Roles of the helper NLR NRG1 in effector-triggered immunity

Joanna Marie Feehan

A thesis submitted to the University of East Anglia
for the degree of Doctor of Philosophy

The Sainsbury Laboratory

November 2020

Abstract

Plants encode intracellular immune receptors that detect pathogen effectors and activate defence mechanisms. These receptors carry nucleotide-binding and leucine-rich repeat (NLR) domains. NLR receptors may directly bind pathogen molecules (effectors) as sensor NLRs, or act as helper NLRs in signalling pathways initiated by sensor NLRs. NRG1 is a conserved helper NLR that is required for function of sensor NLRs with N-terminal TIR domains (TNLs). NRG1 co-functions with the lipase-like EDS1 and SAG101 immune signalling proteins to mediate cell death in Arabidopsis upon TNL-dependent effector-triggered immunity (ETI).

The initial goal of this research project was to uncover novel ETI signalling components. However, a forward-genetics screen revealed numerous false-positive mutant candidates, so my research focus shifted towards the signalling mechanisms of NRG1. Using Arabidopsis complementation lines, the association of NRG1 with EDS1 and SAG101 was investigated in pre- and post-immune activation contexts. In addition, large-scale purification of full-length NRG1 after transient expression in *N. benthamiana* was optimized for structural investigations by cryo-electron microscopy.

This thesis describes an optimized protocol for recovery of highly pure, though low yield, NRG1 protein after transient expression in *N. benthamiana* and immunoprecipitation. This resulted in a low-resolution map of NRG1 reconstructed from negative stain electron microscopy data. Co-immunoprecipitation assays in Arabidopsis revealed that NRG1 associates with EDS1 and SAG101 upon delivery of a TNL-recognized effector. Blue native PAGE assays indicated that higher-order states of NRG1 are formed upon PAMP-triggered immunity in the absence of effectors. Therefore, PAMP-triggered immunity may prime NRG1 for associations with EDS1 and SAG101 upon ETI initiation.

The research presented in this thesis provides a foundation for future purifications of NRG1 or other NLRs after transient expression in *N. benthamiana* for structural investigations. Additionally, this research has revealed the effector-dependent association of NRG1 with EDS1 and SAG101. Future investigations into the dynamics of these associations upon PAMP- and effector-triggered immunity should further resolve the mechanisms by which NRG1 functions with EDS1 and SAG101 to mediate cell death.

Table of contents

List of tables

List of figures

List of appendices

List of symbols and abbreviations

ADP	Adenosine diphosphate
ATP/ dATP	Adenosine triphosphate/ deoxyadenosine triphosphate
BN-PAGE	Blue native PAGE
CBB	Coomassie brilliant blue
CC	Coiled-coil
CNL	CC-NLR
Da (kDa)	Dalton (kiloDalton)
ETI	Effector-triggered immunity
GF Buffer	Gel filtration buffer
HELL	HeLo-like domain
HeLo	N-terminal pore-forming domain found in fungal HET-S protein
HF	6×His-3×FLAG
hpd	Hours post-effector delivery
hpe	Hours post-β-estradiol infiltration
hpi	Hours post-Agro-infiltration
HR	Hypersensitive response
IP	Immunoprecipitation
LC-MS	Liquid-chromatography-mass spectrometry
LRR	Leucine-rich repeat domain
MHD	methionine-histidine-aspartate motif
MW	Molecular weight
NB-ARC	Nucleotide-binding domain found in Apaf1, R proteins and CED4
NIDP40	Nonidet™ P-40 substitute
NLR	Nucleotide-binding, leucine-rich repeat intracellular receptor
NLR-ID	NLR with an integrated domain
OD_{600}	Optical density at a wavelength of 600 nm
PAGE	Polyacrylamide gel electrophoresis
PAMP	Pathogen-associated molecular pattern
Pf0-1	Pseudomonas fluorescens EtHAn
PTI	PAMP-triggered immunity
RNL	RPW8-NLR
RPW8	RESISTANCE TO POWDERY MILDEW 8 gene
SDS	Sodium dodecyl sulphate
SETI	Super-ETI
TIR	Toll/interleukin-1 receptor/resistance
TNL	TIR-NLR
UV	Ultraviolet
v/v	Volume/volume
vcADPR	Variant-cyclic-ADP-ribose
w/v	Weight/volume

Acknowledgements

I express my sincerest gratitude to Professor Jonathan Jones for the opportunity to conduct my PhD thesis research under his supervision. I am grateful for your guidance and your enthusiasm for science. Thank you for helping me become the skilled and knowledgeable scientist that I am.

Thank you to the Rotation PhD Programme for allowing me the opportunity to pursue my PhD at The Sainsbury Laboratory.

Thank you to my postdoctoral supervisors Dr. Adam Bentham and Dr. Hee-Kyung Ahn for your guidance and support. I appreciate your efforts to help me develop my research projects, ideas, and technical skills. I'd also like to thank my lab members for their continued support and feedback on my research projects.

Thank you to the TSL students for being amazing. Being among the intelligent and wonderful student community has been the highlight of my time at TSL.

Thank you also to the TSL community and the support staff. In particular, Dr. Paul Derbyshire and Dr. Franke Menke within the Proteomics Platform. Thank you also to Jake Richardson within the JIC Bioimaging Platform for your input and effort on performing and optimizing the negative stain EM. I'd also like to thank horticultural services, particularly Timothy Wells and Lesley Phillips, for taking care of my plants.

Thank you to my mother, Anna, and father, Mark. Obtaining my PhD is as much your accomplishment as it is mine and, of course, this wouldn't be possible without you both. Thank you for your love and encouragement.

Thank you to my sisters and my friends for their continued love and support.

Thank you to Professor Jamie Cate for hosting me during my first summer of research, Professor Frank Nargang for allowing me to gain more lab experience, and Professor Orson Mortiz for giving me my first real opportunity to see a research project from beginning to end while completing my Master's degree.

To my aunt and uncle, Shauna and Chris: Thank you for your mentorship, guidance, and encouragement. My career in science began from a conversation with Chris nine years ago. The many subsequent discussions with you both have been so rewarding. Thank you for helping me develop as a scientist, and as a person. Thank you for being an inspiration and for believing in me.

Chapter 1

Introduction

1 Introduction

Plants need to be able to perceive external stimuli and mount coordinated, robust responses for survival. Particularly, plants must fend off pathogens that seek to subvert the host. As stimuli are broad and diverse, many of the survival mechanism's plants have evolved are unknown. As a changing environment increases the disease pressures plants face, there is a growing need to have comprehensive knowledge of plant defence mechanisms. Therefore, my thesis work aims to further our understanding of signalling between pathogen recognition and defence activation during the plant immune response. This introductory chapter provides a general discussion of concepts central to plant-pathogen interaction dynamics, as well as a focused discussion on the components of interest in this thesis research.

1.1 The plant immune system

1.1.1 Plants respond to pathogen threats

Diverse classes of pathogens colonize plants. Bacteria can gain access to the plant apoplast via surface openings, nematodes and aphids can inject a feeding stylet into plant cells, and fungi and oomycetes can either push directly into or build extensive hyphae between cells to colonize and feed. In response, plants have thus evolved mechanisms to detect and defend against these diverse pathogen threats.

Plants have a two-tiered innate immune system to detect and defend against pathogen infections; the first tier is mediated by cell surfaced-localized receptor-like kinases (RLKs) and receptor-like proteins (RLPs) that respond to apoplastic molecules. The second tier is mediated by intracellular receptors with nucleotide-binding and leucine-rich repeat domains (NLRs) (Jones et al., 2016) upon detection of intracellular pathogen-derived molecules. Activation of cell surface-localized receptors triggers downstream signalling events that result in increases in cytoplasmic calcium, cation and anion effluxes, extracellular alkalization, production of reactive oxygen species, and activation of MAP kinase cascades (Tang et al., 2017). NLRs are thought to activate similar responses, with the additional hallmark of programmed cell death, referred to as the hypersensitive response (HR) (Jones and Dangl, 2006). During the defence response, plants also produce the defence hormones ethylene, jasmonic acid, and salicylic acid, the last of which plays an essential role in the amplification of cell surface-localized and intracellular immune

responses by regulating the transcriptional activation of defence genes (Zhou and Zhang, 2020).

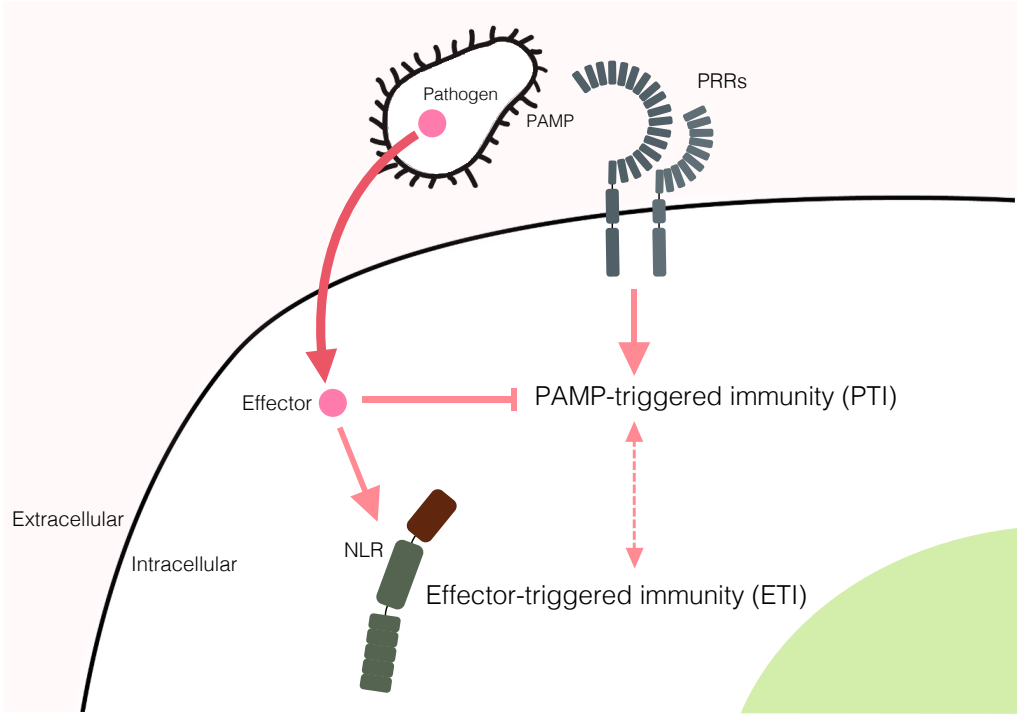

Figure 1.1 Plant immune responses at a glance. Cell-surface localized receptors, pattern recognition receptors (PRRs), detect pathogen-, microbial-, or damage-associated molecular patterns (PAMPs, MAMPs, or DAMPs) or pathogen virulence molecules (effectors) and initiate PAMP-triggered immunity (PTI). Pathogens such as bacteria, fungi, and oomycetes secrete effectors into the intracellular space that suppress the PTI response. Intracellular immune receptors with nucleotide-binding (NB) and leucine-rich repeat (LRR) domains known as NLRs detect these effectors to enhance immune responses through effector-triggered immunity (ETI). Mutual potentiation of PTI and ETI confer a robust immune response for defence (Ngou et al., 2020a). Redrawn from Dodds & Rathjen (2010) *Nature Reviews Genetics*.

The immune response is thought to begin with cell surface-localized receptors, referred to as pattern recognition receptors (PRRs), that detect and respond to the pathogen-, microbial-, or damage-associated molecular patterns (PAMPs, MAMPs, or DAMPs) or pathogen virulence molecules (effectors). This tier of the plant immune system has been referred to as PAMP-triggered immunity (PTI), which can halt further colonization by pathogens. However, pathogens have evolved the use of secreted effector proteins to suppress PTI responses. Some effectors are recognized by plant intracellular immune receptors, which activate what has been referred to as effector-triggered immunity (ETI) (Figure 1.1) (Jones and Dangl, 2006). These two tiers of immunity were initially conceptualized as such in the zigzagzig model, with the

defence response pathways of PTI and ETI had been thought to be distinct from one another. However, two recent publications have provided evidence that these pathways not only crosstalk but mutually potentiate each other. In these publications, simultaneous activation of cell surface-localized and intracellular receptors are required for a complete immune response, and pre-activation of intracellular receptors appears to prime cell surface-localized receptor-mediated defence responses (Ngou et al., 2020a, Yuan et al., 2020). Ngou et al. (2020) showed that ETI signalling functions to "restore" PTI capacity in defence responses, together producing an overall more robust response. These data indicate that the signalling pathways between cell surface-localized and intracellular receptors are intricately linked (Figure 1.1).

In recent years, the "PTI" and "ETI" acronyms seem insufficient for describing the differences between immune response pathways mediated by cell surface-localized and intracellular receptors, respectively. Receptors at the plant cell surface recognize more than just PAMPs, and effectors are also recognized at the cell surface, so the PTI and ETI terms are insufficient. Researchers have proposed other terminology such as extracellularly triggered immunity (ExTI) and intracellularly triggered immunity (InTI) (van der Burgh and Joosten, 2019); replacing ETI with NLR-triggered immunity (NTI) (Lolle et al., 2020); or the use of a spatial invasion model with apoplastic-initiated and cytosol-initiated immune responses, instead of the zigzag model (Kanyuka and Rudd, 2019). Although a consensus on new terminology has not emerged, the general call seems to be for a distinction of the immune pathways based on the localization of receptors, either cell surface or intracellular-localized. However, for simplicity, herein the cell surface-localized receptor immune responses will be referred to as "PTI", and the intracellular immune responses as "ETI", although I acknowledge the deficiencies in these terminologies.

1.1.2 Intracellular receptors mediate resistance in plants

Harold Flor observed that developing plant varieties with resistance genes "was one of the most successful means of controlling plant diseases" (Flor, 1971). Breeding for resistance phenotypes in flax against a fungal rust pathogen, Flor showed that both host resistance and pathogen virulence traits are heritable. He showed that for each resistance (*R*) gene in the host, there is a corresponding pathogen avirulence (*Avr*) gene, referred to as the "gene-for-gene" model (Hammond-Kosack and Jones, 1997). His pioneering contribution used fungal genetics to show that *Avr* genes are dominant.

This discovery of co-evolution between pathogens and host led to research programs that sought to understand the mechanistic basis for these interactions.

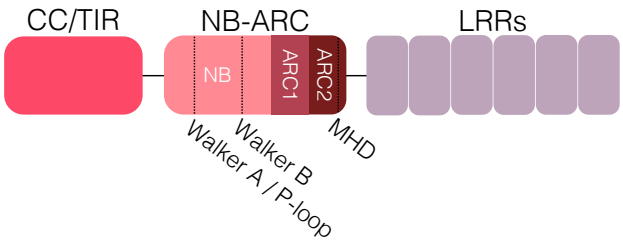

Figure 1.2 Domain architecture of plant NLRs. The canonical architecture of plant NLRs includes an N-terminal coiled-coil (CC) or toll/interleukin-1 receptor/resistance (TIR) domain, a central nucleotide-binding domain that shares homology with human APAF-1, plant *R* genes, and *C. elegans* CED-4 (NB-ARC), and a leucine-repeat rich (LRR) C-terminal domain. Relevant motifs in the NB-ARC related to NLR function are highlighted: Walker A/P-loop important for nucleotide-exchange; Walker B, essential for ATP hydrolysis; MHD, involved in ADP binding. Redrawn from Lukasik & Takken (2009) *Current Opinion in Plant Biology*.

Many *R* genes have been cloned to date, the majority of which code for proteins of NLR architecture (Figure 1.2) (Kourelis and van der Hoorn, 2018). The Arabidopsis pan-NLRome encodes approximately 13,167 NLR genes, with between 167 to 251 genes per accession (Van de Weyer et al., 2019), representing a remarkable within-species diversity. Plant NLRs are defined by a central nucleotide-binding (NB) motif that shares homology with eukaryotic cell death executors, human APAF-1 (APOPTOTIC PROTEASE-ACTIVATING FACTOR 1) and the *Caenorhabditis elegans* homolog CED-4 (CELL DEATH PROTEIN 4) (ARC) (van der Biezen and Jones, 1998). This so-called NB-ARC domain of NLRs belongs to the broad family of STAND (signal transduction ATPases with numerous domains) domains with NTPase activity (Lukasik and Takken, 2009). It is thought that in response to pathogen stimuli, NLRs exchange ADP (adenosine diphosphate) for ATP (adenosine triphosphate), which correlates with oligomerization (Takken and Tameling, 2009, Lukasik and Takken, 2009). Plant NLRs generally also contain an N-terminal signalling domain (discussed further in section 1.2.1) and a C-terminal leucine-rich repeat (LRR). The LRR domain directly binds pathogen effectors in some cases, but likely has a primary function in negative regulation (Faustin et al., 2007). As with animal NLRs, some plant NLRs seem to oligomerize upon effector perception, as was shown recently with the discovery of the ZAR1 (HOPZ-ACTIVATED RESISTANCE 1) “resistosome” (Wang et al., 2019a). Yet, how oligomerization confers cell death is not understood.

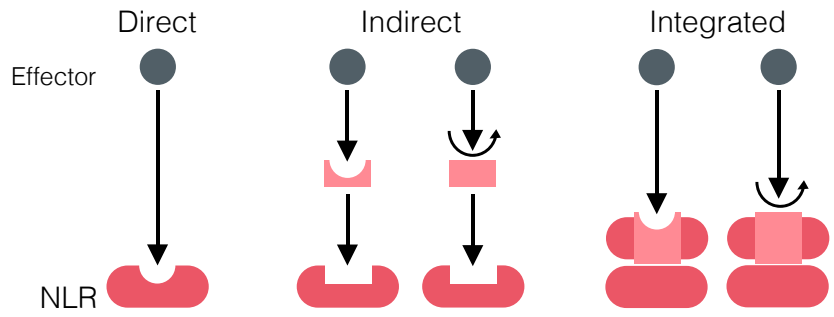

Figure 1.3 Mechanisms of effector perception by NLRs. There are three general mechanisms for perception of pathogen virulence molecules (effectors) by intracellular NLRs (R genes): direct, indirect, or through integrated domains. Direct recognition is the least common, where a host NLR can directly bind a pathogen effector. Indirect recognition may occur via guardees or decoys, either through interactions with, or modifications of, host components. Detection mediated through integrated domains utilise a decoy to perceive pathogens either directly or via modifications (indicated by curved arrows) of the integrated domain. Redrawn from Kourelis & van der Hoorn (2018) *The Plant Cell*.

We now know that NLRs have evolved diverse mechanisms to perceive effectors either directly, indirectly, or via integrated domains (Figure 1.3) (Kourelis and van der Hoorn, 2018). Direct detection may be mediated by the LRR domain, such as with the effector ATR1 and the NLR RPP1 (RESISTANCE TO PERONOSPORA PARASITICA) in Arabidopsis (Krasileva et al., 2010), or through destabilizations of intramolecular interactions such as with AvrL567 and the NLRs L5 and L6 in flax (Ravensdale et al., 2012). Indirect recognition may be mediated by NLR "guardees" that monitor host target proteins, such as RIN4 (RPM1-INTERACTION PROTEIN 4) in Arabidopsis (Axtell and Staskawicz, 2003), or "decoys" that mimic host target proteins such as ZED1 (HOPZ ETI-DEFICIENT 1) in Arabidopsis or Pto in tomato (Baudin et al., 2017, Ntoukakis et al., 2014). While guardees carry-out functions, decoys serve only to bait pathogens into detection through mimicry (van der Hoorn and Kamoun, 2008). Those NLRs that carry integrated domains (NLR-IDs) are so far known to be genetically linked with a "pair" that does not contain an ID (Kourelis and van der Hoorn, 2018). These NLR-ID/NLR pairs utilise the ID as an "integrated-decoy" (Cesari et al., 2014a) to perceive effectors directly or indirectly. The NLR-ID/NLR pair RRS1/RPS4 (RESISTANCE TO PSEUDOMONAS SYRINGAE 4/RESISTANCE TO RALSTONIA SOLANACEARUM 1) directly bind AvrRps4 from Pseudomonas syringae or perceive the acetyl-transferase activity PopP2 from Ralstonia solanacearum (Sarris et al., 2015, Le Roux et al., 2015). By whatever method plant NLRs employ to recognize pathogen effectors, they seem to signal through conserved downstream signalling pathways.

1.2 The signalling mechanisms of intracellular immune receptors

1.2.1 Plants carry TNLs, CNLs, and RNLs

Plant NLR proteins are separated into three ancient and diverged classes based on differences in their N-terminal domain architecture: Toll/interleukin-1 receptor/resistance (TIR) NLRs (TNLs), non-TIR or coiled-coil (CC) NLRs (CNLs), and RPW8 (RESISTANCE TO POWDERY MILDEW 8)-like coiled-coil NLRs (CC_R-NLs or RNLs) (Collier et al., 2011, Shao et al., 2014, Cesari, 2018). Current data suggests that although the RPW8-like domain is a coiled-coil, RNLs are monophyletic (Tamborski and Krasileva, 2020). (RNLs are discussed in further detail in section 1.4). Likely, ancestral fusions of TIR, CC, and RPW8-like domains to NB-ARC domains formed TNLs, CNLs, and RNLs (Figure 1.4). This may have occurred early during the evolution of flowering plants as all three are present in the early-diverging *Amborella* lineage (Figure 1.10) (Tamborski and Krasileva, 2020).

The N-terminal domain of each NLR subtype has been implicated in downstream signalling and shown to be sufficient for cell death when individually expressed (Swiderski et al., 2009, Maekawa et al., 2011, Collier et al., 2011, Adachi et al., 2019). This may, however, reflect cytotoxicity of individual units and not authentic immune activation. Effector perception by NLRs likely leads to conformational changes which facilitate signal transduction via the N-terminal domains. It's also likely that these N-terminal domains facilitate oligomerization in concert with the NB domain (Bernoux et al., 2011, Williams et al., 2014, Maekawa et al., 2011). The TIR-domains of TNLs have been shown to have NADase activity leading to the production of a variant-cyclic-ADP-ribose that is required for immune responses, and TNL proteins with mutations in the NADase active site lose function (Horsefield et al., 2019, Wan et al., 2019). In contrast, oligomerization of CNLs and RNLs may be the terminal point of cell death (Wan et al., 2019, Lapin et al., 2019).

TNLs have expanded in many dicot species, but are missing in some monocot lineages where a subtype of TNLs with a TIR2 N-terminal domain are more prevalent (Shao et al., 2016, Sarris et al., 2016). The structures of several plant TIR domains have been characterized, showing that oligomerization via two distinct interfaces is important for defence signalling (Williams et al., 2014, Nishimura et al., 2017, Zhang et al., 2017) and suggesting a common TNL mechanism for TIR-mediated signalling (Cesari, 2018). EDS1 (ENHANCED DISEASE SUSCEPTIBILITY 1; At3g48090 and At3g48080) was first characterized as essential for the function of all TNL proteins

(Liu et al., 2002). It is not known why TNLs require EDS1 for immune responses; any possible connection between the NADase activity of TNLs and the requirement for signalling via EDS1 remains obscure. Additionally, non-canonical TIR-domain-containing proteins devoid of LRR domains—TIR-nucleotide binding (TN) and TIR-unknown site/domain (TX) families (Nandety et al., 2013)—show some function in immune responses that are dependent on EDS1. However, their full role in immunity is not yet understood.

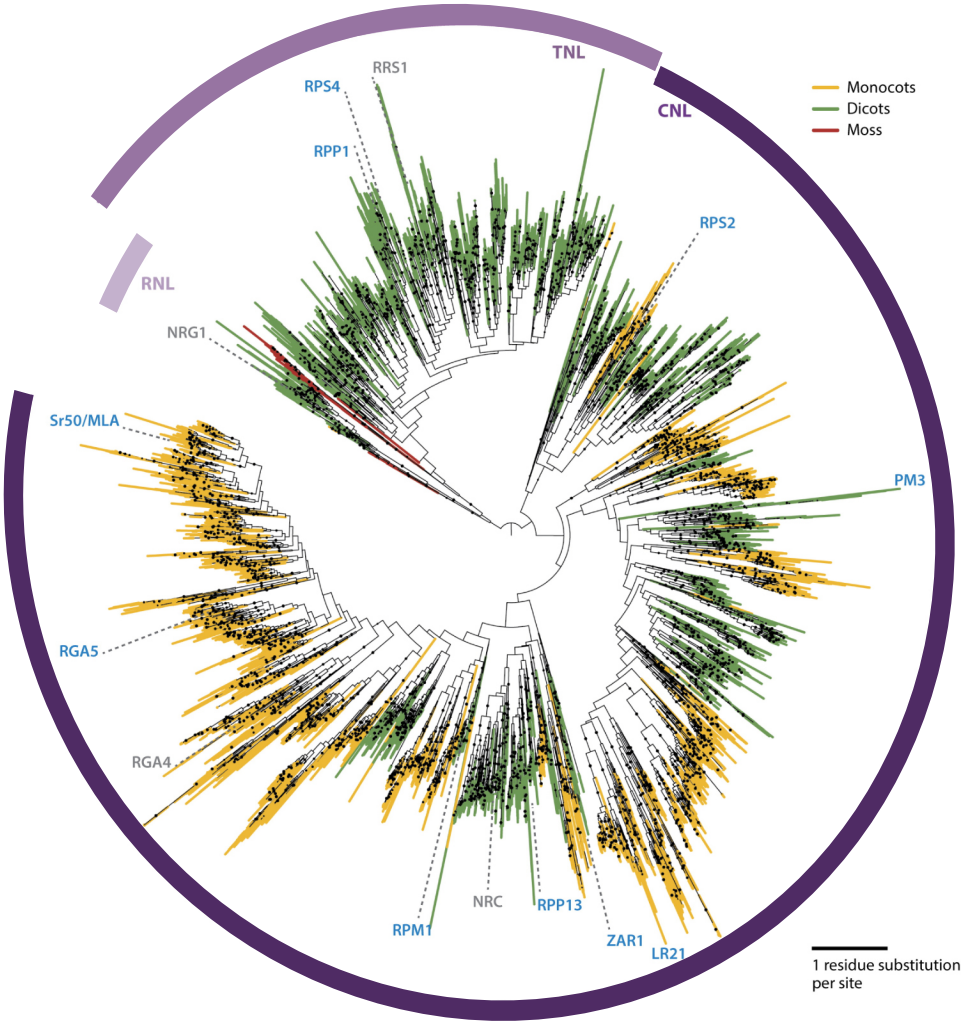

Figure 1.4 NLR evolution in flowering plants. "Maximum likelihood phylogeny of 7,133 NLRs from 11 dicots (green), 7 monocots (yellow), and 1 moss (red) based on NB-ARC domain alignment (11). Major classes of NLRs are depicted as arcs: RNLs (light purple), TNLs (medium purple), and CNLs (dark purple). Examples of well-characterized NLRs with different functions are marked on the tree in blue text (sensors) and grey text (helpers). The tree is rooted on the longest internal branch and is based on the NB-ARC domain. Bootstrap values >80 are indicated on the tree as black circles." Adapted from Tamborski & Krasileva (2020) *Annual Review of Plant Biology*.

The function of the CC domain in CNL signalling is perhaps even more challenging to characterize. It seems that there are at least four distinct classes that have been identified based on sequence-differences: CC_{EDVID}, canonical CC, $CC_{I2\text{-}like}$, and the CC_{SD} of Solanaceous plants. However, the classification of CC domains based on sequence similarities has not revealed conserved functions (Bentham et al., 2018). Additionally, a novel clade of CNLs within Solanaceous plants called the NRCs (NB-LRR PROTEIN REQUIRED FOR HR-ASSOCIATED CELL DEATH), have CC domains that contain both an EDVID motif, which may be involved intramolecular interactions with the NB domain, and a novel signalling sequence called the MADA motif (Wu et al., 2016, Adachi et al., 2019). The CC_{EDVID} domain is characterized by the presence of the signature EDVID motif, while the CC_{SD} subclass is named for the inclusion of an auxiliary N-terminal Solanaceous domain (SD). Notably, the $CC_{I2\text{-}like}$ are a monophyletic clade within the CC_{EDVID} subclass (Wu et al., 2016). CNLs have been shown to function as singletons (e.g. ZAR1), or in sensor-helper pairs to mediate immune responses.

1.2.2 Sensor and helper NLRs coordinate to mediate immune responses

The requirement of one NLR for the function of another was first defined when the Arabidopsis TNL RPP2 (conferring downy mildew resistance) was cloned, revealing that two adjacent TNL genes, RPP2A and RPP2B, are both required for resistance (Sinapidou et al., 2004). Since then, three types of NLR/NLR cooperation can be distinguished in plant immunity: (1) those that function as paired sensor-helper NLR-ID/NLRs, (2) the distinct signalling pathway of CNL or TNL sensor NLRs that signal through RNL helpers, and (3) the Solanaceous-specific group of CNL sensors that signal through NRC helpers (Figure 1.5).

With paired NLRs, a helper NLR acts with a genetically linked sensor NLR-ID to convert effector detection, mediated by the ID as a decoy target, into defence activation. The Arabidopsis RRS1/RPS4 and rice R-GENE ANALOG 4 (RGA5)/RGA4 provide paradigmatic examples of this signalling relationship (Figure 1.5) (Cesari et al., 2014b). The sensor NLR RRS1 contains an integrated WRKY decoy domain and signals with its paired helper RPS4, while the sensor NLR RGA5 contains a HEAVY-METAL BINDING (HMA) domain and signals with its paired helper RGA4. As mentioned previously, it is hypothesized that integrated domains evolved from guarded host targets (Cesari et al., 2014a). While host WRKY transcription factors are targeted by the effector PopP2, which is thus recognized by the RRS1-WRKY ID, host effector targets with HMA domains have not been reported (Cesari, 2018). There is

evidence for 265 distinct IDs fused to NLRs across 37 land plant genomes (Sarris et al., 2016), and the pan-NLRome of Arabidopsis reflects an extensive diversity in NLR-ID/NLR pair architecture (Van de Weyer et al., 2019). These findings may indicate a large repertoire of potential guarded host sites, as well as a diversity of NLR signalling relationships.

The first example of an NLR acting downstream of a genetically unlinked NLR was the RNL *NRG1* (*N-REQUIREMENT GENE 1*). A silencing screen in tobacco for genes that compromised the function of the TNL *N* revealed that NRG1 is required (Peart et al., 2005) but does not directly interact for function (Mestre and Baulcombe, 2006). Subsequently, in Arabidopsis, the *NRG1*-related *ADR1* (*ACTIVATED DISEASE RESISTANCE 1*) gene family was found to be required for full function of several TNLs and CNLs (Figure 1.5) (Bonardi et al., 2011). This highly conserved (Figure 1.9) family of helper NLRs comprises a unique signalling hub acting downstream of many TNL, and some CNL, sensors (Castel et al., 2019a, Wu et al., 2019). Consistent with a helper rather than sensor function, these RNLs usually display low copy number and high conservation in plant genomes (Shao et al., 2016) and pan-genomes (Van de Weyer et al., 2019). A detailed discussion of RNL helpers can be found in section 1.4.

The NRC class of helper NLRs is required for the function of many, but not all, Solanaceae CNLs (Figure 1.5) (Wu et al., 2017). NRCs are CNLs that are phylogenetically more related to NRC-requiring NLRs than non-NRC-requiring NLRs (Wu et al., 2017). Intriguingly, NRCs were first reported as required for full function of the cell surface receptor-like resistance protein Cf-4 (Gabriels et al., 2007), as well as for *Rx, Pto* and *Mi* NLR gene function. Wu et al. (2017) discovered that functionally redundant NRC paralogs can display distinct specificities toward different sensor NLRs that confer immunity to oomycetes, bacteria, viruses, nematodes, and insects (Wu et al., 2017). The helper NLR NRC4 is required for the function of several sensor NLRs, including *Rpi-blb2, Mi-1.2*, and *R1*, whereas either NRC2 or NRC3 are required for the function of the NLR Prf. Interestingly, NRC2, NRC3, and NRC4 redundantly contribute to the immunity mediated by other sensor NLRs, including Rx, Bs2, R8, and Sw5. The NRC superclade is hypothesized to have emerged over 100 million years ago from an NLR pair that diversified to constitute up to one-half of the NLRs of Asterids (Wu et al., 2017).

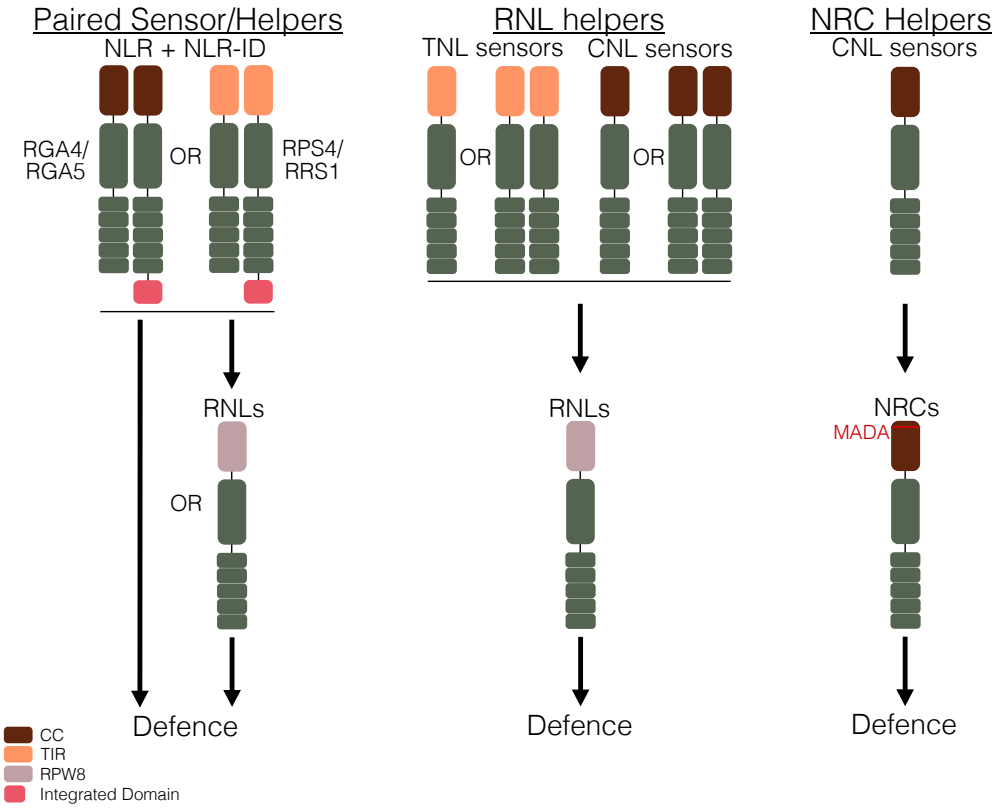

Figure 1.5 Helper NLR signalling pathways. Left; classic NLR/NLR-ID (integrated domain) pairs. Effectors interact with the ID, imposing changes that result in a conformational change within the NLR-ID that activates the helper NLR. The helper NLR may or may not need an additional helper NLR protein to signal. Centre; signalling via the RNL class of helper NLRs (NRG1 or ADR1). CNL or TNL singletons or pairs can activate RNL-dependent signalling. Right; NRC helper signalling. Particularly in Solanaceae, but also in other taxa, many (but not all) CNL sensor NLRs require NRC helper NLRs to activate defence. NRC functionality likely requires a conserved MADA domain at the N-terminus. Feehan et al. (2020) *Current Opinion of Plant Biology*.

1.2.3 RRS1/RPS4 mediate immune responses to AvrRps4 and PopP2

The Arabidopsis TNL pair RPS4 and RRS1 recognize the bacterial pathogen effectors AvrRps4 and PopP2 via an integrated WRKY transcription factor domain at the C-terminus of RRS1-R that mimics the effector's authentic targets (Sarris et al., 2015). The RRS1 represses its RPS4 pair, but upon effector perception, RRS1 releases and activates RPS4, which initiates immune responses (Cesari et al., 2014a). A functional cell death response mediated by RPS4 is dependent on EDS1, SGT1 (SUPPRESSOR OF G-TWO ALLELE OF SKP1), and HSP90 (HEAT SHOCK PROTEIN 90) (Zhang et al., 2004). However, how these proteins work in concert to activate defence upon effector recognition is largely unknown.

Arabidopsis encodes paralogs for both *RRS1* and *RPS4*, deemed the "A" and "B" pair, which are non-functional when inappropriately combined in an A-B cross-pairing (Saucet et al., 2015). Allelic variations between accessions at these loci confer an expanded recognition capacity of effectors from different pathogens (Birker et al., 2009). The RRS1-S allele from Col-0 confers recognition of AvrRps4 from *P. syringae* pv. *pisi*, while the RRS1-R allele, from Ws-2, also recognizes the *Ralstonia solanacearum* effector PopP2 (Sarris et al., 2015) and an unknown effector from the fungus *Colletotrichum higginsianum* (Narusaka et al., 2009). Recognition is mediated through different interactions with the WRKY domain of RRS1; PopP2 acetylates the WRKY domain, while AvrRps4 binds directly (Sarris et al., 2015, Le Roux et al., 2015). These data indicate that the expanded recognition of RRS1/RPS4 is due to the integration of this WRKY domain.

The WRKY domain of RRS1 is also integral to the stability of the RRS1/RPS4 complex. Likely, the WRKY domain helps to maintain the complex in an inactive state as deletion results in an auto-active RRS1 allele. AvrRps4 binding disrupts association of the WRKY with an adjacent domain, triggering derepression of the complex (Ma et al., 2018). In contrast, PopP2-mediated interactions between the RRS1 C-terminus and TIR domain promote derepression. The C-terminus of RRS1-R, but not RRS1-S, is phosphorylated at multiple threonines and serines, the latter of which is required for PopP2 responsiveness (Guo et al., 2020). Thus, effector-triggered and phosphorylation-regulated conformational changes within RRS1 result in distinct modes of RRS1/RPS4 complex derepression by AvrRps4 and PopP2. The intramolecular rearrangements that immediately precede this derepression, and the subsequent translation to defence responses, remain poorly understood. Possibly, RRS1/RPS4 form oligomers which induces proximity of RPS4 TIR domains, leading to NADase activity, recruitment of EDS1, or both.

1.2.4 NLRs across kingdoms share similarities with plant NLRs

The architecture of NLR proteins is deployed across kingdoms in programmed cell death pathways that function in host defence and or self-/ non-self-discrimination (Jones et al., 2016). The core structure of plant, animal, fungal, bacterial, and archaea NLRs generally includes an N-terminal signalling domain, a central NB domain, and a superstructure-forming repeat C-terminal region. However, variability in N-terminal and C-terminal domains is high. Most likely, the NLR architecture of plants and animals arose from two distinct and separate evolutionary events (Urbach and Ausubel, 2017).

The core features of NLRs include the NB domain, which belongs to the family of STAND NTPases. Plants exclusively encode the NB-ARC subtype of STAND NTPases, while animals, filamentous fungi, and prokaryotes can also carry a NACHT (NAIP, CIITA, HET-E, and TP1) subtype (Figure 1.6) (Dyrka et al., 2014, Jones et al., 2016, Dyrka et al., 2020). Typically, LRRs are found as the C-terminal domain in plants and animals, but WD, HEAT, ankyrin, or TPR motifs are also found (Bentham et al., 2017). The C-terminal repeat domains of fungi include WD, ANK, and TPR types, but no LRR motifs have been reported (Dyrka et al., 2014). Like fungal NLRs, prokaryote NLRs usually have WD or TPR repeats but also do not contain any LRR regions (Dyrka et al., 2020). The N-terminal domains are quite variable between kingdoms. Plants predominantly carry TIR or CC domains, as previously mentioned, while animal NLRs may carry CARD, PYD, DD, or BIR domains (Bentham et al., 2017). Fungi contain the highest diversity with 12 possible categories; the most representative examples include Goodbye-like, HeLo-like, sesB-like, and PNP_UDP (Dyrka et al., 2014). The N-terminal domains of prokaryote NLRs are one of ten recently identified bacterial amyloid signalling sequences (BASS), which are proposed to function in prion formation (Dyrka et al., 2020).

In filamentous fungi, NLR proteins function in heterokaryon incompatibility, a self-/ non-self-recognition response that terminates incompatible cell fusions (Dyrka et al., 2014, Heller et al., 2018). However, the high number of STAND-encoding genes in fungi exceeds the number of incompatibility genes (Dyrka et al., 2014), perhaps indicating evidence of innate immunity in fungi (Uehling et al., 2017). Plant NLRs have also been implicated in a form of self-/ non-self-discriminatory programmed cell death termed “hybrid necrosis” (Chae et al., 2014, Tran et al., 2017, Barragan et al., 2019). However, this is thought to be a negative byproduct of innate immunity. In filamentous bacteria, proteins with NLR-like architecture have only recently been identified. Their mechanisms have not yet been determined, yet it is interesting to speculate that they may function in self-/ non-self-recognition in bacteria (Dyrka et al., 2020). Taken together, these data indicate a universal role in self- and non-self-recognition for proteins with NLR architecture.

Though substantial NLR diversity exists, all NLR proteins are thought to involve switch-like activation mechanisms (Yuan and Akey, 2013). This model postulates that pre-activation conformations of NLR proteins are suppressed by intramolecular and intermolecular domain interactions, and this suppression is altered upon perception of self- or non-self-molecules (Jones et al., 2016). Oligomerization of NLRs has been

shown in animals in the formation of inflammasomes after ligand binding (Tenthorey et al., 2017). Two higher-order plant NLR resistosome structures have been reported thus far: the CNL ZAR1, which forms a pentamer upon ligand binding (Wang et al., 2019a, Wang et al., 2019b), and the TNL Roq1 (RECOGNITION OF XOPQ 1) which forms a tetramer in complex with XopQ effectors (Martin et al., 2020).

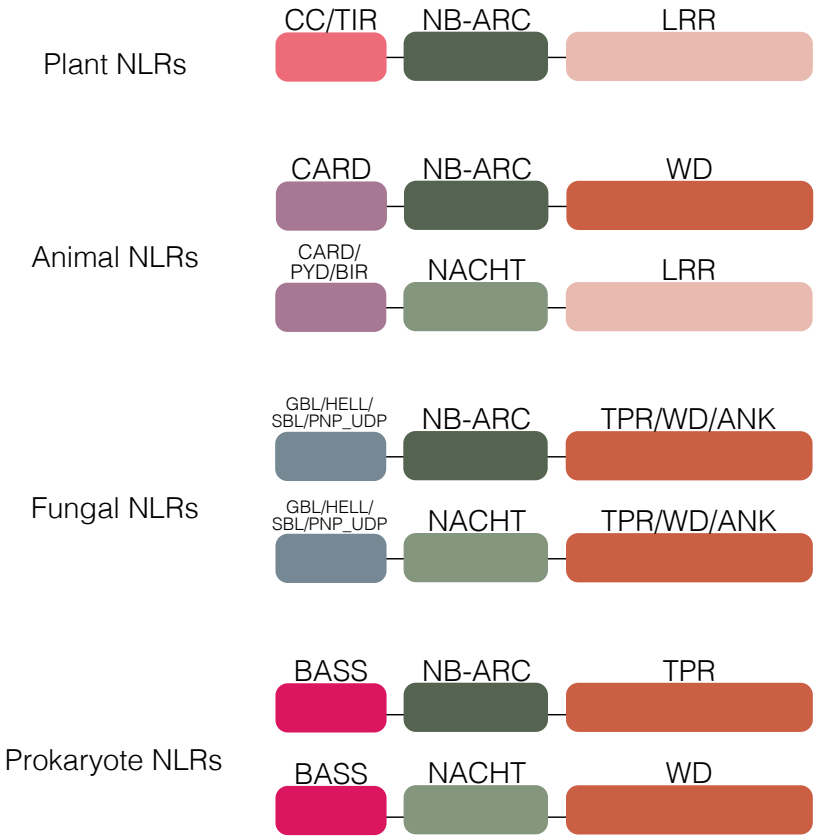

Figure 1.6 Domain architecture of NLRs across kingdoms. Plant, animal, fungal, and prokaryote NLRs and NLR-like proteins carry similar domain architecture. Domains representative only; not to scale. Jones, Vance, & Dangl (2016) *Science*; Dyrka et al. (2014) *Genome Biology and Evolution*; Dyrka et al. (2020) *bioRxiv*.

Oligomerization of NLRs is thought to facilitate signalling by inducing proximity of the N-terminal domains that recruit factors to trigger downstream activation (Danot et al., 2009). In animal NLRs, signalling molecules interact with N-terminal domains, such ASC adaptor protein that recruits caspase-1 via its CARD domain to the PYD domains of NLRP3 (Jones et al., 2016), but analogous signalling elements in plants have not been identified (Jones et al., 2016). The NB domain may exchange ADP for ATP, stabilizing an altered NB-ARC conformation that enables oligomerization. However, nucleotide exchange has not been shown to directly drive oligomerization

of NLRs in plants (Jones et al., 2016). While the details of a Roq1 pre-activation state are not known, ZAR1-RKS1 (-RESISTANCE RELATED KINASE 1) monomers are bound to ADP in the inactive state. When the uridylated (AVRPPHB SUSCEPTIBLE 1)-LIKE 2 ($PBL2^{UMP}$) guardee interacts with ZAR1-RKS1 monomers, ADP is no longer found to be associated (Wang et al., 2019b). A pentamer of ZAR1-RKS1-$PBL2^{UMP}$ protomers forms in the presence of dATP (deoxyadenosine triphosphate) or ATP. The dATP/ATP nucleotides may act to stabilize ZAR1-RKS1-$PBL2^{UMP}$ protomers, thereby contributing to conformational changes that induce formation of the activated ZAR1 resistosome (Wang et al., 2019a). These data indicate that, like animal NLRs, plant NLRs form homomeric oligomers for function.

However, investigations into the interactome of plant NLRs have revealed the potential for heteromeric associations between NLRs to mediate function. This could provide one explanation as to why there is a much greater NLR repertoire in plants than animals (Wróblewski et al., 2018). It is hypothesized that the formation of multimeric NLR complexes might have evolved to compensate for the absence of signalling molecules analogous to those in mammalian systems, e.g. Caspase-1 (Wróblewski et al., 2018). However, currently, there is no evidence of direct interactions between genetically unlinked sensor and helper NLRs in plants.

1.3 Non-NLR components mediate intracellular immune responses

1.3.1 HSP90 and its co-chaperones SGT and RAR1 mediate NLR stability

Molecular chaperones are essential for maturation and activation of NLR proteins in eukaryotes. One of these conserved chaperones is HSP90, which contributes to maintenance of NLR steady-state levels (Kadota and Shirasu, 2012). HSP90 often functions with the co-chaperones SGT1 and the plant-specific RAR1 (REQUIRED FOR MLA12 RESISTANCE) (Takahashi et al., 2003), and has a central role in both biotic and abiotic stress responses (Kadota and Shirasu, 2012, Park and Seo, 2015). These proteins form a symmetric ternary complex consisting of an HSP90 dimer, one molecule of RAR1, and two molecules of SGT1 (Zhang et al., 2010, Siligardi et al., 2018). This complex contributes to immunity in plants either by stabilizing the pre-activation complex of NLR proteins or by facilitating the reconfigurations involved in the conversion from the pre- to post-activation state (Park and Seo, 2015).

Orthologues of SGT1 are essential to the yeast cell cycle (Kitagawa et al., 1999) and in plant immune responses (Azevedo et al., 2002). There are two SGT1 genes in

Arabidopsis, SGT1a and SGT1b, which are redundant in developmental pathways. Only SGT1b is required for innate immunity (di Donato and Geisler, 2019), and experiments in Arabidopsis, Barley, and *N. benthamiana* indicate the requirement of SGT1b for diverse resistance proteins (Takahashi et al., 2003). The central domain of SGT1 contains a CS (CHORD-SGT1) domain that is essential for the disease resistance function of this protein (Botër et al., 2007). The C-terminus holds a highly conserved SGS (SGT1 specific) domain that can associate with LRR domains of NLRs (Siligardi et al., 2018, Shirasu, 2009). Steady-state accumulation of NLRs Rx and N require SGT1 (Azevedo et al., 2006, Mestre and Baulcombe, 2006), for which both the CS and SGS domains are important (Shirasu, 2009).

While SGT1 has a diverse role in plants, RAR1 is more specialized in resistance functions (Muskett et al., 2002). RAR1 is involved in ROS accumulation in infected plant tissue (Shirasu et al., 1999, di Donato and Geisler, 2019) and critical for resistance mediated by multiple NLRs of diverse recognition capacity (Muskett et al., 2002). Arabidopsis *rar1* mutants are defective in NLR-mediated resistance to bacteria and oomycetes (Takahashi et al., 2003). Indeed, the NLR N requires RAR1 for immune function (Liu et al., 2002). Yet, not all alleles of the NLR MLA require RAR1, which seems to be dependent on accumulation of MLA isoforms (Bieri et al., 2004). Notably, several NLRs seem to specifically require RAR1 for protein accumulation (Bieri et al., 2004, Holt et al., 2005). Therefore, RAR1 seems likely to mediate immune responses by maintaining threshold levels of NLR proteins.

As the CS domain of SGT1 is required for association with RAR1, and the SGS domain associates with NLRs, it is possible that SGT1 bridges NLRs to the HSP90-RAR1-SGT1 (Shirasu, 2009). Moreover, the potential to bind two NLRs positions HSP90-RAR1-SGT1 as a regulator of NLR oligomerization (Siligardi et al., 2018). Additionally, roles for chaperones in immunity beyond stabilization have been observed. For example, the HSP90 chaperone complex in rice promotes delivery of a cell-surface-localized receptor from the ER to the plasma membrane to mediate anti-fungal defence responses (Chen et al., 2010). Furthermore, there is evidence that a bacterial effector from a plant pathogen can inactivate the ATPase activity of both human and plant orthologues of HSP90 through phosphorylation, likely mimicking a host binding “client”, highlighting the indispensable role of HSP90 in innate immunity (Chen et al., 2019).

Animal NLRs also require HSP90 chaperones to maintain steady-state levels (Shirasu, 2009). Mammalian orthologues of SGT1 and NLRs also associate (Mayor et

al., 2007), seemingly through associations specific to LRR domains (Mayor et al., 2007, Shirasu, 2009). Unlike plant NLRs, mammalian NLRs seem to require SGT1 only for inflammasome activity and not for accumulation, while HSP90 still functions in both capacities (Mayor et al., 2007). This conservation between NLRs and their chaperones between different kingdoms strengthens the observation that there are intrinsic properties of NLRs that denote their functions.

1.3.2 The lipase-like family of EP proteins: EDS1, PAD4, and SAG101

EDS1, identified during a mutagenesis screen for enhanced susceptibility (Glazebrook et al., 1996), is a necessary component for resistance to oomycete and bacterial pathogens (Parker et al., 1996, Aarts et al., 1998). It was first proposed as a common requirement specifically for TNL-mediated immunity when it was found to be necessary for *N*-mediated defence responses (Liu et al., 2002). Indeed, genetic requirement for EDS1 by TNLs is shared by those acting against bacterial, oomycete, and viral pathogens in dicotyledonous plant species (Peart et al., 2002).

The N-terminal domain of EDS1 shares homology with eukaryotic lipases (Falk et al., 1999). It contains a canonical α/β hydrolase catalytic triad with Ser, Asp, and His residues, and shows structural similarity with lipases (Wagner et al., 2013). Lipases digest water-insoluble ester bonds through glycerol ester hydrolase activity (Wang et al., 2018). EDS1 belongs to the family of class III lipases with PAD4 (PHYTOALEXIN DEFICIENT 4; At3g52430) (Jirage et al., 1999), SAG101 (SENESCENCE-ASSOCIATED GENE 101; At5g14930) (He and Gan, 2002), DAD1 (DEFECTIVE IN DEHISCENCE 1), and DGL (DIACYLGLYCEROL LIPASE) (Wang et al., 2018). EDS1, PAD4, and SAG101 further share a conserved C-terminal EDS1-PAD4 (EP) domain (Feys et al., 2001), which has no significant homology with non-plant proteins; thus, the EDS1 family is defined by the co-occurrence of a lipase-like and EP domain in a single protein (Figure 1.7A) (Wagner et al., 2013). Short EP-like sequences for EDS1 and PAD4 are present in algal genomes (Baggs et al., 2020). However, these may not be truly representative of EP proteins as the strongest evidence for the first occurrence of this domain is found in seed plants (Figure 1.10) (Lapin et al., 2020). As a *pad4 sag101* mutant phenocopies an *eds1* mutant, the EP-family proteins are viewed as a discrete immune signalling hub (Feys et al., 2005), that may require species-specific genetic compatibility (Gantner et al., 2019).

The presence of a lipase domain in EDS1-family proteins would indicate a functional role for catalysis in immunity. However, mutagenesis of in the predicted

catalytic residues in EDS1 and PAD4 do not affect immune function (Wagner et al., 2013), and no enzymatic activity has been reported (Rusterucci et al., 2001, Wiermer et al., 2005, Voss et al., 2019). Interestingly, in vitro catalytic activity of SAG101 has been reported (He and Gan, 2002). However, it does not appear to have residues that would constitute a functional serine hydrolase catalytic triad (Wiermer et al., 2005). It is interesting that although the lipase domain appears to be dispensable for immune function, it has never-the-less been retained throughout the evolution of seed plants. The role of this domain in immunity will be an important mechanism to uncover.

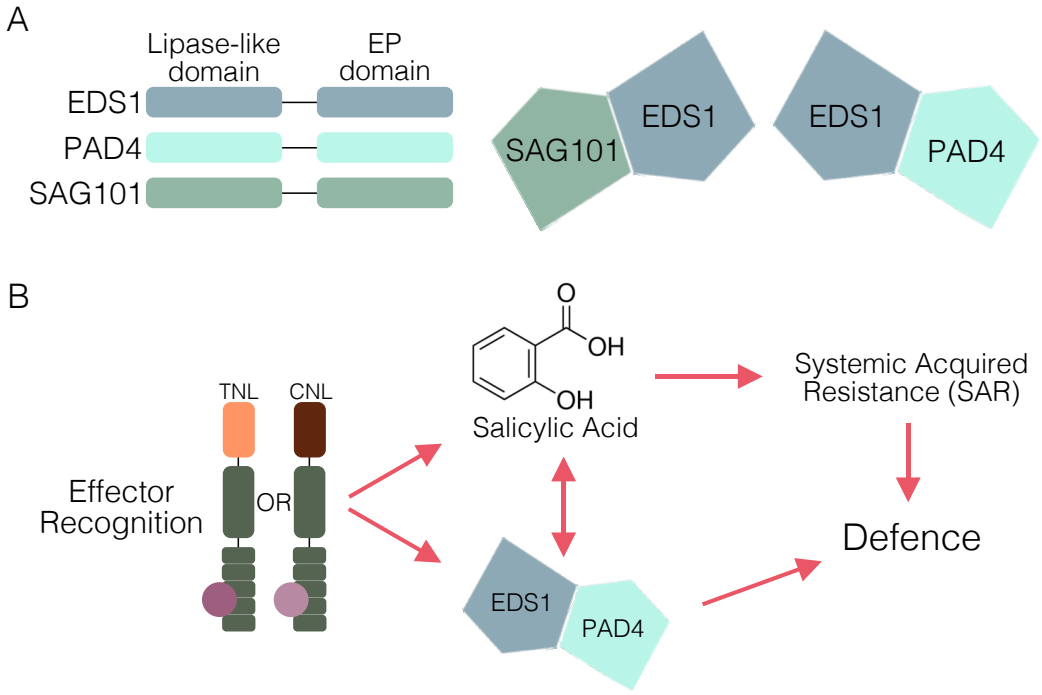

Figure 1.7 The lipase-like EP protein family. EDS1, SAG101, and PAD4 comprise a novel plant-specific family of proteins that encode lipase-like and EP (EDS1-PAD4) domains. EDS1 forms distinct heterocomplexes with SAG101 or PAD4. Redrawn from Lapin et al. (2020) *Annual Review of Phytopathology*. (B) Perception of pathogen effectors by host NLRs activates immune signalling that requires EDS1 and SA for defence. EDS1 and PAD4 promote further accumulation of SA, which in turn positively reinforces EDS1 and PAD4 expression. Venugopal et al. (2009) *PLoS Genetics*. Cui et al. (2016) *New Phytologist*.

EDS1 forms functional heterodimers with either SAG101 or PAD4 (Feys et al., 2005, Wagner et al., 2013), primarily mediated by an N-terminal interface, but with some cooperativity between N- and C-terminal domains (Wagner et al., 2013). There is some evidence that EDR1 (ENHANCED DISEASE RESISTANCE 1) may accomplish its function as a negative regulator of immunity by interfering with EDS1-PAD4 associations (Neubauer et al., 2020). A large cavity in EDS1-SAG101 and EDS1-PAD4

heterodimer structures indicates a possibility for ligand binding (Wagner et al., 2013). Mutants in this cavity have impaired function in immunity (Bhandari et al., 2019), particularly the EDS1^{R493A}, which shows a delay in transcriptional reprogramming but does not break heterodimer formation. Beyond interactions with PAD4 or SAG101, EDS1 may exist in an inactive monomer state but does not appear to form homomers (Voss et al., 2019).

Interactions with PAD4 or SAG101 may direct localizations of EDS1 (Zhu et al., 2011); EDS1-SAG101 complexes appear primarily localized to the nucleus, with some signal in the cytoplasmic space (Gantner et al., 2019), while EDS1-PAD4 associations are nucleo-cytoplasmic (Feys et al., 2005, García et al., 2010). There is an absolute requirement for EDS1 in PAD4 and SAG101 accumulation (Feys et al., 2005). Regulation of a nuclear pool of EDS1 is fundamental to TNL immune pathway maintenance (Stuttmann et al., 2016), and accumulation of nuclear EDS1 either precedes or coincides with transcription of defence-related genes (García et al., 2010). However, cytoplasmic EDS1 seems to have a function specifically in cell death responses (García et al., 2010). Coordinated nuclear and cytoplasmic EDS1 activities may be important for a robust immune response in plants.

There is a functional link between EDS1 and salicylic acid (SA) signalling. Upon immune activation, EDS1 works with PAD4 to promote SA accumulation, required for systemic acquired resistance (SAR) (Figure 1.7B) (Falk et al., 1999, Feys et al., 2001). However, it is likely that EDS1 and SA signal in parallel as they are functionally redundant in CNL-mediated immunity against bacterial, viral, and oomycete pathogens (Venugopal et al., 2009). The EP-domain has been shown to confer transcriptional reprogramming upon TNL-mediated pathogen detection and counters bacterial repression of SA signalling (Bhandari et al., 2019). Indeed, the EDS1-PAD4 complex has been shown to inhibit MYC2, a transcription factor that regulates JA signalling, to boost SA defence independently of EDS1 (Cui et al., 2018, Bhandari et al., 2019). Notably, the function of EDS1 in SA signalling may enable this protein to also contribute to CNL regulation beyond its role in TNL pathways; for example, mutants defective for both EDS1 and SA accumulation phenocopy an *rps2 (RESISTANCE TO PSEUDOMONAS SYRINGAE 2*) mutant (Venugopal et al., 2009). This is further supported by the requirement for a functional EP-domain in EDS1 for RPS2-mediated defence (Bhandari et al., 2019). However, a conclusive role for EDS1 contribution to CNL signalling pathways has not yet been determined—Aarts et al. (1998) found that EDS1 was not required in RPS2-mediated resistance. Nevertheless, EDS1 seemingly

interacts promiscuously with several other cell components to contribute to a broad spectrum of responses in immunity.

EDS1 has been proposed as an effector target (Heidrich et al., 2011), but additional data supporting this hypothesis has not since been reported (Sohn et al., 2012). There is evidence that EDS1 directly interacts with TNLs (Huh et al., 2017), but it is unlikely that this reflects a guard-guardee interaction—Yeast-2-hybrid assays have not shown EDS1 to interact with pathogen molecules, which is in contrast to SA signalling which is disabled by several pathogen effectors (Lapin et al., 2020). Recently, an effector from *Phytophthora capsici* was shown to interact specifically with the lipase domain of EDS1, interfering with PAD4 associations (Li et al., 2020b). This would be the first evidence of suppression of plant immunity by direct targeting of the EP family. However, as EDS1 proteins are highly conserved in seed plants (Figure 1.10), it seems unlikely that so few pathogens would have evolved effectors to target a susceptible host component. Indeed, it is surprising that EDS1 has not been shown to be targeted by pathogens to suppress host immune responses.

Specific mechanisms for PAD4 in defence have been identified. PAD4 is required for SA accumulation and participates in a positive feedback loop that amplifies SA production (Zhou et al., 1998, Jirage et al., 1999). A recently identified a gain-of-function $PAD4^{S135F}$ allele shows enhanced resistance and cell death phenotypes upon powdery mildew infection; however, the mechanism of this is still unknown (Neubauer et al., 2020). In a unique example, PAD4 functions independently from EDS1 and SA for resistance to Green Peach Aphid (GPA) (Pegadaraju et al., 2007, Louis et al., 2012). While the lipase-like domain is not sufficient for conferring resistance, it can limit GPA infestation (Dongus et al., 2020). In contrast to EDS1, mutation of catalytic residues in this domain of PAD4 deterred GPA feeding (Louis et al., 2012). It is remarkable that PAD4 has an EDS1-independent function, as EDS1 is critical for accumulation of, and thought to stabilize, PAD4 (Feys et al., 2005). It is not yet determined whether monomeric PAD4 mediates GPA function, or whether it functions with an unidentified component. Moreover, the specificity for response to insects is notable. This interaction provides a promising context to understand the innate features of EP family proteins.

The role of EDS1, PAD4, and SAG101 in biotic stresses has been well-characterized; however, they also seem to have a function in abiotic stresses, such as freezing responses, in Arabidopsis (Chen et al., 2015). Additionally, EDS1 and PAD4 may function in drought responses (Chini et al., 2004, Szechynska-Hebda et al., 2016).

A link between plant immunity and drought response is supported by conservation of EDS1 and PAD4 with drought response genes throughout plant genomes (Baggs et al., 2020). The contribution of EP family proteins to both biotic and abiotic stress responses reinforces their importance in seed plant species.

1.3.3 RPW8 is required for resistance to powdery mildew

Originally defined as an Arabidopsis powdery mildew resistance gene, RPW8 encodes a protein with an N-terminal signal anchor and several coiled-coil domains, but without NB or LRR domains (Xiao et al., 2001). Despite this unorthodox structure, RPW8-mediated resistance may share similarities with TNL signalling pathways as it is associated with an HR phenotype that is SA-, EDS1-, PAD4-, and SGT1-dependent (Xiao et al., 2005). Targeting to the extra-haustorial membrane after powdery mildew infection in Arabidopsis is key for RPW8-mediated resistance (Wang et al., 2009, Zhang et al., 2015b), but how this change in localization contributes to immune response is not yet understood.

The Arabidopsis Ws-2 accession contains two paralogs of *RPW8*, *RPW8.1* and *RPW8.2*, in a tandem array with three *HOMOLOGOUS TO RPW8* (*HR*) genes, *HR1*, *HR2* and *HR3*. However, in Col-0, *RPW8.1* and *RPW8.2* have been replaced with *HR4* (Xiao et al., 2001). It has been suggested that the Brassicaceae *RPW8* gene family evolved from an *HR3*-like ancestor gene, following duplications and functional diversification of *RPW8* (Xiao et al., 2004). A distant homolog of RPW8, HR5, has been identified but is not predicted to share function (Castel et al., 2019b). Overexpression of HR1, HR2, or HR3 shows enhanced resistance phenotypes to powdery mildew (Berkey et al., 2017). Furthermore, these three paralogs can localize at the extra-haustorial membrane, indicating that extra-haustorial membrane-targeting is an ancestral function of the RPW8 family (Berkey et al., 2017). However, an *rpw8* quadruple mutant in Arabidopsis Col-0 maintains its cell death response even in the presence of compromised resistance phenotypes (Castel et al., 2019b). Thus, the immune-mechanisms of RPW8 are not well elucidated.

A role for RPW8 self-associations in auto-immunity has been shown. The C-terminal region of RPW8 contains repeats that determine auto-immune-incompatible interactions with alleles of the CNL *RPP7* (Barragan et al., 2019), and the HR4 allele from Arabidopsis accession Fei-0 has been reported to trigger the assembly of higher-order RPP7b complexes (Li et al., 2020a). An extended C-terminal repeat region in this allele is implicated in the formation of self-oligomers which are

RPP7-independent and induce cytotoxicity (Li et al., 2020a). Whether these mechanisms extend to immune responses beyond auto-immunity remains to be seen.

1.3.4 RPW8 shares homology with the HeLo domain of HET-S

RPW8 shares homology to the HeLo domain of the fungal HET-S protein (Figure 1.8) (Daskalov et al., 2016). The *het* (*heterokaryon incompatibility*) loci in fungi regulate incompatible hyphal fusions (Glass et al., 2000). Upon incompatible encounters, HET-S proteins form amyloid aggregates mediated by a C-terminal prion-forming domain (Greenwald et al., 2010). Formation of prion aggregates target the HeLo N-terminal domain to membranes, creating pores that correlate with liposome leakage and toxicity-inducing cell death (Seuring et al., 2012).

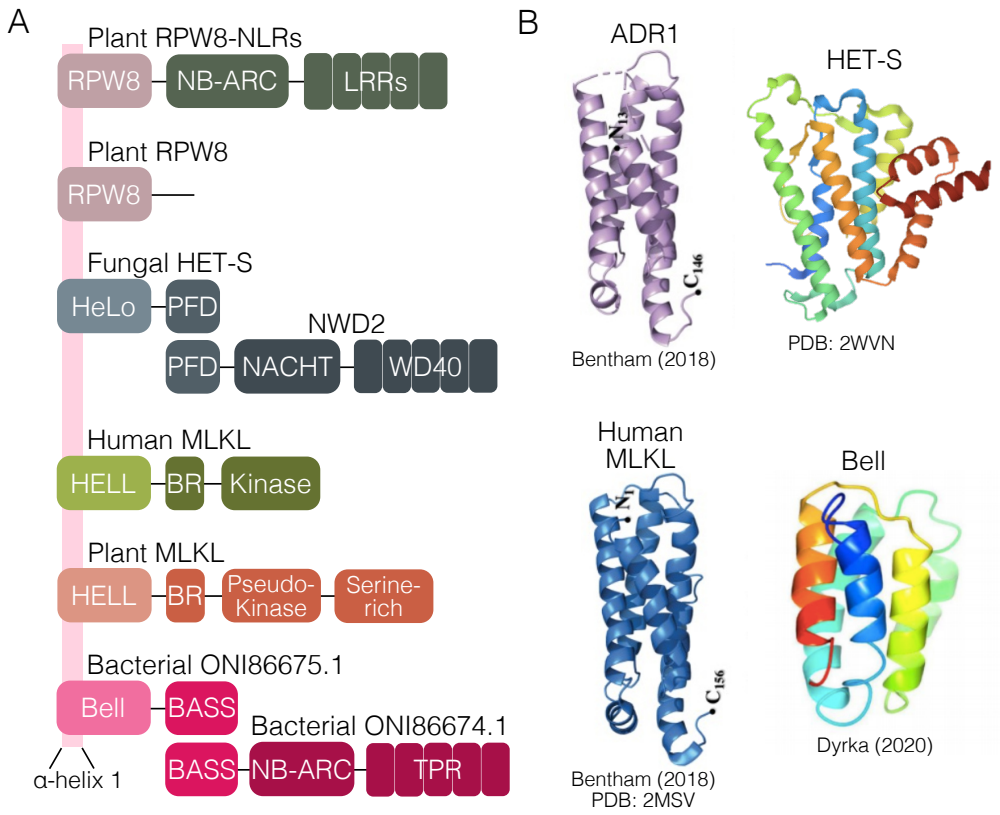

Figure 1.8 HeLo/HELL domain-containing proteins across kingdoms. Domain organizations of NRG1, RPW8, and MLKL-like from Arabidopsis, compared to fungal HET-S, human MLKL, and bacterial ONI86675.1. Genome-adjacent NLR-like proteins are included for fungal HET-S (NWD2) and bacterial ONI6675.1 (ONI86674.1). Pink bar indicates the conserved first α-helix of each protein. HELL: HeLo-like; PFD: Prion-forming domain; BR: Brace Region; Bell: Bacterial domain analogous to Hell; BASS: Bacterial amyloid signalling sequence. (B) Structural similarity of four α-helix bundles for models of *At*ADR1 and bacterial Bell N-terminal domains, alongside solved structures of N-terminal human MLKL (PDB: 2MSV) and fungal HET-S (PDB: 2WVN). Feehan et al. (2020) *Current*

Opinion in Plant Biology; Bentham et al. (2018) *Plant Cell Physiology*; Dyrka et al. (2020) *bioRxiv*; Mahdi et al. (2020) *Cell Host & Microbe*.

RPW8 was found to contain homology to the HeLo domain of HET-S, referred to as the HeLo-like (HELL) domain (Daskalov et al., 2016). This domain is also observed in the fungal HELLP protein (Daskalov et al., 2016), the mammalian necroptosis MLKL (MIXED LINEAGE KINASE DOMAIN-LIKE) protein (Hofmann, 2019), plant MLKL-like protein (Mahdi et al., 2020), and the prokaryote Bell (Bacterial domain analogous to Hell) domain-containing protein (Dyrka et al., 2020). The HET-S HeLo domain has a four α-helix bundle structure (Seuring et al., 2012), which is also true for the solved structure of mammalian MLKL (Su et al., 2014) and plant MLKL-like (Mahdi et al., 2020) (Figure 1.8). Furthermore, this domain structure is predicted for the N-terminal RPW8-like domain of RNLs (Bentham et al., 2018) as well as for the prokaryotic Bell domain (Dyrka et al., 2020). Like HET-S, mammalian MLKL proteins have been shown to form pores following aggregation (Wang et al., 2014, Cai et al., 2014, Chen et al., 2014). There is evidence HELLP and Bell domain-containing proteins also function analogously to HET-S, utilizing their HELL domains for pore-formation and toxicity following aggregation (Liu et al., 2017, Daskalov et al., 2016, Dyrka et al., 2020).

Only recently were Bell domain-containing proteins identified in filamentous prokaryotes genomes (Dyrka et al., 2020). The encoded proteins carry the so-called Bell domain fused to a proposed prion-forming BASS domain (Figure 1.8). Interestingly, NLR-like proteins carrying BASS domains were found adjacent to some of these proteins, indicating potential cooperation between NLR and Bell-domain containing proteins for recognition of self- and or non-self; analogous to HET-S and HELLP mechanisms in fungi (Dyrka et al., 2020).

The tendency for HeLo and HELL domain-containing proteins to associate for function suggests that RPW8 could behave like HET-S. Perhaps via a C-terminal prion-forming domain and the N-terminal pore-forming HELL domain, RPW8 could form prion aggregates with the RPW8-like domain of RNLs to mediate defence responses. However, an Arabidopsis *rpw8* mutant does not phenocopy an *nrg1a/b* mutant (Castel et al., 2019b), and RNL-dependent NLRs such as RRS1/RPS4, RPS2 and WRR4A do not require RPW8 to signal (Castel et al., 2019b). Nevertheless, the *rpw8* mutant is slightly impaired in resistance to adapted and non-adapted strains of powdery mildew, and to *P. syringae* pv tomato strain DC3000 (Castel et al., 2019b). Thus, RPW8 likely

plays a role in plant immunity distinct from RNL helpers, perhaps dependent upon self-associations.

1.3.5 Plant MLKL-like proteins contribute to ETI-mediated immune responses

A family of MLKL-like proteins in plants was recently identified to contribute quantitatively to disease resistance in ETI responses (Mahdi et al., 2020). Although mammalian MLKL has unambiguously been shown to mediate necroptosis via cell death (Wang et al., 2014, Cai et al., 2014, Chen et al., 2014), the cell death mechanism of plant MLKL-like appears uncoupled from resistance (Mahdi et al., 2020). Interestingly, MLKL-like immunity was shown to be TNL specific which may indicate some redundancy with RNLs and EDS1-family proteins (Mahdi et al., 2020). Upon delivery of AvrRps4, which signals through the TNLs RRS1 and RPS4, MLKL-like seems to mediate bacterial growth restriction but not cell death. Perhaps MLKL-like proteins will prove to be redundant with transcriptional activation of defence genes mediated by ADR1, EDS1, and PAD4 (discussed further in 1.4.2). Yet, the full context of their role in plant immunity remains to be determined.

1.4 RPW8-NLRs act as helper NLRs to mediate core immune responses

1.4.1 NRG1 and ADR1 comprise a core signalling hub as helper NLRs

RNLs comprise a distinct helper NLR signalling hub, required downstream in many sensor TNL, and some CNL, immune signalling pathways (Figure 1.9A) (Castel et al., 2019a, Wu et al., 2019, Saile et al., 2020). The sister clades of this subgroup, which diverged after the Gymnosperm and Angiosperm split, are *NRG1* and *ADR1* (Figure 1.10) (Tamborski and Krasileva, 2020, Collier et al., 2011). The Arabidopsis genome encodes three *NRG1* paralogs: *NRG1A* (At5g66900), *NRG1B* (At5g66910), and the truncated *NRG1C* (At5g66890). *NRG1A* and *NRG1B* are functionally redundant in immune responses, while *NRG1C* appears dispensable (Castel et al., 2019a, Wu et al., 2019). An additional non-canonical NLR, DAR5 (DA1-RELATED PROTEIN 5; At5g66630) encodes an N-terminal RPW8-like domain and a central NB-ARC domain, but in place of the C-terminal LRR is instead a LIM (LIN-11, Isl1, MEC-3) domain (Castel et al., 2019a). A role for DAR5 in immunity has not been revealed.

NRG1 appears to be a conserved component required for activity by diverse TNLs that recognized effectors from different pathogen species. However, it does not seem to confer a complete defence response. While an Arabidopsis *nrg1a/b* mutant

shows a loss of cell death upon effector delivery, transcriptional activation signatures of a functional immune response are maintained (Castel et al., 2019a). Additionally, NRG1 seems to be differently required depending on the pathogen treatment: an Arabidopsis *nrg1a/b* mutant still restricts bacterial growth, while restriction of oomycete hyphal growth is only partially compromised (Castel et al., 2019a). Furthermore, overexpression of *Nb*NRG1 in *N. benthamiana* can impair viral replication (Peart et al., 2005, Collier et al., 2011). These data indicate a specialized role for NRG1 in mediating cell death responses whose contribution to resistance may be pathogen-dependent.

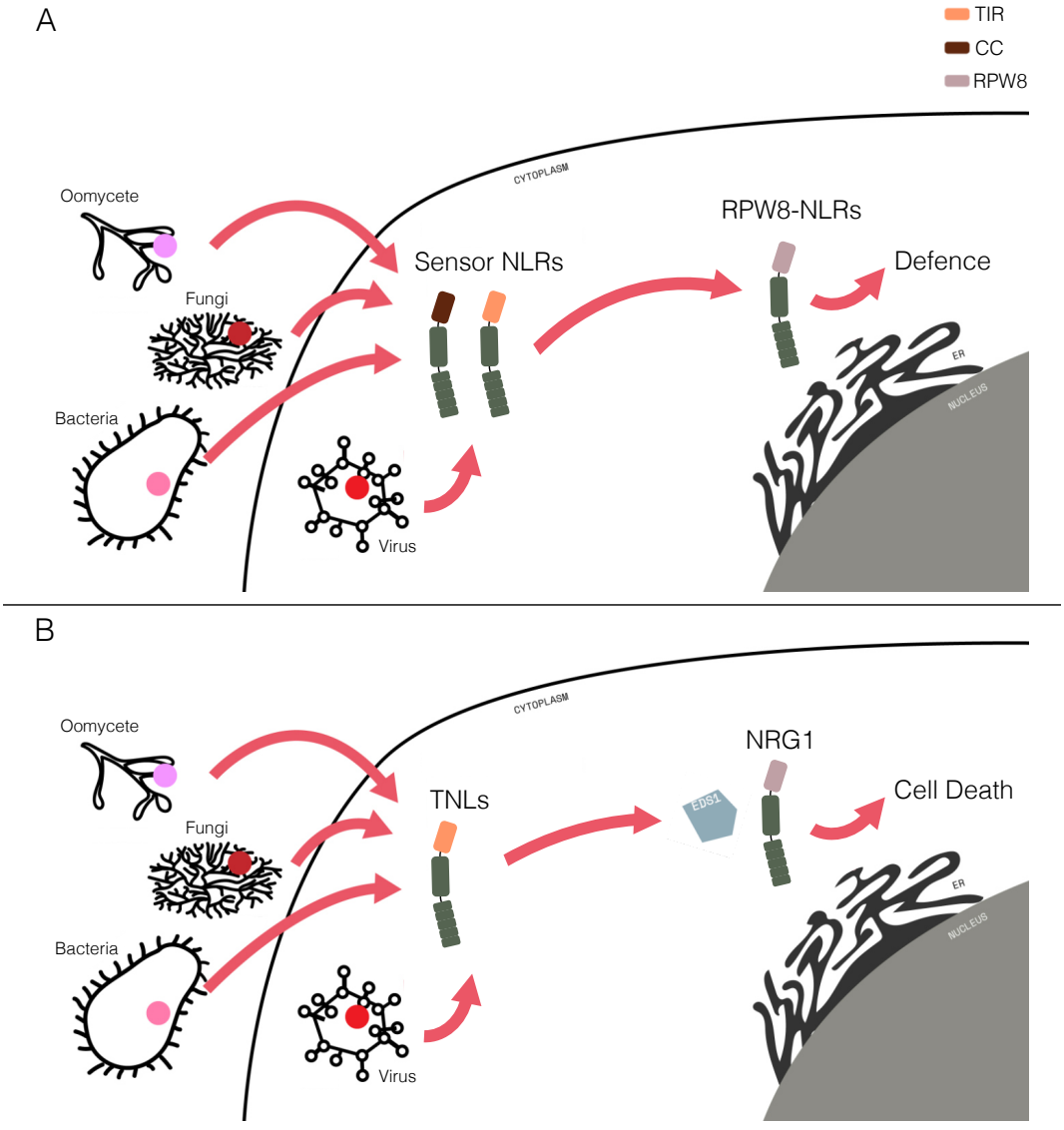

Figure 1.9 RNLs function as helper NLRs downstream of sensor NLRs. (A) RNLs signal downstream of both sensor TNLs and CNLs that recognize broad pathogen effectors to activate defence. (B) NRG1 signals downstream of TNLs in concert with EDS1 to mediate cell death responses. Castel et al. (2019) *New Phytologist*; Wu et al. (2019) *New Phytologist*; Qi et al. (2018) *PNAS*.

How NRG1 mediates cell death is not understood, but EDS1 is somehow involved (Figure 1.9B). NRG1 is localized to the cytosol and endomembrane network, and no change in localization is observed upon effector delivery, indicating a cell death mechanism that is carried out in extranuclear spaces (Wu et al., 2019). As NRG1 contains an N-terminal HeLo-like domain (Daskalov et al., 2016), and as it associates with endomembrane networks, it is plausible that NRG1 executes cell death mechanisms via oligomerization and membrane disruption as is observed for other HeLo/HeLo-like domain-containing proteins. Moreover, as mentioned previously, replacement of ADP with ATP binding is thought to promote oligomerization of NLRs. The Walker A motif of NB-ARC domains, also referred to as the P-loop (Figure 1.2), is proposed to coordinate binding of ATP/ADP by NLRs (Tameling et al., 2006). Indeed, an intact P-loop is required by *Nb*NRG1 for cell death in *N. benthamiana* (Peart et al., 2005). These data would indicate that NRG1-mediated cell death is dependent upon oligomerization. However, the P-loop may be dispensable when signalling downstream of auto-active TNLs in Arabidopsis (Wu et al., 2019). Another feature of NB-ARC domains includes the methionine-histidine-aspartate (MHD) motif (Figure 1.2) which when mutated can induce auto-activity, likely through constitutive binding of ATP (Williams et al., 2011). An NRG1A^{D485V} allele in Arabidopsis is auto-active, again supporting the hypothesis that oligomerization is required for cell death functions (Wu et al., 2019). However, an auto-active Arabidopsis NRG1B allele has not been identified. These discrepancies between alleles and homologs creates some uncertainty around the mechanisms of cell death for NRG1. Therefore, whether NRG1 does oligomerize, and the role of any potential oligomer in cell death, requires further investigation.

There are three paralogs of *ADR1* in the Arabidopsis genome: *ADR1* (At1g33560), *ADR1-L1* (At4g33300), and *ADR1-L2* (At5g04720). *ADR1* was identified in a screen that utilised activation tagging in an Arabidopsis SA-signalling reporter line (Grant et al., 2003). It is notable that a function for NRG1 in SA signalling has not been identified, in contrast to ADR1 (Bonardi et al., 2011). ADR1 was found to function as a helper NLR downstream of CNL sensor NLRs, such as RPS2, and TNL sensors, such as RPP4 and RPP2. However, not all CNLs signal through ADR1—RPM1- and ZAR1-mediated immune pathways are not compromised in an *adr1* triple mutant background (Bonardi et al., 2011, Saile et al., 2020). The requirement for a functional P-loop is also not resolved in ADR1s; it is dispensable for ADR1-L2 function (Bonardi et al., 2011), except for runaway-cell death phenotypes in *lsd1* (*LESION STIMULATING DISEASE 1*) mutants, but is required for the auto-active MHD mutant

ADR1-L2^{D484V} allele (Roberts et al., 2013). Whether ADR1 oligomerizes, and the function of such an oligomer, also requires further investigation.

Although NRG1s are recognized as the specialized helper RNL required downstream of TNLs, there is some evidence for requirement of ADR1: ADR1-L1 was identified in a screen for negative regulators of the TNL *snc1* (*SUPPRESSOR OF NPR1-1, CONSTITUTIVE 1*), and an auto-immune allele of *snc1* is suppressed in the *adr1 triple* mutant background (Dong et al., 2016). Furthermore, there is some evidence that EDS1 acts as a negative regulator of ADR1-L2^{D484V}, both with and independently from its function in SA accumulation (Roberts et al., 2013). Moreover, an ADR1-L2^{D484V} allele requires PAD4 for function (Wu et al., 2019). These data indicate that RNLs are synergistic and upstream sensor NLRs seem to have a preferred helper RNL: TNLs with NRG1 and CNLs with ADR1. However, it is unlikely NRG1s and ADR1s function together, as auto-activity of ADR1-L2^{D484V} is independent of NRG1 (Wu et al., 2019). Interestingly, like EDS1 and PAD4, ADR1 seems to have a function in drought tolerance (Chini et al., 2004), highlighting the potential contribution of RNLs in other plant signalling pathways.

1.4.2 NRG1 and ADR1 signal with the family of EP proteins

An Arabidopsis "*helperless"* mutant that lacks *NRG1A, NRG1B, ADR1, ADR1-L1*, and *ADR1-L2* genes phenocopies *eds1* and *pad4*/*sag101* mutants (Wu et al., 2019, Saile et al., 2020). Moreover, an *adr1 triple* mutant is phenotypically similar to a *pad4* mutant (Wu et al., 2019), and an *nrg1a/b* mutant shares loss of cell death phenotypes with a *sag101* mutant (Lapin et al., 2019). These data are consistent with a model in which RNL and EDS1 family proteins act in parallel (Figure 1.11). In particular, a co-evolved, functional relationship between SAG101, NRG1, and TNLs is further supported by the repeated loss of all three in monocots and in *Aquilegia coerulea* (Figure 1.10) (Baggs et al., 2020).

NRG1 genetically requires EDS1 for function, and previously NRG1 has been positioned downstream of EDS1 in the immune signalling pathway (Peart et al., 2005). However, native expression of *Nb*NRG1 and coexpression with the recognized effector do not induce HR in an *N. benthamiana eds1* mutant background (Qi et al., 2018). These data indicate that EDS1 is required to facilitate an authentic immune response by NRG1, suggesting that these proteins act in parallel. In contrast, overexpression of *Nb*NRG1 does induce HR in an *N. benthamiana eds1* mutant (Qi et al., 2018), revealing that *Nb*NRG1 can induce cell death in an EDS1-independent

manner. However, potentially this HR reflects some toxicity of accumulated *Nb*NRG1. If there is a membrane-disrupting function for *Nb*NRG1, perhaps this can occur above a certain threshold of *Nb*NRG1 protein abundance in the absence of *Nb*EDS1.

Arabidopsis alleles of EDS1, SAG101, or PAD4 fail to complement Solanaceae mutants in the corresponding genes (Gantner et al., 2019). However, addition of *At*NRG1 with *At*EDS1 and *At*SAG101 recapitulates a functional immune response in Solanaceae (Lapin et al., 2019). This supports the hypothesis that RNL and EP proteins act in co-evolved modules that require all components for functionality. As RNLs are more basal, and as RPW8 also requires EDS1 (Xiao et al., 2001) and PAD4 (Xiao et al., 2005), it is likely EDS1-family proteins evolved to function with RNLs (Lapin et al., 2020).

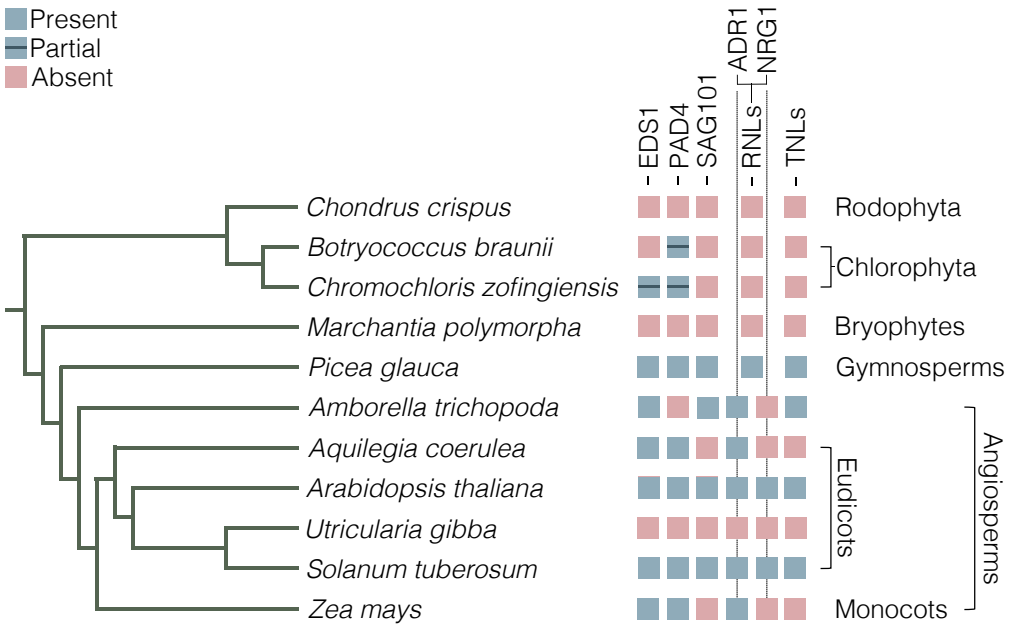

Figure 1.10 Co-occurrence of RNL, TNL, and EP genes across plants. Presence/absence of EP, RNL, and TNL genes in representative plant genomes. Presence is indicated in blue, absence in pink. The emergence of EDS1, RNLs, and TNLs occurred prior to gymnosperm and angiosperm divergence. Partial sequences for EDS1 and PAD4 exist in Chlorophyta genomes but are unlikely to be true orthologues. Co-occurrences of NRG1, SAG101, and TNL loss occurs in monocot genomes, as well as in the *Aquilegia coerulea* dicot genome. Collier et al. (2001) *Molecular Plant Microbe Interactions*; Wagner et al. (2013) *Cell Host & Microbe*; Tamborski & Krasileva (2020) *Annual Review of Plant Biology*.

Indeed, RNL and EP proteins likely form at least two distinct signalling modules that function in immunity downstream of TNL activation. In Arabidopsis, NRG1/EDS1/SAG101 are required for cell death, while ADR1/EDS1/PAD4 mediate

bacterial growth restriction (Figure 1.11) (Lapin et al., 2019). Conversely, Arabidopsis alleles of NRG1/EDS1/SAG101 are sufficient for both cell death and bacterial growth restriction when expressed in *N. benthamiana*, while ADR1/EDS1/PAD4 are not required (Lapin et al., 2019). As there is evidence that these modules have co-evolved and act in parallel, it is highly plausible that they directly interact to mediate immune signalling mechanisms. However, the data are ambiguous; *Nb*EDS1 constitutively associates with *Nb*NRG1 in transient assays in *N. benthamiana* (Qi et al., 2018), while the association between *At*EDS1 and *At*NRG1 alleles has not been conclusively shown (Wu et al., 2019, Lapin et al., 2019). There are no reports of direct interactions between SAG101 and NRG1 nor PAD4 or EDS1 with ADR1.

Further complicating our understanding, NRG1 and SAG101 appear to be in distinct cell compartments. NRG1 is reported to localize primarily to endomembrane networks in Arabidopsis and *N. benthamiana* (Wu et al., 2019, Lapin et al., 2019). However, Arabidopsis SAG101, whether expressed in Arabidopsis or heterologously in *N. benthamiana*, is primarily nuclear-localized, seemingly as a heterodimer with EDS1 (Feys et al., 2005, Wagner et al., 2013). If it is hypothesized that NRG1, SAG101, and EDS1 directly associate to mediate immune function, the impact of spatial separation should be investigated. Furthermore, there no reports on the subcellular localization of ADR1, but EDS1/PAD4 heteromers localize to both the nuclear and cytoplasmic spaces (Feys et al., 2005). Investigations into ADR1 localizations should guide future research questions into their functions with EDS1 and PAD4.

It is not known why TNLs seem to require RNL/EP signalling modules for immune responses. The TIR-domains of TNLs have been shown to have NADase activity leading to production of a variant-cyclic-ADP-ribose (vcADPR) that is required for immune responses, and TNL proteins with mutations in the TIR domain NADase active site lose function (Horsefield et al., 2019, Wan et al., 2019). Any possible connection between the NADase activity of TNLs and the requirement for signalling via RNL/EP modules remains obscure.

Although RNLs were first defined as required upon activation of TNLs, the function of some CNLs is also delayed or reduced in a *helperless* mutant (Saile et al., 2020). This indicates the importance of RNLs beyond TNL immune signalling. Whichever sensor accomplishes recognition, RNLs always regulate transcription of the same set of genes in Arabidopsis—a set that mostly overlaps with CNL-regulated genes (Saile et al., 2020). In summary, RNLs are broadly required helper NLRs that

execute an array of defence functions, and there are many questions yet to be answered about how this is achieved.

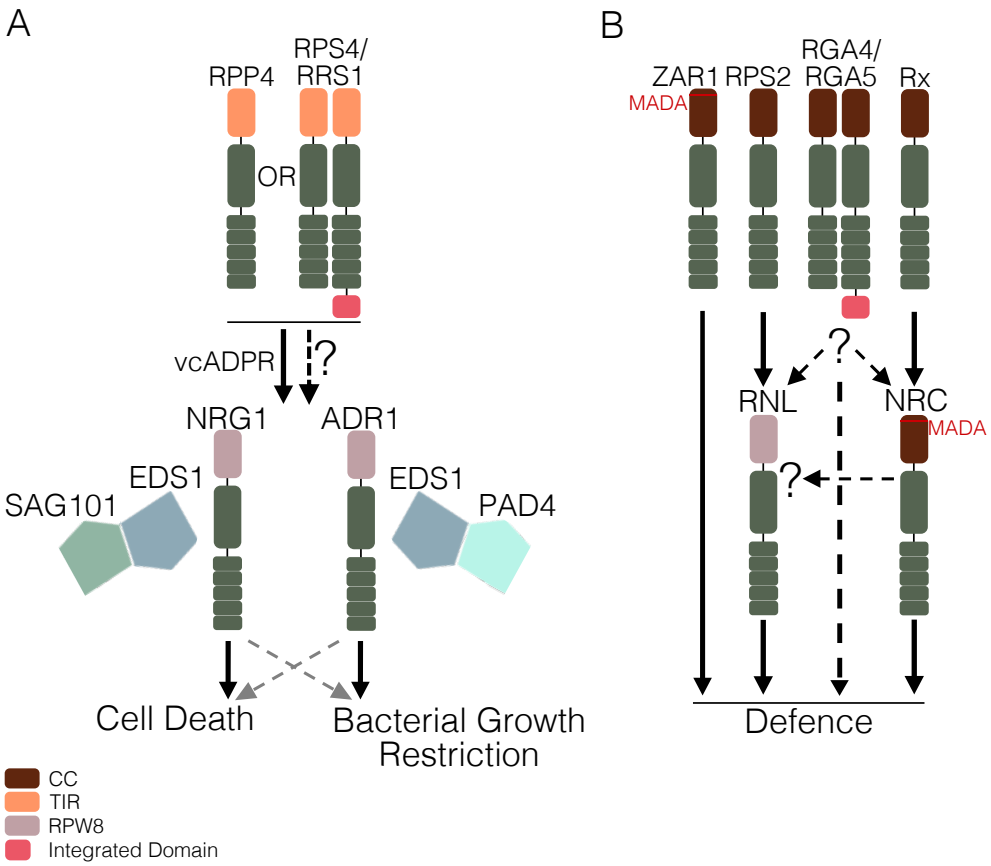

Figure 1.11 TNL sensor NLRs signal through RNL/EP modules. (A) Unpaired or paired TNLs produce variant cyclic-ADP-Ribose (vcADPR) via NADase activity of N-terminal TIR domains. vcADPR, likely in addition to unknown components, signals to RNL/EP modules of either NRG1/EDS1/SAG101 to trigger cell death, or ADR1/EDS1/PAD4 for bacterial growth restriction. Grey dotted arrows indicate the ability of these modules to mediate other defence responses either by compensation or species-specific specializations. (B) CNLs signal either independently of helper NLRs (e.g., ZAR1), through RNLs (e.g., RPS2), or the Solanaceous NRCs (e.g., Rx). It is not known how paired the CNLs RGA4/RGA5 signal downstream in defence. It is not known whether NRCs signal through RNLs to mediate defence. Lapin et al. (2019) The Plant Cell; Castel et al. (2019) New Phytologist; Horsefield et al. (2019) Science; Wan et al. (2019) Science; Feehan et al. (2020) *Current Opinion in Plant Biology*.

1.5 Project aims and objectives

Our understanding of how intracellular NLRs mediate immune responses has progressed significantly since the discovery and cloning of the first NLR almost 30 years ago (Whitham et al., 1994). Yet, while many more NLR—and non-NLR components—have since been identified, it is not fully understood how perception translates to defence. The ultimate goal of this project was to gain insight into the mechanisms employed by plants between pathogen recognition and host immunity.

The first part of this project sought to reveal novel signalling components in ETI through a forward genetics screen. An effector-inducible line of Arabidopsis encoding additional layers of NLR redundancy was employed; however, a high-false positive recovery rate meant that this project was terminated. Improvements for future potential screens are proposed.

In an attempt for more detailed investigations of NRG1 mechanisms, I sought to purify full-length NRG1 protein for structural investigations. Structure determination is a major bottle-neck to our knowledge of plant NLR function, but could provide answers to long-standing questions on how plant NLRs relay signal in immune responses. Purification of full-length NRG1 resulted in reconstruction of a low-resolution map after negative stain electron microscopy. These data lay the foundation for follow-up purifications to resolve higher-resolution structures of NRG1, or for purification of other full-length NLRs for structure determination.

As RNLs and EDS1-family proteins are emerging as core components that relay signals from pathogen detection to defence response, I looked to investigate whether NRG1, EDS1, and SAG101 proteins from Arabidopsis directly associate to mediate function, pre- and post- immune activation. These studies have revealed the existence of effector-dependent associations between these components. The results of this work will guide future investigations into the mechanisms by which these associations confer cell death.

This project sought to reveal details of NLR signalling mechanisms from immune activation to defence response. In particular, I have focused on the broadly conserved NRG1, investigating effector-dependent changes in engagement with other signalling components over a time-course of effector provision. Thus, this data presented in this thesis adds to a growing body of research into the dynamics of helper NLR contributions to plant immunity.

Chapter 2

Materials and Methods

2 Materials and Methods

2.1 General chemicals, reagents, and buffers

2.1.1 Water

The Milli-Q® direct water purification system was used to purify water in this project. Type III (reverse osmosis) was used in preparation of general buffers. Type I (ultra-pure) was used in preparation of reagents and buffers for DNA and protein purification methods.

2.1.2 Chemicals

Unless otherwise specified, chemicals were purchased from Sigma-Aldrich (now Merck), Thermo Fisher Scientific, or VWR (Avantor).

2.1.3 Antibiotics

Stock and working concentrations for *Escherichia coli*, *Agrobacterium tumefaciens*, and *Pseudomonas fluorescens* (Pf0-1) are listed in Table 2.1. Stock solutions of Carbenicillin, Gentamycin, Kanamycin, Spectinomycin, and Chloramphenicol were stored at – 20 °C while Rifampicin was stored at 4 °C. Stock solutions were filter-sterilised using a 0.3 µm Ministart® filters prior to storage.

Table 2.1 Antibiotic stock and working concentrations

		Working (µg/mL)		
Antibiotic	**Stock (mg/mL)**	*E. coli*	*A. tumefaciens*	Pf0-1
Carbenicillin	100 (in water)	100	100	-
Gentamycin	10 (in water)	-	20	100
Kanamycin	50 (in water)	50	50	100
Spectinomycin	100 (in water)	50	50	-
Chloramphenicol	10 (in ethanol)	-	-	30
Rifampicin	10 (in methanol)	-	50	-

2.2 Bacterial methods

2.2.1 Media for bacterial growth

2.2.1.1 Lysogeny broth liquid media and agar plates

Lysogeny broth (LB) was composed of 1% (w/v) tryptone, 0.5% (w/v) yeast extract, and 1% (w/v) sodium chloride at pH of 7.0 in water prior to autoclaving. For

selection plates, 1.5% (w/v) agar was included prior to autoclaving. Molten LB agar was allowed to cool to 65 °C before addition of antibiotics and pouring into 90 cm Petri dishes. LB was used to culture *E. coli* and *Agrobacterium* strains.

2.2.1.2 King's B medium agar plates

King's B medium (KB) was composed of 2% (w/v) proteose peptone, 0.1% (v/v) glycerol, and 0.15% (w/v) potassium phosphate dibasic at pH of 7.0 in water prior to autoclaving. Magnesium sulphate was adjusted to 1.5% (w/v) after autoclaving to prevent precipitation. For selection plates, 1.5% (w/v) agar was included prior to autoclaving. Molten LB agar was allowed to cool to 65 °C before addition of antibiotics and pouring into 90 cm Petri dishes. KB was used to culture Pf0-1 strains.

2.2.2 Bacterial transformation protocols

2.2.2.1 Bacterial strains

Bacterial strains of *A. tumefaciens*, *E. coli*, and *P. fluorescens* were used in this research project. *A. tumefaciens* strains were used for transient expression in *N. benthamiana, E. coli* was used for molecular biology, and *P. fluorescens* was used for pathogen assays in Arabidopsis. Two strains of *A. tumefaciens* were used, GV3101:pMP90 and Agl1, one *E. coli* strain used, DH10β, and one *P. fluorescens* strain was used, Pf0-1. The C58 genotype of GV3101:pMP90 confers natural rifampicin resistance, and this strain carries the nopaline-based Ti plasmid pMP90 which carries the gentamycin selectable resistance cassette. Agl1 genotype is a RecA-type C58 which confers both natural carbenicillin and rifampicin resistance. The Ti plasmid of Agl1 does not carry a selectable cassette. The *E. coli* DH10β strain carries natural resistance to streptomycin. The *P. fluorescens* Pf0-1 strain carries natural chloramphenicol resistance. This project utilised Pf0-1 engineered with the effector-to-host analyser system described further in 2.6.1. Pf0-1 strains were inherited from lab members; therefore, I prepared no Pf0-1 competent cells nor performed transformations.

2.2.2.2 Preparation of electrocompetent E. coli

Electrocompetent *E. coli* cells were prepared first by streaking DH10β onto LB streptomycin 25 µg/mL plates. A single colony was used to inoculate 10 mL of LB and grown overnight shaking 200-250 RPM at 37 °C. Next day, 3 × 500 mL LB were inoculated with 2.5 mL overnight culture and incubated ~ 2-3 h at 37 °C shaking 200-250 RPM until OD_{600} = 0.4-0.6. Cells were cooled on ice and harvested by

centrifugation at 4 °C for 15 min at 4000 x *g*. Pellet was washed three times with 200 mL of cold 10% glycerol solution. Cells were resuspended in 10% glycerol and aliquoted to cold Eppendorf tubes before storage at – 80 °C.

2.2.2.3 Transformation of electrocompetent E. coli

Electrocompetent *E. coli* cells were thawed on ice for 10 min. plasmid DNA (1 pg-100 ng) was added to cells before transfer to cold 0.1 cm electroporation cuvette. Cuvette was placed in MicroPulser™ Electroporation Apparatus (Bio-Rad: 165-2100) and one pulse was applied at 1.8 kV using the "Ec1" pre-programmed setting. Cuvette was transferred back to ice and cells were resuspended in LB before transfer to 1.5 mL Eppendorf. Cells were incubated shaking at 200-250 RPM at 37 °C for 0.5-1 h before plating onto appropriate selection media. When LacZ gene was present in acceptor vectors, 50 µL of 50 mg/mL 5-bromo-4-chloro-3-indolyl β-D-galactopyranoside (X-gal) and 10 µL of 1 M isopropyl β-D-1-thiogalactopyranoside (IPTG) was spread onto selection plates for blue-white colony selection. Plates were transferred to 37 °C incubator for 12-16 h to allow colony growth for downstream applications.

2.2.2.4 Preparation of electrocompetent A. tumefaciens

Electrocompetent *A. tumefaciens* cells were prepared first by streaking onto LB plates with appropriate selection. One colony was used to inoculate 10 mL of LB and grown overnight shaking 200-250 RPM at 28 °C. Next day, 100 mL of LB with appropriate selection antibiotics were inoculated with 5 mL of overnight culture and incubated overnight. Next day, 500 mL of LB with appropriate selection antibiotics was inoculated with 50 mL overnight culture to a starting OD_{600} = 0.1-0.2. Culture was incubated ~ 4-6 h at 28 °C with shaking 200-250 RPM until OD_{600} = 0.5-0.8. Cells were cooled on ice and harvested by centrifugation at 4 °C for 10 min at 4000 x *g*. Pellet was washed in 50 mL of cold 10% glycerol solution before centrifugation at 4 °C for 5 min at 4000 x *g*. Wash steps were repeated twice more. Cells were resuspended in 1 mL cold 10% glycerol and aliquoted to Eppendorf tubes before storage at – 80 °C.

2.2.2.5 Transformation of electrocompetent A. tumefaciens

Electroporation of *A. tumefaciens* cells were performed as described in 2.2.2.3 with the described changes: a) one pulse was applied at 2.2 kV using the "Agr" pre-programmed setting, b) cells were incubated shaking at 200-250 RPM at 28 °C for 1-2 h before plating onto appropriate selection media, c) plates were transferred to 28 °C incubator for ~ 48 h to allow colony growth for downstream applications.

2.2.2.6 Preparation of glycerol stocks

Single colonies were retrieved from selection plates and transferred to appropriate sterile liquid media before incubation at 200-250 RPM 16-24 h at 37 °C for *E. coli* and 28 °C for *A. tumefaciens* or Pf0-1. Cells were pelleted for 10 min at 1900 × *g* and resuspended in 500 µL MES-$MgCl_2$ pH 5.6. Resuspensions were combined with 500 µL 60% sterile glycerol mixtures before storage at – 80 °C.

2.3 DNA methods

2.3.1 Isolation of plasmid DNA from *E. coli*

Single colonies were used to inoculate 10 mL sterile LB supplemented with the appropriate selection antibiotics. Cultures were grown 12-16 h shaking 200-250 RPM at 37 °C. Cells were pelleted 4000 x *g* for 10 min before plasmid DNA isolation with Macherey-Nagel NucleoSpin® Plasmid Mini Kit (28006000) according to manufacturer's instructions. Plasmid DNA was eluted from spin columns in water. Concentration was determined by measuring ultraviolet light absorbance of plasmid DNA at 260 nm by Nanodrop™ spectrophotometer. A ratio of A_{260}/A_{280} = ~ 1.8 was considered pure. Purified plasmid DNA was stored at − 20 °C.

2.3.2 Polymerase chain reaction

Polymerase chain reaction (PCR) was used for mutating restriction nucleotide sites in genes of interest from plasmid DNA. Sigma-Aldrich synthesised DNA oligonucleotide primers for PCR reactions. Lyophilized oligonucleotides were resuspended in water to a final concentration of 100 µM and stored at − 20 °C. Annealing and elongation parameters were applied based on predicted melting temperature (T_m) and base-pair amplicon size. Q5® high-fidelity polymerase (NEB: M0491S) was used in 20 µL PCR reactions run according to manufacturer's instructions. General thermocycling conditions are outlined in Table 2.2. Primers used for domestications are detailed in Table 2.3.

Table 2.2 Q5® thermocycling conditions

Step	Temp	Time
Denaturation	98	30 s pDNA, 5 min gDNA
	98	10 s
×25-30	x	15 s
	72	30 s/kb
Extension	72	2 min
Hold	10	

Table 2.3 Oligonucleotides for gene domestications

ID	Oligonucleotide Sequence 5' to 3'	Details
JF17_F1_F	GGTCTCAAATGGTCGTGGTCGATTGGCTTG	Domest. NRG1B from BCJJ292 for JFJJ25
JF18_F1_R	GGTCTCATCCACAACCAGGAGGACCAGACAC	
JF19_F2_F	GGTCTCATGGAAAGACCACGCTGGTTACTAAGC	
JF20_F2_R	GGTCTCACTCGCGCTTATTTGTCCTGGTAGTAAGTA	
JF21_F3_F	GGTCTCACGAGGACGGTTTTTACAATGAGTTGTTAGTCAC	
JF22_F3_R	GGTCTCATAATGAAACAACTTCGGGGATCCAATATGG	
JF23_F4_F	GGTCTCAATTAAAGACACTTAGCATCACAAACTGTAAC	
JF24_F4_R	GGTCTCACGAAccAAACGTTAGAAGCAACTTCAGGTTATGC	
JF108_pSAG101-F-BbsI	GGGAAGACAAGGAGCCTTCTCGATGAATTAAGGGTTTTATG	Primers to BbsI diglig into L0
JF109_pSAG101-R-BbsI	GGGAAGACAACATTGCGTGAGCTGGAATAGATCTGTGGAGAAGAAAATAC	

2.3.3 Agarose gel electrophoresis

Agarose gels for DNA electrophoresis were prepared by heating molecular biology grade agarose in TAE buffer [40 mM Tris-acetate pH 8.0, 1 mM ethylenediaminetetraacetic acid (EDTA)] to a final concentration of 0.7-1 % (w/v). The agarose solution was allowed to cool to ~ 65 °C before addition of ethidium bromide to a final concentration of 0.5 µg/mL. Molten agarose mixture was poured into gel moulds with well-combs and allowed to cool to room temperature for agarose polymerization. DNA samples were mixed with 4× FOG loading dye [12 % (w/v) Ficoll 400 and 0.25 % (w/v) Orange G] before loading. Molecular weight marker 2-log DNA Ladder (New England Biolabs: 101228) was run alongside DNA samples. Electrophoresis was carried out in TAE buffer, and electrical current was applied across the gel at 100-120 V. DNA bands were visualized by ultraviolet transilluminator.

2.3.4 Purification of DNA from an agarose gel

When appropriate, DNA bands of interest were excised from the agarose gel after electrophoresis. Isolation of DNA from the gel was carried out with Zymoclean™ Gel DNA Recovery Kit (Zymo Research: D4002) according to the manufacturer's instructions.

2.3.5 DNA synthesis

Twist Biosciences performed synthesis of DNA. Sequences for EDS1 promoter and terminator were retrieved from The Arabidopsis Information Resource (TAIR) and domesticated for BpiI (BbsI) and BsaI sites with Golden Gate compatible overhangs

to clone into L0 acceptor vectors. Sequences submitted for synthesis are described in Appendix I.

2.3.6 Golden Gate cloning

Golden Gate cloning was used to generate constructs for transient expression assays in *N. benthamiana*. Golden Gate cloning utilises Type IIS restriction enzymes for DNA assemblies (Engler et al., 2008). The lab has generated a Golden Gate modular cloning toolbox for plants that is available on request through TSL Synbio Platform (Engler et al., 2014). This system utilises a "common syntax" which can be used to generate transcriptional units that can be sequentially assembled into multigene constructs. Level 0 (L0), L1 constructs were assembled with "short" protocol, while L2 constructs were assembled with "long" protocol (Table 2.4). The short protocol called for 100-200 ng acceptor plasmid, a 2:1 molar ratio of insert:acceptor, 10 U BpiI (BbsI) or BsaI (ThermoFisher), 2 µL Buffer G (ThermoFisher), 400 U T4 DNA Ligase (NEB), and 2 µL 10 mM ATP. The long protocol called for 100-200 ng acceptor plasmid, a 2:1 molar ratio of insert:acceptor, 5 U BpiI (BbsI) or BsaI (ThermoFisher), 1.5 µL T4 Ligase Buffer (NEB), 1.5 µL Bovine Serum Albumin (10×), and 200 U T4 DNA Ligase (NEB). Constructs were confirmed by restriction digest using enzymes other than BsaI or BpiI (BbsI) that had sites in backbone as well as in coding sequence. Plasmid DNA was analysed by Sanger sequencing for independent confirmation of accurate sequences or assembly. Constructs generated by Golden Gate cloning are described in Table 2.5. Parts used to assemble these constructs are outlined in Appendix II.

Table 2.4 Golden Gate protocols

Short (BpiI)			Short (BsaI)			Long (BpiI/BsaI)		
10 min	37 °C		10 min	40 °C		20 s	37 °C	
10 min	16 °C	×3	10 min	16 °C	×3	3 min	37 °C	×3
10 min	37 °C		10 min	50 °C		4 min	16 °C	
20 min	65 °C		20 min	80 °C		5 min	50 °C	
Hold	16 °C		hold	16 °C		5 min	80 °C	
						hold	16 °C	

Table 2.5 Golden Gate-assembled constructs

ID	Description
JFJJ14	35S-GUS-4XMyc-OcsT
JFJJ19	35Ss-NRG1B-4XMyc-35S
JFJJ25	NRG1B_AATG-TTCG
JFJJ26	NRG1B_AATG-TTCG
JFJJ27	pSAG101:SAG101-mCherry
JFJJ29	pSAG101:SAG101-mEGFP
JFJJ34	pSAG101_GGAG-AATG
JFJJ36	pEDS1_GGAG-AATG
JFJJ37	EDS1ter_GCTT-CGCT
JFJJ38	pEDS1:EDS1-V5
JFJJ42	HopQ1
JFJJ43	LexA:HopQ1-Myc
JFJJ45	PAD4-HA_EDS1-V5_LexA:HopQ1-Myc_XVE
JFJJ55	35S:NRG1B-V5:OcsT
JFJJ70	pPAD4:PAD4-HA
JFJJ72	pNRG1B_GGAG-AATG
JFJJ79	NRG1Bter_GCTT-CGCT
JFJJ125	NRG1B-mEGFP_SAG101-mCherry

2.3.7 Sanger sequencing of DNA

Sanger sequencing was performed by GENEWIZ. Barcoded pre-mixed reactions were prepared in water with 400-500 ng plasmid DNA and 2.5 µL of 10 µM respective oligo mixture to a final volume of 10 µL. Results were analysed using Geneious Prime software. Common sequencing primers are listed in Table 2.6.

Table 2.6 Sequencing primers

ID	Oligonucleotide Sequence 5' to 3'	Details
JF15_F(0015)	CGTTATCCCCTGATTCTGTGGATAAC	L0 sequencing primer
JF16_R(0016)	GTCTCATGAGCGGATACATATTTGAATG	L0 sequencing primer
JF7_F(0229)	GAACCCTGTGGTTGGCATGCACATAC	L1 sequencing primer
JF8_R(0230)	CTGGTGGCAGGATATATTGTGGTG	L1 sequencing primer

2.4 Protein detection methods

2.4.1 Fusion tags for protein detection

Several different fusion-tags were used for detection of proteins of interest. The HF (6×HIS-3×FLAG®) tag is a string of histidines, which bind immobilized metal ions, fused to the highly specific and artificial 3×FLAG® (DYKDHD-G-DYKDHD-I-DYKDDDDK) antigen. The V5 tag (GKPIPNPLLGLDST) is derived from paramyxovirus. The HA tag (YPYDVPDYA) is derived from human influenza hemagglutinin. The TSL Synbio Golden Gate L0 construct carries six repeats for a 6×HA tag. The Myc (EQKLISEEDL) tag is derived from the human c-Myc. The TSL Synbio Golden Gate L0 construct carries four repeats for a 4×Myc tag. The GFP (green fluorescent protein) is a 238 amino acid fusion-tag (Prasher et al., 1992). mEGFP is a monomeric enhanced GFP with residue mutations of F64L, S65T, and A206K (Cormack et al., 1996, Zacharias et al., 2002). mCherry is a monomeric optimized red fluorescent protein (Shaner et al., 2004).

2.4.2 Polyacrylamide gel electrophoresis (PAGE) assays

2.4.2.1 Sample loading dye

Sample loading dye was prepared to a 4× concentration at 250 mM Tris-HCl (pH 6.8), 8% (w/v) sodium dodecyl sulphate (SDS), 40% glycerol (v/v), 50 mM EDTA, and bromophenol blue for visualization.

2.4.2.2 Preparation of PAGE resolution gels

PAGE resolution gels were either purchased precast (4-20% Mini-PROTEAN® TGX™: 4561095, 4-20% TEO-Tricine RunBlue™: BCG42012) or prepared in the lab. Laboratory procedures used glass plate apparatus to cast 6, 8, 10, or 12% acrylamide resolving gels. Resolution buffer was prepared to a 4× concentration at 1.5 M Tris base, 20% SDS (w/v), and adjusted to pH 8.8 with HCl before autoclaving. Stacking buffer was prepared to a 4× concentration at 0.5 M Tris base, 20% SDS (w/v), and adjusted to pH 6.8 with HCl before autoclaving. Acrylamide was added to 1× resolution buffer with 0.01% APS, and 0.05% Tetramethylethylenediamine (TEMED) before layering with isopropanol. When gel was set, isopropanol was washed away, and 1× stacking buffer with acrylamide, 0.01% APS, and 0.1% TEMED was poured over resolution gel. Well-comb was added, and gel was left to polymerize at room temperature for ~ 20 min. Gels were used fresh or stored in moist blue-roll and plastic wrap at 4 °C before use within one week.

2.4.2.3 SDS-PAGE

SDS-PAGE was performed with precast or prepared gels (as described in 2.4.2.2) assembled in gel tank apparatus (Mini-PROTEAN® system) with 1× SDS buffer [25 mM Tris, 200 mM Glycine, 2% SDS (w/v)] for western blotting or 1× RunBlue™ (TEO-Tricine) Run Buffer for coomassie staining. If frozen, samples were warmed to 37 °C for 5 min, briefly vortexed, and centrifuged at 15,000 x *g* for 1 min. Samples were loaded alongside 5 µL PageRuler™ Prestained Protein Ladder 10-180 kDa (26617). Electrophoresis was run at 90 V for ~ 15 min until ladder had migrated into resolving gel. The electrical current was increased to 135 V for ~ 45 min or until dye-edge had migrated near the end of the gel. Gels were either subjected to western blotting (detailed in 2.4.3) or stained with InstantBlue® Coomassie Protein Stain (ab119211) to visualize protein bands. InstantBlue® is referred to as Coomassie brilliant blue (CBB) throughout this thesis for simplicity.

2.4.2.4 Blue native PAGE (BN-PAGE)

Blue native (BN) PAGE was performed according to the NativePAGE™ Novex® Bis-Tris Gel System with precast NativePAGE™ 3-12% Bis-Tris Mini Protein Gels (10-well BN1001BOX, or 15-well BN1003BOX). Electrophoresis was performed in cold room, and all buffers were cooled prior to use. Samples were prepared on ice with 2.5 µL NativePAGE™ Sample Buffer (4×) and 0.25-1 µL NativePAGE™ 5% G-250 additive to a final concentration of 10 µL. 1× NativePAGE™ anode, light cathode, and dark cathode buffers were prepared fresh. Gel tank apparatus was prepared by loading gels and filling inner chamber with dark cathode buffer to below wells. Wells were flushed with dark cathode buffer by syringe. Samples were loaded into wells alongside 5 µL NativeMark™ Unstained Protein Standard (LC0725). Outer chamber was filled with anode buffer. Electrophoresis was run at 150 V (~ 8-10 mA) until dye-edge ~ 1/3 through gel (~ 35 min) at which point dark cathode buffer in inner chamber was exchanged for light cathode buffer. The electrical current was increased to 200 V (~2-4 mA) for ~ 1 h or until dye-edge was near the end of gel. The gel was subjected to semi-dry transfer as described in 2.4.3. Membrane was incubated in 8% acetic acid, rinsed and allowed to air-dry > 1 h to fix proteins to matrix. The membrane was re-activated with ethanol to visualize molecular weight markers which were marked with pen. The membrane was blocked and probed as described in 2.4.3.

2.4.3 Western blotting

2.4.3.1 Semi-dry protein transfer

Semi-dry transfer of proteins from SDS- and BN-PAGE gels to Immuno-Blot 0.2 µm PVDF (polyvinylidene difluoride) membrane (Bio-Rad: 1620177) was performed using Bio-Rad Trans-Blot® Turbo™ Transfer System. The transfer was performed with the pre-programmed setting for 1.5 mm gel (10 min, 1.3 A for one mini gel or 2.5 A for ≥ two mini gels). Membranes were immediately continued with antibody labelling.

2.4.3.2 Antibody labelling

Following transfer, membrane was blocked with 5% (w/v) milk powder in TBS-T (50 mM Tris-HCl pH 8.0, 150 mM NaCl, 0.1% Tween®-20) for 30-60 min rotating at 50-60 RPM. Probing with conjugated antibodies in 5% milk TBS-T was carried out with dilutions described in Table 2.7 overnight at 4 °C or 1 h at room temperature (RT). The membranes were washed three times for 10 min with TBS-T at RT rotating at 50-60 RPM. The membrane was washed three times for 5 min in TBS at RT rotating at 50-60 RPM. Probing with anti-EDS1 primary antibody was performed in 3% milk TBS-T overnight at 4 °C. The membranes were washed three times for 10 min with TBS-T at RT rotating at 50-60 RPM. Secondary anti-rabbit-horseradish-peroxidase (α-Rb-HRP) in 3% milk TBS-T was probed at RT for 1 h rotating at 50-60 RPM. Membranes were washed three times for 10 min with TBS-T at RT rotating at 50-60 RPM. The membranes were washed three times for 5 min in TBS at RT rotating at 50-60 RPM. The membranes were incubated with SuperSignal™ West Pico PLUS (34580) or West Femto (34095) Chemiluminescent Substrate and imaged with ImageQuant™ LAS 4000 (GE Healthcare) enhanced chemiluminescence system.

Table 2.7 Antibodies and working concentrations

Antibody	Stock keeping unit	Working concentrations
α-GFP-HRP	sc-9996 HRP (Santa Cruz)	0.02 µg/mL (1:10,000)
α-c-Myc-HRP	11814150001	0.2 µg/mL (1:5000)
α-FLAG®-HRP	A-8592	0.03 µg/mL (1:30,000)
α-V5-HRP	AS09 481-HRP (Agrisera)	0.07-0.15 µg/mL (1:75,000)
α-HA-HRP	H6533	1-2.2 µg/mL (1:5000)
α-EDS1	AS13 2751 (Agrisera)	0.3 µg/mL (1:3000)
α-Rb-HRP	A0545	0.4-1.1 µg/mL (1:10,000)

HRP = Horseradish peroxidase for use with chemiluminescence substrates

2.5 Plant growth conditions

2.5.1 Growth of Arabidopsis plants

Arabidopsis plants used for pathogen assays were grown with an 8 h photoperiod in a controlled environment room (CER) at 20-22 °C with 70% relative humidity. Arabidopsis plants used for seed collection were grown at similar conditions with a 16 h photoperiod in a CER.

2.5.2 Growth of *N. benthamiana* plants

N. benthamiana plants used for transient infiltrations and cell death assays were grown with a 16 h photoperiod in a controlled environment room (CER) at a 20-22 °C with 70% relative humidity.

2.6 Arabidopsis Pf0-1 infiltrations

2.6.1 Pf0-1 EtHAn system

The Effector-to-Host Analyzer (EtHAn) system was developed in a non-pathogenic strain of Pf0-1 that has been engineered with the type III secretion system to deliver encoded effectors (Thomas et al., 2009).

2.6.2 Preparation of Pf0-1

Glycerol stocks of Pf0-1 strains carrying effector expression-vectors were struck out on KB agar plates containing appropriate antibiotic selections (detailed in Table 2.8) and incubated ~ 24 h at 28 °C. Cells were collected from plates and resuspended in infiltration buffer ($MgCl_2$-MES pH 5.6). OD_{600} of resuspended cells at 1 in 100 dilution was measured by spectrophotometer. Resuspended cells were diluted to OD_{600} = 0.3 for infiltration into leaves.

Table 2.8 Pf0-1 antibiotic selections

Pf0-1 strain	Selection
Empty vector	Chl, Kan
AvrRps4	Chl, Gen
$AvrRps4^{KRVY}$	Chl, Gen
PopP2	Chl, Gen
$PopP2^{C321A}$	Chl, Gen

Chl = Chloramphenicol, Kan = Kanamycin, Gen = Gentamicin

2.6.3 Pf0-1 infiltration of Arabidopsis leaves for protein purification

Rosette leaves of ~ 5 week-old Arabidopsis leaves were infiltrated with Pf0-1 carrying varying expression vectors. Leaves for protein assays were harvested and flash-frozen in liquid nitrogen. Frozen tissue was stored at – 80 °C for future use.

2.6.4 Pf0-1 infiltration of Arabidopsis leaves for cell death assays

Infiltrations were described as in 2.6.3. Leaves were visualized for tissue collapse representative of a hypersensitive response 24 h post-effector delivery by Pf0-1 infiltration. Pictures were taken, and leaves were discarded as appropriate.

2.7 *N. benthamiana* transient assays

2.7.1 Expression constructs

Expression constructs used in transient assays are described in Table 2.9. Cross-references for thesis figures are indicated. Identifications (ID) correspond to JJ lab construct ID except for those with "SUH" which correspond to Sung Un Huh's *Agro* stock ID. I cloned "JFJJ" constructs by Golden Gate assembly (described further 2.3.6). Constructs were inherited either as *Agro*-stock or were transformed into *Agro* for storage at − 80 °C (described further 2.2.2.5, 2.2.2.6). "At" promoters are Golden Gate-compatible constitutive promoters that have been identified and characterized by TSL members. They are used to drive expression of RRS1-R and RPS4, as native promoter expression does not facilitate detection. pAt2 is the promoter and 5' untranslated region (UTR) region of *SSR16* (*SMALL SUBUNIT RIBOSOMAL PROTEIN 16*; At4g34620) while pAt3 is the promoter and 5' UTR region of *CYSC1* (*CYSTEINE SYNTHASE C1*; At3g61440). The cauliflower mosaic virus promoter (CaMV 35S) is a constitutive over-expression promoter. XVE and pLexAop are components of a β-estradiol-inducible expression system (details can be found in 2.10.2).

Table 2.9 Expression construct designs and details

ID	Antibiotics	Promoter	Gene	Tag	Figure	OD_{600}
BCJJ375	RGK	35S	NRG1B	HF	4.2, 5.1, 5.25	0.5
SUH120	RGK	35S	SAG101	Myc	4.2, 4.20, 4.21, 5.8, 5.25	0.5
SUH186	RGC	35S	EDS1	V5	4.2, 4.20, 5.1, 5.4, 5.5, 5.6, 5.7, 5.9, 5.25	0.5
CS8C1	RK	35S	HopQ1	-	4.2, 4.20, 5.25	0.5
BCJJ310	RGK	35S	NRG1B	GFP	4.19, 4.20	0.5
JFJJ19	RGC	35S	NRG1B	Myc	4.19, 4.21, 5.4, 5.5, 5.6, 5.7, 5.9	0.5
JFJJ14	RGC	35S	GUS	Myc	4.19, 5.4, 5.5, 5.6,	0.1
SUH22	RK	35S	GFP	-	4.19, 5.2	0.5
JFJJ55	RGK	35S	NRG1B	V5	4.21, 5.8	0.5
SUH53	RS	35S	EDS1	HA	4.21, 5.8	0.5
SUH121	RGK	35S	NRG1A	Myc	5.1, 5.2	0.5
SUH175	RGK	35S	GUS	V5	5.1, 5.4, 5.5, 5.6	0.2
SUH48	RK	35S	PAD4	HA	5.1, 5.4, 5.5, 5.6, 5.9	0.5
SUH50	RK	35S	GUS	HA	5.1	0.02
SUH46	RGK	35S	GUS	HF	5.1	0.05
SUH54	RK	35S	EDS1	GFP	5.2	0.5
SUH55	RK	35S	PAD4	GFP	5.2	0.5
BBJJ17	RGK	pAt3 pAt2 pAct2 pLexAop	RPS4 RRS1-R XVE AvrRps4	HA HF - GFP	5.4, 5.5, 5.6, 5.7, 5.8, 5.9	1
BBJJ18	RGK	pAt3 pAt2 pAct2 pLexAop	RPS4 RRS1-R XVE AvrRps4^{E187A}	HA HF - GFP	5.4, 5.7, 5.8, 5.9	1
JFJJ45	RGK	pPAD4 pEDS1 pLexAop pAct2	PAD4 EDS1 HopQ1 XVE	HA V5 Myc -	5.23, 5.25	0.05
JFJJ125	RGK	pNRG1B pSAG101	NRG1B SAG101	mEGFP mCherry	5.23, 5.24, 5.25	1

BC = Baptiste Castel, SUH = Sung Un Huh, BB = Billy Tasker-Brown, JF = Joanna Feehan; JJ = Jonathan Jones lab construct. CS8C1 = inherited from previous Kamoun Lab member Chih-Hang Wu. Antibiotics: R = Rif, G = Gen, K = Kan, C = Carb, S = Spectinomycin.

2.7.2 Preparation of *A. tumefaciens* for infiltration into *N. benthamiana* leaves

Glycerol stocks of *A. tumefaciens* strains carrying expression constructs were struck out on LB agar plates containing appropriate antibiotic selections (detailed in Table 2.9) and incubated 48-72 h at 28 °C. Cells were collected from plates and resuspended in infiltration buffer ($MgCl_2$-MES pH 5.6). OD_{600} of resuspended cells at 1 in 100 dilution was measured by spectrophotometer. Resuspended cells were further diluted in infiltration buffer based on experiment design, each at OD_{600} measurement ranging from 0.1-1 (detailed in Table 2.9). Also included at OD_{600} = 0.5 in each infiltrated was p19 RNA silencing suppressor expression construct (Kontra et al., 2016). Leaves were infiltrated as described below.

2.7.3 *Agro*-infiltration for cell death assays

A. tumefaciens strains were prepared as described in 2.7.2. *N. benthamiana* leaves were infiltrated with resuspended *A. tumefaciens* strains carrying expression vectors when 4-6 week development age. Assays for cell death were spot-infiltrated and covered with foil envelopes to shield from light (Schultink et al., 2017). Foil was removed 48-72 h after infiltration and leaves were noted for hypersensitive response. Pictures were taken while leaves and plants were discarded as appropriate.

2.7.4 *Agro*-infiltration for protein purification

A. tumefaciens strains were prepared as described in 2.7.2. *N. benthamiana* leaves were infiltrated with resuspended *A. tumefaciens* strains carrying expression vectors when 4-6 week development age. Entire leaf surface was infiltrated. Leaves were harvested by removing central vein and flash-freezing 48-72 h after infiltration. Tissue was stored at – 80 °C for future use.

2.8 Protein extraction methodology

2.8.1 Preparation of lysates by heating in SDS sample buffer

For expression testing, protein was extracted by SDS-boiling of leaf discs. Two leaf discs were “punched” with 1.5 mL Eppendorf lid and flash-frozen in liquid nitrogen. One 3 mm tungsten carbide bead (28002675) was added to each tube before tissue homogenization with Geno/Grinder® for 60 s at 1000 RPM. Tissue was heated to 65 °C for 10 min in 100 µL 4× SDS sample dye with 100 mM dithiothreitol (DTT). Sample was centrifuged 10 min at 15,000 x *g*. Supernatant was transferred to

new 1.5 mL Eppendorf, centrifuged again 1 min at 15,000 x *g*, and supernatant was diluted 1 in 3 before running SDS-PAGE.

2.8.2 Arabidopsis lysate preparations

Protein was purified from Arabidopsis leaves that were flash-frozen in liquid nitrogen. Tissue was ground by mortar and pestle in liquid nitrogen and membranes were solubilized in 100 mM HEPES (pH 7.5), 300 mM NaCl, 5 mM $MgCl_2$, 0.5% Nonidet™ P-40 Substitute (11754599001), 10% glycerol, 2% polyvinylpolypyrrolidone (PVPP), 1 tablet cOmplete™, EDTA-free protease inhibitor cocktail tablet, 10 mM DTT. Lysate was incubated inverting 10 min at 4 °C before centrifugation at 4 °C 30 min at 4000 x *g*. Sample was filtered through Miracloth (475855) and normalized with wash buffer [100 mM HEPES (pH 7.5), 300 mM NaCl, 5 mM $MgCl_2$, 0.5% Nonidet™ P-40 Substitute, 10% glycerol] by Bradford Protein Assay (Bio-Rad: 5000006). Input samples were combined with SDS sample buffer and 10 mM DTT and heated 65 °C for 5 min before storage at – 20 °C, if not used fresh.

2.8.3 *N. benthamiana* lysate preparations

Protein was purified from *N. benthamiana* leaves as described in 2.8.2.

2.9 Co-immunoprecipitation methodology

2.9.1 Co-immunoprecipitation with Arabidopsis lysates

Lysates were prepared as described in 2.8.2 from ~ 2.5 g Arabidopsis tissue. Approximately 5 mL of normalized lysates were combined with 125 µL Anti-FLAG® M2 Affinity Gel, previously equilibrated in wash buffer, and incubated inverting at 4 °C ~ 2 h. Samples were centrifuged at 800 x *g* for 5 min at 4 °C before removal of supernatant. Beads were washed with wash buffer inverting at 4 °C for 5 min. Sample was centrifuged at 800 x *g* for 5 min at 4 °C, and wash step was repeated twice more. After final wash and removal of supernatant, 100 µL wash buffer was added to beads with 12.5 µL 3×FLAG® peptide (5 mg/mL). Sample was incubated 2 h at 4 °C shaking 5 min 750 RPM every 20 min. Eluates were removed from beads and transferred to fresh 1.5 mL Eppendorf. Eluates were combined with SDS sample buffer and 10 mM DTT and heated 65 °C for 5 min before storage at – 20 °C, if not used fresh

2.9.2 Co-immunoprecipitation with *N. Benthamiana* lysates

Lysates were prepared as described in 2.8.3 from ~ 0.5 g *N. benthamiana* leaf tissue. Approximately 3 mL normalized lysates were combined with 10-30 µL antibody conjugate agarose beads and incubated inverting 4 °C for ~ 1.5 h. Lysates were centrifuged at 800 x *g* for 5 min at 4 °C to pellet beads before removal of supernatant. Beads were washed with wash buffer inverting at 4 °C for 5 min. Sample was centrifuged at 800 x *g* for 5 min at 4 °C, and wash step was repeated twice more. After final wash and removal of supernatant, 100 µL SDS sample buffer and 10 mM DTT was added to beads and heated at 65 °C for 5 min before storage at – 20 °C, if not used fresh.

2.10 Forward genetics screen methodology

2.10.1 The Super-ETI (SETI) Arabidopsis line

The Super-ETI (SETI) line (generation T1-8 T3) served as the parental line that was mutagenized in this forward genetics screen (Ngou et al., 2020b). This line was generated by Dr. Pingtao Ding. This line utilised the XVE cassette for β-estradiol-inducible AvrRps4-mNeon that induced a stunted growth phenotype. mNeon is an enhanced, monomeric variant of GFP (Shaner et al., 2013). Fluorescence in roots was visualized using the Leica DM5500 upright microscope with L5 filter cube. The AtuMas and AtuOcs terminators are from *A. tumefaciens;* Mas1 agropine synthesis reductase and octopine synthase, respectively. Details of XVE system can be found in 2.10.2. This line also utilised FAST-R selection and further details can be found in 2.10.3. Details of SETI T-DNA assembly can be found in Table 2.10.

Table 2.10 SETI T-DNA design details

Pr + 5' UTR	Gene	Tag	Term	Module
pAtOleosin	gAtOleosin	RFP	TerOleosin	FastRed
pAtCYSC1 (pAt3)	gRPS4	6×HA	Ter35S	RPS4:HA
pSSR16 (pAt2)	gRRS1-R	6×His:3×FLAG®	TerRRS1-R	RRS1-R:HF
pAtActin2	XVE	-	TerMas	XVE
pLexAop	AvrRps4^{WT}	mNeon	TerOcs	LexA:AvrRps4-mNeon

Pr = promoter. Term = terminator; pLexAop = LexA operator fused to 35S promoter

2.10.2 The XVE system for β-estradiol induction

The XVE inducible-expression system utilizes a LexA operator which suppresses expression in the absence of β-estradiol. When β-estradiol is supplied to the system, the chimeric trans-activator XVE moves into the nucleus to de-repress the expression (Zuo et al., 2000).

2.10.3 The FAST-R system for T-DNA selection in seed

The FAST-R (fluorescence-accumulating seed technology with OLE1-TagRFP) selecting cassette (Shimada et al., 2010) allows visualization of transgenic seeds by fluorescence. This utilises the promoter and 5' UTR region of the Oleosin (At4g25140) which is expressed in seed coat tissue. Fluorescence in seed was visualized using the Leica M165 fluorescent stereo microscope with DSR filter.

2.10.4 Ethyl methanesulfonate mutagenesis of SETI parental seed

Ethyl methanesulfonate (EMS) mutagenesis was carried out by Dr. Pingtao Ding and other lab members prior to my arrival in the lab. They mutagenized ~ 0.38 g (~ 5000 seeds / 0.1 g) seed which generated ~19,000 M0 seed. Seeds were exposed to ~243 mM EMS for 16 h. 400 pools of 16 M1 plants (6400 total) were bulked.

2.10.5 Screening for immune-signalling mutants in Arabidopsis

Mutation rate for the phenotype of interest was ~ 1 in 2000-5000 M2 plants. Approximately 50-80 M2 plants per pool were initially planned to be screened for a total of ~ 20,000. Therefore, they hoped to yield 4-20 mutants. Details on final counts and screening can be found in Chapter 3 of this thesis.

2.11 Large-scale protein purification methodology

2.11.1 Large-scale purifications of NRG1B-HF from *N. benthamiana*

Large-scale protein purifications after transient expression in *N. benthamiana* were used for structure investigations described in Chapter 4 of this thesis. Purifications started with *Agro*-infiltration of ~ 30 g (~ 45 mL lysate) *N. benthamiana* leaf tissue with strains carrying BCJJ375 binary vectors for expression of 35S:NRG1B-6×His-3×FLAG® (Table 2.9). Tissue was flash-frozen and stored at –80 °C. Tissue was ground by motor and pestle in liquid nitrogen. Membranes were solubilized in varying buffer conditions described in 2.11.1. Protein was

immunoprecipitated by anti-FLAG® M2 affinity gel unless otherwise specified. Protein was eluted with 3×FLAG® peptide for 30 min at 150 ng/µL followed by a subsequent overnight elution at 300 ng/µL, unless otherwise specified. Combed eluates were diluted 4× in the respective buffer for gel filtration chromatography. This solution was concentrated by ultracentrifugation with 50 kDa molecular-weight cut-off concentrators pre-incubated with water, unless otherwise specified. Protocol for preparation of concentrators can be found in 2.11.2. Unless otherwise specified, a 4 mL (UFC805024) Merck Amicon® Ultra concentrator brought the eluate solution to 500 µL. This was further concentrated to < 200 µL with a 0.5 mL Sartorious Vivaspin® 500 concentrator (VS0131). Concentrated eluates were subjected to gel filtration chromatography (described further in 2.12). Recovery of NRG1B-HF was evaluated by SDS-PAGE and western blotting. Purity of NRG1B-HF was evaluated by SDS-PAGE and coomassie-staining. Purified NRG1B-HF was subjected to negative stain EM performed by Jake Richardson within the John Innes Centre (JIC) Bioimaging Platform (described further in 2.14). Further details can be found in Chapter 4 of this thesis. A detailed copy of the working protocol is added as Appendix III.

2.11.2 Pre-incubation of centrifugal concentrators with water

The membranes of centrifugal concentrators were rinsed with water. Water was again added to membranes and concentrators were subjected to centrifugation according to manufacturer's instructions for 1 min. Water was added to just above membrane height and incubated at RT > 2 h, or overnight. Water was poured away, and device was rinsed with water ×3-4. Water was added above membranes and subjected to centrifugation according to manufacturer's instructions. Protein sample was either applied immediately, or water was added until protein sample was ready. Concentrators were centrifuged briefly to remove water from membranes just before protein sample was applied.

2.11.3 Buffer optimisations for large-scale purifications

Buffer optimisations were extensively performed for large scale protein purifications. Original protocols were based on a "GTEN" buffer which called for 100 mM Tris [2-Amino-2-(hydroxymethyl)propane-1,3-diol]-HCl (pH 7.5), 150 mM NaCl, 1 mM EDTA, 0.1% Tween-20®, and 10% glycerol. When used for cell lysis it included 2% PVPP, 10 mM DTT, and a tablet of cOmplete™, EDTA-free Protease Inhibitor Cocktail. GTEN comprised wash and elution buffers. Buffer was optimized, as described in chapter 4 of this thesis, to the final "GHMN" buffer calling for 100 mM HEPES [4-(2-hydroxyethyl)-1-piperazineethanesulfonic acid] (pH 7.5), 300 mM NaCl,

5 mM $MgCl_2$, 0.5% Nonidet™ P-40 Substitute, and 10% glycerol. When used for cell lysis it included 2% PVPP, 10 mM DTT and tablets of cOmplete™, EDTA-free Protease Inhibitor Cocktail. GHMN comprised wash and elution buffers. Buffers for purifications in chapter 4 were GHMN unless otherwise specified.

Optimisation beyond buffer recipes were also included. Attempts to decrease centrifugation of lysate at 50,000 x *g* from 90 to 60 min was attempted. Centrifugation for only 60 min resulted in loose cellular debris pellets that interfered with removal of supernatants. Therefore, centrifugation at 50,000 x *g* for 90 min was maintained in future purifications without issue.

Initially, 250 µL of anti-FLAG® M2 affinity gel was incubated for 1 h with lysates. This was changed to an initial 30 min incubation with 500 µL followed by a second incubation with a fresh 500 µL of anti-FLAG® M2 affinity gel. Additionally, one round of overnight elution with 3×FLAG® peptide at 150 ng/µL was changed to a 30 min elution with 150 ng/µL and an additional overnight elution with 250 ng/µL. Three rounds of elution was attempted once which included two 30 min elutions with 3×FLAG® peptide at 150 ng/µL and overnight elution with 250 ng/µL. Accomplishing three rounds of elution on each of two protein-bound beads meant six elutions which proved difficult to coordinate. Thus, two elution rounds for each set of protein-bound beads was the standard for future purifications.

2.11.4 Assay for pre-incubation of centrifugal concentrators

Below is the methodology used for the pre-incubation treatments described in Figure 4.14 to assay for improved protein recovery. The membranes of centrifugal concentrators were rinsed with water. Water was again added to membranes which were then subjected to centrifugation according to manufacturer's instructions for 1 min. Pre-treatment solution was added to just above membrane height and incubated at RT ~ 2 h. Pre-treatment was poured away, and device was rinsed with water ×3-4. Water was added above membranes and subjected to centrifugation according to manufacturer's instructions. NRG1B-HF eluates at ~ 4 mL were diluted up to ~ 19 mL with gel filtration buffer and "starting" was sampled. Diluted eluates were transferred to concentrators and pipette-mixed. Another sample was taken. Concentrators were subjected to centrifugation at 4 °C. The 0.5 mL concentrators were concentrated from 500 µL to 100 µL at 15,000 x *g*, 2 mL concentrators were concentrated from 2 mL to 200 µL at 4,000 x *g*, and 4 mL concentrators were concentrated from 4 mL to 400 µL at 4,000 x *g*. Flow-through was collected and 10%

was sampled. Flow-through was then recombined with retentate and pipette-mixed. Combined filtrate with retentate were sampled. The starting sample was compared to the combined filtrate and retentate samples for each concentrator by SDS-PAGE and immunoblotting.

2.12 Gel filtration chromatography

Gel filtration chromatography, or size-exclusion chromatography (SEC), was performed with ÄKTA™ pure modular chromatography system (GE Healthcare) for protein purification. SEC was run at 4 °C using a Superose Increase 10/300 GL (GE Healthcare) equilibrated in gel filtration (GF) buffer. GF buffer was composed of 10 mM HEPES pH 7.5, 150 mM NaCl, 5 mM $MgCl_2$, 5% glycerol, and 1 mM DTT unless otherwise specified. GF buffer was de-gassed with Ultrasonic Cleaner and filter-sterilized with 0.3 µm Ministart® filters under vacuum pressure. Protein samples concentrated to 100-200 µL were injected after equilibration. A volume of 45 mL gel filtration buffer was run over the column at a flow rate of 0.25 mL/min collecting 250 µL fractions, unless otherwise specified. An upper threshold pressure limit of 3.5 MPa was programmed. Experiments evaluating ATP/dATP-induced changes in SEC were performed with a Superdex 200 Increase 10/300 GL column (GE Healthcare) equilibrated in GF buffer.

2.13 Liquid chromatography-mass spectrometry

Samples for liquid chromatography-mass spectrometry were (LC-MS) resolved by SDS-PAGE with RunBlue™ 4-20% TEO-Tricine (BCG42012) and stained with InstantBlue® Coomassie Protein Stain (ab119211). Bands were excised from gel with sterile blade and stored at – 20 °C if not submitted fresh. LC-MS and data processing was carried out by Paul Derbyshire within the TSL Proteomics platform as previously described (Bender et al., 2017). Data was analysed as total spectrum counts in Scaffold Viewer (Proteome Software) and filtered for a protein threshold probability > 99%, peptide threshold probability > 95%, and a minimum of two peptides identified, unless otherwise specified.

2.14 Negative stain electron microscopy

Negative stain electron microscopy (EM) was carried out by Jake Richardson within the JIC Bioimaging platform. 3.5 µL of sample was placed on a carbon film 400 mesh copper grid (EM Resolutions, Sheffield, UK) which had been glow discharged for 20 seconds at 10 mA in an Ace 200 (Leica Microsystems (UK) Ltd, Milton Keynes, UK). After 60 seconds, the excess sample was wicked away using Whatman No. 1 filter paper and negatively-stained for 30 seconds using 2% (w/v) uranyl acetate in distilled water, excess wicked then allowed to air dry. Grids were imaged using a Talos F200C transmission electron microscope (Thermo Fisher Scientific, Eindhoven, The Netherlands) operated at 200 kV, equipped with a 4k OneView CMOS detector (Gatan UK, Abingdon, Oxfordshire, UK).

2.15 Confocal microscopy

A leaf disc was cut with a cork borer and loaded onto glass slides that contained a perimeter of vacuum grease. Water was pipetted onto leaf disc, and a coverslip was placed over the top. Water was added between slide and coverslip within vacuum grease-perimeter to maintain humidity. Confocal microscopy was performed with a Leica TCS SP5 utilizing ×63/1.20 water-immersion objective. Bright-field images were collected to visualize cell boundaries. The Argon ion 488 nm laser was used for excitation of GFP fluorophores. Emission was collected for 495-550 nm wavelengths with PMT detector. The Yellow DPSS 561 nm laser was used for excitation of mCherry fluorophores. Emission was collected for 570-690 nm wavelengths with PMT detector. Scan resolution was 1024 × 1024, and pixel average was set on 2 per frame. Zoom was 1-2.5×. Pinhole size was set to at Airy 1. All other settings were set to default as indicated in standard operating procedure. Images for GFP and RFP fluorophores were collected separately and overlayed in ImageJ when appropriate.

Chapter 3

A screen for novel ETI-signalling components utilizing an inducible-effector line of Arabidopsis

3 A screen for novel ETI signalling components utilizing an inducible-effector line of Arabidopsis

3.1 Introduction

Plants carry *R* genes which encode proteins that trigger immune activation upon perception of pathogen effectors to confer defence responses. While the downstream signalling events of cell-surface localized receptors are well described, the immediate targets of NLRs remain largely uncharacterized. Forward genetic screens in Arabidopsis using ethyl methanesulfonate (EMS) mutagenesis have been applied extensively to uncover immune-signalling components. However, attempts to uncover elements specific to ETI have shown limited success, seemingly due to genetic redundancy. Therefore, a forward genetics screen utilizing redundant copies of NLRs was employed in an effort to uncover novel ETI-signalling components.

Forward genetics screens are performed with a variety of mutagens. A common and straightforward method for Arabidopsis is EMS mutagenesis of seeds, which introduces randomly distributed mutations throughout the genome. EMS is an alkylating agent that chemically modifies nucleotides, creating mispairings and base changes, the majority of which are cytosine to thymine which results in guanine to adenine substitutions (Kim et al., 2006).

Core components of the Arabidopsis immune response have been determined with forward genetics screens after EMS mutagenesis. A screen for mutants defective in Systemic Acquired Resistance (SAR) uncovered *NPR1* (*NONEXPRESSOR OF PR GENES*) (Cao et al., 1994), and a subsequent screen for suppressors of *npr1* discovered the TNL, *SNC1* (*SUPPRESSOR OF NPR1-1, CONSTITUTIVE 1*). Glazebrook et al. (1996) looked for mutants with enhanced disease susceptibility (eds) to *P. syringae* pv. *maculicola* ES4326 and identified 12 immunity mutants. This included the re-discovery of *NPR1*, but uncovered the requirement for *PAD4* (Glazebrook et al., 1996). *EDS1* was found necessary for resistance conferred by several TNLs in another EMS screen for enhanced susceptibility to the oomycete *Peronospora parasitica* (now *Hyaloperonospora arabidopsidis*) (Parker et al., 1996). Utilizing various mutagens beyond EMS, the negative immunity regulator *EDR1* (*ENHANCED DISEASE RESISTANCE 1*) was identified by testing for reduced susceptibility to the fungus *Erysiphe cichoracearum* (Frye and Innes, 1998).

These initial screens all showed successful recovery of core ETI-signalling components—the mechanisms of which are not fully resolved. However, subsequent screens seem to continually re-identify many of these components. Likely, this results from redundancy in the Arabidopsis genome. Notably, *NPR1*, *PAD4*, and *EDR1* are all single gene copies. However, *EDS1* has two paralogs in Col-0 and was discovered only because the researchers performed their investigation in the single-copy backgrounds of Ws-2 and Ler backgrounds (Parker et al., 1996).

To avoid re-identification of known components, researchers have used innovative techniques in additional screens. To look for gain-of-function mutants in Arabidopsis, activation tagging was employed in a *PR-1 (PATHOGENESIS-RELATED GENE 1*)-driven luciferase-reporter background (Grant et al., 2003). Expression of *PR-1* is induced upon pathogen infection. This led to the identification of *ADR1*, which overcame the barrier of genetic redundancy as there are three paralogs in the Arabidopsis genome. Utilizing cDNA libraries, virus-induced gene silencing (VIGS) in *N. benthamiana* led to the identification of NRG1 (Peart et al., 2005). NRC1 was also identified by VIGS screening in *N. benthamiana* using an enriched cDNA library (Gabriëls et al., 2007). However, not all novel approaches have been successful; Serrano et al. (2010) utilised a chemical library of 6,800 natural compounds in an attempt to mitigate the challenges of genetic redundancy. They looked for chemical interference of AvrRpm1-induced cell death but did not uncover novel signalling components.

Researchers have also met barriers that seem to be due to high mutability of NLR genes. The lab of Xin Li looked to identify suppressors of *snc1* in the mos (modifiers of *snc1*) screen which uncovered 15 mutants with roles in transcriptional regulation, RNA processing, protein modifications, and nucleocytoplasmic trafficking (Johnson et al., 2012). In their muse (mutant, *snc1*-enhancing) screen, they gained knowledge of the mechanisms associated with NLR activation (Huang et al., 2013). This group has also employed reverse genetics to identify three additional NLRs that are redundantly required for *SNC1* function, *sidekick snc1* (*SIKIC1*), *SIKIC2*, *SIKIC3* (Dong et al., 2018). The Jones lab utilised a constitutive mutant of $RRS1^{SLH1}$ in forward genetic screens. However, the group found a strong bias towards mutations in *RPS4*. Notably, this discovery did confirm the requirement for *RPS4* in *RRS1*-mediated immune responses (Sohn et al., 2014).

Other groups have attempted to use inducible effectors in forward genetic screens. The Dangl group screened for signalling mutants in an *AvrRpm1*-inducible

Arabidopsis line. Of 110 mutants yielded, 95 were mutated in the cognate *RPM1* (*RESISTANCE TO PSEUDOMONAS SYRINGAE PV MACULICOLA 1*) gene, and the other candidates were known chaperone components, *RAR1* and *HSP90* (Tornero et al., 2002). The Innes group used a line of Arabidopsis with an inducible *AvrPphB*, this time with redundant copies of the cognate NLR, *RPS5 (RESISTANCE TO PSEUDOMONAS SYRINGAE 5*), and avoided recovering *rps5* mutants (Qi et al., 2014). They expected to find mutants downstream of RPS5 activation but instead recovered mutants of the guardee *PBS1* (*AVRPPHB SUSCEPTIBLE 1*). In both scenarios, the Dangl and Innes groups made lemonade out of lemons and generated detailed studies of RPM1 and PBS1, respectively.

Therefore, the Jones lab designed a screen that would circumvent these barriers to gene discovery. An Arabidopsis line with an inducible effector and redundant copies of cognate NLRs was generated and used in this screen, the so-called Super-ETI (SETI) line (Ngou et al., 2020b). This line carries RRS1-R-HF, RPS4-HA, and β-estradiol-inducible AvrRps4-mNeon on a single transgene (Figure 3.1A). The transgene also carries a FAST-R selection cassette that produces fluorescent seed, and the XVE cassette for β-estradiol-induction, both described in more detail in section 2.10 of this thesis. The RRS1-R allele on the T-DNA is endogenous to Ws-2, and as this line was generated in the Col-0 background with the RRS1-S allele, multiple AvrRps4-recognizing NLRs are present in the SETI line. Furthermore, bias towards mutagenesis in the guarded host target—as was observed for Qi et al. (2014)—was not expected as RRS1 encodes an integrated decoy domain. When SETI seeds are germinated on 50 μM β-estradiol, they exhibit a stunted growth phenotype as the AvrRps4-mNeon is recognized and triggers an immune response (Figure 3.1C). We hypothesized, that with additional NLR redundancy, and with the avirulence target site integrated into those NLRs, that this screen could reveal novel, core ETI-signalling genes.

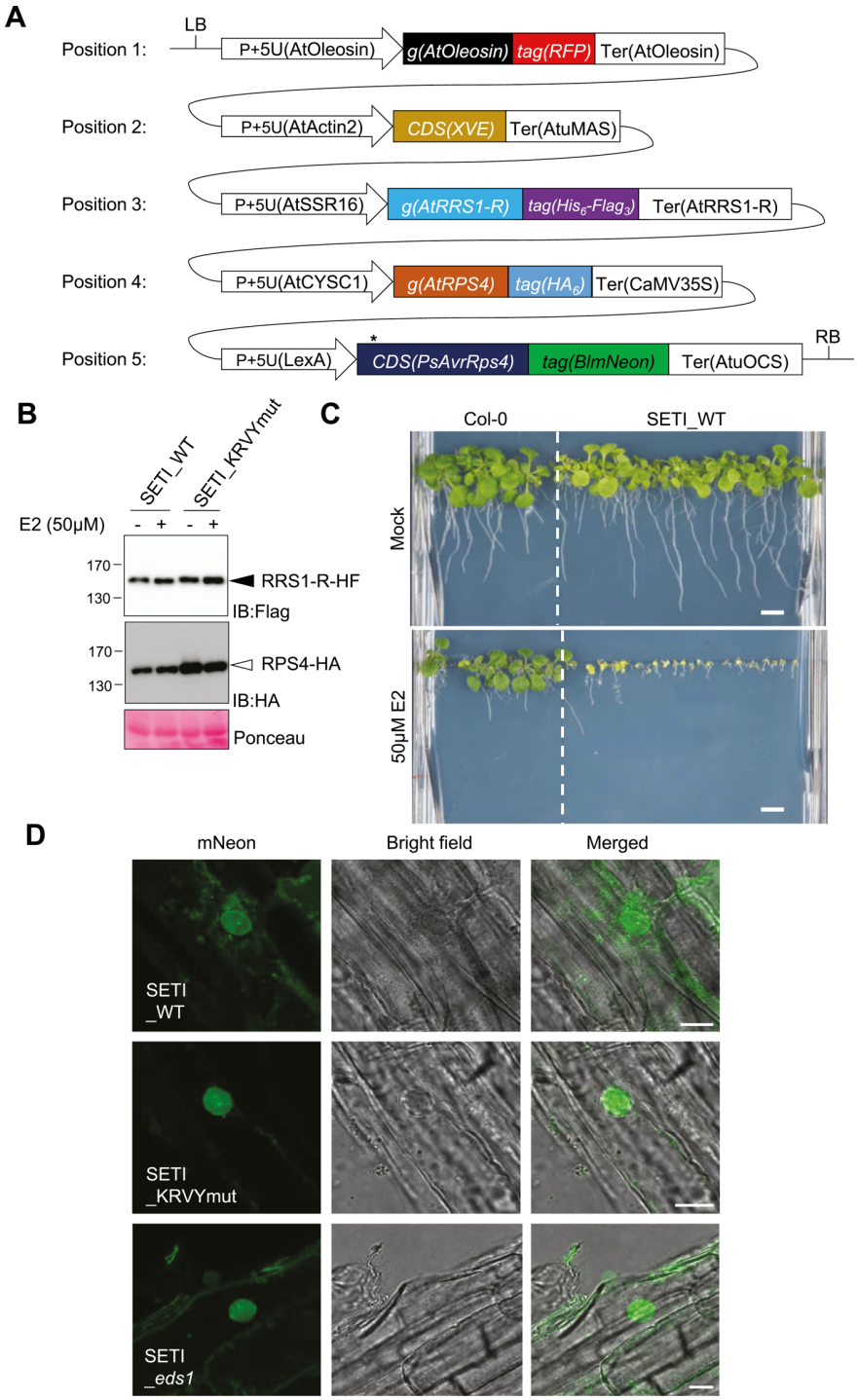

Figure 3.1 Super ETI (SETI) design and phenotypes. "(A) Illustrative layout of the Super-ETI (SETI) construct. There are five individual expression units … the FAST-R selection marker … chimeric trans-activator XVE … and the corresponding LexA-inducible system to express AvrRps4 or its mutant variants under the control of β-estradiol treatment … full-length RRS1-R and RPS4 proteins with epitope tags 6xHis-3xFlag and 6xHA, respectively. (B) Protein accumulation of RRS1-R-HF (IB:Flag, black arrowhead) and RPS4-HA (IB:HA, white arrowhead) of SETI lines expressing AvrRps4 (SETI_WT) or mutant AvrRps4 KRVY-AAAA (SETI_KRVYmut). Seedlings were grown in liquid culture and induced with 50 μM β-estradiol for 2 h at 7 days after germination (DAG). Ponceau staining of Rubisco large subunits was used as a loading control. (C) Seedling phenotype of the SETI Arabidopsis

transgenic line at 14 DAG in GM medium containing mock (0.1% DMSO) or 50 μM β-estradiol. Col-0 was sown as control for the effect of β-estradiol on seedling growth. Scale bar=0.5 cm. (D) Confocal images of SETI_WT, SETI_KRVYmut, SETI_*eds1* root cells expressing AvrRps4–mNeon, and AvrRps4KRVY-AAAA–mNeon induced by 50 μM β-estradiol for 24 h. The mNeon channel shows nucleocytoplasmic localization of AvrRps4–mNeon and AvrRps4KRVY-AAAA–mNeon. Bright field channel and a merged image of mNeon and the bright field channel are shown together. Scale bars=10 μm." Figure adapted with permission from Ngou et al. (2020.) *J Exp Bot*.

3.2 Chapter aims and objectives

This chapter aimed to identify novel components of ETI-signalling in Arabidopsis by forward genetics. We mutagenized and screened a transgenic line of Arabidopsis that carries redundant copies of the paired NLRs RRS1 and RPS4, and an inducible cognate effector. Increasing NLR redundancy served to avoid bias for recovery of NLR mutants and utilizing an inducible effector served to identify ETI-specific signalling components. We hypothesized that novel immune signalling components could be identified by employing these innovations from previous forward genetic screens.

However, the project was terminated during screening, due to identification of only false-positive candidate mutants. In this chapter, I describe the design of the screen, and isolation and discovery of false-positives candidates. Although the reason for a high false-positive recovery rate was not determined, it appears that transgene silencing could be the most likely cause. I discuss other possible explanations for recovery of false-positive candidates and what could be improved for future screens.

3.3 Screening mutagenized SETI seedlings for loss of AvrRps4 recognition

The SETI screen, initiated by Dr. Pingtao Ding before my arrival in the lab, consisted of EMS mutagenesis of approximately 19,000 SETI seeds (M0 seed) (Figure 3.2). These seed were then pooled into 400 groups of 16 M1 seedlings and self-fertilized before screening of the M2 population. While initially the goal was fewer plants to screen, I aimed to screen approximately 125 seedlings per pool which would have equated to 50,000 M2 seedlings (Table 3.1). These numbers correlate with best recommendations for saturation and recovery of mutants (Jander et al., 2003, Kim et al., 2006). More details can be found in section 2.10 of thesis.

Table 3.1 SETI screening counts

	Screening Stage	Possible	Total	Coverage (%)
Pools	Screened	400	310	77.5
	≥ 1 putant	310	162	52.3
	0 putants		148	47.7
M2 Seedlings	Screened for E2 insensitivity	50,000	31,000	62.0
	Insensitive to E2	31,000	2,082	67.2
	E2-insensitive, mNeon (+)	2082	322	15.5
	E2-insensitive, mNeon (-)		1760	84.5
Putants	Re-screened for E2-insensitivity	162	124	76.5
	Retained E2 insensitivity	124	57	46.0
	Screened for AvrRps4 recognition	57	10	17.5
	Loss of AvrRps4 recognition	10 (2)	0	0.0

E2: β-estradiol; (2) indicates two putants (putative mutant) not screened for retention of β-estradiol-insensitivity, but still evaluated for AvrRps4 recognition by Pf0-1 delivery.

The M1 seed of these pools were collected and germinated on 50 μM β-estradiol, and the M2 seedlings were screened for growth inhibition (Figure 3.2). The absence of stunted growth in the presence of β-estradiol indicated the possible mutagenesis of an ETI-signalling component. Seedlings that showed insensitivity to β-estradiol were pricked from the agar plates, and the root was visualized for mNeon signal in nuclei to confirm expression of AvrRps4-mNeon (Figure 3.1D). We specifically screened for roots that showed localization to nuclei, as nuclear localization of AvrRps4 is required for immune activation (Heidrich et al., 2011). Those that showed both insensitivity to β-estradiol and mNeon expression in the roots were transplanted to soil, and M2 seed were harvested. One hundred eleven pools (count 59 to 169 in Appendix IV) were screened before my arrival in the lab by Bruno Ngou and Dr. Pingtao Ding. I continued screening; a total of 310 pools were screened, which yielded 322 putative mutant (putant) candidates from 162 different pools (Table 3.1, Appendix IV). Pools from count 275-287 were excluded from the final count due to poor seed quality after over-sterilization. As each bulked pool theoretically contains a single putant, one representative from a pool was prioritized for further screening in the next generation. The M2 seed were germinated on β-estradiol to screen for retention of β-estradiol-insensitivity in the M3 seedlings. Those that retained insensitivity were prioritized for pathogen challenge assays to independently confirm loss of AvrRps4 recognition (Figure 3.2).

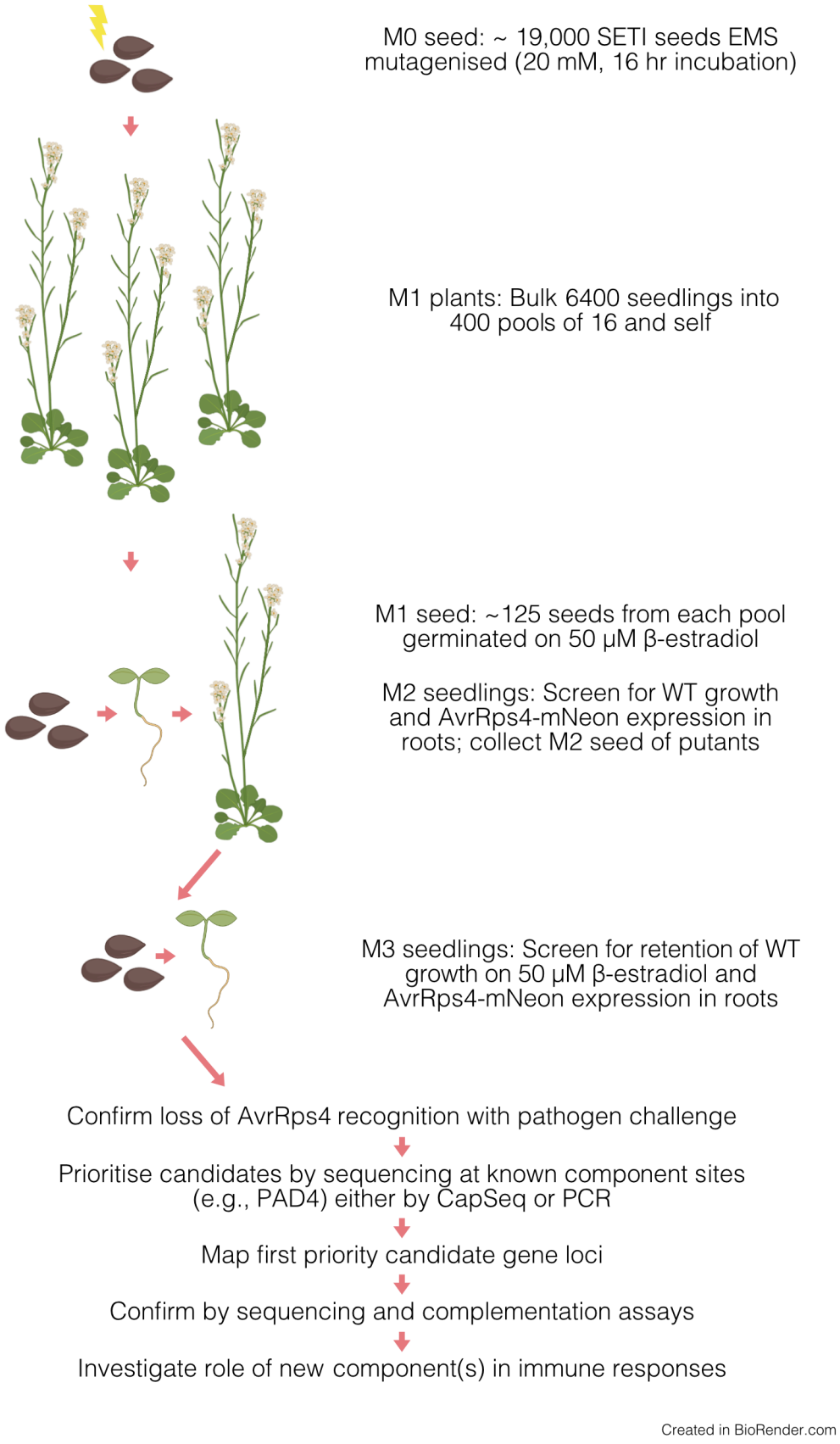

Figure 3.2 SETI screen pipeline.

3.4 Candidate putants maintain AvrRps4 recognition

A representative putant from 124 of the 162 pools with at least one putant was tested in the next generation for sensitivity to β-estradiol. From those, 57 putants retained WT growth phenotypes (Figure 3.3A, Appendix V). Unexpectedly, sensitivity to β-estradiol was variable between sibling seedlings. Therefore, eight sibling seedlings from 13 β-estradiol-insensitive putants were screened for mNeon signal in roots. Only two of those 13 putants showed any AvrRps4-mNeon localization to nuclei: 156-1 and 366-1, and only in 2 and 4 roots respectively of the 8 sibling seedlings examined (Figure 3.3B). These data provoked alarm as consistent growth between putant siblings on β-estradiol, and conservation of AvrRps4-mNeon signal localized to root cell nuclei in the next generation, were expected. These were the first indications of false-positive recovery.

To evaluate whether these putants were indeed false-positives, pathogen-challenge assays were employed. The most rigorous test for mutants defective in ETI signalling is loss of AvrRps4 recognition by pathogen delivery. Therefore, Pf0-1 EtHAn (hereafter Pf0-1) (details in section 2.6.1) strains carrying AvrRps4 were infiltrated into rosette leaves of 5-6-week-old putant plants, and screened for HR 24 h post-effector delivery (hpd). Seven putants of the 57 that retained insensitivity to β-estradiol were infiltrated, and all showed an HR phenotype, indicating no defects in ETI signalling genes (Figure 3.3B). Putants were also evaluated for PopP2 recognition utilizing the Pf0-1 delivery system. Interestingly, there was only a partial recognition of PopP2 in seven of the eight putants tested, and one putant with no PopP2 recognition. This also provoked alarm as maintenance of AvrRps4 recognition but loss of PopP2 recognition indicates mutagenesis or silencing of the SETI transgene. PopP2 is only recognized by the RRS1-R allele carried on the transgene, and not by the endogenous alleles of RRS1-S and RRS1B in the Col-0 background. Furthermore, variable recognition phenotypes between leaves of siblings was observed, potentially due to silencing or perhaps variation in genetic backgrounds. These data indicated that false-positive candidates were being recovered as putants, potentially due to silencing of the SETI transgene.

Putant 156-1 maintained a strong HR to AvrRps4 in all eight leaves challenged, indicating no mutation of ETI signalling genes. Additionally, only partial PopP2 recognition was observed (Figure 3.3B). As mentioned, the reduction/loss of PopP2 recognition may indicate mutagenesis or silencing of the SETI transgene. Silencing is further supported by the uniform insensitivity to β-estradiol (Figure 3.3A) and the lack

of AvrRps4-mNeon localization to nuclei in 6 of 8 sibling seedlings (Figure 3.3B). However, the presence of AvrRps4-mNeon localization to nuclei in two of the eight seedlings does not support transgene silencing. These data indicate that something other than transgene silencing could be the reason for maintenance of AvrRps4 recognition in putant 156-1.

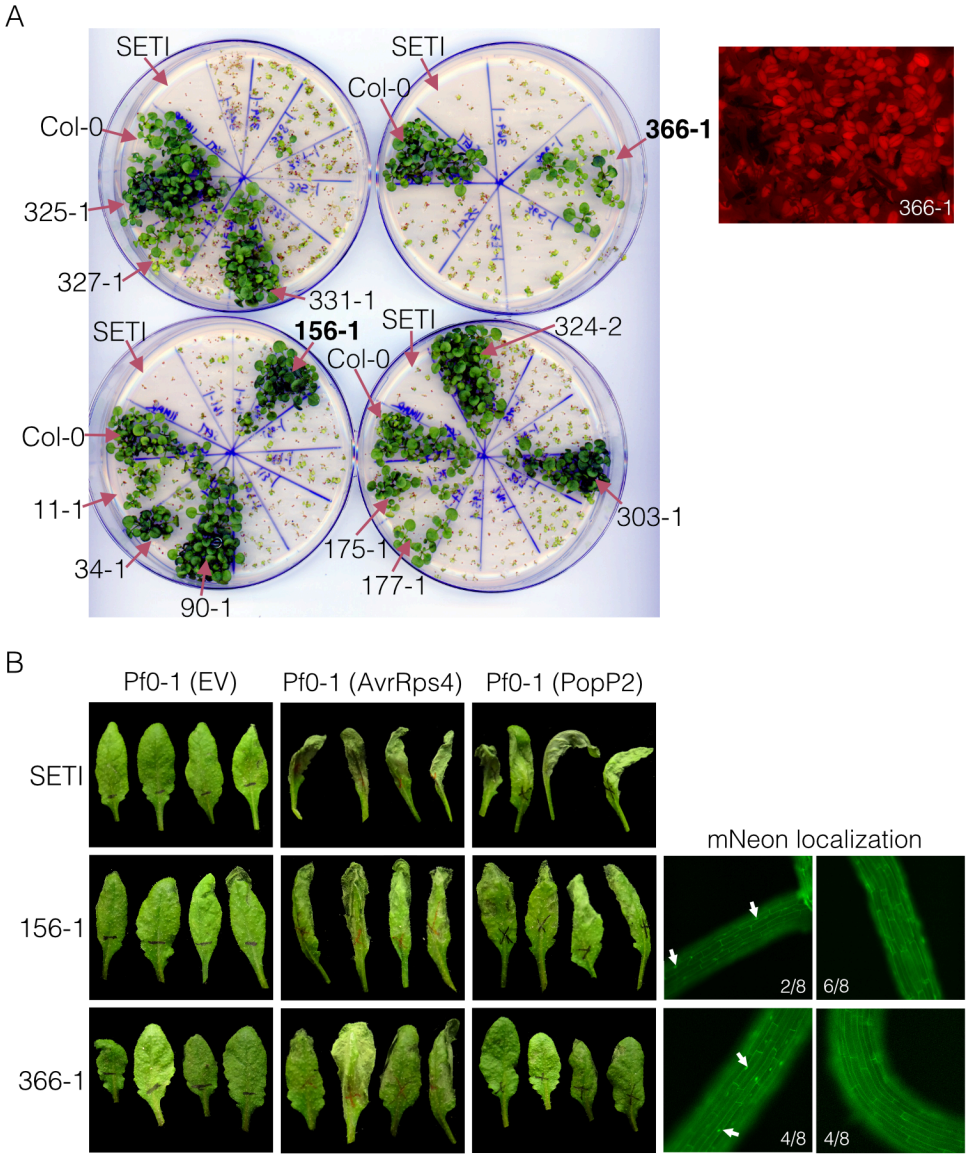

Figure 3.3 Assays for retention of loss of AvrRps4 recognition in next generation. (A) Insensitivity to β-estradiol in M3 generation of putants. M3 seed of 35 putant candidates were plated on GM + 50 μM β-estradiol and evaluated 14 days post-germination for retention of WT growth. Thirteen candidates retained β-estradiol insensitivity. See Appendix V and Appendix IX for other putants re-screened. Fluorescence signal in M2 seed of 366-1 in top right corner. RFP emission was collected with DSR filter. (B) HR assays in M3 generation of putants. Pf0-1 delivery in rosette leaves of 5-6 week old plants shows maintenance of AvrRps4 recognition in 156-1 and 366-1, and partial loss of PopP2 recognition in M3 generation, 24 hpd. mNeon signal in roots of seedlings from plate in "A". GFP emission was collected with L5 filter cube. AvrRps4-mNeon

localization to nuclei is indicated with white arrows. Only 2 out of 8 seedlings had AvrRps4-mNeon localizing to nuclei from 156-1 M3 seed and only 4 out of 8 seedlings for 366-1.

Putant 366-1 showed variable recognition of AvrRps4 or PopP2 between sibling plants. Particularly, a stronger AvrRps4 response was observed over PopP2 response (Figure 3.3B). Variability between sibling seedlings was also observed for the seed germinated on β-estradiol (Figure 3.3A). Potentially these data could indicate inactivation of a component that functions weakly in immune signalling. However, as the T-DNA also carries the FAST-R selection cassette, seed was visualized for fluorescence in the DsRed channel. A variable fluorescence signal between seeds was observed (Figure 3.3A), indicating either silencing of the transgene or heterozygosity of the transgene in the parental background. These data reflect that false-positives had been identified during the initial screening phase, and that likely most of the remaining untested putants were also false-positive candidates.

3.5 Variable seed fluorescence phenotypes indicate transgene silencing

To investigate the possibility that silencing during M2 seedling screening led to recovery of false-positive putant candidates, screening for red fluorescence in M2 seed was deemed the most high-throughput assay. As mentioned previously, the SETI transgene carries a FAST-R selection cassette which produces fluorescent seed. Western blotting to evaluate expression of the tagged variants of RRS1 and RPS4, or RT-PCR assays to evaluate transcripts of RRS1 and RPS4 were other potential and more direct options. However, with 162+ putants to consider for silencing, evaluating by fluorescence in seeds was adopted on the basis of time and effort efficiency. Therefore, the M2 seed for each putant was evaluated for fluorescence, and signal was characterized as either “uniform”, “variable”, or “none” (Figure 3.4A, Appendix **VII**). Only 19% of the 313 M2 putant seed screened were uniform in their fluorescence signal, while approximately 65% had variable signal, and the remaining 17% had no signal (Figure 3.4A). Furthermore, even those deemed “uniform” showed slight variability. Moreover, the parental seed showed variable fluorescence signal (data not shown). As the M0 seed was generated from a single transgenic seed, this variability was cause for concern. These data indicate that potentially there were multiple loci in the parental seed, or that transgene silencing occurred during bulking and harvesting of the parental line.

Additionally, I inherited M2 seed from several putants that were identified by previous lab members. As these seed no longer germinated on β-estradiol (likely due to age), they were germinated and grown on soil and fresh seed was harvested in the next generation (M3 seed). The fluorescence signal was evaluated in the M2 and M3 seed to evaluate maintenance generation-to-generation. Notably, a change in signal was observed in 50% of the 16 putants examined (Figure 3.4B). These data reflect that silencing of the transgene produced false-positive candidates in this screen.

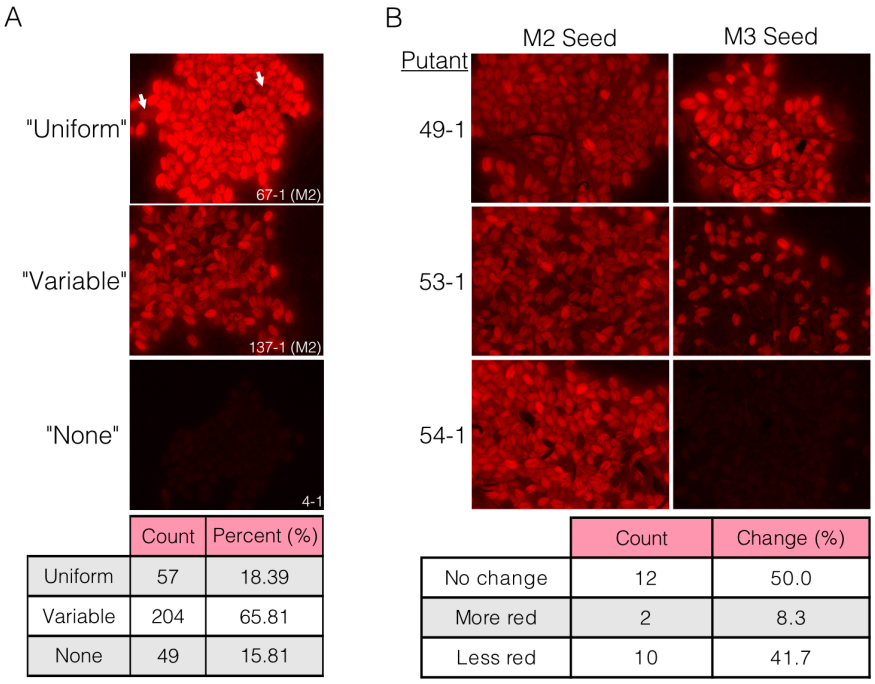

	Count	Percent (%)
Uniform	57	18.39
Variable	204	65.81
None	49	15.81

	Count	Change (%)
No change	12	50.0
More red	2	8.3
Less red	10	41.7

Figure 3.4 FAST-R signal in putant seed. (A) Examples of variable FAST-R signals in 310 putant seed evaluated. Fluorescence signal in seed was “uniform”, “variable”, or “none”. RFP emission was collected with DSR filter. White arrows indicate variable fluorescence in “uniform” example. (B) Screening the M2 and M3 generations of putant seed shows changes in FAST-R signal generation to generation. A total of 24 putants were analysed.

3.6 A high rate of false-positives results in early termination of screen

The remaining most promising candidates were prioritized for pathogen-challenge assays—the best indicator of mutants defective for ETI—to determine whether the screen should be abandoned due to the high false-positive recovery rate. As a correlation was observed for variable fluorescence in seed and variable growth on β-estradiol (Figure 3.3A), putant M2 seed with “uniform” fluorescence signal were prioritized as they were least likely to be false-positive candidates.

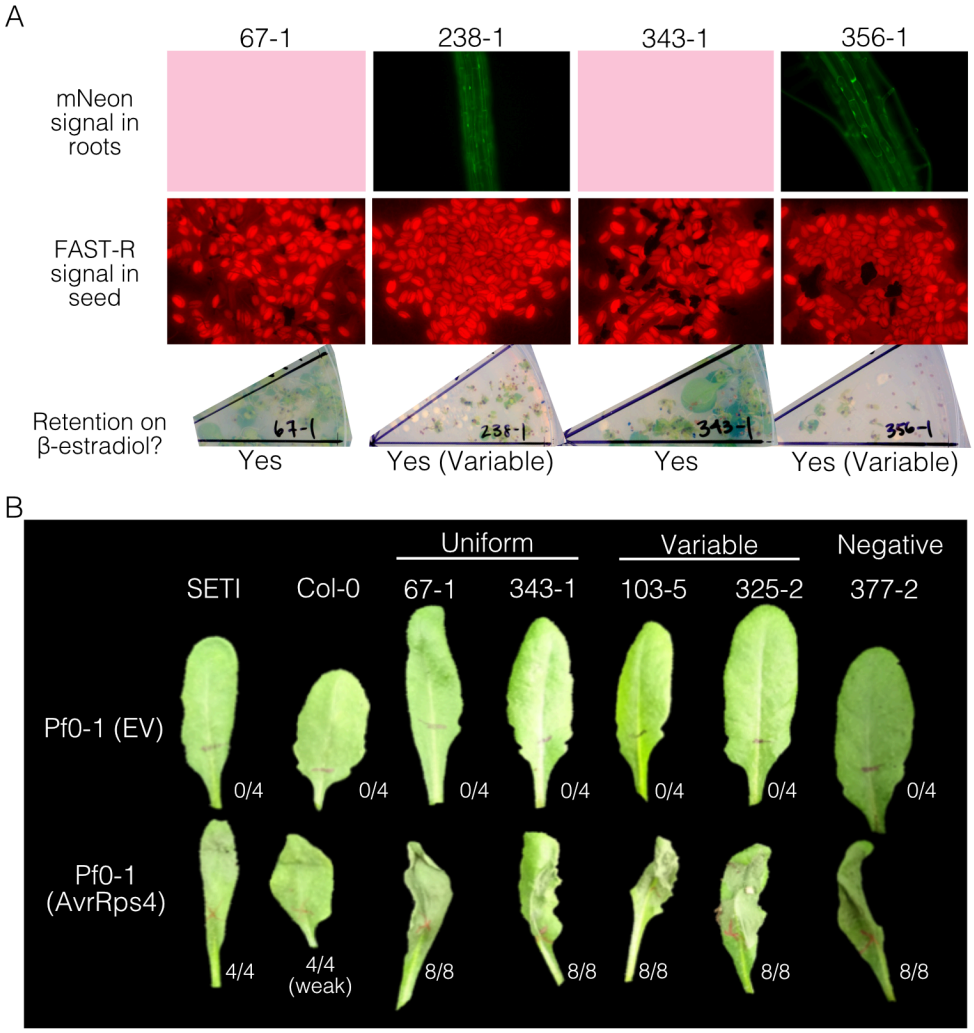

Figure 3.5 Selecting the most promising putants to test for AvrRps4 recognition. (A) Phenotypes of most promising mutants to test. AvrRps4-mNeon signal was localized to the nuclei in M2 seedling roots during screening. GFP emission was collected with L5 filter cube. Fluorescence (FAST-R) signal in M2 seed (M3 for 67-1) of those putants that were screened and bulked. RFP emission was collected with DSR filter. Retention on β-estradiol was evaluated for M3 seedlings (M4 for 67-1). (B) HR assays in M3 (M4 for 67-1) generation of putants. Pf0-1 delivery in rosette leaves of 5-6 week-old plants shows maintenance of AvrRps4 recognition in 67-1 and 343-1 and no cell death with empty vector negative control. HR was evaluated 24 hpd. Numbers indicate technical replicates. Replicate data can be found in Appendix VIII.

Fifty-seven putants showed “uniform” fluorescence signal in seed (Figure 3.4A), of which thirteen had already been evaluated for retention of growth on β-estradiol (Appendix IX). Four of those thirteen putants retained some β-estradiol insensitivity in the next generation: 67-1, 238-1, 343-1, 356-1. Of these, 67-1 and 343-1 showed the most uniform growth on β-estradiol, while 238-1 and 356-1 were highly variable (Figure 3.5A). Furthermore, the fluorescence signal in the seed of 67-1 did not change from the M2 and M3 generation, suggesting stability of the transgene. These were

considered the most promising putant candidates. However, Pf0-1-mediated delivery of AvrRps4 still showed a strong HR in putants 67-1 and 343-1 (Figure 3.5B).

A few paradoxes remain in the data that are not explained by transgene silencing. The sibling seedlings of putants 238-1 and 356-1 show variable sensitivities to β-estradiol, but the fluorescent signal in their seed is more uniform (Figure 3.5A). In another example, M2 seed with uniform fluorescence did not correlate with strong mNeon signal in M2 seedlings (Appendix VII). These data indicate that possibly fluorescence in seed is not indicative of transgene silencing. To directly test whether the fluorescence signal in seed correlates with phenotypes in sibling plants, two "variable" representatives (103-5 and 325-2) and one putant with no signal (377-2) were included in the pathogen challenge assays. Yet, Pf0-1 delivery of AvrRps4 showed a strong HR all representatives tested (Figure 3.5B, Appendix VI). These data indicate that there is no correlation between the fluorescence signal in seeds and recognition of AvrRps4.

Taken together, these data indicated that only false-positive putants were being recovered in this screen. And as the cause of false-positives was not clear, it did not seem likely that mutants defective in ETI-signalling were going to be uncovered in this screen. Therefore, this project was terminated, and other goals were developed to investigate ETI signalling mechanisms.

In summary, 310 of 400 pools were screened and 322 putants were identified from 162 different pools (Table 3.1, Appendix IV). A representative from 124 of those 162 pools was evaluated for retention of β-estradiol-insensitivity in the next generation. Fifty-seven of those 124 retained their insensitivity. Ten of those 57 were tested for AvrRps4 recognition by pathogen challenge; however, 10/10 tested exhibited HR phenotypes, indicating no disruption to ETI signalling pathways. Furthermore, AvrRps4 recognition was shown in representatives from two of the remaining 38 pools that were not evaluated for β-estradiol sensitivity (Table 3.2, Appendix IX). There were 198 putants, but only 36 pools, left to test for retention of insensitivity to β-estradiol. Additionally, there were 47 β-estradiol-insensitive putants left to evaluate for loss of AvrRps4 recognition in pathogen-challenge assays. However, at the coverage rate I have applied to each step of the screen, it is unlikely that any of these putants are true immune signalling mutants.

Table 3.2 Summary of Putant Phenotypes

Putant	Retains insensitivity to β-estradiol?	Character of β-estradiol-insensitivity	mNeon signal in sibling roots	HR? Pf0-1 (AvrRps4)	HR? Pf0-1 (PopP2)	Character of seed fluorescence
11-1	Yes	Variable	0/8	Full	Partial	Variable
34-1	Yes	Variable	0/8	Partial	Partial	Few
67-1	Yes*	Variable*	-	Full*	-	Uniform†
90-1	Yes	Uniform	0/8	Full	Partial	None
103-5	-	-	-	Partial	-	Variable
156-1	Yes	Uniform	2/8	Full	Partial	Variable
175-1	Yes	Variable	0/8	Partial	Partial	Variable
177-1	Yes	Variable	0/8	-	-	Variable
303-1	Yes	Uniform	0/8	-	-	Variable
324-2	Yes	Uniform	0/8	-	-	Few
325-1	Yes	Uniform	0/8	-	-	None
325-2	-	-	-	Full	-	Variable
327-1	Yes	Variable	2/8	-	-	Variable
331-1	Yes	Uniform	0/8	Full	Partial	Variable
343-1	Yes	Variable	-	Partial	-	Uniform
360-1B	Yes	-	0/8	Partial	No	None
366-1	Yes	Variable	4/8	Partial	Partial	Variable
377-2	-	-	-	Full	-	None
	M3 generation					M2 generation

**M4 Generation; †M3 generation*

3.7 Discussion

A forward genetics screen was attempted in an effort to identify novel ETI signalling components utilizing a transgenic line of Arabidopsis that carries an inducible effector with redundant copies of the cognate NLR. However, the screen recovered only false-positive candidates. It is possible that mutations in the transgene, or issues with heterozygosity in the parental line, caused the high false-positive rate. I would propose that the use of excessive, prolonged exposure to β-estradiol induced transgene silencing which led to recovery of false-positive putants. Yet, this has not been unambiguously shown. As a result, I was unable to isolate mutants defective in ETI signalling, and thus unable to identify novel signalling components.

It is expected to find false-positives during chemical screens due to mutagenesis of the gene(s) undergoing screening. However, it is unlikely that the high false-positive recovery rate in this screen is due to mutagenesis in the AvrRps4-recognizing RRS1/RPS4 NLRs. The Col-0 background for SETI carries the endogenous paralogs, *RRS1-S*/*RPS4A* and *RRS1B*/*RPS4B*, which are non-functional if paired with the opposite paralog (Saucet et al., 2015). However, the *RRS1-R*/*RPS4A* alleles on the SETI transgene should be functional with the endogenous “A” paralogs. This design allows for two additional “back-up” RRS1/RPS4 pairs if mutagenesis occurs in any of the six copies. Additionally, if either the endogenous RPS4A or T-DNA RPS4A is mutagenized, the other may likely compensate, maintaining three functional pairs mediating recognition of AvrRps4-mNeon. As recovery of a mutation in a given gene usually requires screening ~ 5000 M2 plants (Greene et al., 2003), it is unlikely that all six copies of RRS1 and RPS4 could be destabilized in the same mutant. Notably, Qi et al. (2014) utilised an additional copy of *RPS5* during their screen of 200,000 M2 seedlings and did not recover any *rps5* mutants. Therefore, I would exclude the possibility of *rrs1-r rrs1-s rrs1b rps4a rps4a rps4b* sextuple mutants to be the cause of the high false-positive rate in this screen.

Mutations introduced into *AvrRps4*-mNeon are also not likely to explain the high false-positive rate. As mNeon signal in root nuclei was also screened, putants with nonsense mutations in *AvrRps4* would have been excluded. It is possible that many putants were the result of missense mutations in *AvrRps4* which produced loss-of-function mutants. Indeed, Qi et al. (2014) found that seven of their 30 candidates were mutated in the induced effector that affected expression or function (Qi et al., 2014).

However, this wouldn't explain the variable fluorescence signal observed in the putant seed, as well as the variability of the AvrRps4-mNeon signal in the roots of the next generation. Nevertheless, it could be revealing to sequence the *AvrRps4*-mNeon of putant candidates to look for mutations. Perhaps encoding another layer of *AvrRps4* redundancy could be recommended in future screens.

It is also possible that some of the variability in seed fluorescence is due to mutagenesis of the FAST-R cassette. However, this would not interfere with AvrRps4 recognition. It is also possible that insensitivity to β-estradiol is due to mutations in the XVE—the regulatory cassette that represses AvrRps4-mNeon expression in the absence of β-estradiol. Mutation in the XVE could conceivably render the AvrRps4-mNeon either un-inducible or constitutively expressed. Un-induced mutants would not be selected during screening as AvrRps4-mNeon would be undetectable. Likewise, constitutive expression of AvrRps4 would show a stunted growth phenotype. Therefore, it is unlikely that mutagenesis in the FAST-R or XVE cassette explains the high false-positive recovery rate observed in this screen.

The variability observed in seed fluorescence may be explained by a heterozygous parental SETI line. Indeed, the rate of change in seed fluorescence between and within generations roughly correlates to a 3:1 segregation (Figure 3.4). However, non-segregating loss of PopP2 recognition, mediated by the *RRS1-R* allele on the T-DNA, undermines this possibility. Furthermore, members of the lab have published data with results that indicate consistent performance of the parental SETI line (Ngou et al., 2020b). A homozygous background is further supported by the consistent β-estradiol-insensitive phenotype for the parental SETI line (Figure 3.3A). However, 50 µM β-estradiol is 10× the saturating concentration required (Zuo et al., 2000). Indeed, SETI escapes were identified when plated on concentrations of β-estradiol < 20 µM (Appendix X). These data may indicate the presence of multiple T-DNA loci in the SETI line which results in different expression for each transcriptional unit dependent on T-DNA segregation. It may be that 50 µM β-estradiol is required to overcome this variability in the stunted-growth phenotypes. Yet, immunoblotting indicates that expression of RRS1-R-HF and RPS4-HA on the T-DNA are relatively even between sibling plants (Figure 3.1B). Therefore, it is unlikely that the variability observed in this screen for this line can be attributed to heterozygosity or multiple copies of the SETI T-DNA in the parental line.

The assays used by Ngou et al. (2020) and the assays used in the screen are different. They infiltrate 5-6-week-old rosette leaves with β-estradiol to induce AvrRps4-mNeon expression. However, in this screen the seedlings were germinated on β-estradiol and left to grow for two weeks. It is conceivable that the excessive exposure to β-estradiol induced transgene silencing which resulted in a high rate of false-positive candidate recovery. Yet, although small dosage changes from 5-8 μM β-estradiol can negatively impact Arabidopsis root morphology (Siligato et al., 2016), there are no specific reports of excessive β-estradiol exposure with the XVE system inducing silencing. Yet, there is some evidence that environmental conditions can induce transgene silencing (Meyer et al., 1992). Given these considerations, it may have been better to spray seedlings to better mimic the short pulse-treatment of β-estradiol performed by Ngou et al. (2020), as opposed to germination on β-estradiol.

Two routes for transgene silencing have been proposed: transcriptional gene silencing (TGS) which abolishes transcription of the introduced gene, or post-transcriptional gene silencing (PTGS) which degrades transgene RNA (Schubert et al., 2004, Rajeevkumar et al., 2015). TGS correlates with heavy methylation of promoter regions which blocks transcription, and PTGS is a mechanism by which cytosolic mRNA is degraded (Rajeevkumar et al., 2015). TGS may not be likely as there are no issues with silencing in the parental SETI line. However, if the dosage of β-estradiol was too high during screening, that would silence the AvrRps4-mNeon by PTGS, which would produce false-positives during screening. This could explain why there were approximately 1700 seedlings that were insensitive to β-estradiol but with no mNeon signal in their roots (likely some of these were also *AvrRps4*-mNeon mutants).

One “hallmark” symptom of PTGS is systemic acquired silencing—where silencing is propagated throughout tissue development (Rajeevkumar et al., 2015). This may explain putants that were insensitive to β-estradiol but still had AvrRps4-mNeon in their roots. Potentially, expression was so strong in early root tissue, perhaps before immune signalling can cause developmental defects, that the gene was silenced in the developing tissue. As mNeon signal in leaf tissue was not investigated, I cannot report on whether those signals were present or not. Silencing of developing tissue would also explain changes from generation to generation.

However, PTGS of AvrRps4-mNeon does not explain the loss of PopP2 recognition in putants. Loss of PopP2 recognition clearly indicates disruption of the *RRS1-R* allele on the T-DNA. It is unlikely that RRS1-R-HF expression is so high that it

induced PTGS, as similar expression levels are observed in the presence or absence of β-estradiol (Figure 3.1B). Yet, if PTGS did silence the SETI transgene, it is possible that the endogenous copies of RRS1 and RPS4 were co-suppressed. This may explain insensitivity to β-estradiol in the presence of AvrRps4-mNeon signal in root nuclei. If the NLRs are silenced in the presence of AvrRps4-mNeon, this would give rise to false-positive putants. Silencing of NLRs during screening may explain why the offspring were then able to recognize AvrRps4 by pathogen challenge. Future investigations could use RT-PCR to evaluate co-suppression of endogenous NLRs.

The definitive cause of the high false-positive recovery rate in this screen has not been determined. While the data points to the use of β-estradiol to over-express AvrRps4-mNeon, it is not clear whether silencing of AvrRps4-mNeon could result in silencing of the entire transgene. Furthermore, the variability of fluorescence signal in seeds did not directly correlate with AvrRps4 recognition phenotypes. It is unclear why some components on the T-DNA would be silenced and others not. Therefore, to directly implicate silencing as the cause of false-positive putants, future investigations could investigate the SETI line in mutant backgrounds for silencing components.

In conclusion, 31,000 mutagenized seedlings were screened for loss of AvrRps4 recognition. We recovered 322 putants from 162 different pools. A representative putant from 57 of the 124 pools tested retained insensitivity to β-estradiol in the next generation. However, 10 of those 57 (and 2 untested for β-estradiol sensitivity) still showed an HR upon AvrRps4 delivery by Pf0-1 infiltration. These data indicate that ETI-signalling mutants were not recoverable in this screen. Although I have not conclusively demonstrated silencing as the definitive cause of the high false-positive rate in this screen, it does not negate the fact that every tested putant maintained AvrRps4 recognition. In addition to the phenotypes of variable fluorescence signal in seeds, variable sensitivity to β-estradiol in subsequent generations, loss of AvrRps4-mNeon signal in subsequent generations, and loss of PopP2 recognition, it was clear that a fundamental error existed in this screen. It was better that I halted progress on this work and re-focused on other lines of investigation related to ETI signalling pathways. Therefore, I join the ranks of other researchers unable to uncover novel immune signalling components via mutagenesis screens in Arabidopsis. I am forced to make lemonade out of lemons in the form of insights and learning experiences gained from this project.

Chapter 4

Purification of full-length NRG1 protein for structure investigations

4 Purification of full-length NRG1 protein for structure investigations

4.1 Introduction

Although genetic and biochemical investigations have revealed general features of plant immune responses, our understanding of the precise mechanisms by which NLRs activate immunity is limited. Solving NLR structures pre- and post-activation should enable a greater comprehension of plant immune response mechanisms. Only recently were the first full-length structures solved for two plant NLRs: the CNL ZAR1 (Wang et al., 2019b, Wang et al., 2019a) and the TNL Roq1 (Martin et al., 2020). The activated forms are both wheel-like "resistosome" structures, although ZAR1 is a pentamer while Roq1 is a tetramer. As no RNL structures have been solved to date, this project aimed to elucidate NRG1 mechanisms through structure determination.

A wheel-like structure is also observed for mammalian NLRs which form an "inflammasome" upon activation. The best characterized is the NAIP/NLRC4 pairs which oligomerize in a heteromeric inflammasome composed of a single NAIP that recruits 9 (Tenthorey et al., 2017) or 10-12 NLRC4 protomers upon ligand binding (Hu et al., 2015, Zhang et al., 2015a). NAIP/NLRC4 structures reveal that mammalian NLRs progress to activation via ligand binding-dependent conformational changes and oligomerization (Hu et al., 2015, Zhang et al., 2015a, Tenthorey et al., 2017). However, while mammalian NLR structures can inspire mechanistic investigations, they do not share a common ancestor with plant NLRs (Urbach and Ausubel, 2017). Thus, what is known for mammalian NLRs may not directly apply to plant NLRs. Yet, the similarities between plant and animal NLRs for oligomerization of activated forms indicates that likely the function of a plant resistosome is to convert ligand recognition into immune activation.

Structural information on plant NLRs is limited. An individual NB-ARC domain of NRC1 has been solved (Steele et al., 2019). The LRR domain of full-length ZAR1 represents the first solved structure of an LRR domain for a plant NLR. And, as is observed for the solved structures of the CC domains from CNLs MLA10 (Maekawa et al., 2011), Rx (Hao et al., 2013), Sr33 (Casey et al., 2016), the CC domain of ZAR1 forms a four-helix bundle (Wang et al., 2019b). The activated ZAR1 structure shows changes in conformation wherein the first α-helix of this domain is released and associates with the first α-helix of other activated ZAR1 CC domains (Wang et al., 2019a). This is reminiscent of HeLo/HeLo-like domain-containing proteins (discussed

in section 1.3.4), yet ZAR1 does not show homology to those domains. As mentioned, the TNL Roq1 forms an activated tetramer (Martin et al., 2020), but the pre-activation state is not known. These data indicate that much is left to discover regarding the immune-signalling mechanisms of plant NLRs.

It might be expected that the NB-ARC and LRR domains of NRG1 are structurally similar to those of TNLs and CNLs. Homology modelling has shown that the RPW8-like domain of ADR1 is a four-helix bundle like the CC domain of CNLs (Bentham et al., 2018). It is conceivable that the RPW8-like domain of NRG1 is also a four-helix bundle. Like ZAR1, the pre-activation state of NRG1 may be an auto-inhibited monomer (Wang et al., 2019b). As mentioned (section 1.3.4), NRG1 shares homology with HeLo/HeLo-like domain-containing proteins. It is conceivable that a similar mechanism is true upon activation of NRG1: the first α-helix unfolds to form transmembrane homooligomerizations which may cause toxicity-inducing membrane disruptions, like HET-S (Seuring et al., 2012), or formation of ion channels which function in immune signalling, like MLKL (Chen et al., 2014, Cai et al., 2014). However, without solved structures for pre- and post-immune activated NRG1, this activation mechanism remains speculative.

NRG1 is reported to localize with endomembrane networks (Wu et al., 2019). Proteins that associate with membranes require solubilization in detergents to mimic phospholipid bilayers. Detergent-solubilized membrane proteins exist in protein-detergent complexes (PDCs), found in solution and existing alongside free detergent monomers and micelles (le Maire et al., 2000). These interactions are highly dynamic; there is a constant exchange of protein-associated detergent molecules with the reservoir of unbound detergent (le Maire et al., 2000). Detergent can contribute to 30-70% of PDC mass, and the amount of associated detergent is a property of both protein and detergent (Privé, 2009). Detailed knowledge of PDC composition and detergent concentration are essential for structural studies with membrane proteins (Gimpl et al., 2016).

X-ray crystallography is the most widely used technique for protein structure determination. Despite its ubiquity, historically, X-ray crystallography has struggled with the “crystallization bottleneck”—Proteins must be purified at high concentrations and then coaxed into crystalline forms before X-ray diffraction data can be collected and a structure can be solved (Shoemaker and Ando, 2018). Additionally, while, nuclear magnetic resonance (NMR) spectroscopy was previously applied routinely for structure determination, recent years have seen fewer structures solved with this

methodology. Notably, the number of structures solved by electron microscopy has almost doubled from 2018 to 2020.

Moreover, cryo-electron microscopy (cryo-EM) has emerged as an alternate technology that does not suffer from the same constraints as X-ray crystallography (Wu and Lander, 2020). However, structure determination for < 200 kDa proteins by cryo-EM represents the edge of current technical limitations, although shape contributes to limitations (Hebert, 2019). The primary challenge presented for solving small particle structures by cryo-EM requires balancing trade-offs between maximal signal-to-noise ratios while minimizing radiation damage (Wu and Lander, 2020). Particles of low molecular mass have fewer scattering atoms when frozen in vitreous ice. This low contrast makes it hard to detect protein particles unambiguously, and smaller complexes that are also conformationally flexible or lacking in distinguishing features may make the computation required for 3D reconstructions impossible.

Notably, X-ray crystallography was not explored as an approach to structure determination in this project. As mentioned, although proteins at < 100 kDa are not limiting for this technology, promotion of crystal formation requires exceptionally high concentrations and purity. Previously, Hannah Brown, a recent PhD from the Jones lab, attempted purifications of the full-length TNLs RRS1 and RPS4 from multiple different expression systems for structure determination. She trialled purifications from *E. coli*, insect cells, cell-free wheat germ, transgenic Arabidopsis, and transient *N. benthamiana* expression systems. *E. coli*, insect, and wheat germ expression systems are high-yielding such that X-ray crystallography studies should have been feasible. However, Dr. Hannah Brown found that soluble full-length RRS1 protein could only be purified from in planta expression-based systems, yet at yields that were too low for X-ray crystallography. Notably, ~ 200 g of *N. benthamiana* tissue was required to reconstruct the Roq1 resistosome by cryo-EM (Martin et al., 2020).

While the ZAR1 inactive and activated forms were purified after expression in insect cells, these structures were also solved by cryo-EM (Wang et al., 2019b, Wang et al., 2019a). Indeed, only one full-length NLR structure has been solved by X-ray crystallography—the mammalian NLRC4 (Hu et al., 2013). This is likely not due to a lack of effort but rather an issue with NLRs packing and forming a crystal lattice due to their dynamic nature and propensity to undergo conformational changes. Therefore, in planta expression and cryo-EM appears to be the most promising platform for structure determination of full-length plant NLRs. The protocol for purification of NRG1 described in this chapter built upon Dr. Hannah Brown's work.

4.2 Chapter aims and objectives

The aim of this chapter was to purify full-length NRG1 protein for structural investigations. Purification of the inactive form of NRG1 was prioritized to facilitate optimisation of methodologies. This work provides a foundation for future purifications of activated NRG1 forms, and other full-length NLRs, for structure determination. As NRG1 appears to signal in immune responses by triggering cell death, solving structures of full-length pre- and post-activated forms would help reveal the mechanisms by which cell death is mediated.

Some of the work described in this chapter was carried out by Jake Richardson within the John Innes Centre (JIC) Bioimaging Platform (Jake Richardson, personal communication with permission), Dave Lawson who manages the Protein X-ray Crystallography Platform at JIC (Dave Lawson, personal communication with permission), and Huang Shijia, (Tsinghua University in Beijing, personal communication with permission) in collaboration with Jijie Chai (Max Planck Institute for Plant Breeding Research, personal communication with permission). Jake Richardson prepared negative stain EM grids and carried out EM imaging as indicated throughout this chapter. Dave Lawson carried out a 2D reconstruction from negative stain EM images (Section 4.12). Huang Shijia ran SDS-PAGE and Coomassie brilliant blue staining, prepared negative stain EM grids, and carried out EM imaging in Figure 4.25.

4.3 Purification of NRG1B-HF by anti-FLAG® immunoprecipitation after *Agro*-infiltration and transient expression in *N. benthamiana*

Purification of full-length NRG1 was performed by *Agro*-infiltration and transient expression in *N. benthamiana*, followed by immunoprecipitation or affinity purification before size exclusion chromatography (Figure 4.1). NRG1B was chosen for purification over NRG1A as transient expression of NRG1A in *N. benthamiana* seems to produce a mis-spliced variant (Figure 5.2). Peak fractions were collected, combined, and concentrated with ultrafiltration centrifugal concentrators. Concentrated NRG1 protein was loaded onto EM grids, stained with uranyl acetate, and imaged by transmission electron microscopy.

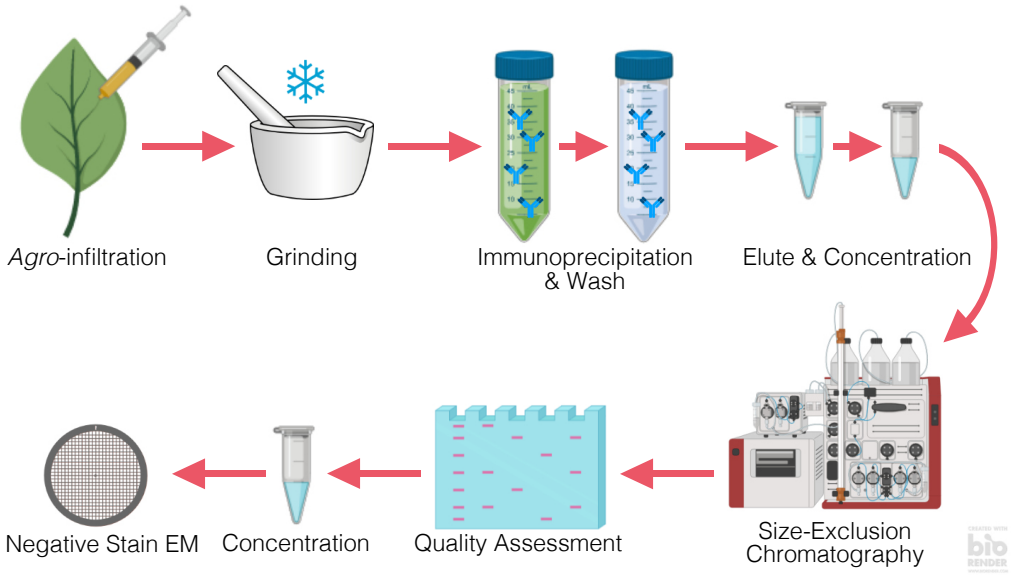

Figure 4.1 General schematic for in planta purification of NRG1. *Agrobacterium tumefaciens* strains carrying 35S:NRG1B-6×HIS-3×FLAG® (NRG1B-HF) expression constructs were infiltrated into 5-6-week-old *N. benthamiana* at OD_{600} = 0.5. Tissue was flash frozen and ground in liquid nitrogen. Lysates were clarified and incubated with affinity resins before elution. Eluates were combined and concentrated and subjected to SEC. Peak elution fractions were collected and assessed for quality by SDS-PAGE. Fractions were combined and concentrated before negative stain EM for structure determination.

To confirm that purified *At*NRG1 is functional when heterologously in *N. benthamiana*, HR assays were performed. The bacterial effector HopQ1 was used as it is recognized by the endogenous TNL Roq1, which signals through *Nb*EDS1 and *Nb*NRG1 (Schultink et al., 2017). An *Agrobacterium strain* carrying 35S promoter-driven *At*NRG1B-6×HIS-3×FLAG® (NRG1B-HF) was co-infiltrated with strains carrying 35S promoter-driven *At*EDS1-V5, *At*SAG101-Myc, and HopQ1 into wild-type, *nrg1,* or *eds1_pad4_sag101a_sag101b* (*epss*) *N. benthamiana* leaves. Co-delivery of NRG1B-HF with Arabidopsis alleles of SAG101 and EDS1 recapitulated HR in the presence of HopQ1 in both the *Nb_nrg1* and *Nb_epss* mutant backgrounds (Figure 4.2) (Lapin et al., 2019). These data indicate that the NRG1B-HF construct encodes a functional protein.

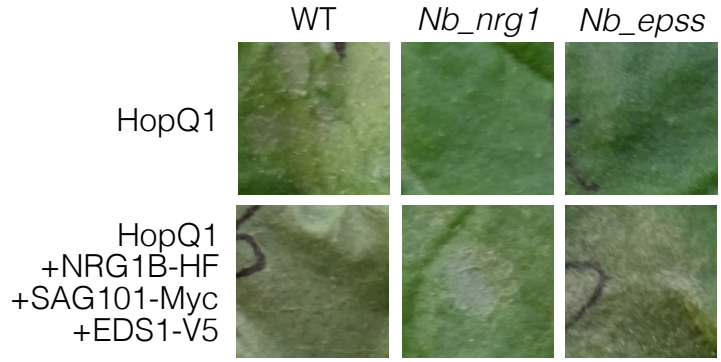

Figure 4.2 NRG1B-HF recapitulates HR with SAG101 and EDS1. HR assays by *Agro*-infiltration in 5-6-week-old *N. benthamiana* leaves. HopQ1 infiltration shows HR in wild-type leaves. Co-delivery of 35S promoter-driven *At*NRG1B-HF, *At*SAG101-Myc, and *At*EDS1-V5 with HopQ1 recapitulates HR in *nrg1* or *epss* mutant leaves.

To determine the best time-point for purification of NRG1B-HF from *Agro*-infiltrated (OD_{600} = 0.5) *N. benthamiana* leaves, accumulation at 1, 3-7 days post-infiltration (dpi) was evaluated by SDS-PAGE and antibody labelling (Figure 4.3). The predicted molecular weight (MW) of NRG1B-HF is ~ 99 kDa. Anti-FLAG® immunodetection indicated that NRG1B-HF migrates slightly slower than the ~ 100 kDa marker. Protein did not accumulate 1 dpi, and accumulation did not change from 3-7 dpi; therefore, tissue was harvested 3 dpi for all purifications.

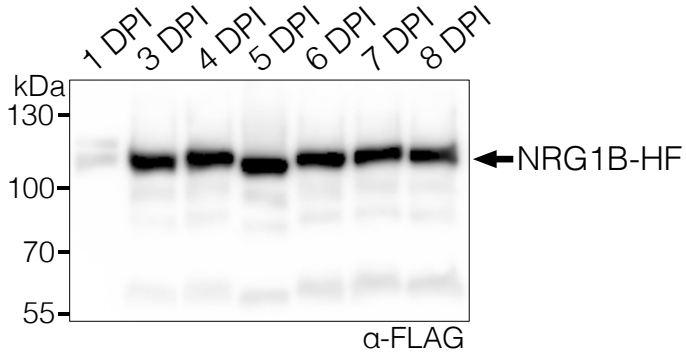

Figure 4.3 NRG1B-HF accumulates 3 dpi in *N. benthamiana*. Western blot after *Agro*-infiltration at OD_{600} = 0.5 of a strain carrying NRG1B-HF in the presence of p19 in 5-6-week-old *N. benthamiana* leaves. Tissue was harvested 1 or 3-7 dpi. Lysates were resolved by SDS-PAGE and bands were visualized by anti-FLAG® antibody labelling.

As NRG1B-HF carries tandem polyhistidine and 3×FLAG® tags, His-Nickel affinity purifications were compared against anti-FLAG® immunoprecipitation (IP). NRG1B-HF was transiently expressed in 5-6-week-old *N. benthamiana* leaves and harvested 3 dpi. Lysates for His-Nickel affinity purifications were solubilised in

phosphate-buffered saline (PBS), as recommended by manufacturer. Lysates for anti-FLAG® IPs were solubilized in a Tris-HCl-based buffer. However, PBS solubilization showed lower levels of NRG1B-HF protein in lysates compared to solubilization in Tris-HCl buffer (Figure 4.4, left). These data indicate that protein extraction with Tris-HCl-based buffers are more optimal than PBS-based buffers.

Lysates were incubated either with Nickel-nitrilotriacetic acid (Ni-NTA) magnetic beads or anti-FLAG® M2 affinity gel (hereafter agarose beads). Elution was performed either with imidazole or 3×FLAG® peptide, respectively. Variable elution conditions were compared: either with no dithiothreitol (DTT) or 5 mM DTT for the His-nickel affinity purification, or with a "long" (3 h binding, 2 × 1 h elution) or "short" (30 min binding, 2 × 15 min elution) for the anti-FLAG® IPs. Samples were evaluated by SDS-PAGE and anti-FLAG® immunodetection to compare yields. The absence of DTT during elution resulted in "streaking" on SDS-PAGE, even though 10 mM DTT was included in SDS sample loading buffer. This streaking interfered with evaluation of protein accumulation. The greatest increase is signal from input to eluates (elution product) is observed in the "5 mM DTT Ni-NTA" sample, while anti-FLAG® eluates show a lower signal vs their respective inputs (Figure 4.4). These data indicate that a higher yield is obtained from His-Nickel affinity purification than anti-FLAG® IP.

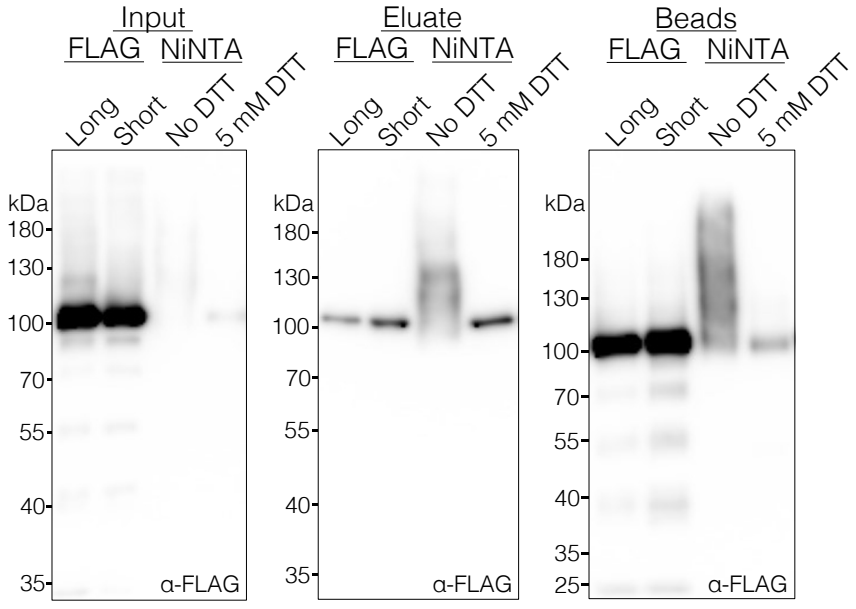

Figure 4.4 His-Nickel affinity purification is higher yielding than anti-FLAG® IP. Western blot of NRG1B-HF after anti-FLAG® IP or NiNTA affinity purification. Lysates were incubated either with anti-FLAG® agarose beads or HisPur™ Ni-NTA magnetic nickel-immobilized metal affinity chromatography (IMAC) before elution with 3×FLAG® peptide or imidazole, respectively. "Long" anti-FLAG® elutions included a 3 h incubation with beads followed by 2 rounds of 1 h 150 ng/µL 3×FLAG®

peptide elutions, while “Short” was 30 min binding followed by 2 rounds of 15 min elutions. “FLAG®” buffer: 50 mM Tris-HCl (pH 7.5), 150 mM NaCl, 0.1% Tween-20®, 10% Glycerol. NiNTA affinity purifications were performed either in the presence of no DTT or 5 mM DTT. NiNTA buffer: 100 mM sodium phosphate (pH 8.0), 600 mM NaCl, 0.1% Tween-20®, 10% Glycerol. Lysis without DTT. Equilibration with 30 mM imidazole. Wash with 0.05% Tween-20®, 50 mM imidazole. Elution with 250 mM imidazole. Bands were resolved by SDS-PAGE and immunolabelled with anti-FLAG®.

While anti-FLAG® IPs were lower yielding, no differences in recovery were observed between the “long” and “short” samples. These data indicate that saturation is met with a 30 min binding and 2 × 15 min elution. Additionally, recovery of NRG1B-HF was evaluated by heating beads in SDS sample buffer to release un-eluted NRG1B-HF. After heating, supernatant was resolved by SDS-PAGE and labelled with anti-FLAG® antibody. Substantial amounts of NRG1B-HF was present in the SDS sample buffer supernatant, especially from anti-FLAG® agarose beads, indicating that elution of NRG1B-HF was not complete (Figure 4.4, right). These data indicate that recovery of NRG1B-HF after His-nickel affinity purification or anti-FLAG® IP requires further optimisation.

As immunoblotting indicated that His-Nickel affinity purifications were higher-yielding than anti-FLAG® IP, coomassie brilliant blue (CBB)-staining of eluates was utilised to evaluate purity. Lysates were solubilized in a Tris-HCl- or HEPES-based buffers instead of PBS, and incubated with Ni-NTA magnetic affinity beads before elution with imidazole. Each of the Tris-HCl- and HEPES-based buffers showed comparable accumulation of NRG1B-HF in inputs (Figure 4.5A). Although DTT can reduce the iron in magnetic beads thereby disrupting function, low concentrations were included in lysis and elution buffers to prevent the streaking observed in Figure 4.4. Addition of 2.5 mM DTT during lysis and elution showed no streaking in SDS-PAGE (Figure 4.5A). Notably, release of iron during lysis was not observed, indicating that each of the Tris-HCl-based buffers, with 2.5 or 5 mM DTT, and the HEPES-based buffer with 5 mM DTT were compatible with Ni-NTA beads. These data indicate that 5 mM DTT is tolerated during His-Nickel affinity purifications with HisPur™ Ni-NTA magnetic beads, and that Tris-HCl- or HEPES-based buffers are comparable for solubilization of NRG1B-HF from plant tissue.

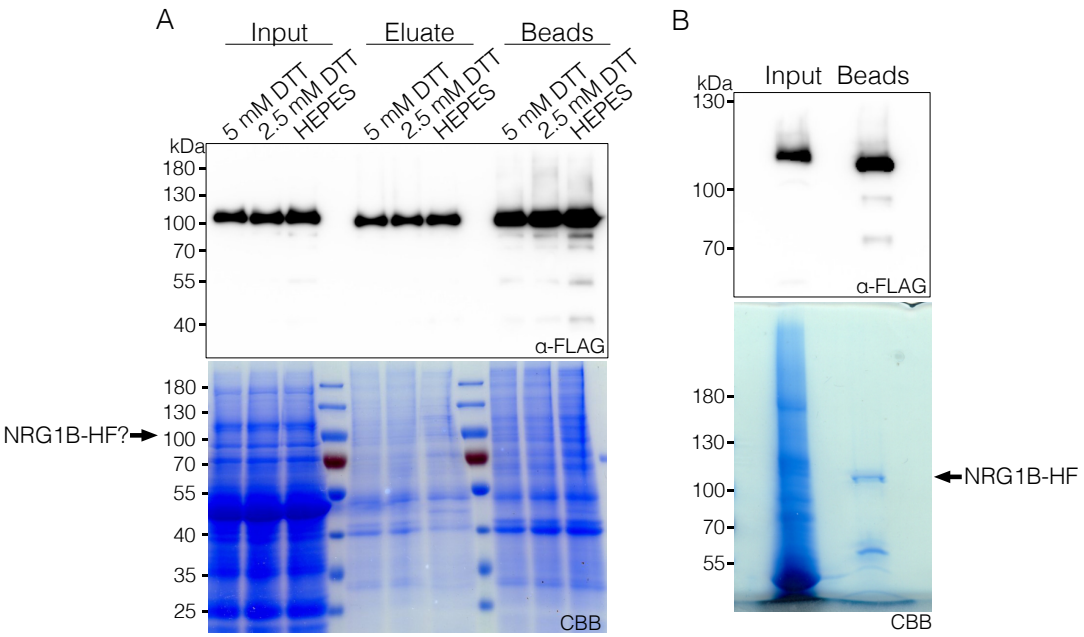

Figure 4.5 Anti-FLAG® IP is higher purity than His-Nickel affinity purifications. (A) HisPur™ Ni-NTA magnetic IMAC followed by imidazole elution. Bands resolved by SDS-PAGE followed by anti-FLAG® western blot (above) and CBB staining (below). CBB indicates the presence of contaminants after imidazole elution. (B) Anti-FLAG® IP. Bands resolved by SDS-PAGE followed by anti-FLAG® western blot (above) and CBB staining (below). CBB indicates the lack of contaminants present after bead boiling.

However, when imidazole eluates were resolved by SDS-PAGE and stained with CBB, many co-purifying proteins were observed (Figure 4.5A). Yet, when NRG1B-HF-bound anti-FLAG® beads were heated in SDS sample buffer, SDS-PAGE of supernatant showed very specific isolation of NRG1B-HF (Figure 4.5B). Therefore, although His-Nickel affinity purifications yielded greater recovery of NRG1B-HF, anti-FLAG® IP yielded higher purity NRG1B-HF. Thus, future purifications were performed with anti-FLAG® IP for purification of full-length NRG1B-HF.

To confirm the identity of NRG1B-HF migrating just above the ~ 100 kDa marker in SDS-PAGE, 3×FLAG® peptide eluates were resolved by SDS-PAGE and stained with CBB, and bands were excised and submitted for liquid chromatography-mass spectrometry (LC-MS) analysis (Figure 4.6A). Spectra correlating to NRG1B-HF peptides were observed in the sample for the band migrating near the ~ 100 kDa marker (Figure 4.6C). These data confirm the identity of this band as NRG1B-HF.

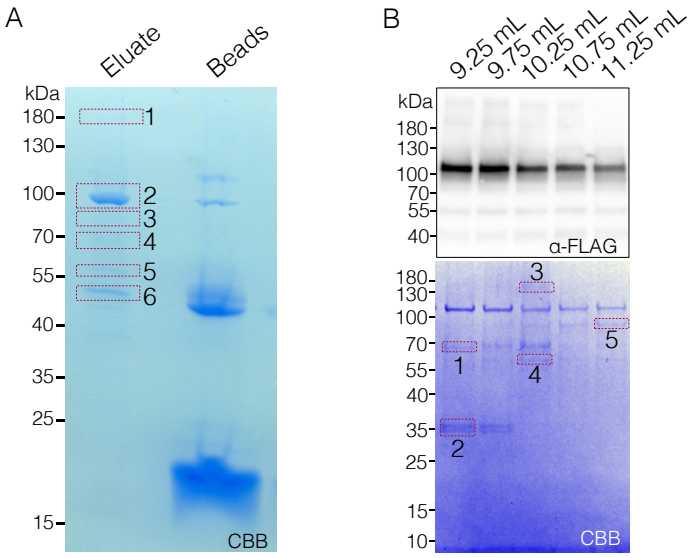

C

		Band ID					
Identified Proteins	MW (kDa)	1	2	3	4	5	6
*At*NRG1B-HF construct	99	100	**1368**	147	73	25	99
RuBisCO large subunit	54	30	20	18	28	46	**453**
Heat shock cognate 70 2-like	71	5	11	29	**221**	5	5
Proteasome activator subunit 4	204	**105**	10			4	
Ultraviolet-b receptor	62				9	**157**	
		Total Spectrum Count					

D

		Band ID				
Identified Proteins	MW (kDa)	1	2	3	4	5
RuBisCO large subunit	54	**53**	10	9	**5**	5
Ultraviolet-b receptor	62	**34**				
Heat shock cognate 70 2-like	71					**26**
VAMP-associated protein (VAP)	30		**33**			
		Total Spectrum Count				

Figure 4.6 Mass spectrometry of NRG1B-HF co-purifying components. (A) SDS-PAGE resolution and CBB staining of NRG1B-HF eluates after *Agro*-infiltration-mediated transient expression in *N. benthamiana*, anti-FLAG® IP and 3×FLAG® peptide elution 150 ng/µL. Bands excised for LC-MS analysis are outline in red boxes. (B) SDS-PAGE and anti-FLAG® western blot (above) or CBB-staining (below) of co-purifying bands with NRG1B-HF after purification and SEC (Figure 4.24). Bands excised for LC-MS analysis are outlined in red boxes. (C) Total spectrum counts for spectra that correlate peptides derived from bands in (A). (D) Total spectrum counts for spectra that correlate to peptides derived from bands in (B).

Co-purifying bands were also excised and sent for LC-MS analysis, all of which contained some spectra that correlated to peptides of NRG1B-HF, which may indicate some degree of protein degradation. However, there were spectra that correlated to peptides derived from other proteins: the band migrating above ~ 180 kDa is likely Proteasome activator subunit 4, the band migrating near ~ 70 kDa is likely HSC70-2, the band migrating near ~ 55 kDa is likely UVR8 (ULTRAVIOLET-B RECEPTOR), while the band running just below the ~ 55 kDa marker showed the highest number of peptide hits to RuBisCO. The MW of proteins measured by LC-MS all correlated to

estimated MW markers when resolved by SDS-PAGE. These data indicate that either these co-purifying components are contaminants, or associate with anti-FLAG® beads or NRG1B-HF.

At a later date in this project, fractions after size-exclusion chromatography (SEC) (Figure 4.24) were also evaluated by LC-MS. These data showed similar results as RuBisCO, HSC70-2, and UVR8 were found to co-purify with NRG1B-HF after anti-FLAG® IP (Figure 4.6B, Figure 4.6D). However, a vesicle-associated membrane protein (VAMP)-associated protein (VAP) was newly identified. As these components eluted at the same time as NRG1B-HF during SEC, it is indicated that they are in complex with NRG1B-HF. These data may indicate a functional relationship between NRG1B-HF and the co-purified proteins.

4.4 Large-scale purification with Tween-20® yields highly pure NRG1B-HF

Larger-scale purifications were initiated to recover NRG1B-HF for structural investigations. Approximately 30 g of *N. benthamiana* leaf tissue was infiltrated with *Agrobacterium* carrying NRG1B-HF and harvested 3 dpi. Protein was solubilized in Tris-HCl-based buffers with 0.1% Tween-20®. Lysates were resolved by SDS-PAGE and anti-FLAG® antibody labelling which showed soluble NRG1B-HF protein (Figure 4.7A). Lysates were incubated with anti-FLAG® agarose beads before elution with 3×FLAG® peptide. Eluates were resolved by SDS-PAGE and anti-FLAG® antibody labelling, which showed recovery of NRG1B-HF. However, signal in supernatant indicated that NRG1B-HF protein remained unrecovered in lysates. Furthermore, there is evidence of protein loss during bead washing steps prior to elution. Yet, this may be attributable to contaminating supernatant in wash buffer. Eluate was separated from beads by centrifugation with spin column, which did not result in loss of protein. Notably, significant protein loss was observed while concentrating eluates by centrifugation with 50 kDa molecular-weight cut-off (MWCO) ultrafiltration devices (hereafter concentrators). NRG1B-HF signal was not detected in the flow-through, and as no protein precipitation was observed, it was conceivable that NRG1B-HF protein was lost directly to the ultracentrifugation materials. Taken together, these data indicate that larger-scale purifications of NRG1B-HF by anti-FLAG® IP result in specific recovery of NRG1B-HF, although losses are compounded at several steps during purification. Therefore, further optimisations of large-scale purifications are required.

Eluates were buffer-exchanged, concentrated to < 200 µL and subjected to SEC on a Superose 6 Increase 10/300 GL column (fractionation range 5-5000 kDa). Multiple peaks were observed; however, the elution peak at 16.5 mL correlated to NRG1B-HF by SDS-PAGE and anti-FLAG® immunolabelling (Figure 4.7B). Notably, some NRG1B-HF signal is observed in earlier fractions and trailing in later fractions (Figure 4.7B). These data may indicate non-specific interactions of NRG1B-HF with column resin.

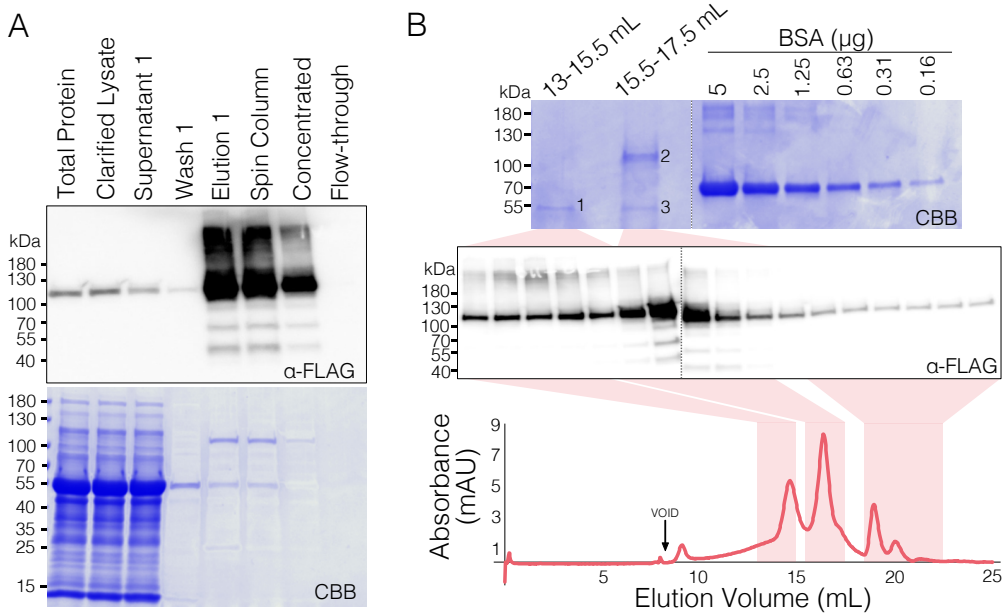

C

Identified Proteins	MW (kDa)	Band ID 1	2	3
AtNRG1B-HF	54	1	**14**	2
RuBisCO large subunit	62	**10**		2
Chaperonin 60 subunit beta 2 chloroplastic	71			4
		Total Spectrum Count		

Figure 4.7 Large-scale purifications with Tween-20® yield highly pure NRG1B-HF. SDS-PAGE and anti-FLAG® western blot (above) or CBB-staining (below) of purification samples. Buffers: 100 mM Tris-HCl pH 7.5, 1 mM EDTA pH 8.0, 150 mM NaCl, 0.1% Tween-20®, 10% Glycerol. Eluted with 3×FLAG® peptide at 150 ng/µL. (B) SEC of protein purified in (A). SEC fractions (bottom) were analyzed by SDS-PAGE and anti-FLAG® western blot (middle) and combined before SDS-PAGE and CBB-staining (top). Numbers beside bands indicate Band IDs in C. BSA standards were run alongside for quantification. SEC buffer did not include $MgCl_2$. SEC flow rate was 0.5 mL and 0.5 mL fractions were collected. (C) Total spectrum counts for spectra that correlate to peptides derived from bands in (B).

Fractions from the first peak (13-15.5 mL) and the NRG1B-HF peak (15.5-17.5 mL) were combined and concentrated, and resolved by SDS-PAGE before CBB

staining (Figure 4.6B). LC-MS of excised bands indicated that the 14.5 mL peak was RuBisCO contamination, and confirmed the identity of the 16.5 mL peak as NRG1B-HF (Figure 4.7C). RuBisCO exists as a tetramer complex and thus is likely eluting in native state at ~ 550 kDa. The presence of a chaperone co-purifying with NRG1B-HF is observed. As the MW of this chaperone is 64 kDa, it would be expected to elute later from this column when unbound to NRG1B-HF. These data indicate that this chaperone may associate with NRG1B-HF.

Quantification by Bradford protein assay indicated that total NRG1B-HF yield after SEC was 2.73 µg in 100 µL (0.027 mg/mL) (Figure 4.7B). However, ultraviolet (UV) absorption at 280 nm reported a concentration of 0.1131 mg/mL. Absorption would measure both NRG1B-HF and the contaminating chaperone. Yet, by CBB-staining, the chaperone band quantification was 0.005 mg/mL, which does not account for the difference between absorption and Bradford protein assay quantification for NRG1B-HF. These data indicate quantifying NRG1B-HF yields by A_{280} is not accurate.

The NRG1B-HF sample was loaded onto EM grids and negatively stained with uranyl acetate (UA). Grids were imaged with a transmission electron microscope (TEM). The buffer used during SEC [gel filtration (GF) buffer] was also stained with UA as a negative control. The GF buffer showed little staining while some darker staining sections were visible in the NRG1B-HF grid (Figure 4.8). However, no obvious particles were present. These data indicated that the GF buffer background was clean, and further optimisation of purifications and UA staining procedures was required.

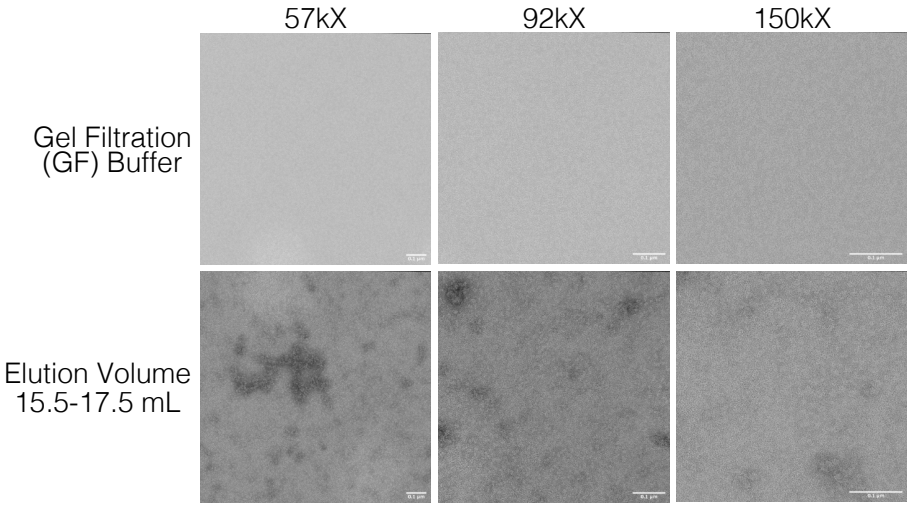

Figure 4.8 Negative stain EM of purified NRG1B-HF does not show clear particles. Micrograph of EM grids negatively stained with UA. The SEC GF buffer shows minimal background noise. Samples from Figure

4.7 show darker staining patches that are not indicative of clear protein particles. Formvar carbon-coated grids were used. This work was carried out by Jake Richardson (Jake Richardson, personal communication with permission).

4.5 Artefacts are present with Tween-20® on negative stain EM grids

Initially, the lysis buffer recipe I inherited was indicated for general protein extraction from plant tissue. I wanted to optimize buffer conditions to ensure purification of stable NLR protein. Changes were made to the lab lysis buffer which called for 50 mM Tris-HCl (pH 7.5), 150 mM NaCl, 1 mM EDTA, 10% glycerol, and 0.1% Tween-20®. As the Walker B motif of NLRs binds Mg^{++} ions, $MgCl_2$ was added to ensure native conformations of NRG1B-HF. Additionally, EDTA was removed as it would chelate Mg^{++} away from NRG1B-HF. EDTA is a common lysis buffer component as chelation of metal ions helps to inhibit metalloproteases; therefore, removal of EDTA could subject proteins to degradation. Importantly, no protein degradation was observed in the absence of EDTA (Figure 4.9A). Lastly, Tris-HCl was exchanged with HEPES, as HEPES has a greater buffering capacity and is more thermostable than Tris-HCl. Indeed, protein was soluble in the optimized HEPES-based buffer (Figure 4.9A). These data indicated that the buffer changes I introduced facilitated purification of stable NRG1B-HF.

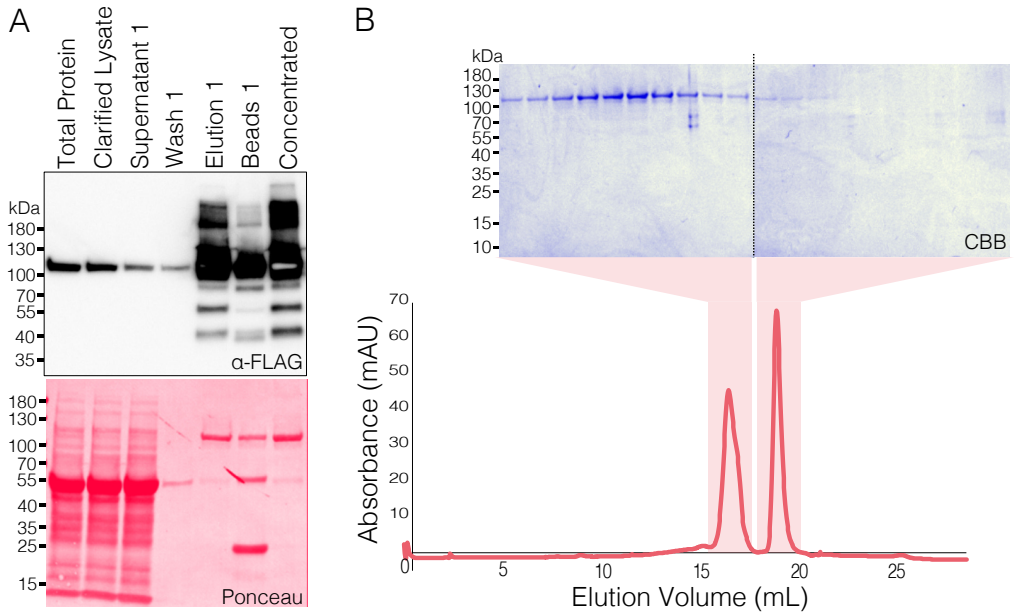

Figure 4.9 SEC with Tween-20® shows higher NRG1B-HF yield. (A) SDS-PAGE followed by anti-FLAG® western blot (above) and ponceau-staining (below) of purification samples. Buffers: 100 mM HEPES (pH 7.5), 150 mM NaCl, 5 mM $MgCl_2$, 10% Glycerol, 0.1% Tween-20®. Eluted with 3×FLAG® peptide at 300 ng/µL. (B) SEC of protein purified in (A). SEC fractions (below) were subjected to SDS-PAGE and

CBB-staining (above). SEC buffer included 0.1% Tween-20® but not $MgCl_2$.

Notably, NRG1B-HF was again detected in supernatant and in buffer after bead washes (Figure 4.9A). Furthermore, although the concentration of 3×FLAG® peptide was doubled from 150 ng/µL to 300 ng/µL, elution was not complete: supernatant of SDS-boiled anti-FLAG® beads after IP and elution were resolved by SDS-PAGE, which showed significant levels of un-eluted NRG1B-HF. These data indicate that while purification of NRG1B-HF by anti-FLAG® IP and elution with 3×FLAG® peptide is highly specific, recovery is minimal. Additionally, significant loss of NRG1B-HF to protein concentrators is again observed (Figure 4.9A). These data indicate that concentration of eluates by centrifugation requires further optimisation.

Concentrated NRG1B-HF was subjected to SEC and two discrete peaks are observed in the chromatogram (Figure 4.9B). NRG1B-HF eluted evenly across the 16.5 mL peak, as visualized by CBB. Interestingly, a band for co-purifying chaperones is no longer observed. Notably, 0.1% Tween-20® was included in the GF buffer to test for improve yields. Indeed, the NRG1B-HF peak A_{280} was ~ 40 mAU vs. ~ 5 mAU in Figure 4.7B. The peak at 19 mL likely represents eluting buffer solutes. These data indicate that the optimized HEPES-based buffer and the addition of 0.1% Tween-20® during SEC improves yield of NRG1B-HF. However, it is possible that a higher input was run over the column, although eluate quantifications were not directly compared.

The elution fractions at 16.25-16.5 mL were combined and sent for negative stain EM. In contrast to Figure 4.8, darkly staining spheres are now observed in both the GF buffer control and NRG1B-HF after UA-staining (Figure 4.10A). Notably, GF buffer now includes 0.1% Tween-20®. While the dark marks were not characteristic of glycerol or uranium salts precipitating, it was not clear that protein particles were present. However, Jake Richardson later determined that the formvar carbon-coated grids that were being used produced background noise at high magnifications when stained with UA alone. He found that carbon-only grids showed a cleaner background in the presence of UA alone (data not shown). These data indicate that either these darkly staining spheres are background noise, or Tween-20® artefacts.

Therefore, NRG1B-HF SEC fractions from 15-16.5 mL were combined and loaded onto carbon-only grids before UA staining, either undiluted or diluted in GyrA buffer (50 mM Tris pH 7.5, 100 mM KCl, 2 mM DTT, 1 mM EDTA) (Figure 4.10B). With these conditions, the undiluted NRG1B-HF sample looked clean and small,

lighter-staining “blobs” were visible. These data indicated that the darkly staining spheres in Figure 4.10A may have been background noise.

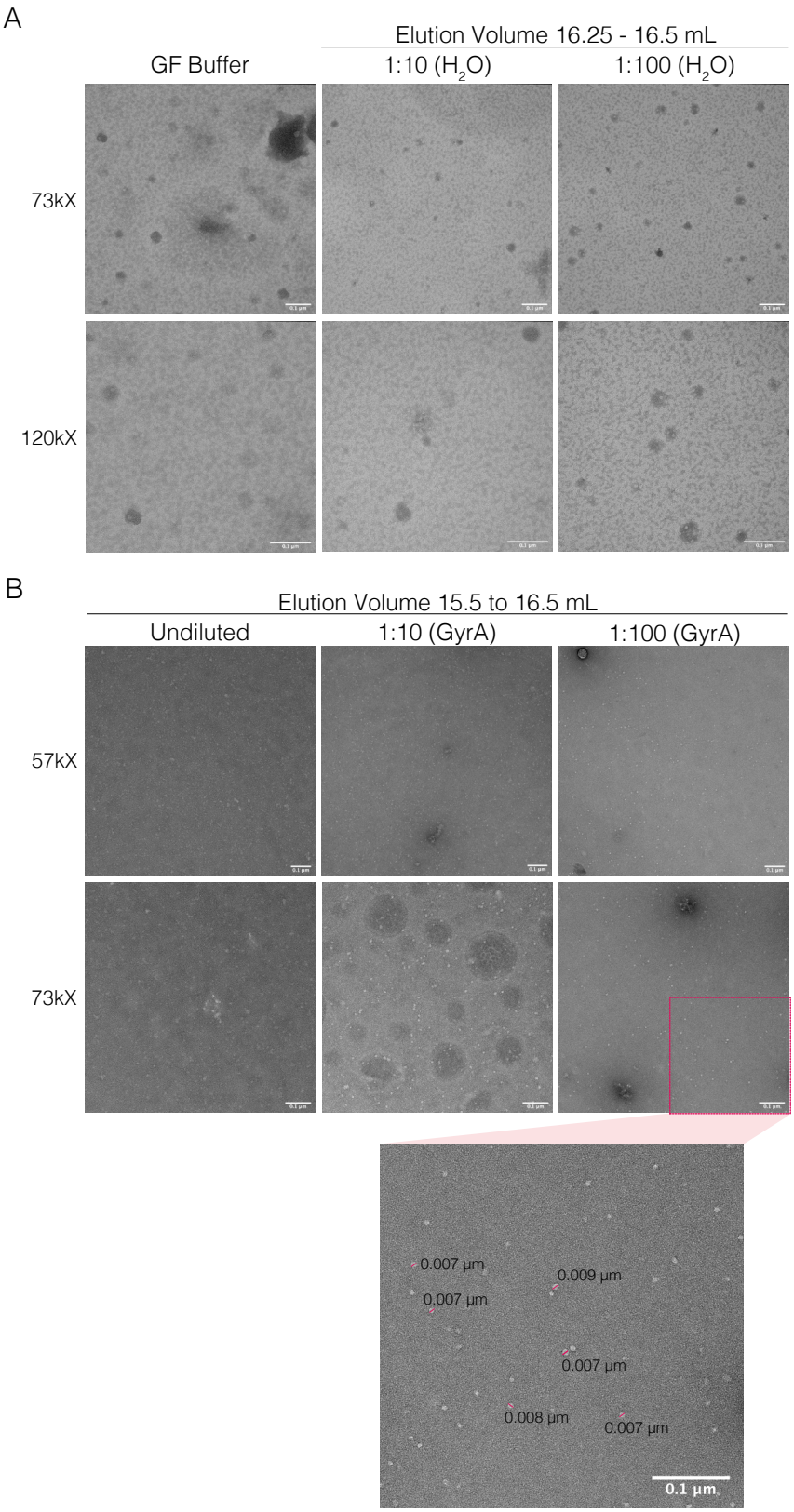

Figure 4.10 Carbon grids show less background noise and candidate NRG1B-HF particles are visible after negative stain EM. Micrograph of negative staining with UA on formvar carbon coated EM grids with sample

from Figure 4.9. Darkly staining spots are observed in both the control and the sample, indicating high background noise of these grids. (B) Negative staining with UA on carbon-only EM grids with sample from Figure 4.9. The presence of light, white blobs is indicative of protein that roughly correlates to NRG1B-HF monomer sizes predicted to be ~ 6.5 nm. Probable NRG1B-HF particles were measured in ImageJ to be 7-9 nm. This work was carried out by Jake Richardson (Jake Richardson, personal communication with permission).

The lighter-staining blobs were measured in ImageJ to be ~ 7-9 nm in diameter. MyCalcTool (https://www.calctool.org/CALC/prof/bio/protein_size) predicts the size of NRG1B-HF monomers to be ~ 6.5 nm in diameter. As the density of these blobs could be easily adjusted with dilutions, they were considered candidate NRG1B-HF protein particles.

To further ensure the NRG1B-HF identity of the blobs, buffer and detergent controls were stained with UA and imaged by TEM. Notably, Tween-20® detergent diluted in GyrA buffer showed very similar lighter-staining blobs (Figure 4.11A). Furthermore, Jake Richardson measured the Tween-20® particles to be 8.5 nm on average (Figure 4.11B)—directly correlating with the sizes measured in Figure 4.10B. These data indicated that the identity of the candidate NRG1B-HF blobs could be Tween-20® artefacts. Therefore, Tween-20® was no longer included as the detergent in purifications.

A

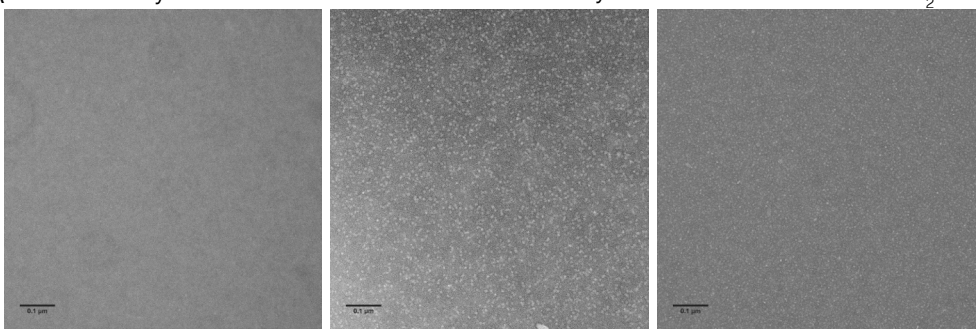

B

Sample	0.02% Tw-20 in GyrA	0.02% Tw-20 in H_2O
Size average nm (longest length)	8.563	6.434
Standard deviation	0.843	1.310

Figure 4.11 Tween-20® Negative stain EM shows particles similar to NRG1B-HF. Micrograph of tween-20® was stained with UA on EM grids, diluted either in GyrA buffer or water. The presence of lighter staining blobs indicates artefacts that are similar in size and contrast to NRG1B-HF probable protein particles. (B) Measurements of particles in A. This work was carried out by Jake Richardson (Jake Richardson, personal communication with permission).

4.6 Nonidet™ P-40 shows fewer artefacts in negative stain EM than Tween-20®

In an effort to better visualize NRG1B-HF particles on EM grids after UA staining, Tween-20® was replaced with Nonidet™ P-40 substitute (NIDP40; IUPAC = octylphenoxypolyethoxyethanol) in subsequent purifications. Both are non-ionic detergents—mild surfactants that are used to break protein-lipid and lipid-lipid interactions but should not interfere with protein-protein interactions. Thus, they function to lyse membranes, particularly helpful in extracting membrane-bound proteins, without interfering with native conformations or associations.

To evaluate whether NIDP40 also shows particle-like artefacts in negative stain EM, a dilution series of NIDP40 in GF buffer were stained with UA and imaged (Figure 4.12). As the critical micelle concentration (CMC) of NIDP40 is 0.25 mM (0.02% [w/v]), concentrations above and below 0.02% NIDP40 were stained with UA to evaluate for micelles in parallel. In contrast to Tween-20®, the NIDP40-containing grids did not stain differently from the GF buffer control. However, some sparse lighter-staining particles are observed in the grid with 0.002% NIDP40 in GF buffer. This may be an artefact of thick UA staining as it was not observed in lighter areas of the grid. A second grid staining showed similar results. Thus, these data indicate that NIDP40 neither shows the presence of small particles nor stained-micelles that would interfere with our ability to detect NRG1B-HF particles.

To ensure that negative stain EM conditions were optimized to visualize NRG1B-HF particles, buffer controls were also stained with UA to evaluate for background noise. Tris (50 mM Tris-HCl 7.5, 100 mM KCl, 5 mM $MgCl_2$, 2 mM DTT)- or HEPES (50 mM HEPES 7.5, 150 mM NaCl, 5 mM $MgCl_2$, 2 mM DTT)-based buffers may better stabilize NRG1B-HF protein than water or GF buffer during dilutions to decrease density on grids. While the Tris buffer did precipitate, the HEPES buffer was clean (Figure 4.12). Therefore, this HEPES-based buffer was used for NRG1B-HF dilution before UA staining in final grid preparations.

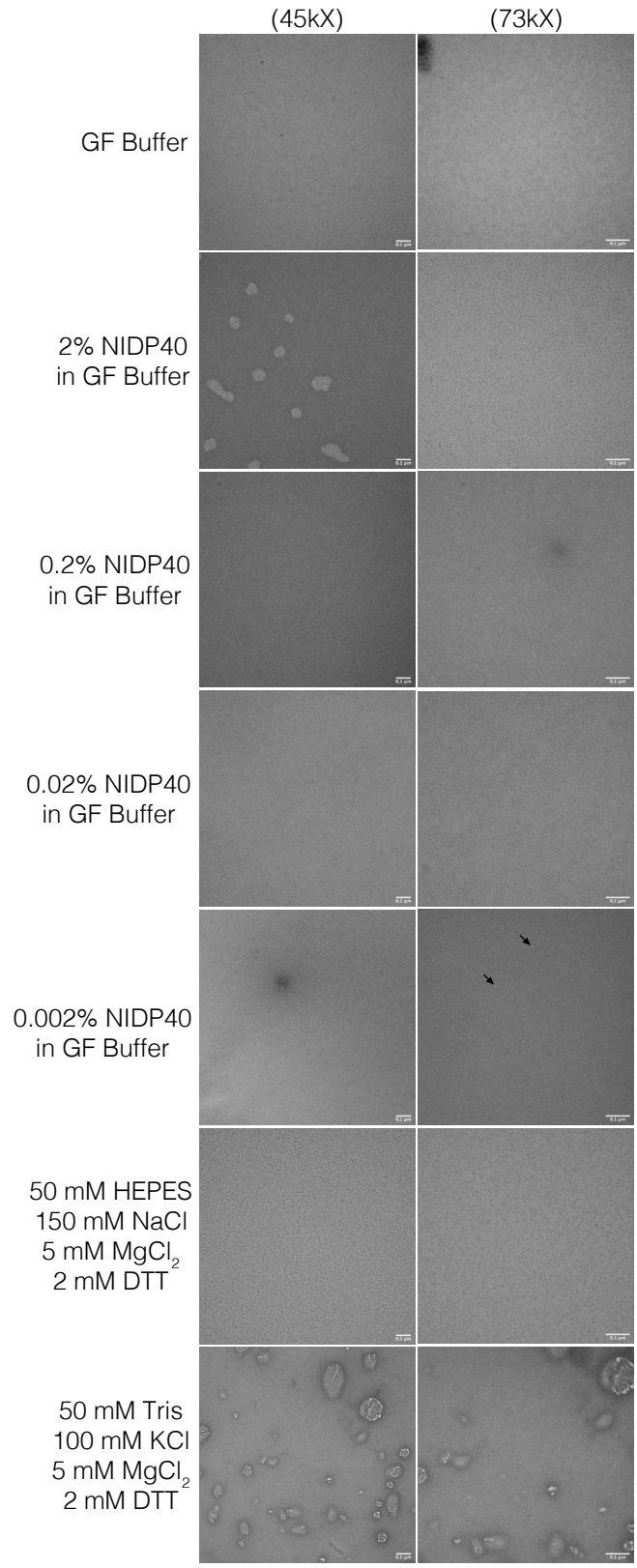

Figure 4.12 NIDP40 does not show artefacts in negative stain EM. Micrograph of varying concentrations of NIDP40 and buffers were negative stained with UA and imaged by TEM. Dilutions of NIDP40 in the GF buffer used during SEC does not produce lighter contrast blob artefacts, except a few in the 0.002% images in darker staining sections of grids (indicated with black arrows). HEPES buffer is clean while Tris precipitates in UA. This work was carried out by Jake Richardson (Jake Richardson, personal communication with permission).

4.7 Optimisation of large-scale purifications with Nonidet™ P-40 substitute

Purifications of NRG1B-HF after transient expression in *N. benthamiana* were attempted with NIDP40 instead of Tween-20® with comparable results. In addition, three rounds of elution with 3×FLAG® peptide were attempted in an effort to increase protein yield. Indeed, each subsequent elution yielded similar recovery to the first (Figure 4.13A). Furthermore, detection of NRG1B-HF protein in the supernatant decreased across elutions. These data indicate that additional elution steps increase NRG1B-HF protein recovery.

As concentration by centrifugation resulted in significant protein losses, dialysis tubing was evaluated as an alternative method to concentrate eluates. Half of buffer-exchanged eluates were transferred to a 50 KDa MWCO Float-A-Lyzer G2 Dialysis Device (Repligen: G235058), while the other half was concentrated by centrifugation. Dialysis tubing was coated in Spectra/Gel® absorbent (Repligen: 292600) and left at 4 °C for ~ 6 h. Volume inside tubing reduced from 5 mL to 0.5 mL indicating removal of water and < 50 kDa solutes. However, concentration with dialysis tubing showed comparable protein loss to concentration by centrifugation (Figure 4.13B). These data indicate that concentration of eluates by dialysis tubing did not improve recovery of NRG1B-HF protein, and that concentration by centrifugation was still preferable although losses persisted.

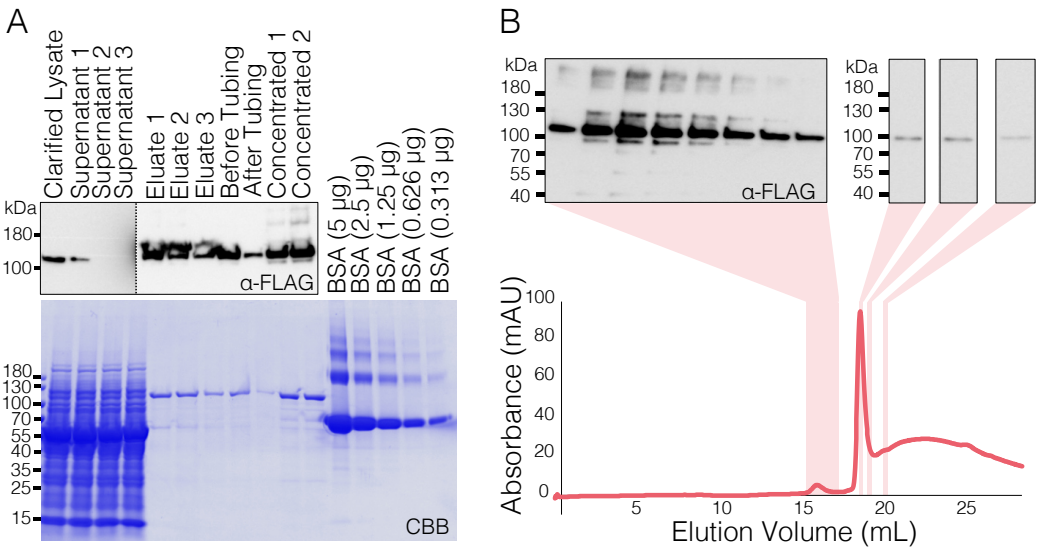

Figure 4.13 NIDP40 is used to purify NRG1B-HF instead of Tween-20®. (A) SDS-PAGE followed by anti-FLAG® western blot (above) and CBB-staining (below) of purification samples. Buffers: 100 mM HEPES (pH 7.5), 150 mM NaCl, 5 mM $MgCl_2$, 10% Glycerol, 0.1% NIDP40. Three 3×FLAG® peptide were employed: two × 30 min at 150 ng/µL followed by an overnight elution at 250 ng/µL. BSA standards were run in CBB gel to compare eluate quantities. (B) SEC of protein purified in (A). SEC fractions

(below) were analyzed by SDS-PAGE and anti-FLAG® western blot (above). SEC buffer did not include $MgCl_2$.

Eluates concentrated by dialysis tubing and by centrifugation were combined and subjected to SEC. Again, two distinct peaks are observed; however, NRG1B-HF protein eluted at 16 mL instead of 16.5 mL. This peak shift may be attributable to the change from Tween-20® to NIDP40 during lysis. While trailing NRG1B-HF is observed by immunoblot as in previous purifications, the chromatogram now shows a novel trail after the 19 mL peak. Potentially, this trail represents eluting monomers of NIDP40. As NIDP40 was not included in GF buffer, these data may indicate that NIDP40 associates with NRG1B-HF during lysis and dissociates during SEC.

While concentration by centrifugation was superior to dialysis tubing, protein losses using this technique were still inhibitory. Therefore, pre-treatment of varying concentrators was attempted to improve protein recovery. I tested a 0.5 mL Sartorious Vivaspin® 500 concentrator (VS0131), made with a polyethersulfone membrane. I also tested 2 mL (UFC205024) or 4 mL (UFC805024) Merck Amicon® Ultra concentrators made with regenerated cellulose membranes. Remarkably, although the assay is semi-quantitative only, pre-incubation with water resulted in no observable protein losses for the 0.5 mL and 4 mL concentrators (Figure 4.14). Notably, pre-incubation with detergent, BSA, or milk resulted in protein losses for the 0.5 and 2 mL concentrators (Figure 4.14). Indeed, all earlier purifications included pre-incubation of concentrators with buffers that contained either Tween-20® or NIDP40. Therefore, subsequent purifications used a water pre-incubated 4 mL concentrator to concentrate eluates to ~ 0.5 mL. At that point, a water pre-incubated 0.5 mL concentrator was used to concentrate eluates to 100-200 µL.

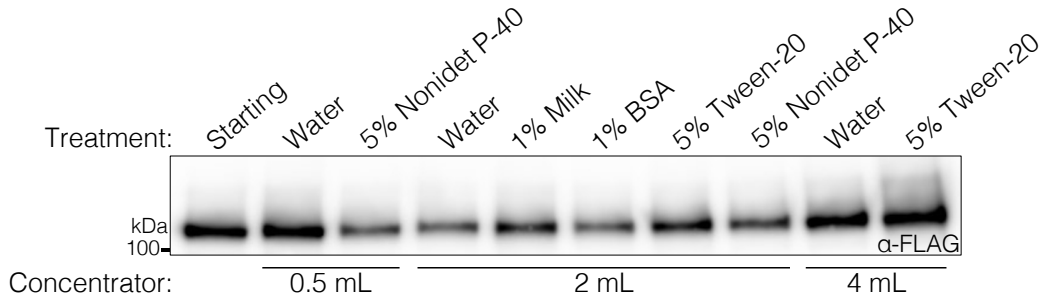

Figure 4.14 Concentrators pre-treated with water improve recovery of NRG1B-HF. SDS-PAGE and anti-FLAG® western blot of NRG1B-HF after centrifugation through pre-incubated concentrators. Lanes indicate concentrator and blocking reagent trialed. All concentrators were incubated overnight except those with 5% Nonidet™ P-40 substitute (NIDP40) which were blocked for 2 h. NRG1B-HF eluate was concentrated

according to manufacturer's instructions, filtrate and retentate were recombined. 0.5 mL = Sartorius Vivaspin® 500 Polyethersulfone, 2 mL and 4 mL = Merck Amicon® Regenerated Cellulose. Detailed description of protocol can be found in section 2.11.4 of this thesis.

A new purification with further optimisations to increase NRG1B-HF recovery was attempted. Lysates were incubated a second round with anti-FLAG® agarose beads, and concentrators were pre-incubated with water. Eluates from each elution showed a similar band intensity in SDS-PAGE (Figure 4.15A). These data indicate that two rounds of anti-FLAG® agarose bead incubation with the same lysate sample increases recovery of NRG1B-HF. SDS-PAGE and CBB-staining also showed an increase in NRG1B-HF band intensity between eluates and concentrated samples (Figure 4.15A). These data indicate that pre-incubation of concentrators with water also yields higher NRG1B-HF recovery. However, the rate of recovery was not determined as the presence of NIDP40 interfered with quantification by UV absorbance at 280 nm (Figure 4.17B).

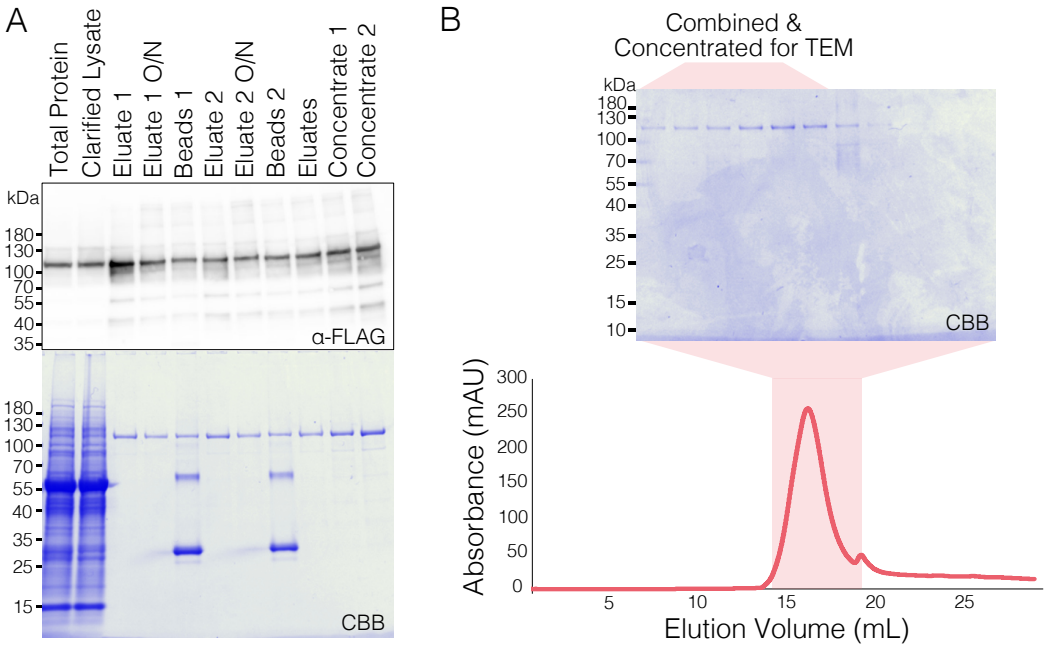

Figure 4.15 Lysis with 0.5% NIDP40 indicates detergent-bound NRG1B-HF. (A) SDS-PAGE and anti-FLAG® western blot (above) or CBB-staining (below) of purification samples. Buffers: 100 mM HEPES (pH 7.5), 150 mM NaCl, 5 mM $MgCl_2$, 10% Glycerol, 0.5% NIDP40. Two rounds of lysate incubation with anti-FLAG® agarose beads were included. (B) SEC of protein purified in (A). SEC fractions (below) subjected to SDS-PAGE and CBB-staining (above). SEC buffer did not include $MgCl_2$.

The concentrated sample was then subjected to SEC. Again, a trail is observed in the chromatogram, likely due to small molecules of NIDP40 eluting. SDS-PAGE and CBB-staining of the 16 mL peak elution fractions showed highly pure NRG1B-HF (Figure 4.15B). Notably, the A_{280} of the NRG1B-HF peak is ~ 250 mAU; however, as NIDP40 absorbs at 280 nm, it is likely that this peak height is due to the use of 0.5% NIDP40 during lysis. These data indicate that protein-detergent complexes are formed between NRG1B-HF and NIDP40. Additionally, these data indicate that NIDP40 interferes with quantification of NRG1B-HF by UV absorbance at 280 nm.

NRG1B-HF peak fractions from elution volumes 14-17 mL were combined, concentrated from 3 mL to 1 mL and an aliquot was sent for negative stain EM. Samples were diluted in water, GF buffer, and GyrA buffer before loading onto grids (Figure 4.16). The HEPES-based buffer—mentioned previously (Figure 4.12)—for diluting samples prior to negative stain EM had not yet been optimized. Dilution in GF buffer seemed to mask protein and induce precipitations, while dilution in water or GyrA buffer provided the best contrast such that particles were easily distinguished and consistency in size and shape was observed (Figure 4.16). Thus, the lighter-staining rounded blobs ~ 10 nm in diameter were considered putative NRG1B-HF monomer particles.

The remaining sample was further concentrated from 1 mL to 150 µL and sent for SEC-small-angle X-ray scattering (SAXS). This technique is used to discern the biophysical characteristics of protein in solution such as shape, oligomeric state, and molecular mass. However, no scattering data was observed for NRG1B-HF (data not shown). At the time, results indicated that no protein was present in the sample. Yet, UV absorbance at 280 nm indicated a concentration of 8.5 mg/mL of NRG1B-HF. Notably, this experiment was performed before the realization that NIDP40 absorbs at 280 nm. Therefore, it is likely that the concentration of protein submitted was far overestimated. This may explain the negative result of the SEC-SAXS assay, as a concentration of > 0.5 mg/mL would be required to observe X-ray scattering with this technique.

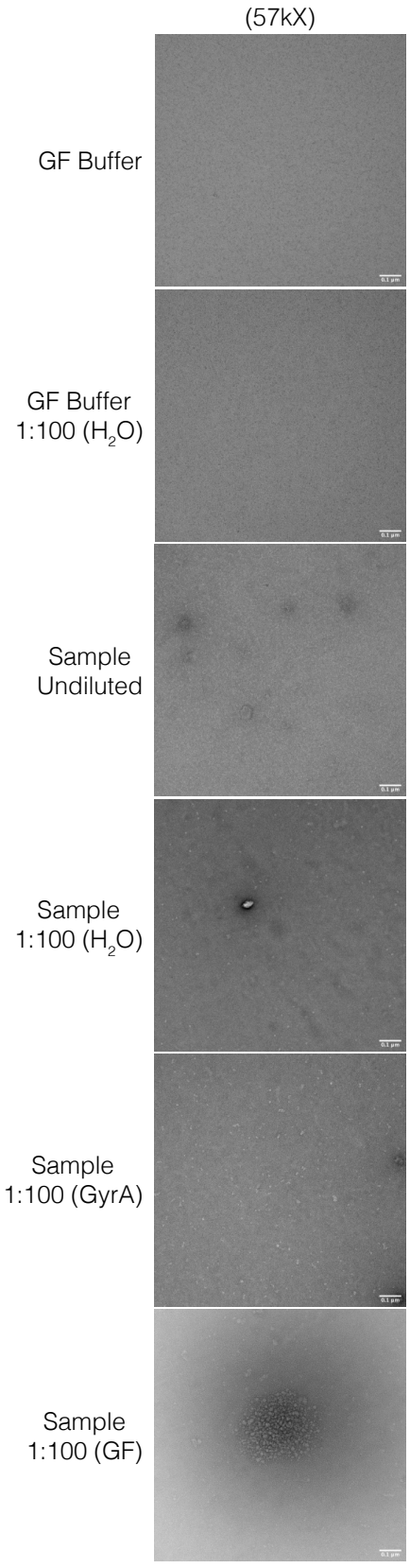

Figure 4.16 Dilution of NRG1B-HF in water or GyrA shows improved contrast in negative stain EM. Micrograph of eluates diluted in varying buffers before negative staining with UA and imaging by TEM. Undiluted sample in SEC (GF) buffer indicates this buffer masks protein particles. Dilutions in water or GyrA provided the best signal-to-noise ratios. Dilution in SEC (GF) buffer resulted in aggregation. This work was carried out by

Jake Richardson (Jake Richardson, personal communication with permission).

4.8 Nonidet™ P-40 substitute absorbs at 280 nm, does not elute as micelles

As there was evidence of protein-detergent complexes being formed between NIDP40 and NRG1B-HF, this meant that NIDP40 micelles could be eluting with NRG1B-HF during SEC. Therefore, NIDP40 was subjected to concentration and SEC in parallel with purified NRG1B-HF. To evaluate NRG1B-HF in a detergent-less context, it was purified with the optimized HEPES-based buffer condition and NIDP40 was decreased from 0.5% to 0% during bead washing steps (Figure 4.17A). To generate the NIDP40 control, HEPES-based wash buffer with 0.5% NIDP40 was concentrated in the absence of NRG1B-HF. Both the NRG1B-HF eluate and HEPES-based wash buffer with 0.5% NIDP40 were concentrated by centrifugation with water pre-incubated ultrafiltration devices.

When concentrated down to ~ 200 µL , the retentate of NRG1B-HF and the NIDP40 control were evaluated for UV absorbance at 280 nm. Indeed, NIDP40 measured 6.36 mg/mL (A_{280}), while NRG1B-HF measured 0.32 mg/mL (A_{280}) (Figure 4.17B). These data indicate that NIDP40 absorbs UV light at 280 nm, likely attributable to the presence of an aromatic ring in the molecular structure (Figure 4.17D). More importantly, these data indicate that the presence of NIDP40 in NRG1B-HF samples is resulting in overestimations of recovery.

Additionally, filtrate of the NIDP40 control measured 1 mg/mL (A_{280}). This indicates that NIDP40 does pass through the 50 kDa MWCO concentrators to some degree, likely as ~ 650 Da monomers (data not shown). However, the majority of NIDP40 did seem to be retained. As the aggregation number of NIDP40 is 100-155, micelles would be 60-100 kDa, which is above the MWCO for these concentrations. Therefore, when NIDP40 is included in elution buffer, NIDP40 micelles are likely present with NRG1B-HF protein after concentration of eluates.

To determine whether NIDP40 micelles elute at the same time as NRG1B-HF, the concentrated NRG1B-HF sample and the NIDP40 control were subjected to SEC. A broad elution peak for concentrated NIDP40 is observed from ~ 22 mL until the end of the chromatogram (Figure 4.17C). These data indicate that NIDP40 does not elute as micelles with NRG1B-HF near ~ 15-16 mL. Conceivably, NIDP40 dissociates into smaller molecules that elute as they are diluted during SEC. Furthermore, these data

correlate with the trail observed in Figure 4.13B and Figure 4.15B. Therefore, it is unlikely that detergent micelles are eluted with NRG1B-HF during SEC.

Notably, although NRG1B-HF was present in SDS-PAGE after elution from agarose beads (Figure 4.17A) no peak for NRG1B-HF was observed during SEC (Figure 4.17C). These data may indicate that NRG1B-HF stability was perturbed when detergent was washed away during elution. Therefore, the presence of detergent appears to be important for NRG1B-HF recovery.

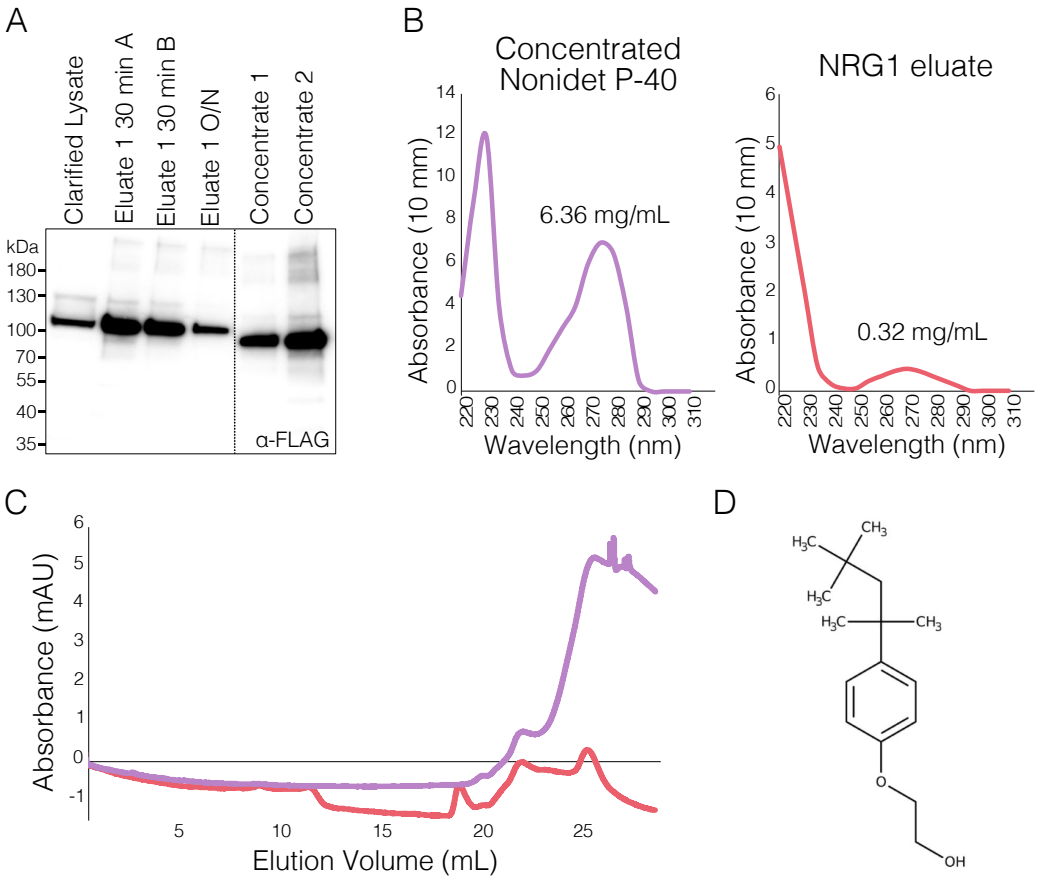

Figure 4.17 NIDP40 absorbs at 280 nm and does not elute as micelles. (A) SDS-PAGE and anti-FLAG® western blot of purification samples performed with optimized protocol from Figure 4.15. (B) Absorbance spectra of concentrated NIDP40 absorbs at 280 nm. (C) Chromatogram of NIDP40 subjected to SEC which elutes > 20 mL. (D) Structure of NIDP40 contains an aromatic ring.

As each purification yielded a variety of results in SEC, elution peaks (annotated Peak A – D) from Figure 4.7B, Figure 4.9B, Figure 4.13B, and Figure 4.15B were compared to better understand what was facilitating the most optimal NRG1B-HF yields. Peak A (Figure 4.7B) was performed with 0.1% Tween-20® in the lysis and wash buffers, but no detergent was present in the SEC buffer. Peak B (Figure 4.9B) was performed with 0.1% Tween-20® in the lysis, wash, and SEC buffers. Peak C

(Figure 4.13B) was performed with 0.1% NIDP40 in the lysis and wash buffers, but no detergent in SEC buffer. Peak D (Figure 4.15B) was performed with 0.5% NIDP40 in the lysis buffer and wash buffers, but no detergent in the SEC buffer. Notably, the salt peak at 19 mL is consistent between each purification, and the trail in Peak C and Peak D reach a similar mAU plateau, indicating reproducible elution of NIDP40 monomers. Peak A and Peak C both used 0.1% detergent during lysis, Tween-20® and NIDP40 respectively, and both showed an NRG1B-HF elution peak below 20 mAU. However, CBB-staining indicates that inclusion of 0.1% Tween-20® in the GF buffer (Peak B) and 0.5% NIDP40 during lysis and washing (Peak D) resulted in better yields of NRG1B-HF. Importantly, Tween-20® does not absorb at 280 nm. These data indicate that optimal NRG1B-HF recovery is dependent upon the presence of detergent in buffers.

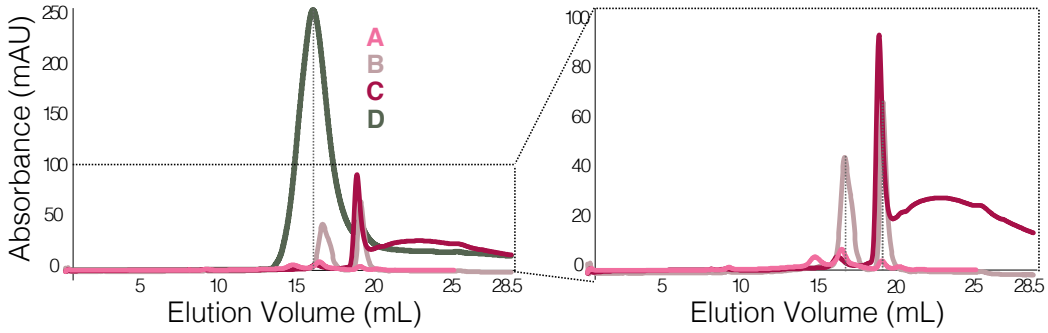

Figure 4.18 Detergent in SEC and lysis buffers influences elution peaks. Comparison of SEC chromatogram peaks during purification optimisations. Peak A (Figure 4.7B) was performed with 0.1% Tween-20® in the lysis and wash buffers, but no detergent was present in the SEC buffer. Peak B (Figure 4.9B) was performed with 0.1% Tween-20® in the lysis, wash, and SEC buffers. Peak C (Figure 4.13B) was performed with 0.1% NIDP40 in the lysis and wash buffers, but no detergent in SEC buffer. Peak D (Figure 4.15B) was performed with 0.5% NIDP40 in the lysis buffer and wash buffers, but no detergent in the SEC buffer.

4.9 NRG1B does not self-associate, but purifies as three higher-order species

To investigate the MW of purified NRG1B-HF, samples were run for Blue native PAGE (BN-PAGE) analysis. In contrast to negative stain EM data, which shows the presence of NRG1B-HF monomers, samples from Figure 4.7 (Figure 4.19A) and Figure 4.9 (Figure 4.19B) showed that several species were eluting during SEC. One species was between ~ 146 and ~ 242 kDa, a second between ~ 242 and ~ 480 kDa, and a third between ~ 480 and ~ 720 kDa MW markers. As the predicted MW of NRG1B-HF is ~ 99 kDa, these data indicate that NRG1B-HF is purifying not as a monomer, but in higher-order states. It is conceivable that these species represent

dimers (~ 200 kDa), tetramers, (~ 400 kDa), and hexamers (~ 600 kDa) of self-associated NRG1B-HF. It is also possible that these MWs reflect complexes of NRG1B-HF with other proteins or detergent molecules.

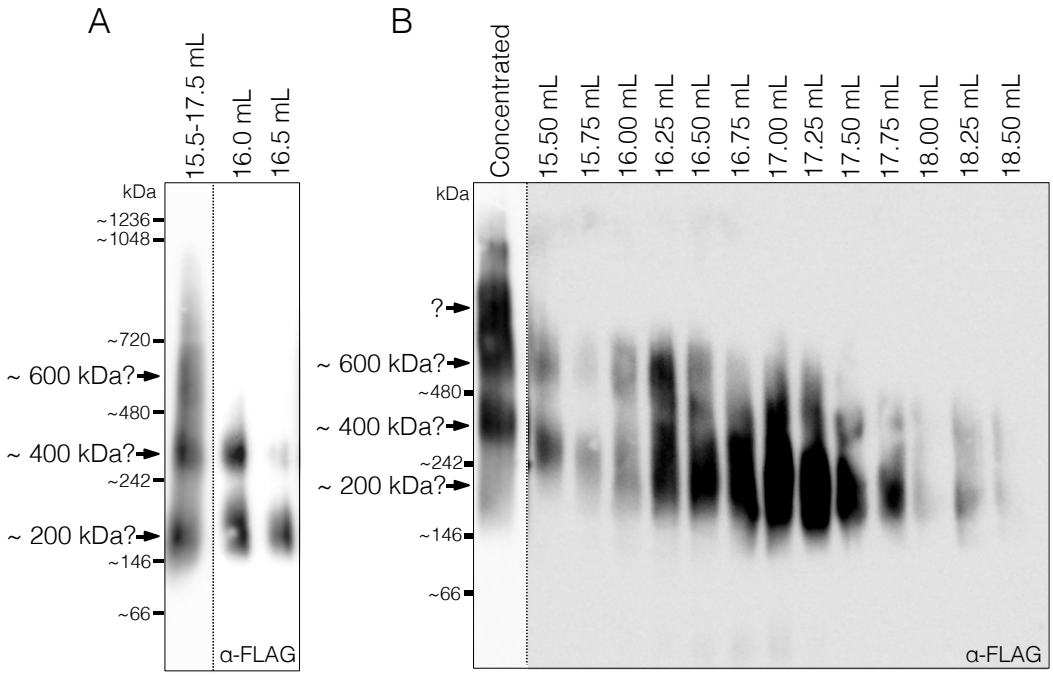

Figure 4.19 Higher-order species of NRG1B-HF are observed in BN-PAGE. BN-PAGE and anti-FLAG® western blot of NRG1B-HF SEC peak fractions followed. Three bands are visualized ~ 200, ~ 400, and ~ 600 kDa. (A) Fractions after SEC from purification in Figure 4.7. (B) Fractions after SEC from purification in Figure 4.9. A band at an unknown MW is indicated with a "?" as markers above ~ 480 kDa were not visualized in this blot.

To evaluate whether the higher-order species of NRG1B-HF observed in BN-PAGE were indeed self-associated dimers, tetramers, and hexamers, co-immunoprecipitation (co-IP) assays after transient in *N. benthamiana* were performed. Lysates with NRG1B-Myc and NRG1B-GFP were incubated with anti-GFP or anti-Myc agarose beads, which were then heated in SDS sample buffer. Supernatants were resolved by SDS-PAGE and immunolabelled. Notably, NRG1B-GFP does not associate with NRG1B-Myc, while NRG1B-Myc does not associate with NRG1B-GFP (Figure 4.20). These data indicate that NRG1B does not self-associate.

However, these data may be unreliable as co-delivery of NRG1B-GFP with EDS1-V5, SAG101-Myc, and HopQ1 does not recapitulate HR in *N. benthamiana nrg1* or *epss* mutants (Figure 4.21). This is in contrast to the recapitulated HR with NRG1B-HF (Figure 4.2). These data indicate that the GFP tag on NRG1B-GFP may

interfere with function. Therefore, it is possible that self-associations are not observed in this assay when they otherwise would be with a functional tag.

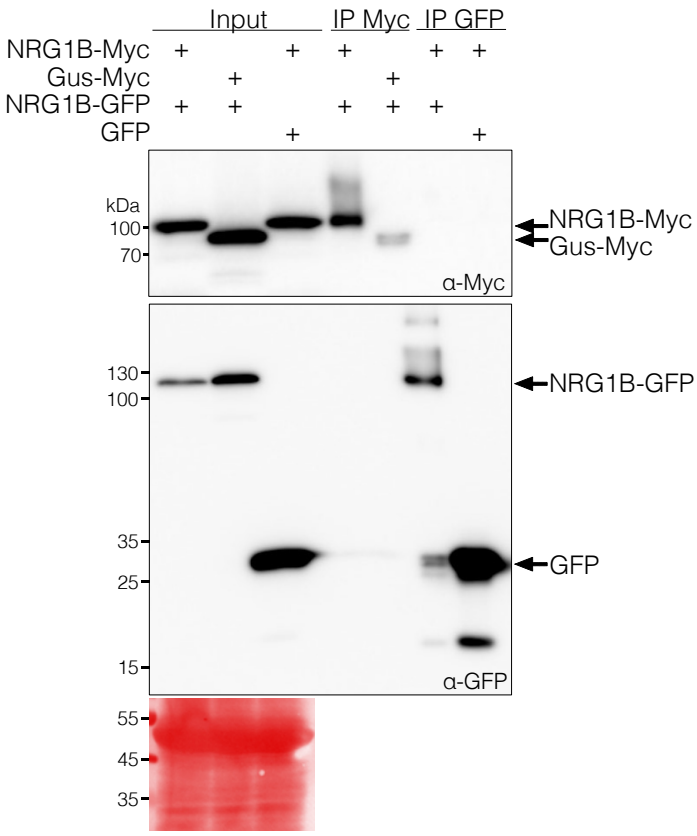

Figure 4.20 NRG1B does not self-associate. SDS-PAGE and western blot of co-IP with 35S promoter-driven NRG1B-GFP and NRG1B-Myc after *Agro*-infiltration and transient expression in *N. benthamiana*. Anti-Myc and anti-GFP IPs were anti-Myc and anti-GFP immunolabelled. NRG1B-GFP did not co-IP with NRG1B-Myc, and NRG1B-Myc did not co-IP with NRG1B-GFP.

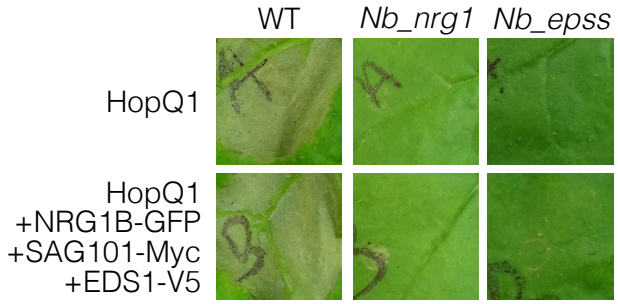

Figure 4.21 NRG1B-GFP does not recapitulate HR with EDS1 and SAG101. Leaf images of HR assays by *Agro*-infiltration in *N. benthamiana* leaves. HopQ1 infiltration shows an HR when infiltrated into WT tissue. Co-delivery of Arabidopsis alleles of NRG1B-GFP, SAG101-Myc, and EDS1-V5 with HopQ1 does not recapitulate HR in *nrg1* or *eds1_pad4_sag101a_sag101b* (*epss*) mutant leaves. Refer to Figure 4.2 which shows that co-delivery of Arabidopsis alleles of NRG1B-HF, SAG101-Myc, and EDS1-V5 with HopQ1 recapitulates HR in *epss* or *nrg1* mutant *N. benthamiana*.

It is possible that self-associations of NRG1B depend on the presence of additional components. As mentioned, Arabidopsis NRG1 requires genetically compatible *At*EDS1 and *At*SAG101 alleles to recapitulate HR in *N. benthamiana* (Lapin et al., 2019). Contrasting the lack of NRG1B self-associations observed in Figure 4.20, a separate co-IP after transient expression in *N. benthamiana* shows that *At*NRG1B-Myc associates with *At*NRG1B-V5 in the presence of HA-*At*EDS1 (Figure 4.22). These data may indicate that NRG1 self-associations are EDS1-dependent. However, additional experiments are required to directly test whether the self-associations observed in Figure 4.22 are due to the use of different protein fusion tags or the presence of *At*EDS1.

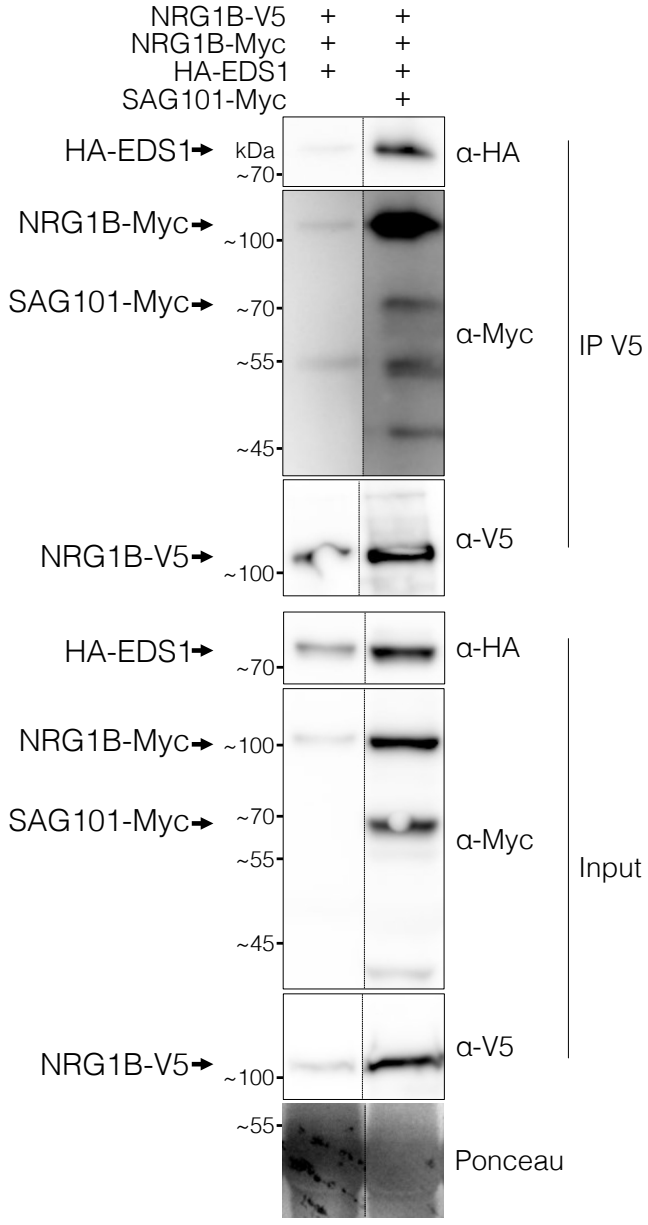

Figure 4.22 NRG1 self-associates in the presence of EDS1. SDS-PAGE and western blot from co-IP of NRG1B-Myc, HA-EDS1, and SAG101-Myc

after *Agro*-infiltration and transient expression in *N. benthamiana*. Anti-V5 IP was anti-HA, anti-Myc, and anti-V5 immunolabelled. Dotted black line indicates cropping of membranes at same exposure.

It is also possible that the higher-order states observed for NRG1B-HF in BN-PAGE are attributable to the presence of additional components. Indeed, HA-EDS1 co-IPs with NRG1B-V5, in the presence or absence of SAG101-Myc. Notably, SAG101-Myc co-IPs with NRG1B-V5 in the presence of HA-EDS1. Additionally, higher accumulation was observed for HA-EDS1, NRG1B-Myc, and NRG1B-V5 when co-expressed with SAG101-Myc. These data may indicate that NRG1 associates with EDS1 and SAG101. However, as purification of *At*NRG1B-HF from *N. benthamiana* was performed in the absence of *At*EDS1 and *At*SAG101, and as *N. benthamiana* homologs were not identified as co-purifying components, it is unlikely that the higher-order states observed in BN-PAGE can be attributed to EDS1-SAG101 associations with NRG1. The potential for NRG1 associations with EDS1 and SAG101 will be covered in more detail in chapter 5 of this thesis.

4.10 NRG1B-HF particles are not observed in vitreous ice cryo-EM grids

To evaluate whether it would be possible to visualize NRG1B-HF particles in cryo-EM grids, vitreous ice sample preparations were attempted with purified NRG1B-HF. Eluates from Figure 4.29 (top right) were first evaluated for the presence of particles by negative stain EM, which again showed uniform, rounded blobs with consistent sizes and shapes that were more distinct when diluted (Figure 4.23A). Notably, this sample was purified in the absence of glycerol which can decrease contrast in cryo-EM grids (Drulyte et al., 2018). However, cryo-EM images did not show obvious evidence of NRG1B-HF particles (Figure 4.23B). This is not likely due to an issue with the quality of the sample submitted, as ice on the grids formed well and did not crystallize. The images show “black blotches” due to “mushroom clouds” of water evaporating and freezing again. However, as particles indicative of NRG1B-HF were not observed, no further cryo-EM preps were attempted. Importantly, a negative result was expected due to the small size of NRG1B-HF protein and the technical limitations of the microscope available. These data were collected to confirm that expectation.

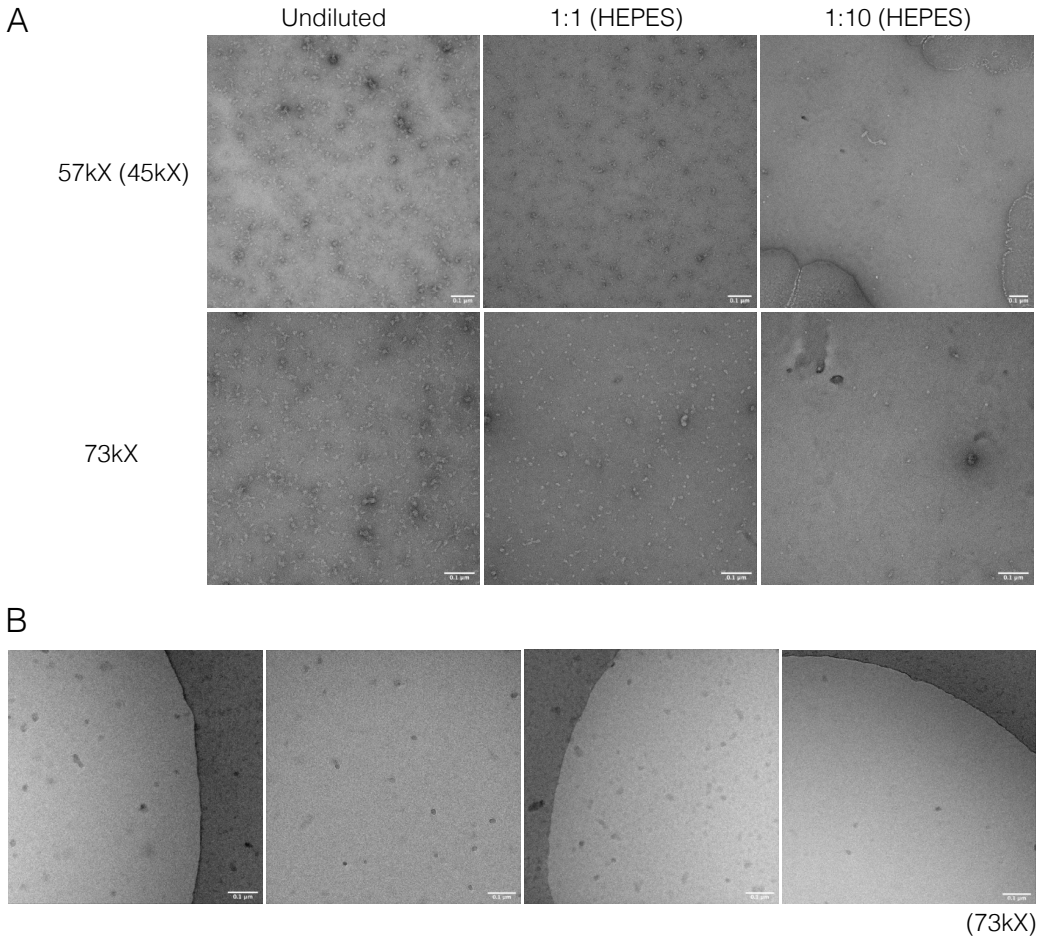

Figure 4.23 NRG1B-HF particles are not observed in vitreous ice cryo-EM grids. Micrograph of eluates from Figure 4.29 (right) were stained with UA and imaged by TEM. Uniform, rounded blob particles are evidence by deceases in density upon further dilutions. (B) Vitreous ice samples were prepared with samples from (A). No particles are visualized. Black blotches are observed, likely due to mushroom clouds of water evaporating and re-freezing. This work was carried out by Jake Richardson (Jake Richardson, personal communication with permission).

4.11 Collaborators unable to visualize NRG1B-HF particles in negative stain EM

Although the TEM microscope available through the JIC Bioimaging Platform does have cryo-EM capabilities, it is missing advanced technical features that may be required to detect proteins at ~ 99 kDa. Thus, an attempt was made to send purified protein to collaborators of the structural biologist Professor Jijie Chai in China. Protein was purified using the optimized conditions in Figure 4.15. Notably, the presence of contaminating bands was more pronounced in the peak elution fractions compared to previous purifications. This may be attributable to the use of a new stock of anti-FLAG® agarose beads, quality of plants infiltrated, or issues with low expression of NRG1B-HF; however, the definitive cause was not determined.

As NIDP40 should not absorb light at 205 nm, A_{205} was evaluated in an effort to more accurately quantify NRG1B-HF. Peak elution fractions from 12-14.25 mL were combined and concentrated from ~ 2.5 mL at 0.042 mg/mL (A_{205}) to ~ 350 µL at 0.465 mg/mL (A_{205}). Possibly, some absorbance at 205 nm is attributable to contaminating proteins. Negative stain EM showed uniform, rounded blobs with consistent sizes and shapes that were more distinct when diluted (Figure 4.24). These data indicated that NRG1B-HF protein was purified and that the sample was suitable to send to collaborators. Therefore, the remaining sample was flash frozen and shipped to Beijing on dry ice.

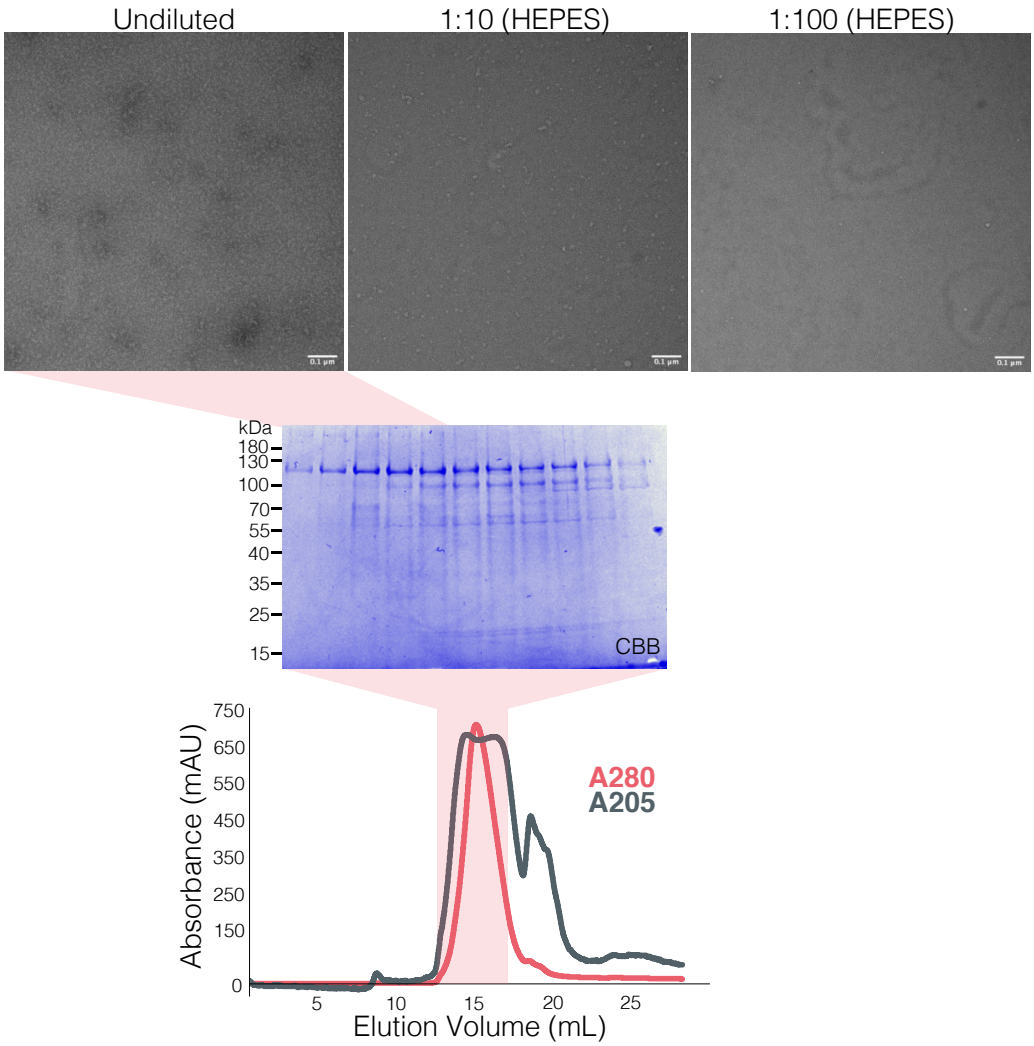

Figure 4.24 Negative stain EM of purified NRG1B-HF before submission to collaborators. Micrograph of NRG1B-HF eluates on EM grids after purification with the optimized protocol described in Figure 4.15 (Appendix III). Peak fractions were resolved by SDS-PAGE and stained with CBB to visualize NRG1B-HF. Fractions were collected, combined, and concentrated before negative stain EM. Dilutions in HEPES buffer correlate with a decrease in density of probable particles. EM images collected by Jake Richardson (Jake Richardson, personal communication with permission).

However, our collaborators noted issues with the quality of the sample that meant they did not prepare cryo-EM grids. They reported that the band visualized in SDS-PAGE migrated faster than what is observed in our SDS-PAGE. Yet, the band in their gel migrated just above the ~ 95 kDa marker, correlating to ~ 99 kDa of NRG1B-HF (Figure 4.25). They reported concern that this band was a contaminating protein and not NRG1B-HF, which contrasted with our interpretations.

Negative stain with UA by the collaborators did show the presence of protein particles on EM grids (Figure 4.25). However, they noted aggregation, likely due to freeze-thawing during shipping. Yet, the sample did arrive with dry-ice present. They indicated that aggregation may be more distinct in frozen samples. They also indicated that the concentration of the sample was too low—possibly due to degradation during shipping. Therefore, the collaborators did not prepare cryo-EM grids with the NRG1B-HF sample submitted.

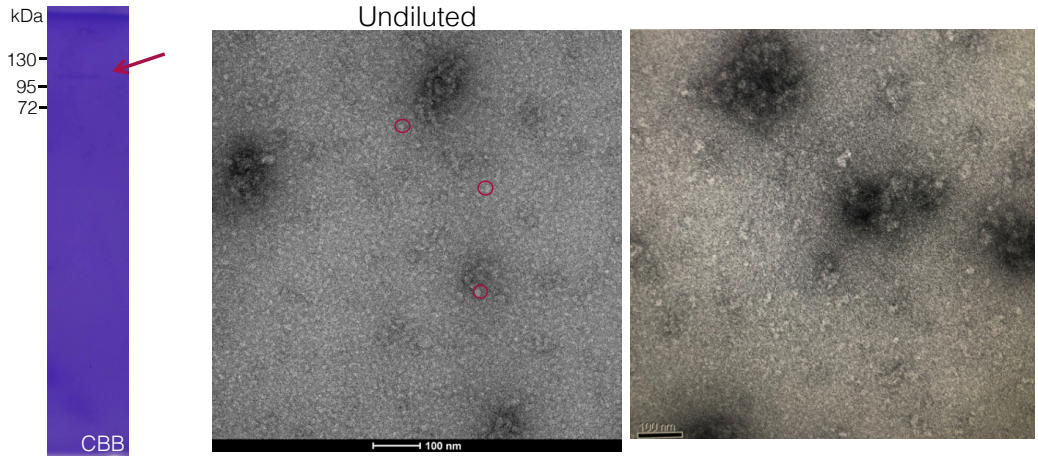

Figure 4.25 Collaborators indicate aggregation of NRG1B-HF in negative stain EM. Data from collaborators. SDS-PAGE and CBB staining of submitted sample (left). TEM micrograph of negatively stained sample (right). This work was carried out by Huang Shijia (Huang Shijia and Jijie Chai, personal communication with permission).

4.12 2D reconstruction of NRG1B-HF particles in negative stain EM grids

As cryo-EM grid preparations were not successful, single particle analysis from negative stain EM grids was attempted. The grids prepared with 1:100 water-diluted NRG1B-HF in Figure 4.15 were imaged using automated EPU (*E Pluribus Unum*) software. The program stopped at 60% through automation for an unknown reason; yet, 374 micrographs were still collected at a resolution of 3.5 Å/pixel. Notably, intense white spots were visible that were not particles of interest Figure 4.26. An initial

attempt to generate 2D reconstructions from these data by Dave Lawson (herein D.L.) revealed that the images had overloaded pixels. D.L. indicated that the software which generates 2D classifications focused on these intense white areas, rather than the particles which were less defined. Therefore, good 2D classifications were inhibited by these intense white spots on negative stain EM grids.

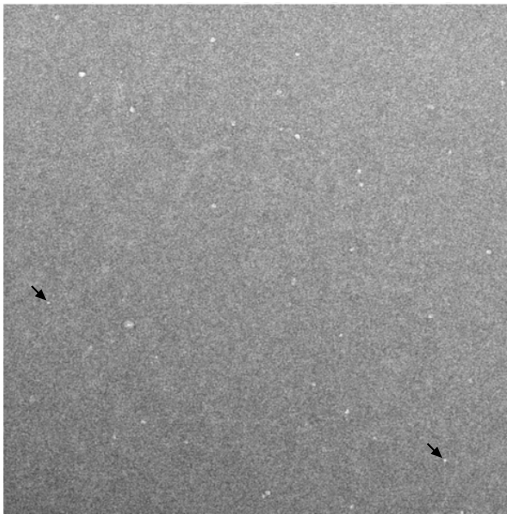

Figure 4.26 High-intensity white artefacts are observed in negative stain EM. Micrograph of quadrant from EPU run of negative stain EM grids. High-intensity white spots are indicated with black arrows. This work was carried out by Jake Richardson and Dave Lawson (Jake Richardson and Dave Lawson, personal communication with permission).

In a second attempt, D.L. processed the data with cryoSPARC (version 2.15.0) and used particle-picking software to generate 2D classifications from probable NRG1B-HF particles. These particles correlated in size with the predicated diameter of NRG1B-HF monomers at ~ 6.5 nm. D.L. noted that this approach could mean a higher likelihood for falsely-identifying background noise as NRG1B-HF particles. Initially, D.L. searched for elliptical blobs that might correspond to monomers or dimers with diameters in the range 40-120 Å. D.L. used several rounds of 2D classification to filter the least probable classes, but found that none were well defined. D.L. discarded classes with intense white features as they likely corresponded to the white spots in Figure 4.26. D.L. then fed the remaining 273 k particles into an initial model job requesting 3 classes (Figure 4.27). He indicated that the first two classes looked similar but were probably too small for NRG1B-HF (Figure 4.27A, upper, middle). The third “tadpole” class (Figure 4.27A, lower) was made up of 112 k particles and had some features that could be indicative of a real structure rather than noise. Corresponding 2D class averages for the tadpole class were generated, though

they were not well resolved (Figure 4.27B). Thus, they were processed for homogeneous refinement (Figure 4.27C) and a 2D reconstruction map was generated.

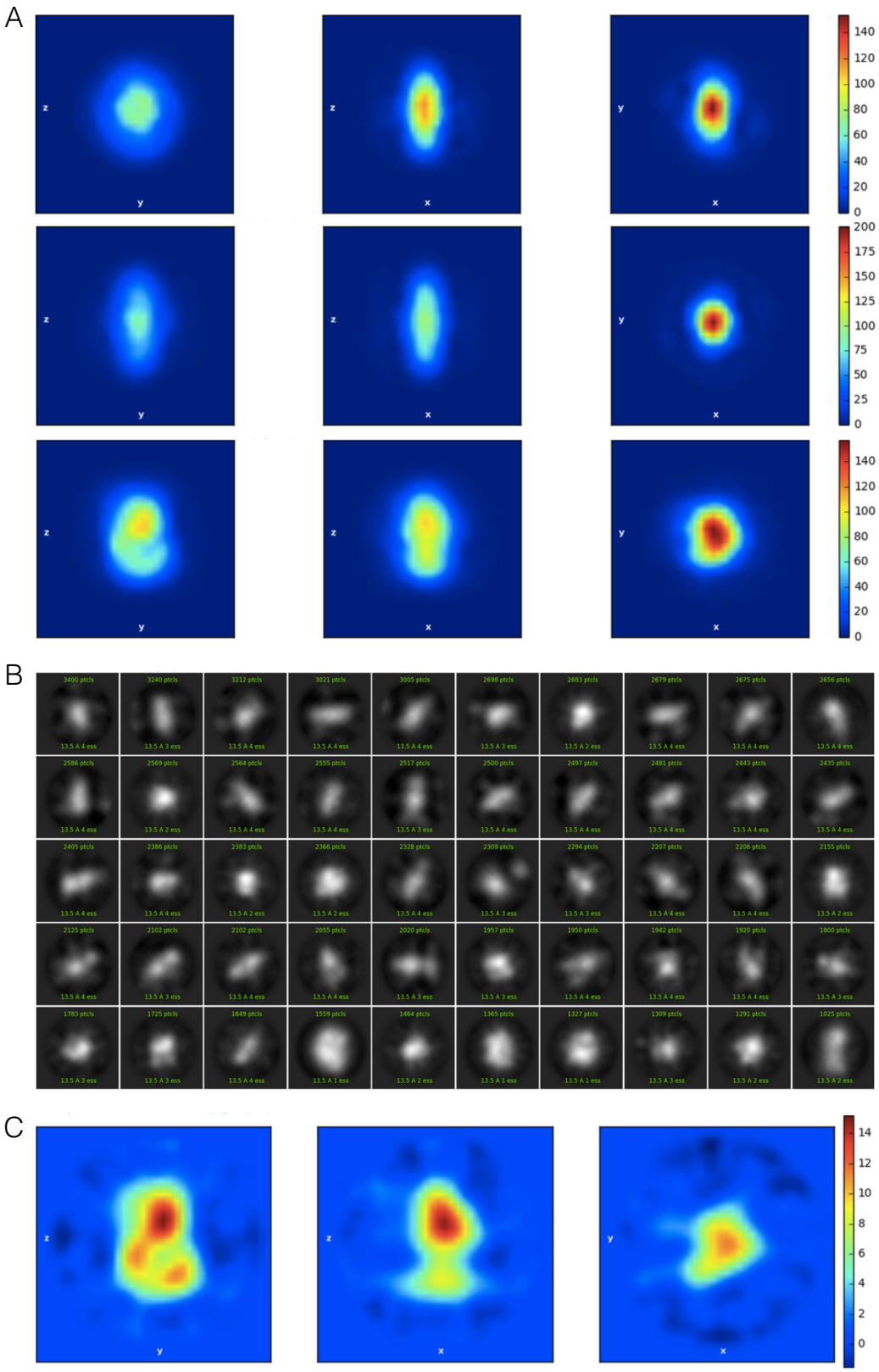

Figure 4.27 2D classifications generated by Dave Lawson. Orthogonal sections for three 2D classifications generated with cryoSPARC version

2.15.0 from 374 micrographs collected at a resolution of 3.5 Å/pixel. First two classes (top and middle) were discarded. “Tadpole” class (bottom) made of 112 000 particles was continued. (B) Corresponding 2D class averages for tadpole class. (C) Homogeneous refinement of 112 000 tadpole particles. This work was carried out by Dave Lawson (Dave Lawson, personal communication with permission).

D.L. generated a homology model of NRG1 using SwissModel and the activated ZAR1 structure (PDB: 6J5T) as a template, which shares ~ 19% sequence identity. The homology model was fit to the NRG1 2D reconstruction map (Figure 4.28). D.L. tested other homologues with different conformations, but the model in Figure 4.28 represented the best fit. He indicated that the NRG1 model included a number of initial surface loops that weren’t present in the template structure. Therefore, these loops were removed from the model as they projected out of the map. These data indicate that likely it is NRG1B-HF particles observed on negative stain EM grids. However, the resolution of this map is too low for detailed mechanistic insights. More data is required to better resolve an NRG1B-HF monomer structure, if it will be possible by EM techniques at all.

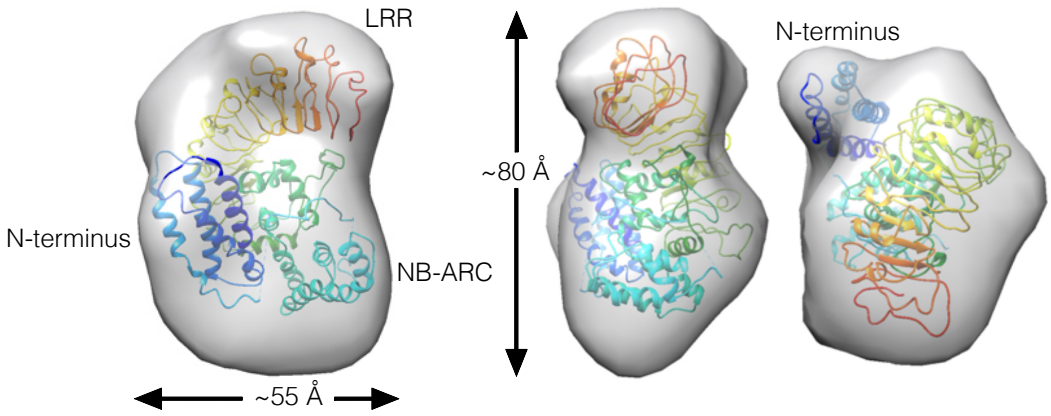

Figure 4.28 Reconstruction map fits NRG1B-HF homology model. Map generated from 2D classifications in Figure 4.27. Homology model (inside map) created with SwissModel with template from 6J5T. This work was carried out by Dave Lawson (Dave Lawson, personal communication with permission).

4.13 SEC peak-shifts not observed for NRG1 after incubation with ADP or dATP

It is thought that NLRs exchange ADP for ATP upon activation, which correlates with oligomerization (Takken and Tameling, 2009). Indeed, the inactive ZAR1-RKS1 monomers bind ADP, while formation of the activated ZAR1-RKS1-PBL2^{UMP} resistosome was induced in the presence of ATP or dATP (Wang et al., 2019b, Wang

et al., 2019a). NRG1B-HF eluates were incubated with dATP or ADP to investigate whether the addition of nucleotides affects the shape or size of NRG1B-HF during SEC. The purifications were performed with a higher resolution Superdex S200 Increase 10/300 GL column (fractionation range 10-600 kDa). NRG1B-HF eluted at ~ 12 mL with this column, and no peak shifts were observed upon incubation with dATP nor ADP (Figure 4.29). A novel peak at ~ 21 mL was observed in the dATP- and ADP-treated samples—likely this represents elution of the ADP or dATP nucleotides.

Two purifications were attempted on separate occasions. In the first attempt, NRG1B-HF protein was lost during concentration after the initial SEC run (Figure 4.29, left). It was not yet known that concentrators required water pre-incubation or that NRG1B-HF losses were minimized in the presence of NIDP40. Thus, no NRG1B-HF peak is observed at ~ 12 mL in the dATP- or ADP-treated traces. The presence of NRG1B-HF was therefore confirmed by immunoblot. Paradoxically, NRG1B-HF is only present at ~ 12 mL in the ADP-treated sample. Moreover, NRG1B-HF is present at ~ 21 mL in both the dATP- and ADP-treated samples, although SDS-PAGE indicates MW is still ~ 100 kDa. A vitamin B (1.3 kDa) standard elutes at ~ 20 mL on this column, which roughly correlates to the MW of ADP/dATP at 650 Da. Therefore, likely the peak at ~ 21 mL is unbound ADP or dATP.

In a second attempt, fractions were collected after SEC and NIDP40 was added to 0.5% prior to concentration with water pre-incubated concentrators (Figure 4.29, top right). No significant protein loss was observed. Concentrated NRG1B-HF was split into three aliquots. An un-treated aliquot was subjected again to SEC in 500 mM NaCl, to better resolve the NRG1B-HF peak (Figure 4.29, second from the top, right). The other aliquots were incubated with dATP or ADP and also subjected to SEC in 500 mM NaCl (Figure 4.29, right bottom). Again, no peak shifts were observed at ~ 12 mL between samples. Likewise, a novel peak at ~ 21 mL was present for the dATP- and ADP-treated samples. As the peak height for NRG1B-HF at ~ 12 mL is unchanged between samples, it is unlikely that the peak at ~ 21 mL is attributable to NRG1B-HF absorbance. These data indicate that NRG1B-HF does not bind ADP nor dATP, or that no changes in size or shape occur upon binding.

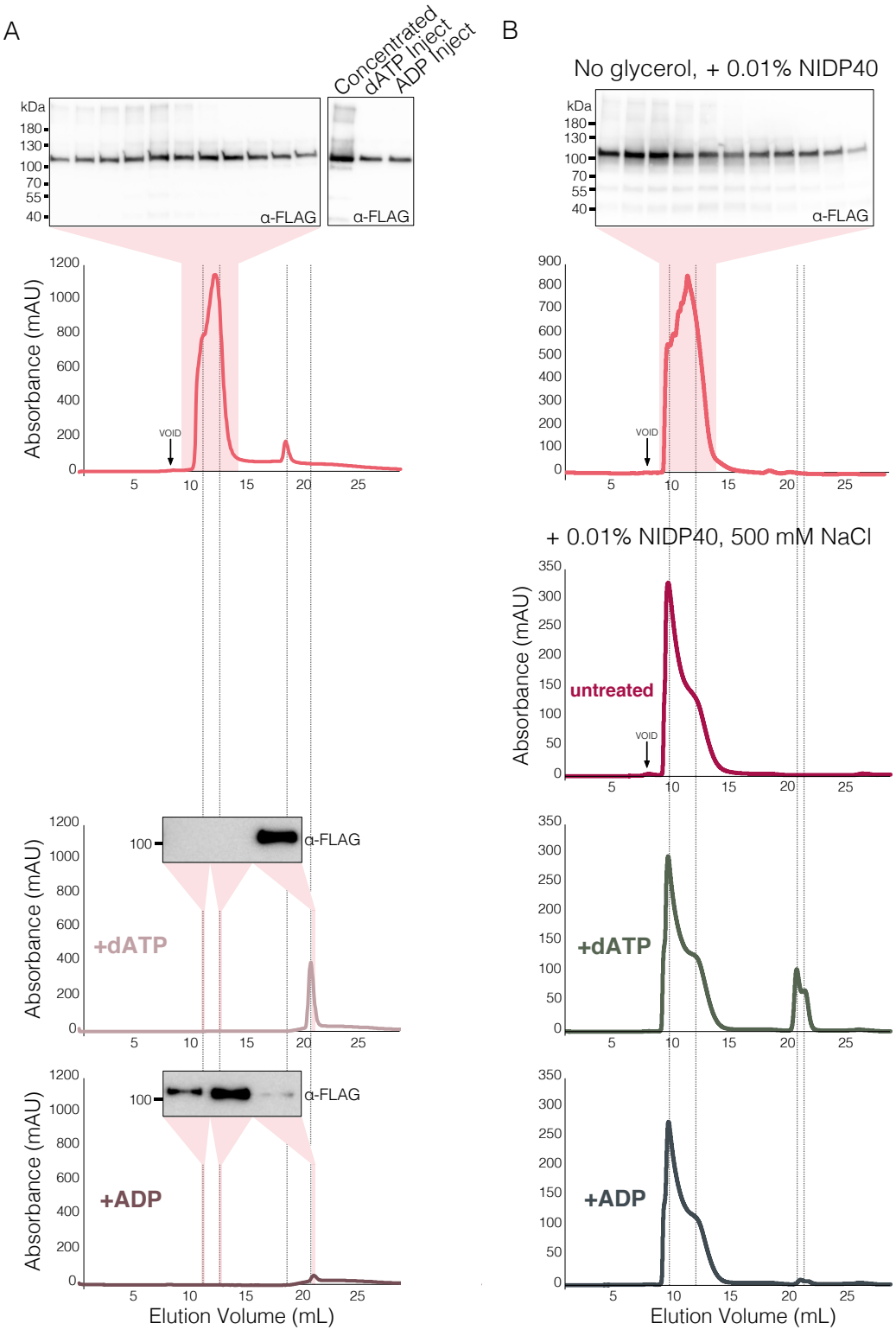

Figure 4.29 SEC peak shifts not observed after incubation with nucleotides. NRG1B-HF was purified with optimized buffer conditions with differences indicated above chromatograms. (A) SDS-PAGE and anti-FLAG® western blot (top) of peak fractions which were combined and concentrated (water pre-incubated concentrators were not used) and split into two 190 µL aliquots incubated either with 2 µL 0.1 M dATP (20 min) or 2 µL 0.1 M ADP (~ 2.5 h) before SEC. (B) SDS-PAGE and anti-FLAG® western blot (top) of peak fractions which were combined, adjusted to 0.5% NIDP40 and 5% glycerol, and concentrated with water pre-incubated concentrators, then split into three 90 µL aliquots either

untreated or incubated 10 min either with 5 µL 0.1 M dATP or 5 µL 0.1 M ADP before SEC.

4.14 Discussion

4.14.1 Large-scale purification recovers low yields of highly pure NRG1B-HF

Purification by anti-FLAG® IP after *Agro*-infiltration-mediated transient expression in *N. benthamiana* resulted in recovery of highly specific, but low yield, NRG1B-HF protein. Although a low-resolution tadpole-shaped map of NRG1B-HF was reconstructed from 2D class averages of negative stain EM particles, nothing about biological mechanism should be inferred from these data. This tadpole map serves only to provide some confidence that NRG1B-HF particles are being visualized on negative stain EM grids. Due to the technical limitations of the EM microscope available at JIC, collaboration with external groups and application of advanced methodology is likely required for high-resolution structures of NRG1B-HF monomers. Therefore, the optimized purification protocol presented in this chapter provides a foundation for future purifications of full-length NLRs.

Anti-FLAG® IP yielded highly pure NRG1B-HF, yet, recovery was not complete. A single band correlating to the MW of NRG1B-HF was observed in CBB-stained gels after elution, indicating exceptionally pure recovery of NRG1B-HF. However, even when additional bead incubations were added to the protocol, each with three rounds of elution, an excess of NRG1B-HF remained in lysates. Likely, this excess contributed to the high-purity recovery observed. It is conceivable that in excess NRG1B-HF, the anti-FLAG® epitopes on agarose-beads are quickly saturated mediating highly specific IP. Therefore, while recovery was not optimal, it may be the reason for the clean isolation of NRG1B-HF.

Although an accurate method for quantifying NRG1B-HF protein in the presence of NIDP40 was not determined (discussed further in section 4.14.4), optimisation of this protocol may have resulted in yield improvements as much 60×. Bradford protein assay in an early purification indicated recovery of ~ 100 µL at 0.027 mg/mL of NRG1B-HF protein (Figure 4.7B). The final purification for collaborators yielded ~ 100 µL at 1.63 mg/mL (A_{205}) [~ 350 µL at ~ 0.465 mg/mL (A_{205})] (Figure 4.24). However, the material input required to recover this level of NRG1B-HF protein is not feasible as a long-term purification strategy. In the final protocol, ~ 30 g of tissue (~ 90 leaves), 1 mL of anti-FLAG® agarose beads (~ £70), and 80 µL of 3×FLAG® peptide

(~ £15) was required. Moreover, NRG1B-HF often remained un-eluted from anti-FLAG® beads, and potentially some of the 1.63 mg/mL observed in the final purification is attributable to contaminating proteins. Therefore, future investigations of lower-cost and higher-affinity purification strategies for recovery of NRG1B-HF are required

4.14.2 Purification of NRG1B-HF requires the presence of detergent

Notably, NRG1B-HF stability seems to be dependent on the presence of detergent. When Tween-20® was present in the SEC buffer, a much higher elution peak is present than with no Tween-20® included (Figure 4.18). As Tween-20® does not likely absorb UV light at 280 nm, the peak height can be attributed solely to NRG1B-HF. When NIDP40 detergent was washed from eluates before concentration, no peak was observed during SEC (Figure 4.17C). Additionally, protein loss was observed when concentrating detergent-less SEC peak fractions (Figure 4.29, left). This was resolved when NIDP40 was added to 0.5% prior to concentration (Figure 4.29, right). These data indicate that the presence of detergent is important to recover NRG1B-HF protein after transient expression in, and extraction from, *N. benthamiana*.

Membrane proteins are prone to aggregate and precipitate if detergent concentrations are too low (Gimpl et al., 2016). As NRG1 is reported to associate with endomembrane networks (Wu et al., 2019), it may carry an N-terminal transmembrane domain that requires associations with detergents to mimic membranes upon cell lysis. Analysis with SignalP 4.1 software indicated the presence of a transmembrane domain but no signal peptide for NRG1B (Nielsen, 2017). Indeed, Collier et al. (2011) reported the likelihood of an N-terminal transmembrane domain in *Nb*NRG1 and *At*NRG1B alleles (Collier et al., 2011). Moreover, they noted it was unlikely the *Nb*NRG1 allele was cleaved at a signal peptide, as it migrated more slowly than an N-terminal deletion variant in SDS-PAGE. These data support the evidence for a single-pass transmembrane domain at the N-terminus of NRG1.

As mentioned, the first α-helix of HeLo/HELL domain-containing proteins interact in transmembrane oligomers to form a hydrophobic channel (1.3.4). Importantly, these proteins do not insert into membranes prior to prion-domain-induced associations. Conceivably, a predicted transmembrane domain for NRG1 indicates that this protein can insert into membranes but is not constitutively inserted as a single-pass transmembrane protein.

If NRG1 is not a transmembrane protein, why does stability appear affected by detergent presence or absence? Non-ionic detergents like NIDP40 do little to maintain water-soluble proteins in native states as they do not seem to interact (Yang et al., 2014). However, there are exceptions wherein detergents have been found to associate with hydrophobic pockets of proteins. It appears that the N-terminal α-helix bundles of CNLs form a hydrophobic core (Burdett et al., 2019), but it is not likely that these hydrophobic residues are exposed enough to require stabilization via detergent molecules. Other sites for potential hydrophobic patches in NRG1B-HF are not obvious. Notably, Tenthorey et al. (2017) used a non-ionic detergent to purify the mammalian NLRC4/NAIP5 inflammasome from cell cultures, and Martin et al. (2020) used NIDP40 to purify the plant Roq1 resistosome from *N. benthamiana* leaves. However, it is not clear whether they experienced similar issues with protein stability dependent upon detergent. They could have included detergent solely to facilitate membrane solubilization for extraction. The presence of detergent is not indicated in lysis buffers that were used to purify active and inactive forms of ZAR1 (Wang et al., 2019b, Wang et al., 2019a). Nevertheless, while the requirement for detergent remains unclear, inclusion throughout purification proves crucial for recovery of NRG1B-HF.

An approximate 50× increase in elution peak mAU is observed during SEC when 0.5% NIDP40 was used in lysis buffer versus 0.1% NIDP40 (Figure 4.18). Yet, a 50× increase in protein recovery is not indicated. As NIDP40 absorbs UV light at 280 nm, and as the SEC buffer did not include detergent, the higher mAU is likely attributable to NIDP40 associations with NRG1B-HF during lysis. Notably, concentrated NIDP40 does not elute at 16.5 mL (Figure 4.17C). Therefore, the higher mAU of the 16.5 mL peak during SEC of purified NRG1B-HF is not attributable to NIDP40 micelles. Although it is unclear how or where NIDP40 detergent would associate with NRG1B-HF, it seems to be that there are associations that persist from lysis through to SEC.

There is evidence that monomeric concentrations of non-ionic detergents in solution can destabilize proteins (Yang et al., 2014). However, maintaining concentrations above CMC facilitates native protein conformations. The concentration of NIDP40 is kept above its CMC throughout purification with 0.5% NIDP40 in the lysis buffer. However, the concentration of NIDP40 during purifications with 0.1% drops below its CMC during buffer exchange before concentrating eluates, and again during SEC. Potentially, transitioning from above CMC to below and back again is deleterious

to protein stability. Therefore, the lower mAU for the NRG1B-HF peak observed in purifications with 0.1% NIDP40 may be attributable to, (1) fewer NRG1B-HF associations with NIDP40, (2) protein destabilization and loss due to drops below CMC, or (3) both. Therefore, it is recommended to keep the concentration of detergent above CMC throughout purification to avoid protein loss.

4.14.3 Water pre-treatment of concentrators improves NRG1B-HF recovery

Pre-incubation of centrifugal concentrators with water contributed to protein recovery (Figure 4.14), yet, it is not clear why this was so effective. Although the 2 mL and 4 mL concentrators are made of the same materials (regenerated cellulose membranes and polypropylene tubes), the 2 mL concentrator showed protein loss after water pre-incubation while the 4 mL did not. The 2 mL collection tubes seem to have a lower surface area than the 4 mL collection tubes. It is conceivable that protein is lost to the walls of the collection tubes. This may explain the consistent decrease in protein recovery in all 2 mL pre-incubation treatments. Alternatively, the 0.5 mL concentrator membranes are made of polyethersulfone. While pre-incubation of the 0.5 mL concentrator with Tween-20® was not tested, a decrease in protein recovery with NIDP40 pre-incubation was observed when compared to water. These data may explain the protein losses in early purifications, as those included concentrators that were pre-incubated with wash buffer, which either contained Tween-20® or NIDP40. Importantly, both pre-incubation with water and detergent independently contributed to improved NRG1B-HF recovery. Purifications wherein detergent was washed away showed losses even with water pre-incubated concentrators (Figure 4.17C). Therefore, water pre-treated 4 mL and 0.5 mL concentrators should be used to concentrate NRG1B-HF protein in the presence of detergent.

4.14.4 Quantification of NRG1B-HF in the presence of NIDP40 is not optimized

It was not determined until late in this project that NIDP40 absorbs UV light at 280 nm (Figure 4.17B). Therefore, the concentration of NRG1B-HF in the presence of NIDP40 is over-estimated when measuring A_{280}. Absorbance at this wavelength is mediated primarily by the presence of aromatic rings in amino acids. Indeed, the structure of NIDP40 clearly shows the presence of an aromatic ring (Figure 4.17B, D). Thus, follow-up work is required to determine an accurate method for quantifying NRG1B-HF recovery in the presence of NIDP40.

It is also possible to quantify protein by measuring absorbance at 205 nm, primarily mediated by peptide bonds in amino acids. NIDP40 does not contain peptide

bonds (Figure 4.17D); therefore, A_{205} was used to quantify NRG1B-HF recovery before shipping protein to collaborators (Figure 4.24). However, they indicated that the concentration of NRG1B-HF protein was much lower than we reported (Figure 4.25). One possibility is that the protein degraded during shipping, as they suggested, but it is also possible that A_{205} is not an accurate method for quantifying protein. Therefore, A_{205} should be directly tested for NIDP40 to determine whether this protein quantification method is accurate.

Other options could be explored for quantifying NRG1B-HF recovery in the presence of NIDP40. Bradford protein assays alongside BSA standards, as was done in early purifications (Figure 4.7B), may be the most reliable methodology. Additionally, NIDP40 could be exchanged for other non-ionic detergents that do not absorb UV light. While current yields seem sufficient for negative stain EM, higher accuracy quantification of NRG1B-HF protein may be crucial for setting up future collaborations. Likely, collaborators will require a minimum quantity of protein before they invest time and resources to solve structures by cryo-EM. Therefore, it will be important to know with greater certainty how much NRG1B-HF is being recovered.

4.14.5 dATP/ADP treatment does not influence NRG1B-HF elution during SEC

NRG1B-HF was incubated with nucleotides to investigate whether an inactive or active form could be stabilized and purified. Theoretically, ADP may stabilize inactive forms of NRG1B-HF, while dATP may stabilize oligomers. However, peak shifts that would indicate changes in size/shape for NRG1B-HF after incubation with dATP or ADP were not observed (Figure 4.29). Notably, a novel peak at ~ 21 mL is observed in those samples with dATP or ADP added. This peak is likely the unbound nucleotides—molecules that elute at ~ 20 mL on this column are expected to have a MW of ~ 1 kDa. Indeed, the MW of dATP or ADP is ~ 650 Da. Curiously, SDS-PAGE confirmed the presence of NRG1B-HF in the ~ 21 mL peak. This was unlikely to be a degradation product as it still migrated near the ~ 100 kDa MW marker. However, this could be attributable to the trailing effect for NRG1B-HF as observed in previous purifications (Figure 4.7). Therefore, future investigations are required to more thoroughly elucidate whether different states of NRG1B-HF are formed upon the addition of dATP or ADP.

4.14.6 The pre-activation state of NRG1 is poorly understood

The purification state of pre-activated NRG1B-HF has not been resolved. Co-IP assays indicate that NRG1B-HF does not self-associate (Figure 4.20), which correlates

with the presence of monomers visualized on negative stain EM grids (Figure 4.24). Yet, BN-PAGE of SEC fractions indicates that NRG1B-HF exists as higher-order species at MWs of ~200, ~ 400, and ~ 600 kDa (Figure 4.19). Notably, in an earlier purification, NRG1B-HF seemed to elute after the ~ 550 kDa RuBisCO complex (Figure 4.7B). These data would indicate that the MW of NRG1B-HF eluting on SEC is near but not > ~ 550 kDa. However, SEC accounts more for shape than size, and a ~ 15% error-range is expected for BN-PAGE. Therefore, the MWs observed for NRG1B-HF after SEC do roughly correlate for the MWs observed in BN-PAGE. Thus, the contrasting data between negative stain EM and BN-PAGE obscures the pre-activation state for purified NRG1B-HF.

Co-IP data indicates that NRG1B does not constitutively self-associate (Figure 4.20). However, co-IPs were performed with GFP- and Myc-tagged NRG1B variants, which were unable to recapitulate HR in transient assays (Figure 4.21). As NRG1B-HF was able to recapitulate HR in the same context (Figure 4.2), these data indicate that the GFP tag renders NRG1B non-functional. The GFP tags fused to NRG1B may be forming dimers which inhibit higher-order self-associations. Indeed, NRG1B fused to monomeric GFP can complement an *nrg1a/b* Arabidopsis mutant (Wu et al., 2019). Perhaps the formation of NRG1B-GFP dimers inhibits further associations with NRG1B-Myc. These data indicate that the pre-activation state for NRG1B-HF has not been rigorously tested in co-IP assays. Therefore, co-IP assays with the functional NRG1B-HF should be directly tested to evaluate NRG1B self-associations.

Notably, NRG1B-V5 was able to associate with NRG1B-Myc in the presence of *At*EDS1 (Figure 4.22). However, this association was not tested in the absence of co-expressed *At*EDS1. It could be that EDS1 mediates NRG1B-NRG1B associations, or that the V5 tag does not interfere with NRG1B self-associations. As *Nb*EDS1 was not identified as a co-purifying component with NRG1B-HF in LC-MS data, it is unlikely that the higher-order states observed in SEC and BN-PAGE are attributable to *At*NRG1B-HF associations with *Nb*EDS1.

The higher MW observed for NRG1B-HF by BN-PAGE and SEC may be attributable to co-purifying components. Indeed, a chaperone subunit did purify with NRG1B-HF after SEC in an early purification (Figure 4.7). The HSC70 chaperone was also later identified to purify with NRG1B-HF after SEC (Figure 4.6D). The MW for each of these components is ~ 70 kDa, which could roughly correlate to the higher-order states observed for NRG1B-HF. It's also possible that the co-purifying UVR8 or VAP (Figure 4.6D) are present in higher-order NRG1B-HF states. UVR8 may

be a homolog of RCC1 (REGULATOR OF CHROMOSOME CONDENSATION 1), which has been co-lost with EDS1, PAD4, and ADR1 in angiosperm genomes (Baggs et al., 2020). However, a role in defence has not been identified. A possible explanation for co-purification of VAPs with NRG1B-HF will be discussed further in section 5.13.7 of this thesis. However, it is not obvious from these data that NRG1B-HF forms higher-order states as heteromers with other components.

As mentioned previously, 30-70% of protein-detergent complexes can be made of bound detergent (Privé, 2009). It could be that detergent associations with NRG1B-HF increase MW. However, as the nature of detergent binding to proteins is dynamic, the presence of distinct bands might not be expected. More likely, BN-PAGE would show "streaking" reflecting many different states of NRG1B-HF-detergent complexes. However, detergent molecules bound to NRG1B-HF would likely be masked during negative stain EM, which could explain why NRG1B-HF monomers are observed with that technique.

If multiple species of NRG1B-HF are being recovered, it should be possible to resolve them by SEC before negative stain EM. Indeed, some separation of the different species is observable (Figure 4.19). However, the fractions often still contained mixtures of different NRG1B-HF states. Future purifications could investigate whether other columns can better resolve NRG1B-HF species. Therefore, whether NRG1B-HF does purify as monomers or higher-order states requires follow-up investigation. This will be discussed in more detail in section 6.3 of this thesis.

4.14.7 An attempt at cryo-EM with collaborators was unsuccessful

Although it is possible that the quantity of protein sent to collaborators of Professor Jiije Chai in Beijing was lower than initially calculated (discussed in 4.14.4), their quality control assays did not match ours. They thought that the band visualized by CBB-staining may have been a contaminating protein, and not NRG1B-HF, as it migrated faster in their SDS-PAGE than ours (Figure 4.25A). However, it is more likely that the use of an alternative MW marker and varying SDS-PAGE conditions explains the migration differences. We also questioned their use of undiluted NRG1B-HF sample to visualize particles by negative stain EM (Figure 4.25B). Perhaps a dilution series would have more confidently shown soluble protein as we observed in our negative stain EM grids (Figure 4.24). Yet, they still saw evidence for protein aggregation, possibly due to freeze-thawing during shipping. They indicated that aggregates might be more distinct in frozen samples, and chose not to proceed with

cryo-EM grid preparations. Therefore, future collaborations could be sought within the UK to ensure protein quality is preserved during shipping.

4.14.8 Low-resolution map of NRG1B-HF generated from negative stain EM

This work resulted in a very low-resolution tadpole map of NRG1B-HF, which fits the NRG1B homology model (Figure 4.28). These data indicate that NRG1B-HF samples imaged on negative stain EM grids do contain NRG1B-HF particles. Collecting more negative stain EM data might eventually provide greater resolution; however, it is unlikely that more than a general shape of the individual domains of NRG1B-HF would be solved. Moreover, as mentioned, it is unlikely that the facilities at JIC will be able to visualize frozen NRG1B-HF particles by cryo-EM. Therefore, the negative stain EM data could be used as preliminary data to set-up a collaboration with a group that has access to cryo-EM microscopes with more advanced technologies.

Notably, Dave Lawson did report the presence of intense white spots—excluded from 2D classifications—on negative stain grids during EPU data collection (Figure 4.26). Intense white spots were independently reported by Jake Richardson in the 0.002% NIDP40 negative stain EM control, although they were sparsely distributed and could have been artefacts of thick UA staining (Figure 4.12). The final concentration of NIDP40 on the EPU-imaged grids would have been ~ 0.002%. Therefore, perhaps different preparations or staining methods will need to be further optimized to reduce NIDP40 background noise. However, it could also be advisable to investigate other non-ionic detergents that do not show intense white spots like NIDP40 upon UA staining.

4.14.9 In summary

The data presented in this chapter describes an optimized purification protocol utilizing transient expression in *N. benthamiana* and anti-FLAG® IP for recovery of highly pure NRG1B-HF. Recovery of NRG1B-HF was found to depend on the presence of detergent in solution. It was also determined that water pre-incubation of protein concentrators improves yields. However, follow-up work is required to resolve the best quantification method for purified NRG1B-HF in the presence of detergent. Future investigations are required to resolve the pre-activation state of NRG1B-HF. Yet, reconstruction of a low-resolution NRG1B-HF map from negative stain EM data indicates that it is present as monomers.

While this project focused primarily on purification of inactive NRG1B-HF species, these data also serve as a foundation for future purifications of activated NRG1 species. Comparison of inactive and activated forms of NRG1 would better inform cell death mechanisms. Indeed, comparing the ZAR1-RKS1 inactive monomer to the activated ZAR-RKS1-PBL2^{UMP} oligomer revealed more details on the activation mechanism (Wang et al., 2019b, Wang et al., 2019a). In contrast, while the activated Roq1 tetramer is the first example of an oligomerized TNL (Martin et al., 2020), without an inactive form to compare to, it is difficult to discern the details of how Roq1 carries out its immune signalling function(s). Therefore, any future investigations of NRG1 structure should include plans to purify and solve structures of both inactive and activated forms. A more detailed discussion on what the potential activated forms of NRG1B-HF might be can be found in chapter 6 of this thesis.

Chapter 5

Interactions of NRG1 with EDS1 and SAG101 pre- and post-immune activation

5 Interactions of NRG1 with EDS1 and SAG101 pre- and post-immune activation

5.1 Introduction

The genetic requirement for compatible alleles of NRG1, EDS1, and SAG101 to mediate immune responses suggests that they could function through the formation of a signalling complex (Lapin et al., 2019). However, whether EDS1 and SAG101 interact with NRG1, directly or indirectly, to mediate cell death mechanisms has not been conclusively shown. NRG1 and SAG101 are seemingly localized to different subcellular compartments and conflicting reports on whether they associate exist in the literature. A thorough investigation into the signalling dynamics for EDS1, SAG101, and NRG1 is required.

RNL and EDS1-family proteins seem to act in parallel, as an Arabidopsis *helperless* mutant lacking *NRG1A*, *NRG1B*, *ADR1*, *ADR1-L1*, and *ADR1-L2* phenocopies *eds1* and *pad4 sag101* mutants (Wu et al., 2019, Saile et al., 2020). Notably, upon TNL activation, loss of cell death response is observed in *nrg1a/b* and *sag101* mutants (Lapin et al., 2019). A coevolving relationship between NRG1 and SAG101 with TNLs is indicated by their repeated losses in monocot and *Aquilegia coerulea* genomes (Figure 1.10) (Baggs et al., 2020). Therefore, it would appear that SAG101 and NRG1 have evolved to function downstream of TNLs to mediate cell death responses.

However, the mechanism by which NRG1 and SAG101 mediate cell death upon TNL activation is unclear. Notably, NRG1 seems spatially separated from SAG101 in plant cells. Transient expression of native promoter-driven Arabidopsis NRG1A and NRG1B in *N. benthamiana* shows co-localization with ER markers. A strong signal is detected at the periphery of nuclei, but no signal is detected within nuclei (Wu et al., 2019). Plasmolysis also shows that both paralogs may be cytoplasmic. However, fractionation data collected by the TSL proteomics team indicates that both paralogs are found only in microsomal fractions (Paul Derbyshire, personal communication with permission). These data indicate that NRG1 is primarily localized to endomembrane networks but perhaps is also present to some degree in the cytosol.

Particle bombardment of *eds1-1 pad4-5* Arabidopsis mutants shows that 35S promoter-driven *EDS1* localizes to both cytosol and nuclei while SAG101 localizes exclusively to nuclei (Feys et al., 2005). Additionally, SDS-PAGE and native antibody

labelling show EDS1 in soluble and nuclear extracts with SAG101 only in nuclear extracts. The structure of EDS1-SAG101 heterodimers has been solved (Wagner et al., 2013), and Fluorescence resonance energy transfer (FRET) assays suggest localization to nuclei (Feys et al., 2005). These data indicate that SAG101-EDS1 heterodimers are exclusively nuclear-localized and spatially separated from extranuclear NRG1.

Whether EDS1 and SAG101 directly associate with NRG1 has not conclusively been shown. Paradoxically, the *N. benthamiana* alleles of NRG1 and EDS1 show a constitutive association (Qi et al., 2018), while the Arabidopsis alleles of EDS1 and SAG101 do not show a convincing association with NRG1, whether pre- or post-immune activation (Wu et al., 2019). Notably, the Arabidopsis alleles were tested for association after heterologous expression in *N. benthamiana*. It could be that expression in *N. benthamiana* does not provide the best genetic context for investigating *At*EDS1 and *At*SAG101 associations with *At*NRG1. Therefore, as convincing evidence for the genetic requirement of NRG1, EDS1, and SAG101 together in cell death-responses exists, a more rigorous investigation of associations in Arabidopsis is required.

5.2 Chapter aims and objectives

This chapter aimed to investigate the signalling mechanisms mediated by NRG1, downstream of RRS1 and RPS4 activation. As NRG1, EDS1, and SAG101 are genetically required together to trigger HR, we hypothesized that these proteins associate to mediate immune responses. Transient co-IP assays in *N. benthamiana* were initially attempted; however, results were highly variable and found to be inconsistent with Arabidopsis in vivo observations. Thus, associations were investigated in an Arabidopsis Ws-2*_nrg1a/b* complementation line carrying native promoter-driven NRG1B-HF. This chapter aimed to investigate whether associations between NRG1 with EDS1 and SAG101 were affected by immune activation states.

5.3 Evaluating EDS1 associations with NRG1 in transient assays

Evidence has emerged for the genetic requirement of *At*NRG1, *At*EDS1, and *At*SAG101 to mediate cell death immune responses (Lapin et al., 2019). However, whether NRG1 associates directly with EDS1 and SAG101 to mediate immune

responses is not known. Therefore, initial association assays were performed by co-IP after *Agro*-infiltration-mediated transient expression in *N. benthamiana*. These experiments were initiated prior to our knowledge for the specificity of SAG101 over PAD4 in cell death with NRG1 and EDS1. Thus, initial assays investigated the associations between NRG1 with EDS1 and PAD4.

As Arabidopsis carries two functionally-redundant NRG1 paralogs, each were evaluated for associations with EDS1 or PAD4. NRG1A-Myc was co-delivered with EDS1-V5 or PAD4-HA, using GUS-V5 or GUS-HA as controls, respectively, via *Agro*-infiltration in *N. benthamiana* leaves (Figure 5.1A). IP was performed with lysates using anti-Myc, anti-V5, or anti-HA agarose beads before band resolution by SDS-PAGE and antibody labelling. Anti-Myc IP shows that EDS1-V5 but not PAD4-HA associates with NRG1A-Myc. Furthermore, reciprocal anti-V5 IP shows the presence of NRG1A-Myc associating with EDS1-V5. These data indicate that NRG1A associates with EDS1 but not PAD4.

To evaluate whether NRG1B also associates with EDS1, NRG1B-HF or GUS-HF was co-delivered with EDS1-V5 and PAD4-HA or GUS-HA (Figure 5.1B). IP was performed with lysates using anti-FLAG® or anti-V5 agarose beads followed by SDS-PAGE and antibody labelling. In contrast to what was observed for NRG1A, anti-FLAG® IP shows that EDS1-V5 associates both with NRG1B-HF and the GUS-HF negative control. Furthermore, the reciprocal anti-V5 IP also shows that NRG1B-HF and GUS-HF associate with EDS1-V5. These data do not indicate a specific association between NRG1B-HF and EDS1-V5.

As the data indicated that NRG1A-Myc may associate with EDS1-V5, but that NRG1B-HF associations were inconclusive, differently-tagged versions of EDS1 and PAD4 were evaluated for associations with NRG1. NRG1A-Myc was co-delivered with GFP-EDS1, GFP-PAD4, or GFP. A band migrating near the ~ 70 kDa marker in the anti-Myc blot is present after anti-GFP IP indicating association of NRG1A-Myc with GFP-EDS1 (Figure 5.2). However, this band may be a mis-spliced variant of NRG1A. Three splice variants are reported for NRG1A that when C-terminally Myc-tagged correlate to MW of ~ 105 kDa (At5g66900.1), ~ 110 kDa (At5g66900.2), and ~ 81 kDa (At5g66900.3). The Arabidopsis information resource (TAIR) annotation indicates that At5g66900.3 is an alternate splice form that does not include the most 3' end of the last exon. Therefore, this variant should not be detectable when expressed with an in-frame Myc C-terminal fusion-tag. Notably, expression of NRG1B-Myc does not produce a band migrating near the ~ 70 kDa marker (Figure 5.4). Therefore, this likely

represents a mis-spliced variant of NRG1A-Myc associating with GFP-EDS1. Furthermore, the band migrating near the ~ 100 kDa marker (correlating to the MW of At5g66900.1 or At5g66900.2 or both) is not present in the anti-Myc immunoblot after anti-GFP IP (Figure 5.2). In contrast to Figure 5.1A, these data indicate that NRG1A-Myc associations with GFP-EDS1 are not specific. Also in contrast to Figure 5.1A, GFP-PAD4 is observed associating with NRG1A-Myc, and vice versa (Figure 5.2). These data indicate that fusion-tags influence associations between EDS1 and PAD4 with NRG1.

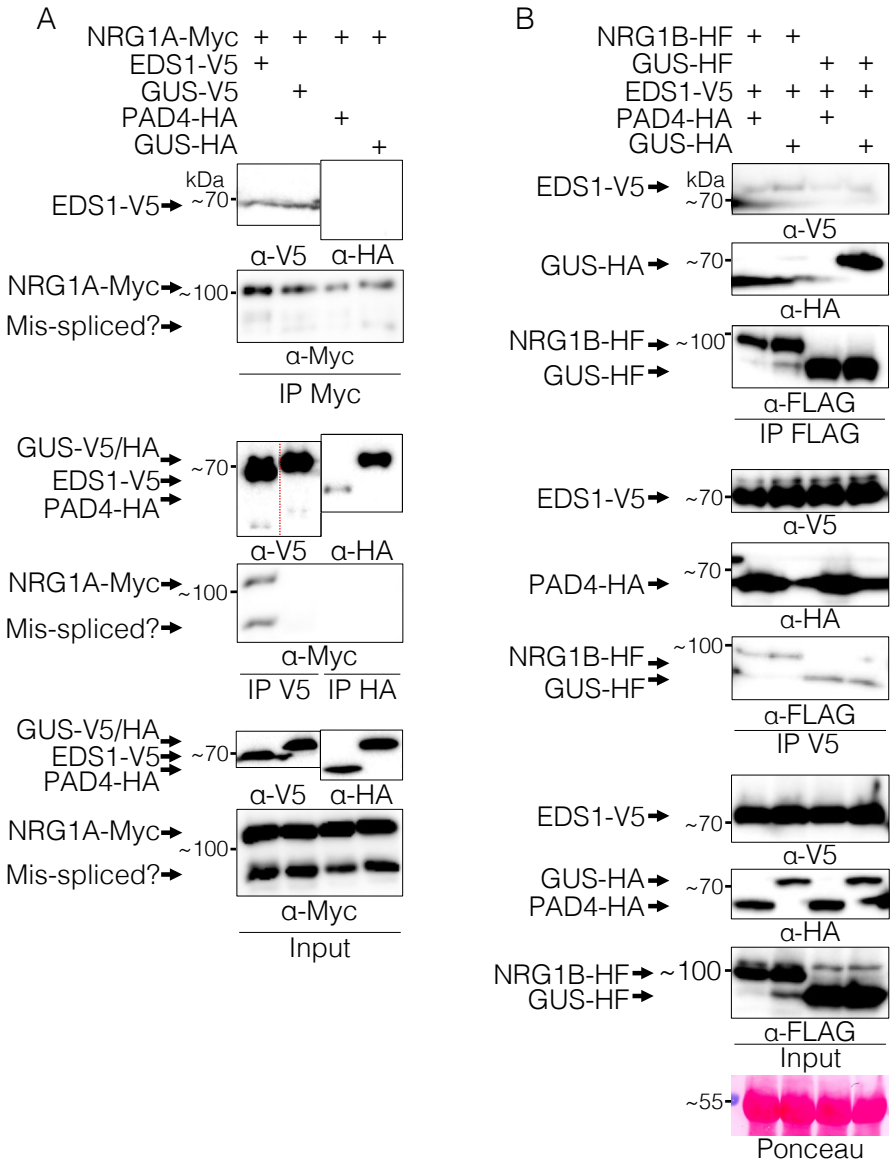

Figure 5.1 EDS1 may associate with NRG1A but not NRG1B. SDS-PAGE and western blots of co-IPs after *Agro*-infiltration and transient expression in *N. benthamiana*. (A) NRG1A-Myc may associate with EDS1-V5. Co-IP of 35S promoter-driven NRG1B-Myc, EDS1-V5, GUS-V5, PAD4-HA, and/or GUS-HA. Lysates were incubated with anti-V5, anti-HA, or anti-Myc agarose beads. Membranes were immunolabelled with anti-V5, anti-HA, and anti-Myc antibody. (B) NRG1B-HF does not associate with EDS1-V5. Co-IP 35S promoter-driven NRG1B-HF, GUS-HF, EDS1-V5, PAD4-HA, and/or GUS-HA. Lysates were incubated with anti-V5 or anti-

FLAG® agarose beads. Membranes were immunolabelled with anti-V5, anti-HA, or anti-FLAG® antibody. Membranes were Ponceau-stained as the loading control. Dotted red line indicates different cropping to visualize bands at different exposure times. Construct details can be found in section 2.7.1 of this thesis.

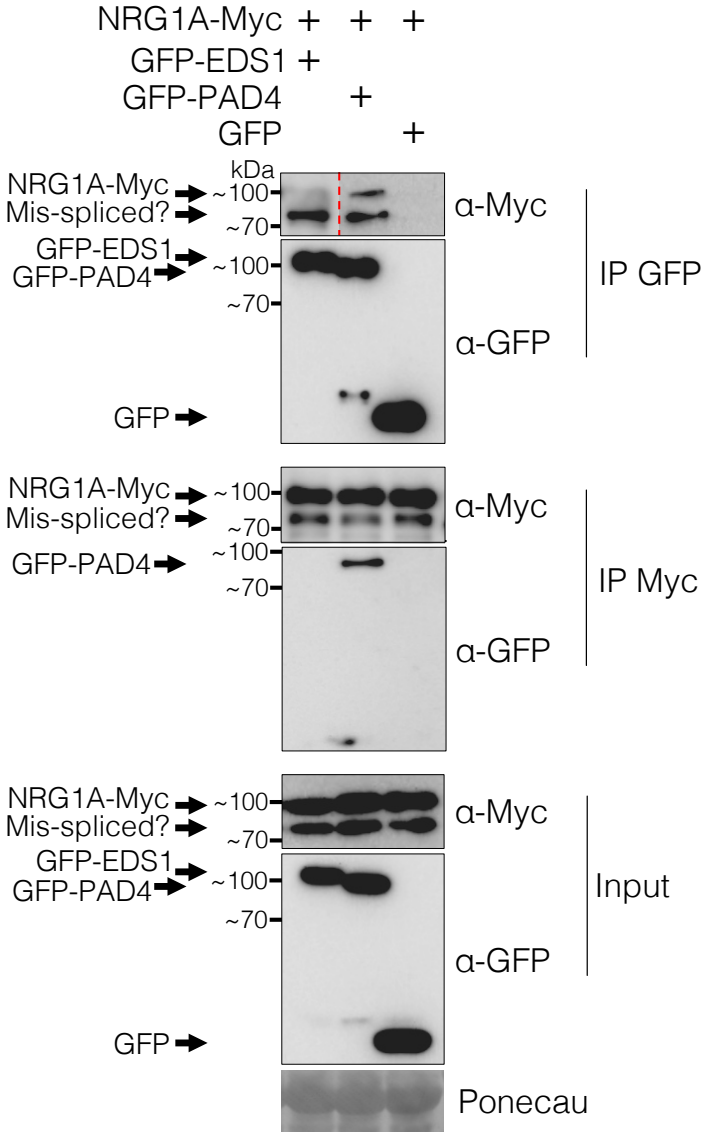

Figure 5.2 EDS1 associates with a mis-spliced variant of NRG1A. SDS-PAGE and western blot of co-IPs after *Agro*-infiltration and transient expression in *N. benthamiana* of 35S promoter-driven NRG1A-Myc, GFP-EDS1, GFP-PAD4, and/or GFP. Lysates were incubated with anti-GFP or anti-Myc agarose beads. Membranes were immunolabelled with anti-GFP or anti-Myc antibody. Loading controls were evaluated by Ponceau-staining of membranes. Dotted red line indicates different cropping to visualize bands at different exposure times. Construct details can be found in section 2.7.1 of this thesis.

5.4 Evaluating EDS1-NRG1 associations upon effector induction in transient assays

Investigations of NRG1B with EDS1 were prioritized in follow-up experiments, as heterologous expression of NRG1A in *N. benthamiana* seemed to produce a mis-spliced variant that showed non-specific associations with EDS1. Additionally, transient expression assays were designed to investigate changes upon immune activation as a constitutive association between NRG1B and EDS1 was not observed. NRG1B-Myc was co-delivered with EDS1-V5, PAD4-HA, and RRS1-R-HF, RPS4-HA, and either AvrRps4-GFP or non-recognized AvrRps4^{E187A}-GFP on a single expression vector (Figure 5.3). The TNL RRS1 mediates recognition of AvrRps4 and signals with its pair RPS4 to trigger immune activation. Three days after *Agro*-infiltration, β-estradiol was infiltrated to induce expression of either AvrRps4-GFP or AvrRps4^{E187A}-GFP. Tissue was harvested 6 h post-estradiol infiltration (hpe) and IP of lysates was performed before SDS-PAGE and immunoblotting.

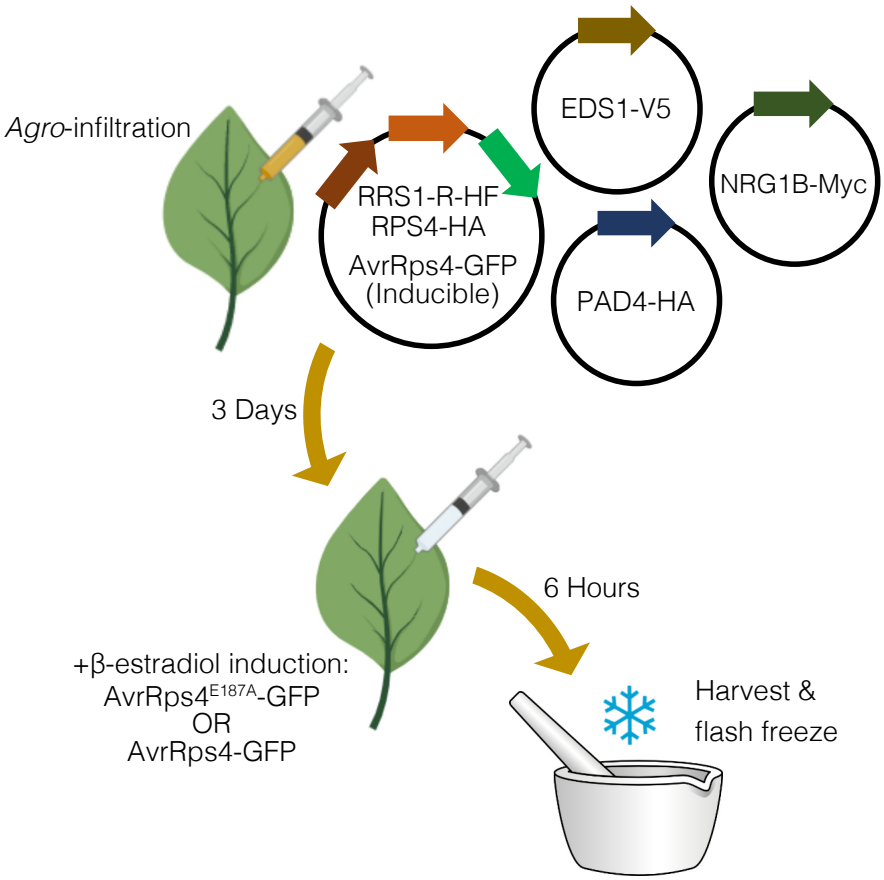

Figure 5.3 Schematic for transient assays pre- and post-immune activation. *Agrobacterium* strains carrying expression vectors were infiltrated into *N. benthamiana* at varying OD_{600}. At 3 dpi, β-estradiol was infiltrated into the same leaves, to induce the expression of AvrRps4-GFP or AvrRps4^{E187A}-GFP. Tissue was flash frozen and harvested 6 hpe. Construct details can be found in section 2.7.1.

Upon induction of AvrRps4-GFP, anti-Myc IP showed that EDS1-V5 associates with NRG1B-Myc (Figure 5.4). These data indicate an effector-dependent association between NRG1 and EDS1. However, a weak association is also observed between EDS1-V5 and NRG1B-Myc in the presence of AvrRps4^{E187A}-GFP. RRS1 weakly binds AvrRps4^{E187A}, but this recognition is insufficient to induce immune activation (Sarris et al., 2015). Therefore, it is possible that NRG1-EDS1 are induced to associate upon AvrRps4 or AvrRps4^{E187A} binding by RRS1, and that NRG1-EDS1 associations are insufficient to induce immune responses.

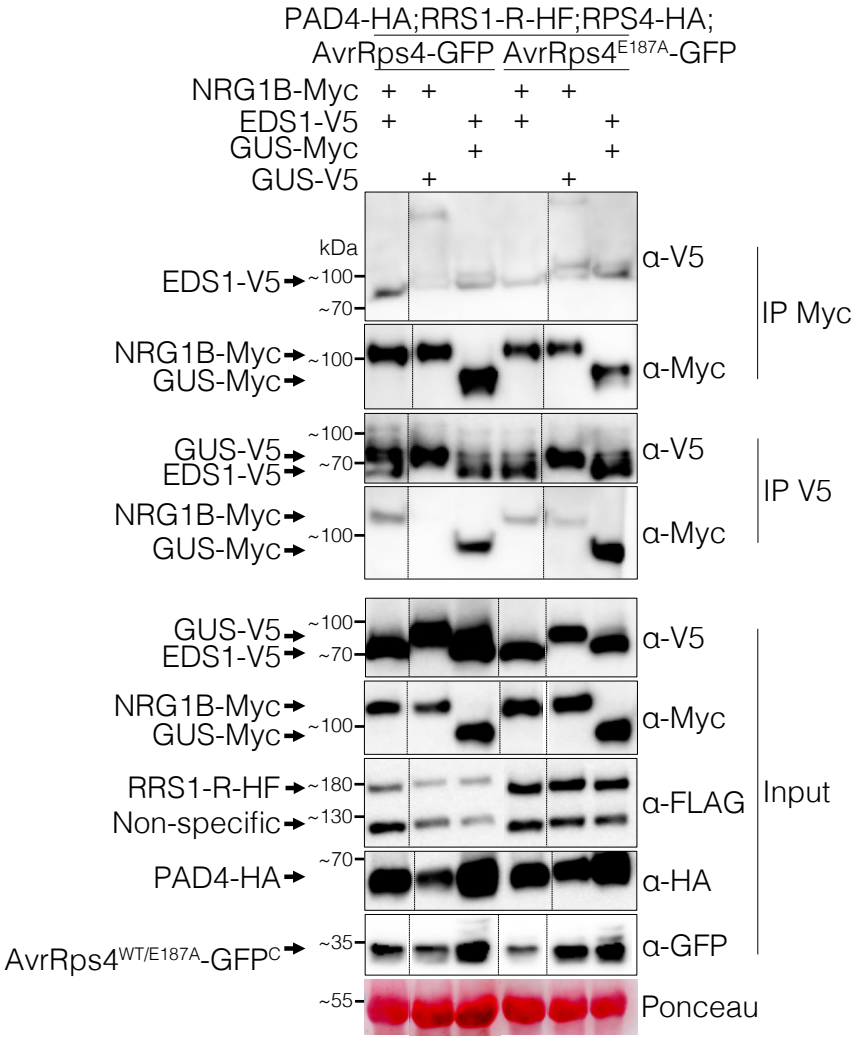

Figure 5.4 NRG1B may associate with EDS1 upon immune activation. SDS-PAGE and western blot of co-IPs after *Agro*-infiltration and transient expression in *N. benthamiana* of 35S promoter-driven NRG1B-Myc, GUS-Myc, EDS1-V5, GUS-V5, and/or PAD4-HA, with pAt2:RRS1-R-HF, pAt3:RPS4-HA, and β-estradiol-inducible AvrRps4-GFP. Lysates were incubated with anti-Myc or anti-V5 agarose beads. Membranes were immunolabelled with anti-V5, anti-Myc, anti-FLAG®, anti-HA, or anti-GFP antibody. Recognized C-terminal cleavage product of AvrRps4 indicated. Loading controls were evaluated by Ponceau-staining of membranes. Tissue was harvested 24 hpe. Dotted black line indicate cropping to remove lanes or same

exposure times with separate membranes. Construct details can be found in section 2.7.1 of this thesis.

However, a weak association is observed between NRG1B-Myc and the GUS-V5 control upon anti-Myc IP in the presence of either AvrRps4-GFP or AvrRps4^{E187A}-GFP. Likewise, a strong association is observed between EDS1-V5 and the GUS-Myc control upon anti-V5 IP in the presence of either AvrRps4-GFP or AvrRps4^{E187A}-GFP. These data indicate that NRG1B-EDS1 associations in the presence of AvrRps4 are not specific. Thus, optimisations of transient co-IP assays were required to reduce non-specific interactions between NRG1B and EDS1 with GUS controls.

5.5 Buffer optimisations reduce non-specific interactions in transient assays

The non-specific associations between NRG1 and EDS1 with GUS controls interfered with data interpretation. Therefore, buffer recipes were optimized to find conditions in which co-IP was no longer observed for GUS with NRG1 or EDS1. Detergent concentrations were varied in an effort to perturb non-specific protein-protein and protein-bead interactions. Nonidet^{TM} P-40 substitute (NIDP40) was increased from 0.1% during lysis and IP, to 0.3% during lysis and 0.5% during IP. Adjusting detergent conditions reduced the non-specific association between GUS-Myc and EDS1-V5 after anti-V5 IP, while maintaining an association between NRG1B-Myc and EDS1-V5 (Figure 5.5A).

Sodium chloride concentration was also adjusted in an effort to reduce non-specific protein-protein or protein-bead interactions. However, increasing sodium chloride concentration from 150 mM to 300 mM in addition to 0.3% NIDP40 during lysis and 0.5% NIDP40 during IP showed a weak NRG1B-Myc and EDS1-V5 association (Figure 5.5A). Yet, when co-IP assays were performed in the presence of 300 mM NaCl with 0.5% NIDP40 during lysis and 0.5% NIDP40 during IP, a specific association between NRG1B-Myc and EDS1-V5 was observed in the absence of GUS-Myc associations with EDS1-V5 (Figure 5.5B). Three biological replicates were performed with 300 mM NaCl and 0.5% NIDP40 conditions. In each replicate, associations between EDS1-V5 and NRG1B-Myc after anti-V5 IP were reproducibly specific (Figure 5.6). These data indicate that buffer conditions were optimized for transient co-IP assays utilizing anti-V5 IP to investigate NRG1B-EDS1 associations.

However, co-IP of NRG1B-Myc with the GUS-V5 control was still observed upon anti-Myc IP in the optimized buffer conditions (Figure 5.6). Subsequently, other negative controls were trialled, but all associated with EDS1-V5 or NRG1B-Myc (Table 5.1). These data indicate that co-IP utilizing anti-V5 agarose beads with optimized buffer conditions was the most ideal assay for investigating associations between NRG1 and EDS1 by heterologous expression in *N. benthamiana*.

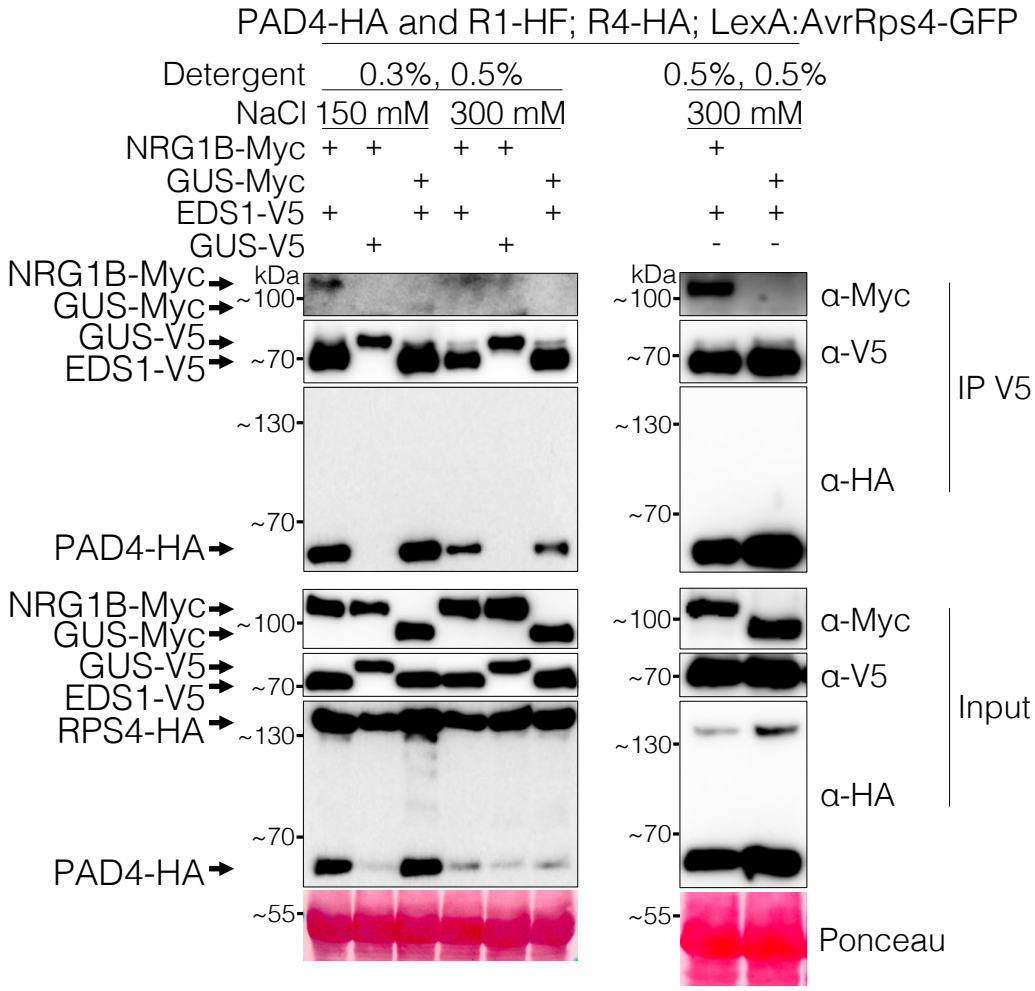

Figure 5.5 Buffer optimisations reduce non-specific interactions. SDS-PAGE and western blot of co-IPs after *Agro*-infiltration and transient expression in *N. benthamiana* of 35S promoter-driven NRG1B-Myc, GUS-Myc, EDS1-V5, GUS-V5, and/or PAD4-HA, with pAt2:RRS1-R-HF ("R1-HF"), pAt3:RPS4-HA ("R4-HA"), and β-estradiol-inducible AvrRps4-GFP. Lysates were incubated with anti-V5 agarose beads. Membranes were immunolabelled with anti-Myc, anti-V5, or anti-HA antibody. Loading controls were evaluated by Ponceau-staining of membranes. Tissue was harvested in the absence of β-estradiol. Construct details can be found in section 2.7.1 of this thesis.

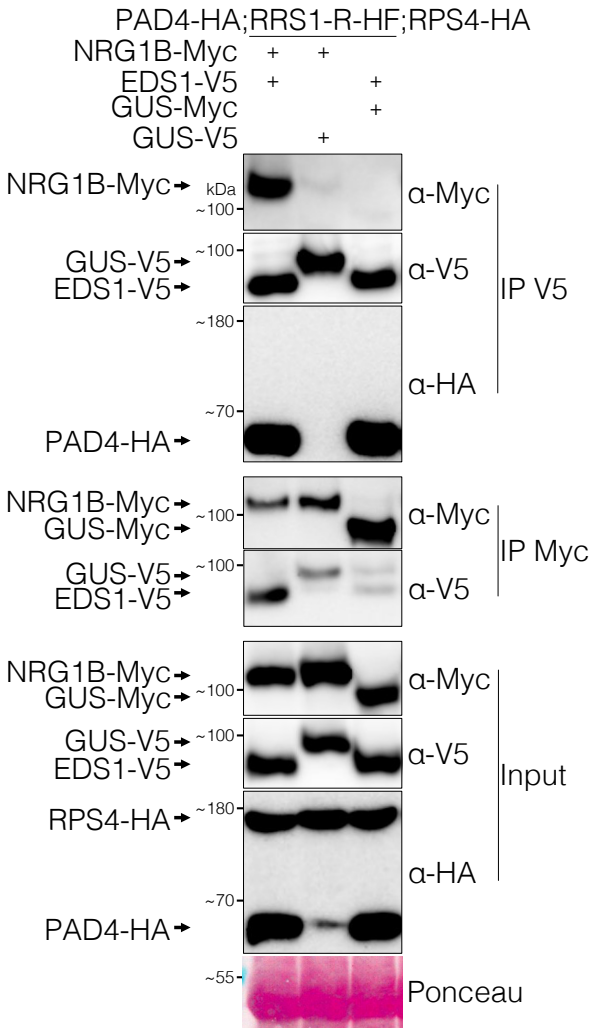

Figure 5.6 Buffer optimisations specific for anti-V5 immunoprecipitations. SDS-PAGE and western blot of co-IPs after *Agro*-infiltration and transient expression in *N. benthamiana* of 35S promoter-driven NRG1B-Myc, GUS-Myc, EDS1-V5, GUS-V5, and PAD4, with pAt2:RRS1-R-HF, pAt3:RPS4-HA, and β-estradiol-inducible AvrRps4-GFP were incubated with anti-V5 or anti-Myc agarose beads. Membranes were immunolabelled with anti-Myc, anti-V5, or anti-HA antibody. Loading controls were evaluated by Ponceau-staining of membranes. Tissue was harvested in the absence of β-estradiol. Construct details in section 2.7.1.

Table 5.1 Negative controls for EDS1-V5 or NRG1B-Myc co-IPs

IP		Co-immunoprecipitant					
-	-	EDS1	GUS	mVenus	NRG1B	GUS	mVenus
	Tag	V5			Myc		
EDS1	V5	-	-	-	YES	NO	NO
GUS		-	-	-	NO	-	-
mVenus		-	-	-	YES (W)	-	-
NRG1B	Myc	YES	YES (W)	NO	-	-	-
GUS		YES (W)	-	-	-	-	-
mVenus		YES (S)	-	-	-	-	-

"YES" = association observed; "NO" = no associations; "(W)" = association is weak; "(S)" = association is strong; western blots for mVenus in Appendix XI.

5.6 Transient assays for EDS1-NRG1 associations are inconclusive

Utilizing the optimized buffer conditions for anti-V5 IP, transient co-IP assays to investigate NRG1B-EDS1 associations were re-attempted. Using the experimental design described in Figure 5.3, associations between NRG1B-Myc and EDS1-V5 were evaluated pre- and post-β-estradiol-induction of AvrRps4-GFP or AvrRps4^{E187A}-GFP. Upon induction of AvrRps4-GFP, the NRG1B-Myc association with EDS1-V5 was shown to decrease, while no change was observed upon induction of AvrRps4^{E187A}-GFP (Figure 5.7). In contrast to Figure 5.4, these data indicate that NRG1B-Myc dissociates from EDS1 upon induction of AvrRps4-GFP. Notably, no change in PAD4-HA association with EDS1-V5 is observed upon induction of AvrRps4-GFP. These data indicate that the change in NRG1B-Myc associations with EDS1-V5 is specific to the presence of AvrRps4-GFP.

Data collection at this time correlated with the publication of Lapin et al. (2019) which indicated the requirement of genetically compatible alleles of NRG1, EDS1, and SAG101 together to recapitulate immune responses. Therefore, co-IP assays were performed in the presence of SAG101-Myc instead of PAD4-HA. To accommodate Myc-tagged SAG101, assays were performed with NRG1B-V5 and HA-EDS1. Upon induction of AvrRps4-GFP or AvrRps4^{E187A}-GFP and anti-V5 IP, a weak constitutive SAG101-Myc association with NRG1B-V5 is observed. Furthermore, no changes in HA-EDS1 associations with NRG1B-V5 are observed. These data are in contrast to what was observed in Figure 5.4 (increase in NRG1-EDS1 association) and Figure 5.7 (decrease in NRG1-EDS1 association). Collectively, these data indicate that transient co-IP assays to investigate pre- and post-immune activation associations between EDS1 and SAG101 with NRG1 are inconsistent and unreliable.

Notably, a constitutive association between RPS4-HA and NRG1B-V5 is observed upon anti-V5 IP (Figure 5.8). However, although optimized buffer conditions were not used, anti-Myc IP did not show RPS4-HA association with NRG1B-Myc (Figure 5.9). These data indicate that RPS4 associations with NRG1B are dependent upon fusion-tag variants used, and thus are likely not specific.

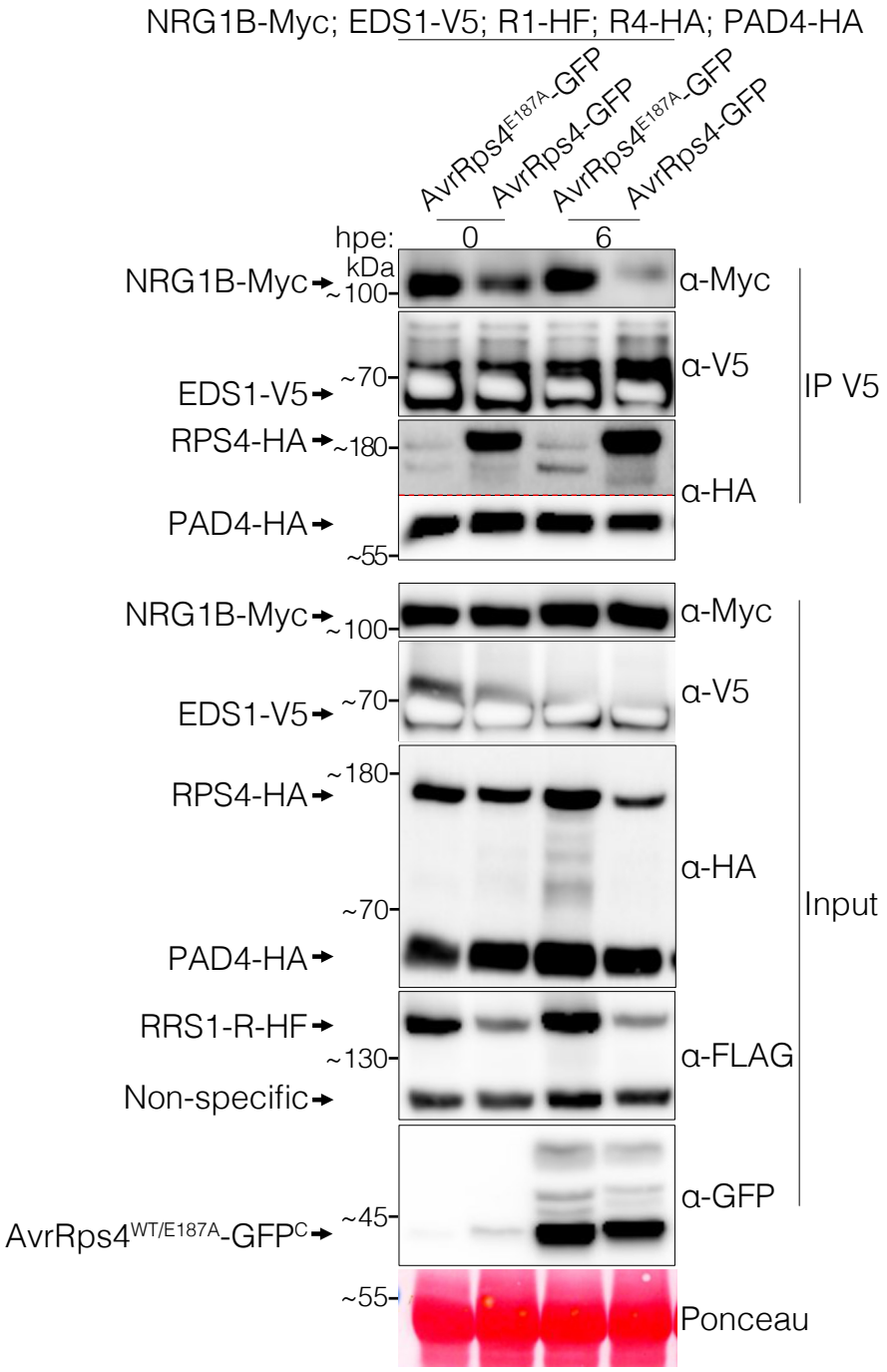

Figure 5.7 NRG1B may dissociate from EDS1 upon immune activation. SDS-PAGE and western blot of co-IPs after *Agro*-infiltration and transient expression in *N. benthamiana* of 35S promoter-driven NRG1B-Myc, EDS1-V5, and/or PAD4-HA, with pAt2:RRS1-R-HF, pAt3:RPS4-HA, and β-estradiol-inducible AvrRps4-GFP. Lysates were incubated with anti-V5 agarose beads. Membranes were immunolabelled with anti-Myc, anti-V5, anti-HA, anti-FLAG®, or anti-GFP antibody. Loading controls were evaluated by Ponceau-staining of membranes. Red dotted line indicates membrane cropped to expose different band intensities. Tissue was harvested either in the absence of β-estradiol or 6 hpe. Recognized C-terminal cleavage product of AvrRps4 indicated. Construct details can be found in section 2.7.1 of this thesis.

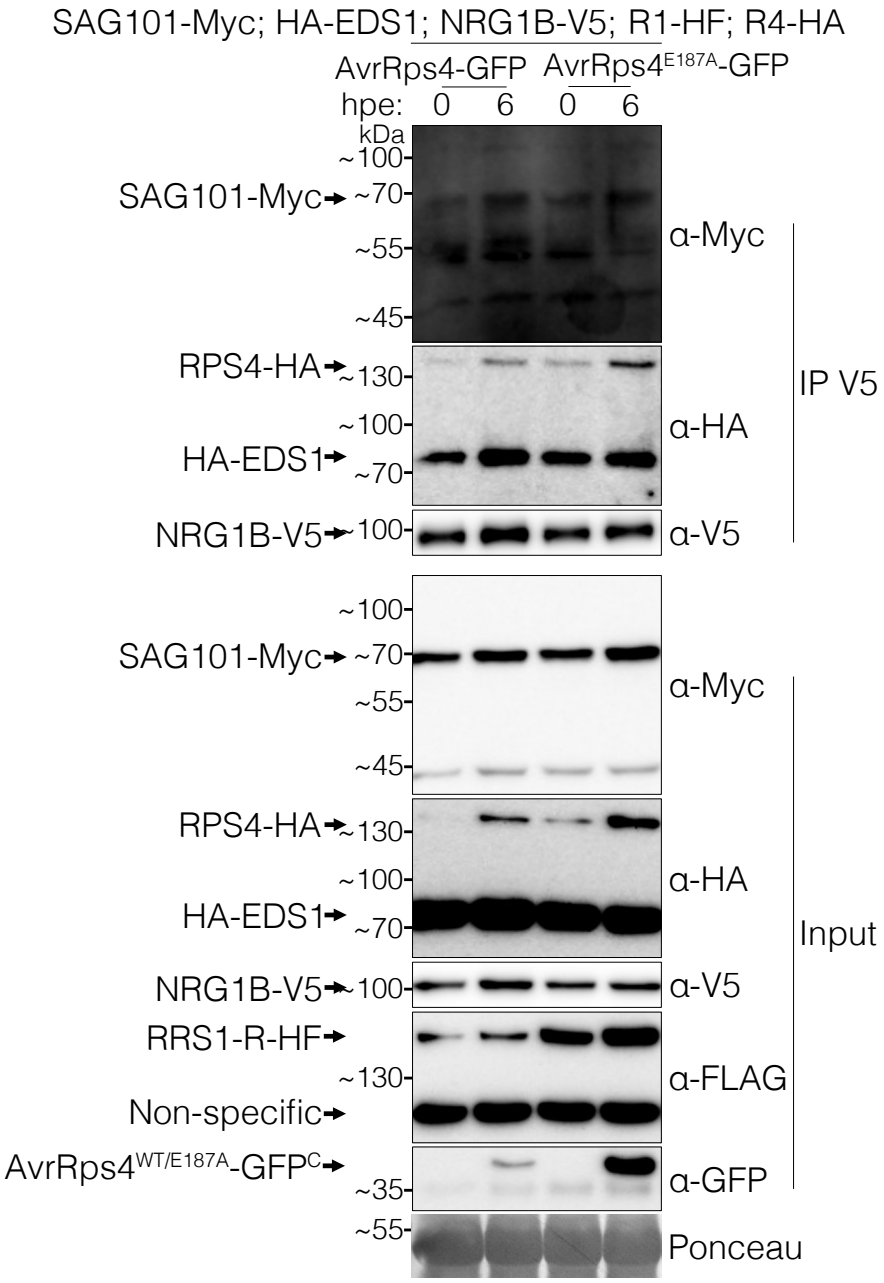

Figure 5.8 EDS1 may constitutively associate with NRG1B upon immune activation. SDS-PAGE and western blot of co-IP after *Agro*-infiltration and transient expression in *N. benthamiana* of 35S promoter-driven SAG101-Myc, NRG1B-V5, and/or HA-EDS1, with pAt2:RRS1-R-HF, pAt3:RPS4-HA, and β-estradiol-inducible AvrRps4-GFP. Lysates were incubated with anti-V5 agarose beads. Membranes were immunolabelled with anti-Myc, anti-HA, anti-V5, anti-FLAG®, or anti-GFP antibody. Loading controls were evaluated by Ponceau-staining of membranes. Tissue was harvested either in the absence of β-estradiol or 6 hpe. Recognized C-terminal cleavage product of AvrRps4 indicated. Construct details can be found in section 2.7.1 of this thesis.

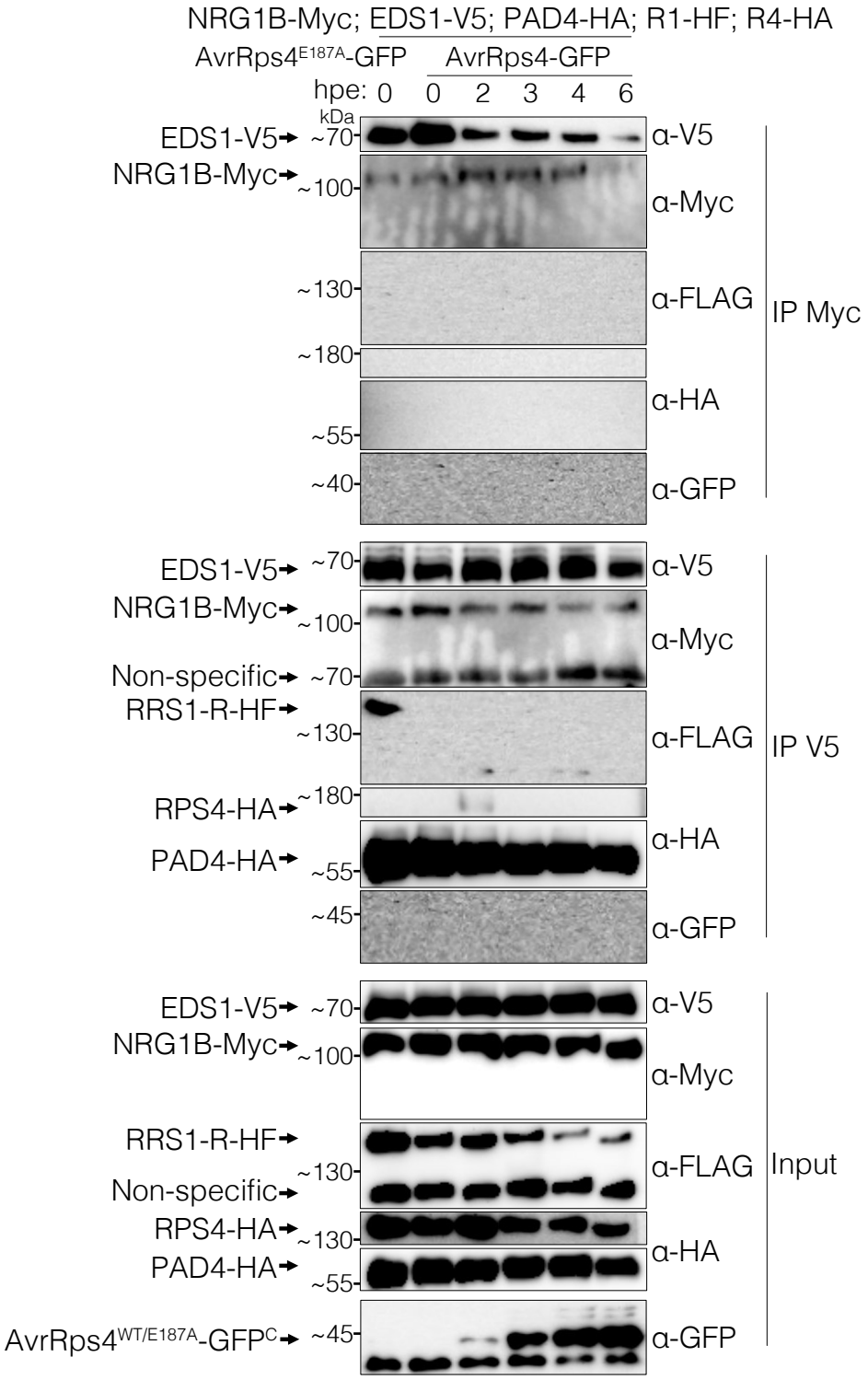

Figure 5.9 RRS1 and RPS4 do not associate with NRG1B. SDS-PAGE and western blot of co-IPs after *Agro*-infiltration and transient expression in *N. benthamiana* of 35S promoter-driven NRG1B-Myc, EDS1-V5, and/or PAD4-HA, with pAt2:RRS1-R-HF, pAt3:RPS4-HA, and β-estradiol-inducible AvrRps4-GFP. Lysates were incubated with anti-Myc or anti-V5 agarose beads. Membranes were immunolabelled with anti-V5, anti-Myc, anti-FLAG®, anti-HA, or anti-GFP antibody. Loading controls not evaluated. Tissue was harvested either in the absence of β-estradiol or 2, 3, 4, 6 hpe. Recognized C-terminal cleavage product of AvrRps4 indicated Construct details can be found in section 2.7.1 of this thesis.

5.7 EDS1 does not constitutively associate with NRG1 in Arabidopsis

To better evaluate associations between EDS1 and NRG1B, the Ws-2_*nrg1a/b* complementation line carrying pNRG1B:NRG1B-HF from Castel et al. (2019) was used for in vivo co-IP assays. A control line was made in the same background carrying 35S:GUS-HF. Lysates were resolved by SDS-PAGE and probed with anti-FLAG® antibody (Figure 5.10A). A band migrating just above the ~ 100 kDa MW marker and between the ~ 70 kDa and ~ 100 kDa markers were observed for the NRG1B-HF complementation line and GUS-HF line, respectively. These bands were resolved by SDS-PAGE and stained by CBB before being excised and sent for LC-MS analysis which confirmed their identities (Table 5.2).

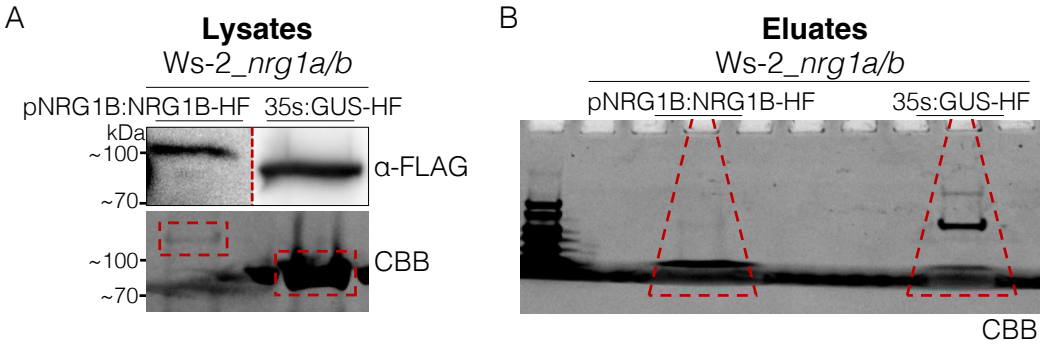

Figure 5.10 Band identification for NRG1B-HF and GUS-HF in Arabidopsis. (A) SDS-PAGE and anti-FLAG® western blot (above) or CBB-staining (below) of lysates from Ws-2_*nrg1a/b* complemented with pNRG1B:NRG1B-HF or carrying 35S:GUS-HF. Bands excised from CBB-stained gel for LC-MS are outlined with red dotted square. (B) SDS-PAGE and CBB-staining of eluates after anti-FLAG® IP and 3×FLAG® peptide elution. for LC-MS. Eluates excised from CBB-stained gel for LC-MS are outlined with red dotted triangle.

Additionally, lysates were incubated with anti-FLAG® agarose beads before elution with 3×FLAG® peptide. Eluates were run into SDS-PAGE gel before excision and submission for LC-MS analysis (Figure 5.10B). LC-MS identified spectra that correlated to peptides derived from RCA (RUBISCO ACTIVASE), HSC70-1 (HEAT SHOCK COGNATE 70-1), HTB1 (histone superfamily protein), RBCL (the large subunit of RuBisCO), CAB1 (CHLOROPHYLL A/B BINDING PROTEIN 1), PVA12 (PLANT VAP HOMOLOG 12), FTIP1 (C2 calcium/lipid-binding plant phosphoribosyltransferase family protein), a ribosomal protein L11 family protein, and ATPA (ATP synthase subunit alpha). The presence of RCA, RBCL, and HSC70-1 peptides co-purifying with NRG1B-HF in Arabidopsis is consistent with what was observed after transient expression in *N. benthamiana* (discussed in chapter 4 of this

thesis). Additionally, BLAST of the co-purifying vesicle associated membrane protein (VAMP)-associated protein (VAP) from *N. benthamiana* (NbS00019865g0007.1) showed 58.8% sequence identity to the PVA12 identified here. The presence of the FTIP1, ribosomal protein, ATPA, and HTB1 likely indicate contaminants with no functional relevance.

To investigate whether EDS1 associates with NRG1 in Arabidopsis, native anti-EDS1 antibody was obtained from Agrisera and evaluated for specificity in Col-0, Ws-2, Col-0_*eds1-2,* and Ws-2_*eds1-1* lysates. Bands were resolved by SDS-PAGE and probed with anti-EDS1 antibody. A band migrating just above the ~ 70 kDa marker was observed in the Col-0 and Ws-2 lysates, but was missing in the Col-0_*eds1-2* and Ws-2_*eds1-1* lysates (Figure 5.11). A higher-migrating band below the ~ 100 kDa marker was observed in all lysates. As the predicted MW for EDS1 is ~ 72 kDa, these data indicate that the faster migrating band near the ~ 70 kDa marker is EDS1 while the slower migrating band is non-specific.

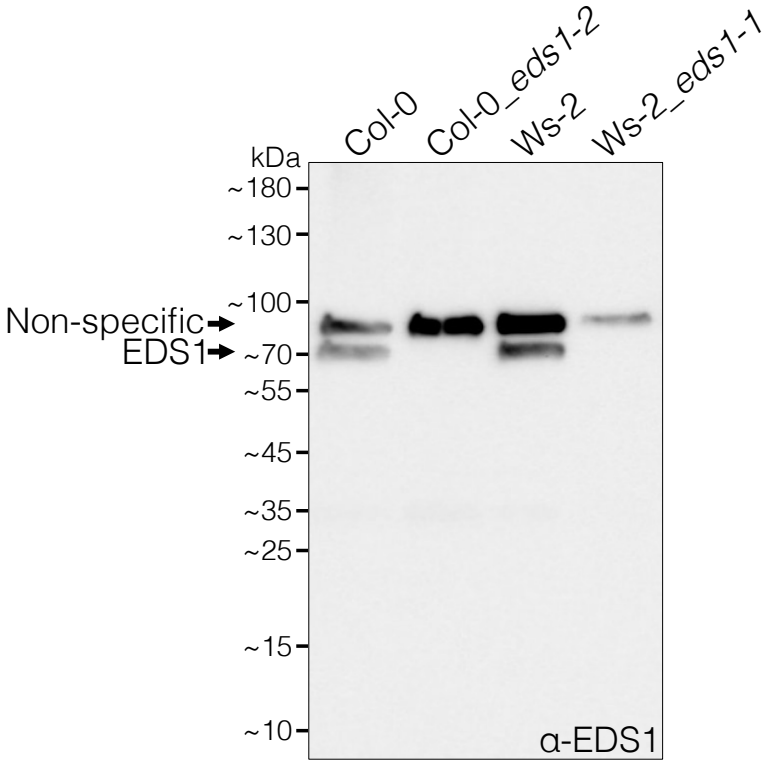

Figure 5.11 Native anti-EDS1 antibody is specific to EDS1 in Arabidopsis. SDS-PAGE and anti-EDS1 western blot of Col-0, Col-0_*eds1-2*, Ws-2, Ws-2_*eds1-1* lysates. Band migrating near ~ 70 kDa marker is absent in the Col-0_*eds1-2* and Ws-2_*eds1-1* lysates indicating specificity for EDS1 while a band migrating below ~ 100 kDa marker is present in all lysates indicating non-specific for EDS1.

Table 5.2 Mass Spectrometry for band identification and NRG1B-HF interactors

		Ws-2_*nrg1a/b*			
		pNRG1B:NRG1B-HF		35S:GUS-HF	
Identified Proteins	MW	Band ID	Co-IP	Band ID	Co-IP
NRG1B-HF	99 kDa	69	55	0	2
GUS-HF	75 kDa	0	0	575	144
RCA | rubisco activase	52 kDa	0	14	0	3
HSC70-1 | heat shock cognate 70-1	71 kDa	0	11	7	0
HTB1 | Histone superfamily protein	16 kDa	1	8	0	0
RBCL | ribulose-bisphosphate carboxylases	53 kDa	0	6	0	3
CAB1 | chlorophyll A/B binding protein 1	28 kDa	0	4	0	2
PVA12 | plant VAP homolog 12	26 kDa	0	4	0	0
FTIP1 | C2 calcium/lipid-binding plant phosphoribosyltransferase family protein	91 kDa	1	3	0	0
Ribosomal protein L11 family protein	18 kDa	0	3	0	0
ATPA | ATP synthase subunit alpha	55 kDa	0	2	0	0
			Total Spectrum Count		

Bands and eluates from Figure 5.10. Table generated with top hits for NRG1B-HF Band ID, top hit for GUS-HF Band ID, and all hits for NRG1B-HF Co-IP. Further results in Appendix XII. Further data in scaffold file jfe190130.

Association of EDS1 with NRG1B-HF was evaluated by anti-FLAG® IP of Ws-2_*nrg1a/b*:pNRG1B:NRG1B-HF lysates and elution with 3×FLAG® peptide. Eluates were resolved by SDS-PAGE and anti-EDS1 immunolabelling, and no band was detected in the anti-EDS1 blot after anti-FLAG® IP (Figure 5.12). These data indicate that EDS1 does not constitutively associate with NRG1B-HF in Arabidopsis.

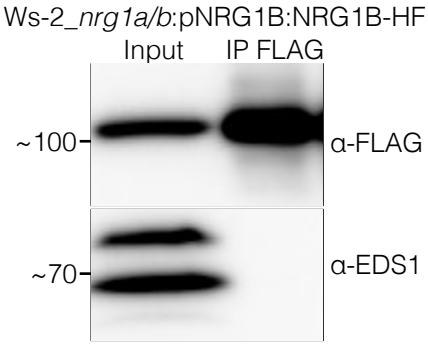

Figure 5.12 EDS1 does not constitutively associate with NRG1 in Arabidopsis. SDS-PAGE and anti-FLAG® or anti-EDS1 western blot of Ws-2_*nrg1a/b*:pNRG1B:NRG1B-HF lysate and eluate after anti-FLAG® IP and 3×FLAG® peptide elution.

5.8 Effector dependent association of EDS1 and SAG101 with NRG1 in Arabidopsis

To evaluate whether EDS1 associates with NRG1 upon immune activation, co-IP assays were performed after Pf0-1 delivery of AvrRps4 in Arabidopsis *Ws-2_nrg1a/b* complementation lines (Figure 5.13). As mentioned, AvrRps4 is recognized by Arabidopsis sensor TNL RRS1 which signals with RPS4 through EDS1, SAG101, and NRG1, mediating cell death immune responses. Associations were evaluated 4 h post-effector delivery (hpd) by Pf0-1 infiltration, as this time-point shows significant accumulation of PTI- and ETI-related transcripts upon estradiol-induction of AvrRps4 in the Super-ETI (SETI) line (Ngou et al., 2020a).

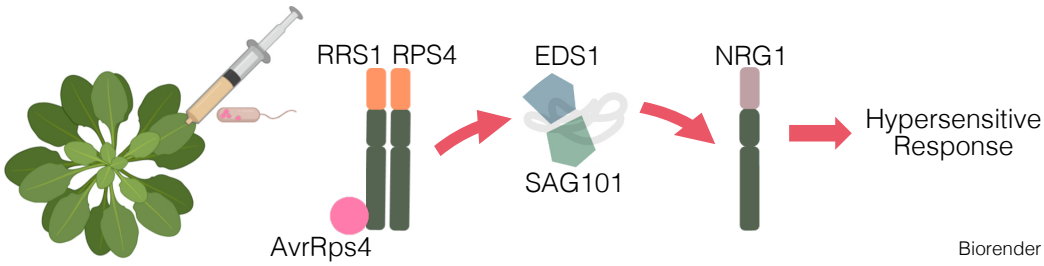

Figure 5.13 Schematic for Arabidopsis assays pre- and post-immune activation. Rosette leaves of 5-6-week-old Arabidopsis are infiltrated with Pf0-1 carrying AvrRps4. AvrRps4 is recognized by TNL sensors RRS1 and

RPS4 which require EDS1, SAG101, and NRG1 to mediate cell death responses.

Rosette leaves of 5-6-week-old Ws-2*_nrg1a/b* complemented with pNRG1B:NRG1B-HF or carrying 35S:GUS-HF were infiltrated with Pf0-1 that delivered either AvrRps4 or empty vector. Leaves were harvested 4 hpd and lysates were incubated with anti-FLAG® agarose beads before elution with 3×FLAG® peptide. Eluates were resolved by SDS-PAGE and probed with anti-FLAG® and anti-EDS1 antibodies. The presence of a band migrating near the ~ 70 kDa marker in the anti-EDS1 blot after anti-FLAG® IP is observed only in lysate from the AvrRps4-treated leaves. These data indicate that EDS1 associates with NRG1 upon AvrRps4 delivery.

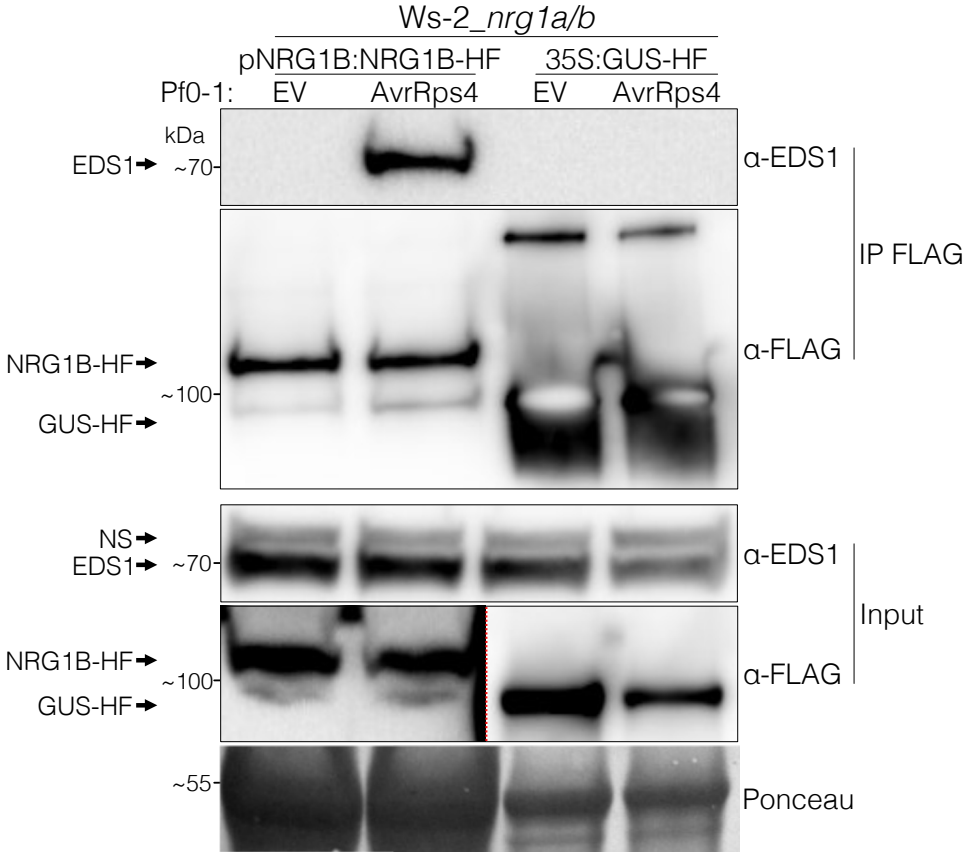

Figure 5.14 EDS1 associates with NRG1 upon AvrRps4 delivery in Arabidopsis. SDS-PAGE and anti-FLAG® or anti-EDS1 western blot of Ws-2*_nrg1a/b*:pNRG1B:NRG1B-HF or Ws-2*_nrg1a/b*:35S:GUS-HF lysates 4 hpd by Pf0-1 carrying empty vector or AvrRps4. Lysates were incubated with anti-FLAG® agarose beads and eluted with 3×FLAG® peptide. Anti-FLAG® membrane was ponceau-stained to evaluate loading control. GUS-HF inputs were less than NRG1B-HF due to a greater accumulation of GUS-HF. Dotted red line indicates different exposure times. Eluates were submitted for LC-MS; data in Table 5.3.

Table 5.3 SAG101 and EDS1 associate with NRG1 upon effector delivery in Arabidopsis

			Ws-2_*nrg1a/b*			
			pNRG1B:NRG1B-HF		35S:GUS-HF	
Identified Proteins	MW	Pf0-1:	EV	AvrRps4	EV	AvrRps4
NRG1B-HF	93 kDa		170	144	0	0
GUS-HF	-		18	35	697	466
RBCL | ribulose-bisphosphate carboxylase	53 kDa		51	95	19	17
RCA | rubisco activase	52 kDa		41	51	20	15
ATPA | ATP synthase subunit beta	54 kDa		34	87	7	10
HSC70-1 | heat shock cognate 70-1	71 kDa		63	46	7	5
ATPB | ATP synthase subunit alpha	55 kDa		30	45	12	8
GAPB | glyceraldehyde-3-phosphate dehydrogenase B subunit	48 kDa		17	31	6	3
FTIP1 | C2 calcium/lipid-binding plant phosphoribosyltransferase family protein	91 kDa		30	23	0	0
TKL1 | Transketolase	80 kDa		10	29	0	0
HSP70 | Heat shock protein 70 family protein	71 kDa		44	37	0	0
HSP70 | Heat shock protein 70 family protein	71 kDa		45	36	0	0
PVA12 | plant VAP homolog 12	26 kDa		12	9	0	0
SAG101 | senescence-associated gene 101	62 kDa		0	5	0	0
EDS1 | enhanced disease resistance 1	72 kDa		0	4	0	0
				Total Spectrum Count		

Eluates from Figure 5.14. Table generated from top 10 EV- and AvrRps4-treated hits. Below dash line contains proteins of interest > top 10 hits. Top 55 out of 218 for AvrRps4-treated in Appendix XIII. Further data in scaffold file jfe190320.

Eluates were submitted for LC-MS analysis and a table was generated from the top ten hits (11 total) for empty vector- and AvrRps4-treated samples (Table 5.3). Similar to Table 5.2, peptides were identified for RBCL, RCA, HSC70-1, ATPA, and FTIP1. These data indicate that these co-purifying components do not change upon immune activation. Notably, while not represented in the top ten hits, spectra for peptides derived from EDS1 and SAG101 were present in eluates isolated from AvrRps4-treated tissue. These data indicate that SAG101, like EDS1, associates with NRG1B-HF upon AvrRps4 delivery.

While overexpression of GUS-HF served as a technical control for non-specific interactions, it should be noted that GUS-HF would not be expected to complement *nrg1a/b* mutants. Therefore, as empty vector-treated samples showed no association of EDS1 and SAG101 with NRG1, Pf0-1 delivery of empty vector was utilised further as a biological control. Additionally, to evaluate whether NRG1-EDS1 associations are damage-induced, mock treatment was added as a control. Indeed, EDS1 only associated with NRG1B-HF upon AvrRps4 delivery (Figure 5.15).

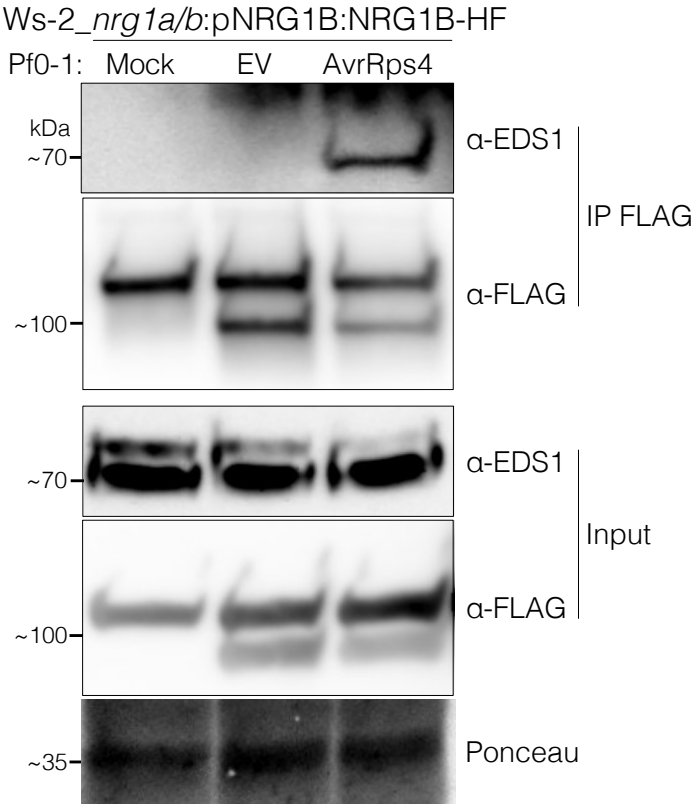

Figure 5.15 EDS1 association with NRG1 is specifically induced by ETI activation. SDS-PAGE and anti-FLAG® or anti-EDS1 western blot of lysates from Ws-2_*nrg1a/b*:pNRG1B:NRG1B-HF 4 h after $MgCl_2$-MES (mock) infiltration or 4 hpd by Pf0-1 carrying empty vector or AvrRps4. Lysates were incubated with anti-FLAG® agarose beads and eluted with

3×FLAG® peptide. Membranes were Ponceau-stained to evaluate loading controls. Eluates were submitted for LC-MS; data in Table 5.5.

Eluates were sent for LC-MS analysis which identified co-purifying components as seen previously (Appendix XIV). Although EDS1 association with NRG1 was observed in western blots, no spectra for EDS1 or SAG101 peptides were present in LC-MS analysis of mock-, Pf0-1 empty vector- or AvrRps4-treated eluates (Table 5.5). This may be due lower anti-FLAG® IP efficiency or variability in EDS1 accumulation between biological replicates.

Notably, the presence of spectra that correlated to an RRS1-R-HF construct in the LC-MS reference database were observed in all samples (Table 5.4). RRS1/RPS4 are the endogenous TNLs that recognize AvrRps4. Spectra for peptides derived from the HF tag were predominantly observed, and as no RRS1-R-HF was present in lysate, these were deemed false-positive spectra. Likely, those spectra correlated to peptides from the HF fusion-tag on NRG1B-HF. However, two spectra correlating to peptides in the RRS1-R sequence were observed: SLPNmANLEFLK, present only in the mock- and AvrRps4-treated samples, and mTDmEEFQDNmEVDNDVVDTR, present only in the mock- and empty vector-treated samples. Notably, mTDmEEFQDNmEVDNDVVDTR is unique to RRS1-R in the C-terminal extension not present in the Col-0 RRS1-S allele. These data indicate a constitutive association between RRS1-R and NRG1B-HF.

When spectra were assembled against a reference database that did not include the peptide sequence for the RRS1-R-HF construct, the total spectrum counts of RRS1 were many fewer—and only when the threshold was reduced to one minimum peptide (Table 5.5). However, only spectra for the SLPNmANLEFLK peptide were present, as this reference database included only the Col-0 RRS1-S allele. These data provide support for the authenticity of the RRS1-R peptides in these LC-MS results. Yet, with this reference database and these threshold settings, spectra for peptides that correlated to other uncharacterized TNLs were also present: one spectrum for At4g16900 was present in the mock- and empty vector-treated samples, and one spectrum for At1g65850 was present in the mock-treated samples (Table 5.5). These data may indicate that NRG1B-HF constitutively associates with multiple TNLs. However, convincing spectra for RRS1, At4g16900, or At1g65850 were not present in other LC-MS analyses utilizing Pf0-1 delivery of AvrRps4. Therefore, follow-up investigations directly testing for NRG1 associations with TNLs are required.

Table 5.4 Mass spectrometry for NRG1B-HF interactors pre- and post-activation

		Ws-2_*nrg1a/b*:pNRG1B:NRG1B-HF			
Identified Proteins	MW (kDa)	Mock	Pf0-1:	Empty Vector	AvrRps4
NRG1B-HF	99	196		185	134
RRS1-R-HF	162	11		11	4
		Total Spectrum Counts			

Eluates from Figure 5.15. EV = empty vector. Top 50 for AvrRps4-treated in Appendix XIV. Further data in scaffold file jfe190528.

Table 5.5 Mass spectrometry of TIR-NLR associations with NRG1B-HF

		Ws-2_*nrg1a/b*:pNRG1B:NRG1B-HF			
Identified Proteins	MW (kDa)	Mock	Pf0-1:	Empty Vector	AvrRps4
NRG1B-HF	99	196		185	134
RRS1 (At5g45260)	146	1		0	1
TIR-NLR (At4g16900)	118	1		1	0
TIR-NLR (At1g65850)	119	1		0	0
		Total Spectrum Counts			

Minimum of one peptide. Eluates from Figure 5.15. Further data in scaffold file jfe190528-NoConstructs.

As mentioned, the Arabidopsis Ws-2 accession has an endogenous RRS1-R allele that in addition to AvrRps4, recognizes the bacterial effector PopP2 and an unknown effector from *Colletotrichum higginsianum*. The Ws-2_*nrg1a/b* complementation line carrying pNRG1B:NRG1B-HF recognizes AvrRps4 (Castel et al., 2019a); however, PopP2 recognition has not been evaluated. Pf0-1 delivery of PopP2 showed HR 24 hpd while delivery of non-recognized PopP2^{C321A} did not (Figure 5.16). These data indicate that pNRG1B:NRG1B-HF complements Ws-2_*nrg1a/b* for both AvrRps4 and PopP2 recognition.

Figure 5.16 NRG1B-HF complements PopP2 recognition in Ws-2_*nrg1a/b*. Images of rosette leaves of 5-6-week-old Ws-2_*nrg1a/b* complementation lines carrying pNRG1B:NRG1B-HF infiltrated with Pf0-1 carrying empty vector, AvrRps4, AvrRps4^{KRVY}, PopP2, or PopP2^{C321A}. HR was evaluated 24 hpd. Further replicates in Appendix XV.

To evaluate the conservation of EDS1-SAG101 associations with NRG1B-HF upon activation of RRS1/RPS4, co-IPs were performed after AvrRps4 or PopP2 delivery by Pf0-1. Immunoblot showed that EDS1 associates with NRG1B-HF both upon AvrRps4 and PopP2 treatment (Figure 5.17). However, band intensity in the overexposed (OE) anti-EDS1 blot after anti-FLAG® IP for the PopP2-treated sample is far weaker than that for the AvrRps4-treated sample. These data indicate that either EDS1 association with NRG1B-HF is not as strong upon PopP2 treatment, or that associations are not provoked 4 h post-effector delivery. Additional timepoints should be tested after PopP2 delivery to better evaluate whether EDS1 association with NRG1 is comparable between PopP2 and AvrRps4 treatment. These data indicate that EDS1 association with NRG1 is a conserved RRS1-RPS4-mediated immune response.

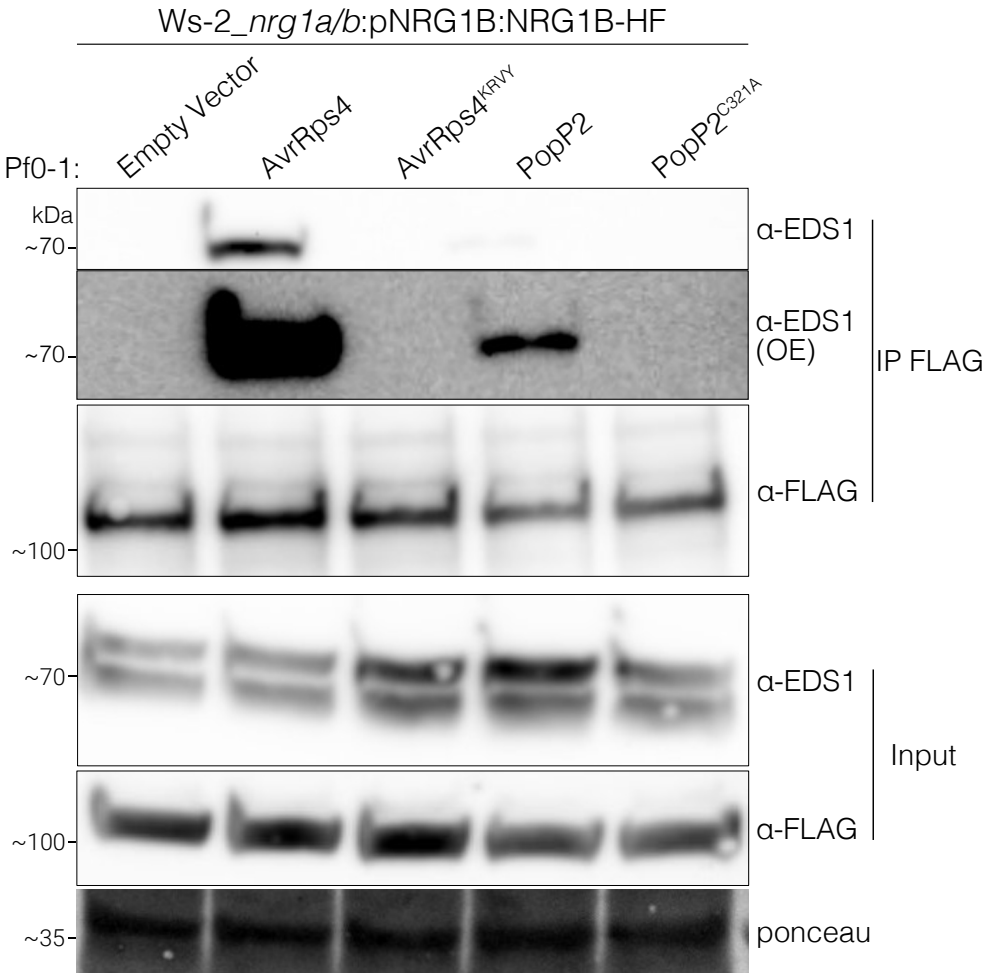

Figure 5.17 EDS1 associates with NRG1B-HF upon PopP2 delivery in Arabidopsis. SDS-PAGE and anti-FLAG® or anti-EDS1 western blot of lysates from Ws-2_*nrg1a/b*:pNRG1B:NRG1B-HF 4 hpd by Pf0-1 carrying empty vector, AvrRps4, AvrRps4^{KRVY}, PopP2, or PopP2^{C321A}. Lysates were incubated with anti-FLAG® agarose beads and eluted with 3×FLAG® peptide. "OE" indicates membranes were over-exposed. Membranes were Ponceau-stained to evaluate loading controls. Eluates were submitted for LC-MS; data in Table 5.6.

Eluates were sent for LC-MS analysis with similar co-purifying proteins identified as before (Appendix XVI). Again, spectra that correlate to peptides derived from EDS1 and SAG101 were present in eluates from tissue that was infiltrated with Pf0-1 delivering AvrRps4 (Table 5.6). However, only one spectrum for EDS1 was counted in the eluates from the PopP2-treated sample. No spectra that correlate to SAG101 peptides are observed when thresholds are lowered to < 5% probabilities. However, it is likely that SAG101 was not detected due to a lower IP efficiency in the presence of PopP2 compared to that in the presence of AvrRps4. This experiment should be repeated with optimized timings for PopP-2-induced associations between NRG1 and EDS1. However, these data provide further support for effector-dependent associations of EDS1 and SAG101 with NRG1B-HF.

Table 5.6 Mass spectrometry for NRG1B interactors downstream of RRS1/RPS4

			Ws-2_*nrg1a/b*:pNRG1B:NRG1B-HF				
Identified Proteins	MW (kDa)	Pf0-1:	EV	AvrRps4	KRVY	PopP2	C321A
NRG1B	93		237	228	277	247	248
SAG101	62		0	15	0	0	0
EDS1	72		0	11	0	1	0
			Total Spectrum Count				

EV = Empty Vector, KRVY = AvrRps4^{KRVY}, C321A = PopP2^{C321A}. Eluates from Figure 5.17. Top 50 for AvrRps4-treated in Appendix XVI. Further data in scaffold file jfe190905.

5.9 Time-resolved associations of EDS1 with NRG1 upon AvrRps4 delivery

To investigate the timing of associations between EDS1 and NRG1, samples were harvested 2, 4, and 12 hpd by Pf0-1 carrying AvrRps4 or empty vector. SAG101 association was not evaluated, as eluates were not submitted for LC-MS analysis. Association of EDS1 with NRG1B-HF is observed 4 hpd, as with other experiments (Figure 5.18). Notably, overexposure of the anti-EDS1 blot also shows some weak EDS1 association with NRG1 12 hpd. These data indicate that either EDS1-NRG1B-HF associations are transient, or that cell viability was compromised in those cells that contained EDS1-NRG1B-HF associations leading up to 12 hpd.

Notably, an increase in protein accumulation over time is observed for NRG1B-HF and EDS1 in the empty vector-treated samples compared to the AvrRps4-treated samples (Figure 5.18). Pf0-1 delivery of empty vector triggers PTI-mediated immune responses (Thomas et al., 2009, Ngou et al., 2020a). These

data may indicate that accumulation of NRG1 and EDS1 occurs upon PTI induction; however, follow-up investigations are required that include un-activated controls.

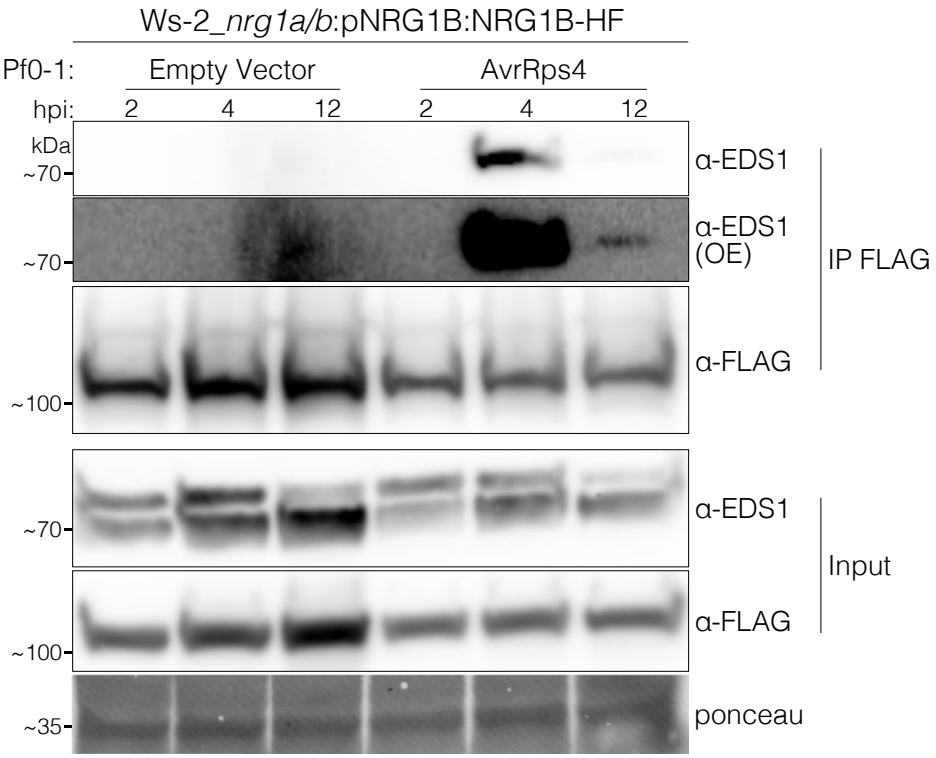

Figure 5.18 EDS1 is not associated with NRG1B-HF 12 h post-AvrRps4 delivery. SDS-PAGE and anti-FLAG® or anti-EDS1 western blot of lysates from Ws-2_*nrg1a/b*:pNRG1B:NRG1B-HF 2, 4, or 12 hpd by Pf0-1 carrying empty vector or AvrRps4. Lysates were incubated with anti-FLAG® agarose beads and eluted with 3×FLAG® peptide. "OE" indicates overexposed membrane. Membranes were Ponceau-stained to evaluate loading controls.

To better elucidate the timings of EDS1 and NRG1 associations, samples were harvested after Pf0-1-mediated delivery of AvrRps4 3, 4, 6, or 8 hpd. Although these data are semi-quantitative only, there is an observable increase in EDS1 associations with NRG1 from 4 to 8 hpd (Figure 5.19). However, this may be partially attributable to the higher IP efficiency at 8 hpd, as a stronger band intensity is observed in the anti-FLAG® blot after anti-FLAG® IP. Notably, no association is observed between EDS1 with NRG1 at 3 hpd. These data indicate that EDS1 associations with NRG1 initiate 4 h post-effector delivery, and continue to accumulate from 4 to 8 hpd. Notably, a weak association is observed 4 hpd; likely explained by decrease in anti-EDS1 antibody sensitivity.

Additionally, accumulation of NRG1B-HF and EDS1 in total protein lysates increases from 4 to 8 hpd (Figure 5.19). Therefore, NRG1-EDS1 associations over

time may be a passive result of increased protein accumulations. However, as mentioned, changes in accumulation of EDS1 and NRG1B-HF was not observed 2, 4, or 12 h post-AvrRps4 delivery (Figure 5.18). Therefore, follow-up investigations are required to comprehensively evaluate PTI- and PTI+ETI-induced NRG1 and EDS1 accumulations.

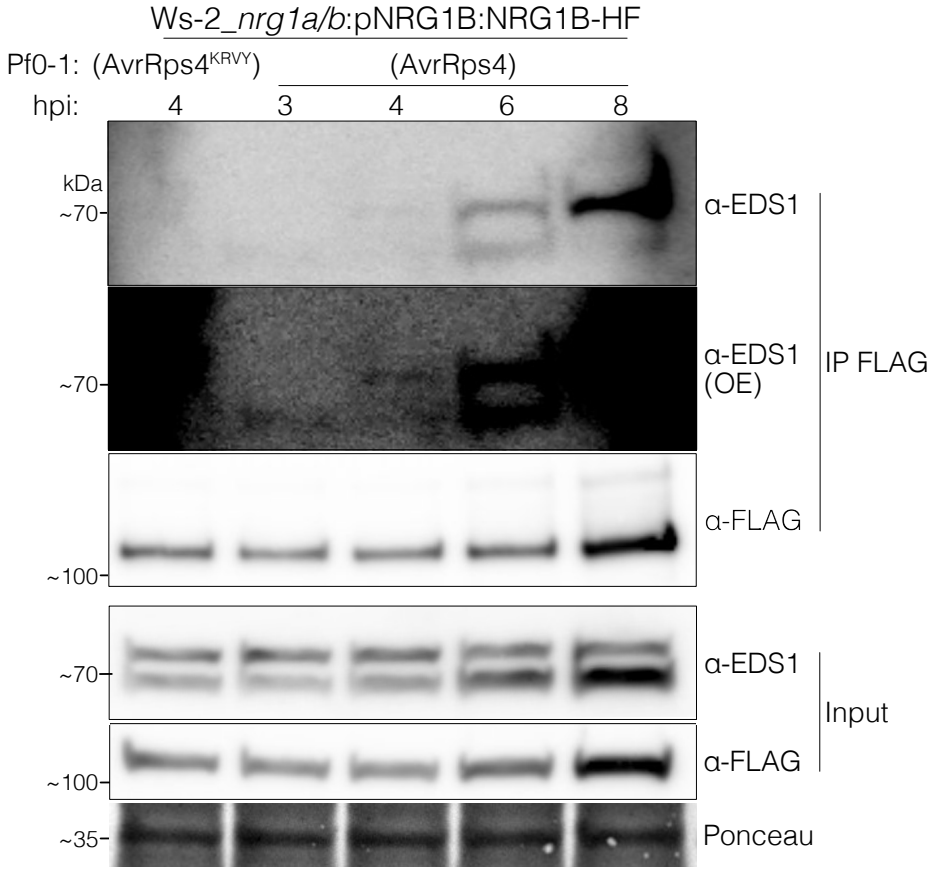

Figure 5.19 EDS1 association with NRG1B-HF increases from 4 to 8 h post-AvrRps4 delivery. SDS-PAGE and anti-FLAG® or anti-EDS1 western blot of lysates from Ws-2_*nrg1a/b* complemented with pNRG1B:NRG1B-HF 4 hpd by Pf0-1 carrying AvrRps4^{KRVY}, or 3, 4, 6, 8 hpd by Pf0-1 carrying AvrRps4. Lysates were incubated with anti-FLAG® agarose beads and eluted with 3×FLAG® peptide. Membranes were Ponceau-stained to evaluate loading controls. Eluates were submitted for LC-MS; data in Appendix XVII.

Eluates were sent for LC-MS analysis with similar co-purifying components detected as in previous assays (Appendix XVII). However, no spectra correlating to EDS1 or SAG101 peptides were observed. If filters were decreased to a protein probability threshold > 80%, peptide probability threshold > 90%, and one minimum peptide identified, one SAG101 peptide is observed in the AvrRps4-treated sample harvested 8 hpd (data not shown). No spectra that correlate to EDS1 peptides are

observed even when thresholds are lowered to < 5% probabilities. These data may indicate that SAG101 also associates with NRG1 8 h post-effector delivery; however, these data are not conclusive.

5.10 Non-specific native anti-EDS1 antibody halts progress in Arabidopsis

Although the assays utilizing eluates after anti-FLAG® IP in Arabidopsis Ws-2_*nrg1a/b* complementation lines carrying pNRG1B:NRG1B-HF were working well, a new lot of anti-EDS1 antibody (Lot 1908) from Agrisera no longer showed the same specificity as the lot used in this chapter (Lot 1609; Figure 5.20). optimisations were attempted which included variable dilutions, blocking reagents, and probing timings; however, none of these improved the resolution of the EDS1-specific band (Appendix XVIII). Without a specific anti-EDS1 antibody, assays were discontinued in Arabidopsis and generation of NRG1, EDS1, and SAG101 immuno-tagged complementation lines were initiated. These lines will not be available until late 2020, and thus will not be included in this thesis.

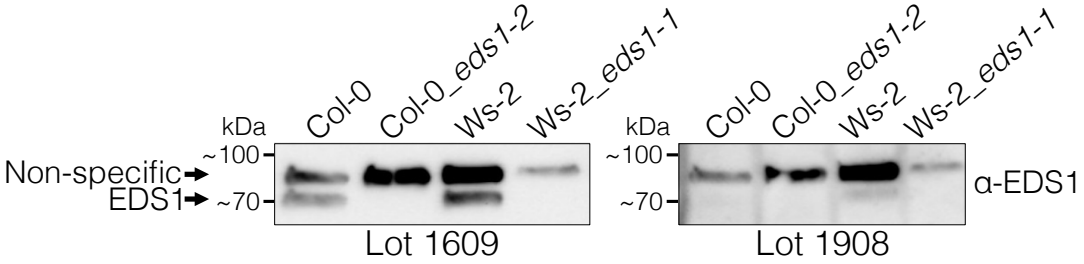

Figure 5.20 New lot of anti-EDS1 antibody not specific to EDS1. SDS-PAGE and anti-EDS1 western blot of Col-0, Col-0_*eds1-2*, Ws-2, Ws-2_*eds1-1* lysates. Anti-EDS1 Lot 1609 (reproduced from Figure 5.11) shows that the band migrating near ~ 70 kDa marker is absent in Col-0_*eds1-2* and Ws-2_*eds1-1* lysates indicating specificity for EDS1 while a band migrating below 100 kDa marker is present in all lysates indicating non-specific for EDS1. Anti-EDS1 Lot 1908 shows a band migrating below ~ 100 kDa marker which indicates non-specific for EDS1.

5.11 NRG1 forms higher-order states upon PTI and PTI+ETI by Native PAGE

To investigate formation of higher-order states of NRG1 upon effector delivery, BN-PAGE assays were performed with lysates from Figure 5.15, and bands were visualized by anti-FLAG® antibody labelling. The presence of a single band migrating as a smear between the ~ 146 and ~ 480 kDa MW marker is observed in the mock-, empty vector-, and AvrRps4-treated samples, while the presence of a slower, distinct

band migrating just below the ~ 480 kDa marker is observed in the empty vector- and AvrRps4-treated samples (Figure 5.21, left). These data indicate that a higher-order complex containing NRG1 forms upon PTI-activation alone.

With longer exposure, the presence of a slower-migrating band just above the ~ 720 kDa marker is observed in the empty vector- and AvrRps4-treated samples (Figure 5.21, middle). CBB-staining of the membrane indicates equal loading of lysates (Figure 5.21, right). Additionally, CBB-staining reveals that RuBisCO is masking signal in the overexposed blot, and a band above the ~ 480 kDa marker may be present. Although there are no differences in band migrations between empty vector- and AvrRps4-treated samples, the relative intensity appears changed. These data indicate that higher-order states of NRG1 formed during PTI activation are maintained upon PTI+ETI activation, and that these states are further accumulating upon PTI+ETI activation.

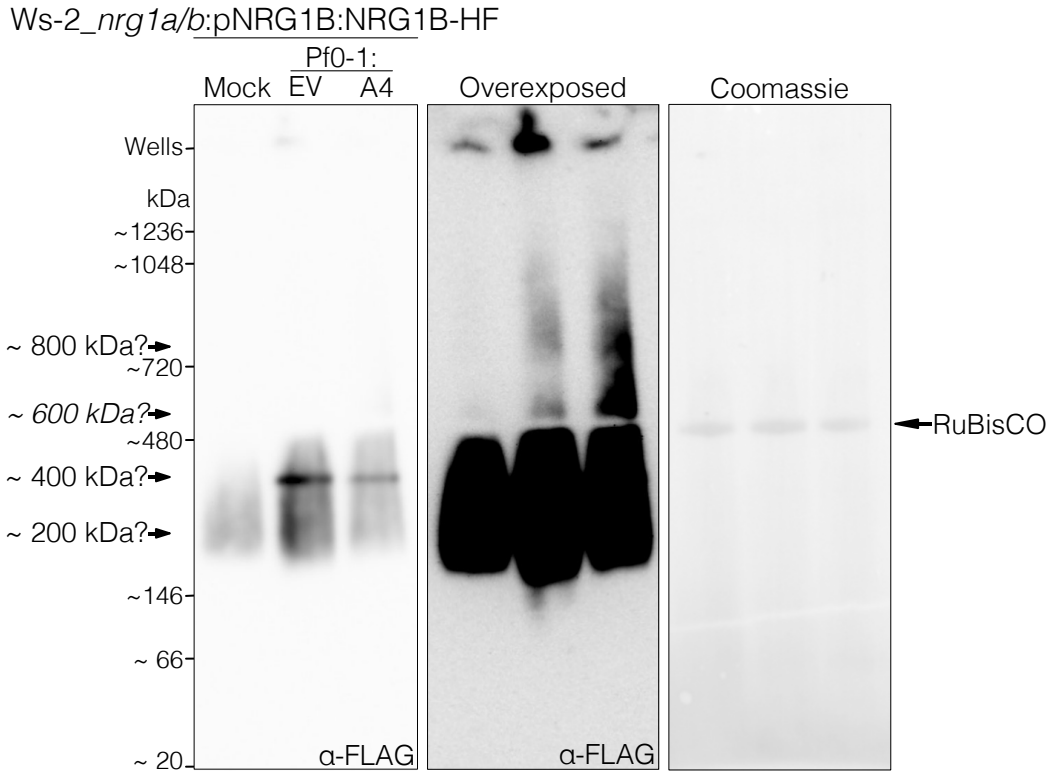

Figure 5.21 NRG1B-HF forms higher-order states upon PTI and PTI+ETI. BN-PAGE and anti-FLAG® western blot of lysates from Figure 5.15 (left). Blot was overexposed to visualize slower-migrating bands (middle). Membrane was stained with CBB to visualize RuBisCO (right). Mock = MES-$MgCl_2$, EV = empty vector, A4 = AvrRps4. Bands are indicated with arrows and potential MWs are described. The band at ~ 600 kDa is in italics as it may be masked by RuBisCO.

BN-PAGE was also performed with lysates from Figure 5.19, and bands were visualized by anti-FLAG® antibody labelling. Again, in the uninfiltrated sample, only a band migrating near the ~ 146 kDa marker is observed. However, upon delivery of AvrRps4 or the AvrRps4^{KRVY}, the presence of a slower migrating band is observed near the ~ 480 kDa marker. Pf0-1-mediated delivery of AvrRps4^{KRVY} would still trigger PTI activation. These data are consistent with Figure 5.21—PTI activation induces formation of higher-order NRG1 species that are maintained upon PTI+ETI activation. Notably, an increase in band intensities is observed from 4 to 8 h post-AvrRps4 delivery. These data provide additional support for accumulation of higher-order NRG1 species upon PTI+ETI activation.

However, in contrast to Figure 5.21, two bands are now observed near the ~ 146 kDa marker, and the presence of a band migrating near the ~ 720 kDa marker is not observed (Figure 5.22). Moreover, streaking artefacts interfere with data interpretation. Therefore, more replicates are required with optimized BN-PAGE conditions to further evaluate the PTI- and PTI+ETI- activation states of NRG1.

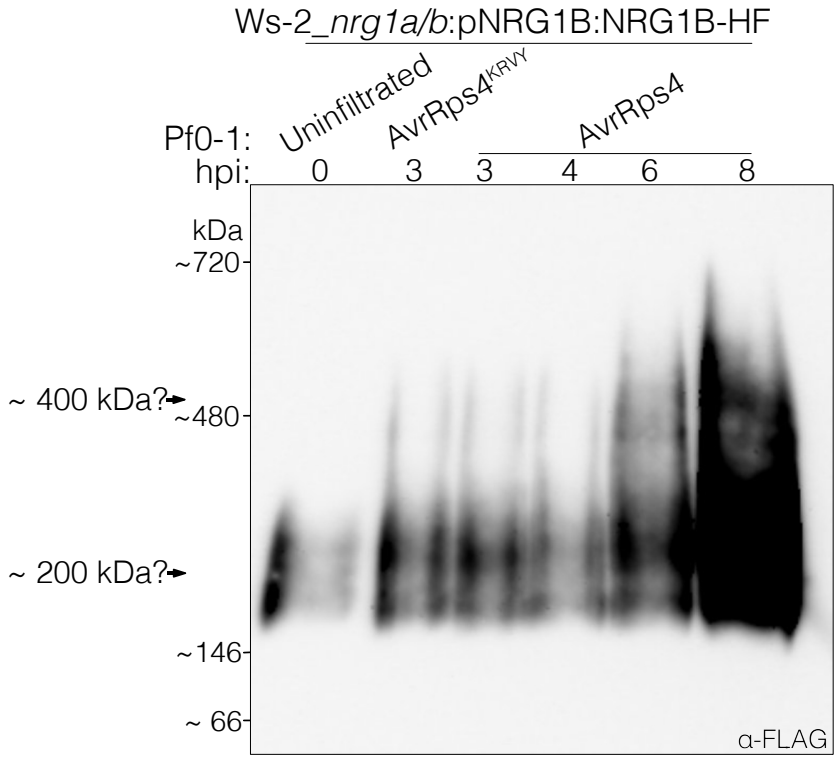

Figure 5.22 Higher-order state of NRG1B-HF accumulates from 4 to 8 h post-AvrRps4 delivery. BN-PAGE and anti-FLAG® western blot of lysates from Figure 5.19. Bands are indicated with arrows and potential MWs are described.

5.12 Localizations of SAG101 and NRG1 pre- and post-immune activation are not resolved

As the literature indicates that NRG1 and SAG101 are primarily localized to different cellular compartments, effector-dependent localization changes were evaluated by transient expression and effector-induction in *N. benthamiana*. Two vectors were co-delivered via *Agro*-infiltration carrying either native promoter-driven NRG1B-mEGFP and SAG101-mCherry, or EDS1-V5 and PAD4-HA. The EDS1-V5_PAD4-HA construct also carried β-estradiol-inducible HopQ1-Myc. HopQ1 is recognized by the TNL Roq1 endogenous to *N. benthamiana* (Schultink et al., 2017). Localization changes would be investigated by first allowing accumulation of these components in *Nb_nrg1* or *Nb_epss*. Upon 2-3 days post-*Agro*-infiltration, induction of HopQ1-Myc would be promoted by infiltration of β-estradiol into the previously *Agro*-infiltrated leaves.

Expression of EDS1-V5 and PAD4-HA was confirmed in lysates after *Agro*-infiltration of *N. benthamiana* by SDS-PAGE and antibody labelling (Figure 5.23). Accumulation was evaluated 48 and 72 h post-*Agro*-infiltration (hpi). β-estradiol was then infiltrated into the previously *Agro*-infiltrated leaves, either 36 hpi or 60 hpi, to evaluate induction of HopQ1-Myc. The most even accumulation of EDS1-V5 and PAD4-HA was observed at 72 hpi, in the presence or absence of HopQ1-Myc (Figure 5.23). Therefore, NRG1B-mEGFP and SAG101-mCherry localizations were assayed by confocal microscopy in *Nb_nrg1* or *Nb_epss* leaves after β-estradiol infiltration 60 h post-*Agro*-infiltration. Mock ($MgCl_2$-MES pH 5.7) infiltrations were used as control.

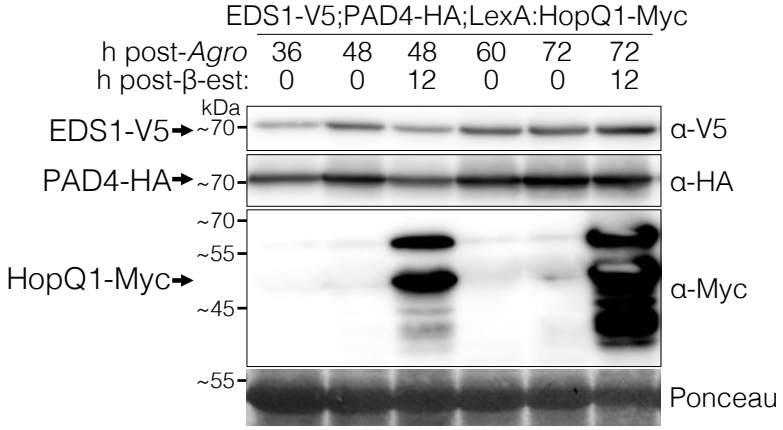

Figure 5.23 Expression tests confirm induction of HopQ1-Myc. SDS-PAGE and western blot of lysates after *Agro*-infiltration and transient expression in *N. benthamiana* of native promoter-driven EDS1-V5 and PAD4-HA with β-estradiol-inducible HopQ1-Myc. Membranes were immunolabelled with anti-V5, anti-HA, or anti-Myc antibody. Loading controls were evaluated by Ponceau-staining of membranes. Construct details described in section 2.7.1.

Leaves were imaged by confocal microscopy every 2 h after β-estradiol or mock infiltration. No changes in NRG1B-mEGFP or SAG101-mCherry localizations were observed (Figure 5.25). These data indicate that NRG1 and SAG101 localization changes do not occur, or are not observable, upon effector induction.

However, co-expression of the native promoter-driven NRG1B-mEGFP, SAG101-mCherry, EDS1-V5, PAD4-HA with 35S promoter-driven HopQ1 does not recapitulate HR (Figure 5.24). Yet, expression of the β-estradiol-inducible HopQ1-Myc in wild type *N. benthamiana* shows HR in the absence of β-estradiol (Figure 5.24, Appendix XIX) This is likely due to "leaky" expression of HopQ1-Myc. Conceivably, recognition of HopQ1-Myc in wild-type *N. benthamiana* would be mediated by the endogenous TNL Roq1 with *Nb*EDS1, *Nb*NRG1, and *Nb*SAG101. Therefore, these data indicate that either the tags utilised for these expression constructs are non-functional, or native expression is insufficient for macroscopic cell death phenotypes. Potentially, the lack of localization changes observed in Figure 5.25 are explained by a lack of immune activation. As a result, this assay was not used further to investigate localization changes. Future experiments are required to establish the functionality of NRG1B-mEGFP, SAG101-mCherry, EDS1-V5, PAD4-HA, and HopQ1-Myc together to recapitulate an HR. Future experiments are also required to more thoroughly investigate the localizations of NRG1, EDS1, and SAG101 pre- and post-immune activation.

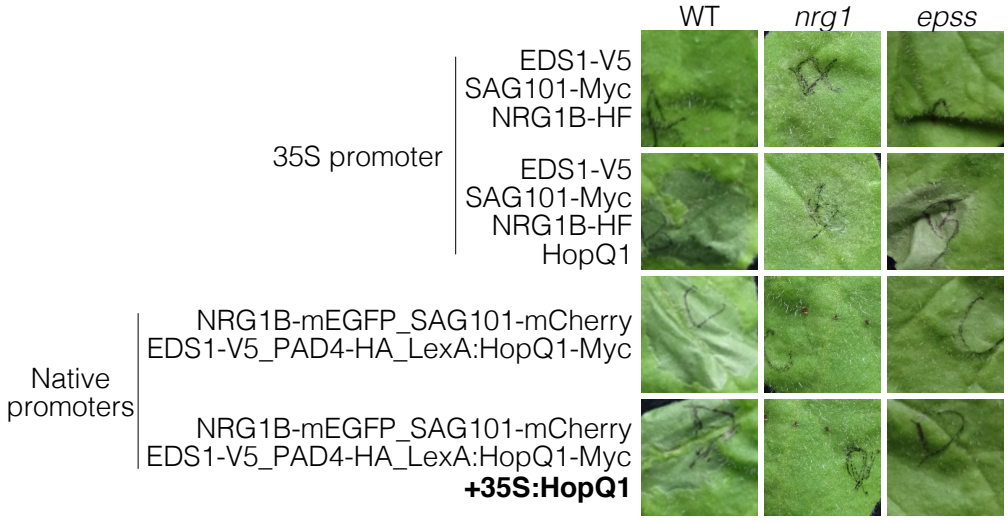

Figure 5.24 Inducible HopQ1-Myc expresses in the absence of β-estradiol and NRG1B-mEGFP and SAG101-mCherry do not recapitulate HR. Leaf images of HR assays after *Agro*-infiltration in 5-6-week-old *N. benthamiana* WT, *nrg1* or *epss* leaves. Infiltration of 35S promoter-driven EDS1-V5, SAG101-Myc, NRG1B-HF and HopQ1 shows HR in WT, *nrg1* (weak), and *epss* leaves. Infiltration of native promoter-driven NRG1B-mEGFP, SAG101-mCherry, EDS1-V5, PAD4-HA and β-estradiol-inducible HopQ1-Myc shows HR in the absence of β-estradiol, while co-delivery with 35S

promoter-driven HopQ1 does not recapitulate HR in the *epss* and *nrg1* mutant backgrounds.

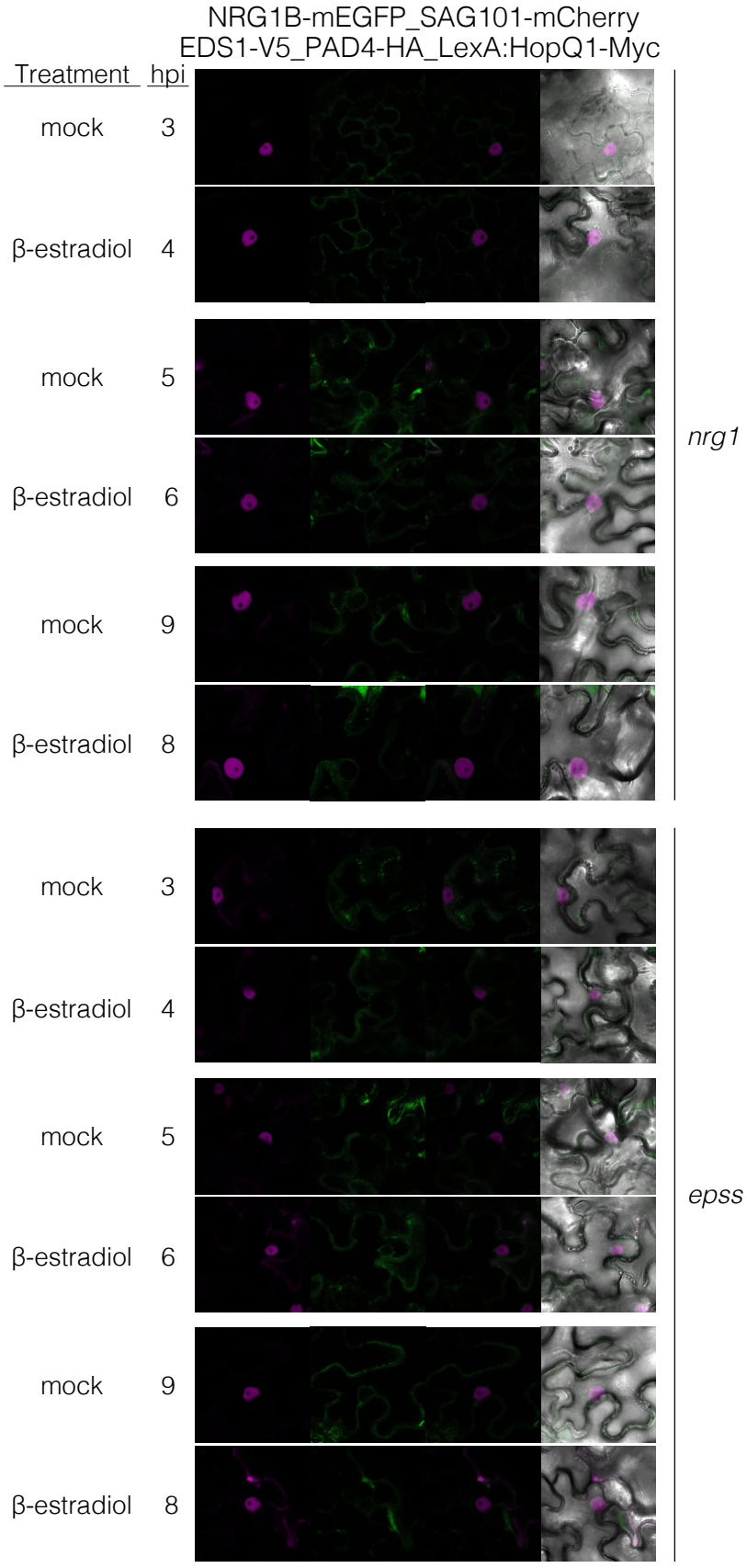

Figure 5.25 No localization changes are observed for NRG1B-mEGFP or SAG101-mCherry upon induction of HopQ1-Myc in transient assays. Confocal

images of *Nb_nrg1* or *Nb_epss* leaves after *Agro*-infiltration and transient expression of native promoter-driven NRG1B-mEGFP, SAG101-mCherry, EDS1-V5 and PAD4-HA with β-estradiol-inducible HopQ1-Myc. Treatment and h post-infiltration (hpi) of mock ($MgCl_2$-MES + 0.1% DMSO) or β-estradiol indicated. Bright field images were taken to visualize cell boundaries. Images were collected separately and merged in ImageJ. Magenta: SAG101-mCherry. Green: NRG1B-mEGFP. Construct details in section 2.7.1. Full dataset in Appendix XX.

5.13 Discussion

5.13.1 EDS1 and SAG101 associate with NRG1 4 h post-AvrRps4 delivery

This project has revealed that EDS1 and SAG101 associate with NRG1B-HF in an effector-dependent manner. Initially, co-IP after *Agro*-infiltration and transient expression in *N. benthamiana* was used to investigate these associations. However, while buffer optimisations resolved issues of non-specific EDS1 and NRG1B associations with controls, results were variable and inconsistent. In contrast, co-IP assays in the Arabidopsis Ws-2*_nrg1a/b* complementation line carrying pNRG1B:NRG1B-HF (Castel et al., 2019a) showed reproducible association of EDS1 and SAG101 with NRG1B-HF 4 h post Pf0-1-mediated AvrRps4 delivery. These data provide a foundation for determining a functional connection to the genetic requirement for NRG1, EDS1, and SAG101 to mediate cell death upon TNL activation.

Transient assays for co-IP have been used extensively in the literature; therefore, it was a logical first approach to investigate associations between EDS1 and NRG1. However, results were highly variable depending on fusion-tags and choice of controls. Buffer optimisations for anti-V5 IP reproducibly showed no interactions of NRG1B-Myc or EDS1-V5 with controls. Yet, non-specific interactions were still observed with anti-Myc IP in the same buffer conditions. This lack of experimental reproducibility created low confidence in the reliability of these results. Furthermore, the optimized buffer conditions saw a constitutive association between NRG1B and EDS1, which were in contrast to what was later observed in Arabidopsis. It's possible that by including an expression construct that carried RRS1-R-HF, RPS4-HA, and inducible AvrRps4-GFP, "leaky" and undetected expression of AvrRps4-GFP in the absence of β-estradiol induced an activated state. This may have promoted associations between NRG1B and EDS1; however, association was still observed between NRG1B-Myc and EDS1-V5 in the absence of the RRS1-R-HF, RPS4-HA, and AvrRps4-GFP (Appendix XI). Furthermore, Wu et al (2019) also showed inconsistent results on whether NRG1 associates with EDS1 by transient co-IP assays in *N. benthamiana*. Collectively, these data indicate that co-IP assays after transient

expression in *N. benthamiana* are not reliable for investigating interactions between Arabidopsis alleles of EDS1 and NRG1.

Therefore, studies on associations between NRG1 and EDS1 were initiated in Arabidopsis. Using native anti-EDS1 antibody and a Ws-2*_nrg1a/b* complementation line carrying pNRG1B:NRG1B-HF, an association of EDS1 was observed with NRG1 after Pf0-1 delivery of AvrRps4. LC-MS confirmed the association of SAG101 with NRG1 in the same samples. Notably, spectra that correlate to PAD4 peptides were not observed to co-IP with NRG1. These data indicate that EDS1 and SAG101 associations with NRG1 contribute to NRG1-mediated immune responses.

The time-course assays revealed that NRG1B-HF associations with EDS1 are detectable by immuno-labelling 4 h after infiltration of Pf0-1 carrying AvrRps4. A further increase in EDS1 associations with NRG1B-HF is observed from 4 to 8 hpd, while a very weak association is observed 12 hpd. As these data were collected from separate experiments, a single time-course evaluating associations from 4 to 12 hpd is required to confirm these results. The weak association at 12 hpd indicates that either EDS1 associations with NRG1 are temporary, or that upon associating with EDS1, the cell death mechanism of NRG1 is initiated. A more detailed discussion on how EDS1 and SAG101 associations with NRG1 may contribute to activation can be found in section 6.2 of this thesis.

5.13.2 NRG1 forms higher-order states upon PTI and PTI+ETI activation

Native PAGE assays have revealed the presence of higher-oligomeric states for NRG1B-HF upon PTI activation. Notably, band shifts are not observed between PTI- and PTI+ETI-activated lysates. These data indicate a “priming” of NRG1 upon PTI activation. As EDS1 is not observed in the eluates of samples under PTI activation, it is unlikely these higher-order states for NRG1B-HF include EDS1 and SAG101 associations; however, EDS1 and SAG101 may be present below the limit of detection. Conceivably, Notably, PTI and ETI are individually insufficient for triggering cell death in Arabidopsis (Ngou et al., 2020a). Perhaps the cell death mechanisms mediated by NRG1 require both PTI for formation of oligomers and ETI for associations with EDS1 and SAG101. Further discussion on the activation state of NRG1 during PTI or PTI+ETI can be found in section 6.2.4 of this thesis.

5.13.3 EDS1 and SAG101 are not always present in mass spectrometry results

Although associations of EDS1 with NRG1 were observed in eluates of every SDS-PAGE and western blot at 4 hpd, only two of the four eluate samples submitted for LC-MS analysis showed spectra correlating to EDS1 and SAG101 peptides: Table 5.3 and Table 5.6. As EDS1 was also absent in those LC-MS results in which SAG101 was absent, and as the literature indicates that SAG101 exists exclusively in heterodimers with EDS1, it is plausible that SAG101 was present in each replicate with EDS1, but not detected. The lack of EDS1 and SAG101 spectra in LC-MS data from Table 5.5 and Appendix XVII. are not due to fewer total NRG1B-HF spectra as they had similar counts to Table 5.3. These data indicate consistent anti-FLAG® IP between biological replicates.

Yet, EDS1 and SAG101 spectra are not consistent in LC-MS results. This may reflect variability in EDS1 and SAG101 associations with NRG1B-HF upon immune activation. Anti-EDS1 bands after anti-FLAG® IP were visualized with 160 s (16 × 10 s standard increments) of exposure in Figure 5.14, with 3060 s (34 × 90 s high increments) in Figure 5.15, with 180 s (4 × 45 s high increments) in Figure 5.17, and with 9,840 s (82 × 120 s high increments) in Figure 5.19. These data indicate that in those samples submitted for LC-MS without EDS1 spectra, a low abundance of EDS1 was associated with NRG1B-HF.

This variability may be attributed to lower abundance of EDS1 in plant tissues or due to multiple uses of the scarce anti-EDS1 antibody. Anti-EDS1 bands for input samples were visualized with 30 s (3 × 10 s standard increments) of exposure in Figure 5.14, 3060 s (34 × 90 s high increments) in Figure 5.15, 180 s (4 × 45 s high increments) in Figure 5.17, and 160 s (16 × 10 s high increments) in Figure 5.19. It is possible that the lower abundance in the input samples for Figure 5.15 was due to infiltrating at ~ 1330 instead of ~ 0930, as there is evidence that accumulation of EDS1 and SAG101 is variable throughout the day (Sano et al., 2014). Likely, the lower abundance of EDS1 in the IP sample for Figure 5.19 is due to > 3 uses of the same antibody aliquot. As the anti-EDS1 antibody is no longer available, future experiments should be performed with stable immuno-tagged Arabidopsis lines. These lines should be evaluated for protein accumulation throughout the day to facilitate more reproducible assays. Taken together, it is conceivable that SAG101 was present with EDS1 when it was found to associate with NRG1B-HF by immunoblotting, but below the limit of detection by LC-MS.

5.13.4 Localizations for NRG1 and SAG101 are not resolved

Notably, the differences in sub-cellular localizations for SAG101 and NRG1 presents a paradox for our observation that they associate upon effector delivery. Transient assays in *N. benthamiana* with Arabidopsis alleles of NRG1B-mEGFP and SAG101-mCherry in the presence of EDS1-V5 and PAD4-HA were attempted to investigate localization changes upon induction of HopQ1-Myc. HopQ1 is recognized by the *N. benthamiana* endogenous TNL Roq1. However, no changes were observed. This may be explained by several factors: a) no mass migrations occur upon immune activation and were thus not visible without quantitative assays, b) the inducible HopQ1-Myc was leaky and the pre-activation control was under immune activation, c) the fluorophore-tagged alleles of NRG1B and SAG101 are not functional, or d) native promoters for EDS1, SAG101, NRG1, and PAD4 provided insufficient expression level to recapitulate a strong immune response. If these assays were attempted again, verification of functionality of the mEGFP tag on NRG1B should be prioritized, as NRG1B-GFP was non-functional in HR assays (Figure 4.21).

However, Wu et al. (2019) complemented *nrg1a/b chs3-2D* mutants with native promoter-driven NRG1A-mNeonGreen or NRG1B-mNeonGreen. As co-expression with 35S promoter-driven Arabidopsis alleles of NRG1B-HF, SAG101-Myc, and EDS1-V5 with HopQ1 is sufficient to recapitulate HR in *N. benthamiana*, 35S promoter-driven NRG1B-mEGFP and SAG101-mCherry should be generated and tested for functionality. Additionally, assays could be conducted in a *roq1* mutant to better evaluate the pre-activation state, as any HopQ1-Myc expression in the absence of β-estradiol will not be recognized. However, I am generating stable transgenic *nrg1a/b sag101* complementation lines carrying native promoter-driven NRG1B-mEGFP and SAG101-mCherry to investigate localization changes pre- and post-immune activation by Pf0-1 delivery of AvrRps4. If NRG1-mEGFP and SAG101-mCherry prove to be functional, these assays should be less prone to expression artefacts that interfere with data interpretation. Further discussion on how the localizations of NRG1 and EDS1-SAG101 may influence signalling mechanisms can be found in section 6.2.3 of this thesis.

5.13.5 EDS1 associates with NRG1 upon PopP2 delivery

The differences in associations between EDS1 with NRG1 upon PopP2 treatment vs. AvrRps4 treatment are notable. It's unlikely that PopP2 would induce a lower association between EDS1 with NRG1B-HF; it is more likely that the association begins shortly after 4 hpd by Pf0-1 infiltration. It's possible this discrepancy can be

attributed to AvrRps4 recognition by both the RRS1-R/RPS4A and RRS1B/RPS4B pairs vs PopP2 recognition by only the RRS1-R/RPS4A. Perhaps activation of both pairs leads to more timely downstream signalling responses. A time-course from 4-12 hpd between AvrRps4 and PopP2 would reveal whether EDS1 association with NRG1 is weaker or begins 4 h post Pf0-1 delivery of PopP2.

5.13.6 NRG1 likely does not associate with RRS1/RPS4

Although AvrRps4 signals through RRS1 and RPS4 as well as EDS1, SAG101, and NRG1, data is inconsistent on whether there are associations between NRG1 and RRS1 and RPS4. We saw RRS1-R-HF hits in one LC-MS data set; however, it is likely that most spectra recovered peptides in the HF tag which increased confidence in the identification of RRS1. Yet, the presence of unique RRS1 peptides in each sample is intriguing. Although some associations were also observed in *N. benthamiana* transient assays, these data were highly variable and inconsistent. While the most reasonable conclusion based on these data would be that NRG1 does not associate with RRS1 or RPS4, it has not been thoroughly tested in this project. To resolve these inconsistencies, future experiments utilizing Arabidopsis in vivo systems could be designed to directly investigate whether NRG1 associates with upstream TNLs. The likelihood of these associations will be discussed in further detail in section 6.4 of this thesis.

5.13.7 HSC70-1 and PVA12 may contribute to immune mechanisms of NRG1

LC-MS results after anti-FLAG® IP of NRG1B-HF indicated spectra for peptides of proteins that localized to chloroplasts and nuclei. Potentially these represent non-specific components associating with anti-FLAG® beads. However, PVA12 and HSC70 were continually identified in the top 10-50 hits for both transient expression and Arabidopsis samples. While co-purification of chaperones is expected, as they regulate protein folding, HSC70 has been implicated in NLR-mediated plant immunity. In contrast, a role for PVA12 in immunity has not been revealed. Yet, it is possible these associations reflect some contribution to NRG1-mediated immunity.

PVA12 was identified as a protein of interest after BLAST of the VAP that co-purified with *At*NRG1B-HF after heterologous expression in *N. benthamiana*. VAPs are tail anchor membrane-associated proteins with an N-terminal cytoplasmic domain, and have been implicated in targeting proteins to the cytosolic surface of the ER in yeast and mammalian cells (Saravanan et al., 2009). However, the role of plant VAP homologs (PVAs) have not been established. PVA12, a member of the larger VAP33

family, has a novel role as an ER receptor for ORP3A [OSBP(OXYSTEROL BINDING PROTEIN)-RELATED PROTEIN 3A] via an WFDE domain (Saravanan et al., 2009). These data may implicate PVA12 in mediating NRG1 localizations to ER networks; however, this is highly speculative. PVA12 has not been implicated in immunity, and NRG1 does not appear to carry a WFDE domain, although that domain could be specific to ORPs. Nonetheless, future investigations could aim to evaluate a functional role for PVA12 in NRG1-mediated immune responses.

In Arabidopsis, HSC70 proteins, also referred to as HSP70, comprise a subset of heat shock proteins which function under stress to facilitate folding and prevent aggregation, amongst other processes (Sung et al., 2001). HSP70-1 and, to a lesser extent, HSP70-2 were found to be important for virulence by the *Pseudomonas syringae* HopI1 effector (Jelenska et al., 2010). Furthermore, silencing of HSP70-1 in *N. benthamiana* impairs defence responses (Kanzaki et al., 2003). These data indicate a role for HSC70s in basal and ETI resistance. As mentioned in the introduction chapter of this thesis, SGT1 is required for RRS1/RPS4-mediated immunity (Zhang et al., 2004), and SGT1b, EDS1, SAG101 were all shown to be positive regulators of the TNL CHS3-mediated defence (Xu et al., 2015). Notably, purification of SGT1 shows stable associations with HSC70-1 (Noël et al., 2007). Therefore, it is tempting to postulate whether HSC70-1/SGT1 associations bridge the EDS1-SAG101 associations with NRG1 via HSC70-1/NRG1 interactions. Indeed, Dr. Pingtao Ding has shown that SGT1b constitutively co-purifies with EDS1 from Arabidopsis lysates (Pingtao Ding, personal communication with permission). However, LC-MS data in this thesis did not show spectra that correlated to SGT1 peptides. Therefore, any role for HSC70 in NRG1-mediated immunity remains speculative, yet, future investigations could investigate this possibility.

5.13.8 Conclusions

Although evidence exists for the genetic requirement of NRG1, EDS1, and SAG101 to mediate cell death together, convincing data on whether or not they associate have not been shown until now. This project has revealed in Arabidopsis an effector-dependent association between EDS1 and SAG101 with NRG1. A clear association is reproducibly observed 4 h post-effector delivery, which seems to increase up to 8 h post-effector delivery and is no longer present 12 h post-effector delivery. The association between EDS1 with NRG1 is induced by two effectors that are recognized by sensor TNLs RRS1/RPS4, indicating that varying inputs generate the same activation outputs. The formation of higher-order states for NRG1 upon PTI

activation indicates some priming that may be required for cell death mechanisms. Follow-up work is required to resolve the exact mechanisms that provoke EDS1-SAG101 associations with NRG1, and whether associations are dependent upon localization changes. Moreover, whether these associations are transient or stable is to be determined. The data presented in this chapter provides a foundation for future investigations into the mechanisms by which NRG1 mediates cell death with EDS1 and SAG101.

Chapter 6

Discussion

6 Discussion

6.1 Summary of research progress

The goal of this project was to gain insights into the mechanisms employed by plants between pathogen recognition by intracellular receptors and host immunity. I used a forward genetics screen with an inducible effector, purifications of full-length NRG1 for structural investigations, and biochemical assays of NRG1 associations to elucidate mechanisms that span immune activation to defence response. While the forward genetics screen was terminated early due to a high false-positive recovery rate, the structural and association investigations were more informative. I optimized an *in planta* purification protocol for recovery of highly pure, though low yield, NRG1 protein which is visible by negative stain EM. Furthermore, I discovered the effector-dependent association between EDS1 and SAG101 with NRG1. These data will provide the foundation for a more detailed understanding of NRG1 signalling mechanisms pre- and post-immune activation. As NRG1 represents a component of the helper NLR clade of RNLs, mechanistic insights may reveal core plant immune response mechanisms.

6.2 Effector-dependent associations between NRG1 with EDS1 and SAG101

6.2.1 How NRG1 forms associations with EDS1 and SAG101 is not clear

RNLs comprise a helper NLR signalling hub that functions in parallel with EDS1-family proteins downstream of sensor TNLs. The RNL NRG1 functions in a co-evolved module with EDS1 and SAG101 to mediate cell death in Arabidopsis (Lapin et al., 2019). Using co-IP assays in Arabidopsis, I revealed that EDS1 and SAG101 associate with NRG1 only upon effector delivery. Additionally, I showed that higher-order states of NRG1 are formed upon immune activation in BN-PAGE assays. These data indicate that NRG1 may form an immune signalling complex with EDS1 and SAG101 to mediate cell death upon TNL-mediated immune activation.

Mass spectrometry data consistently showed SAG101 and EDS1 associations with NRG1 in relatively equal abundance. Although some evidence suggests that EDS1 may exist as a monomer—or in complex with unknown components—when not in heterodimers with either SAG101 or PAD4 (Voss et al., 2019), SAG101 shows instability in the absence of EDS1 (Feys et al., 2005). These data strongly suggest that

SAG101 exists exclusively in heterodimers with EDS1. Therefore, it is unlikely that SAG101 associates with NRG1 in the absence of EDS1. Conceivably, the data presented in this thesis could indicate the formation of NRG1-EDS1-SAG101 associations and not NRG1-EDS1 or NRG1-SAG101 associations. However, this has not unambiguously been shown.

Potential binding sites on NRG1 for EDS1-SAG101 are not obvious. Qi et al. (2018) found that the NB-ARC and LRR domains of *Nb*NRG1 associate with *Nb*EDS1. This likely holds true for the Arabidopsis alleles. Additionally, the presence of a large cavity in EDS1-SAG101 heterodimers was noted when the structure was solved (Wagner et al., 2013). Mutating a residue in this cavity on EDS1 shows maintenance of associations with PAD4 but defective transcriptional activation (Bhandari et al., 2019). As ADR1-EDS1-PAD4 mediate transcriptional activation, perhaps the residues in this cavity mediate EDS1-PAD4 associations with ADR1. It could be revelatory to test whether mutating conserved residues in SAG101 results in loss-of-association with NRG1.

The formation of NRG1-EDS1-SAG101 associations after effector delivery indicates that NRG1 requires these associations to activate cell death mechanisms. If NRG1 does oligomerize to carry out cell death mechanisms, it is possible that EDS1-SAG101 associates with NRG1 to provoke oligomerization. Conceivably, EDS1-SAG101 perceives upstream signals of immune activation, and directly interact with NRG1 to induce conformation changes that facilitate oligomerization (Figure 6.1A). This would mimic the mechanism in which ZAR1-RKS1 monomers perceive the modified PBL2^{UMP} and oligomerize to form a resistosome (Wang et al., 2019b, Wang et al., 2019a).

However, few spectra were counted for EDS1 and SAG101 compared to NRG1 in LC-MS data. While semi-quantitative only, this may indicate either transient association of EDS1-SAG101 with NRG1, or low abundance of EDS1-SAG101-NRG1 stably-associated forms. A transient association is further supported by the absence of EDS1 associated with NRG1 12 h post-effector delivery. It's possible that EDS1 and SAG101 briefly associate with NRG1, either directly or indirectly, to mediate oligomerization before dissociating to produce activated NRG1 resistosomes (Figure 6.1B). However, the absence of EDS1 associated with NRG1 12 h post-effector delivery could also be a result of cell death induced by NRG1-SAG101-EDS1 associations. Yet, accumulation of NRG1 and EDS1 in lysates remained constant from 4-12 h post-effector delivery. It's plausible that total lysates contained enough NRG1

and EDS1 to mask the effect of cell death in those cells that contained NRG1-EDS1-SAG101 complexes. Therefore, future investigations utilizing loss-of-function NRG1 mutants (discussed further in 6.2.2) could be employed. Knowing whether EDS1 and SAG101 are present in the final activated form of NRG1 is essential to better understand the mechanisms of NRG1-mediated cell death.

Additionally, EDS1 associations with NRG1B-HF seemed to increase from 4-8 h after AvrRps4 delivery. This may reflect the active formation of NRG1-EDS1-SAG101 associations upon effector delivery. However, accumulation of NRG1B-HF and EDS1 was also observed in lysates. This may indicate that NRG1-EDS1-SAG101 associations are passively formed as a result of increasing concentrations. Yet, it is not clear whether accumulation is sufficient to induce associations—overexpression of *At*NRG1, *At*EDS1, *At*SAG101 in *N. benthamiana* does not show HR in the absence of a recognized effector (Figure 5.24). In contrast, overexpression of *Nb*NRG1 in *N. benthamiana* does induce effector- and EDS1-independent cell death (Schultink et al., 2017). Therefore, whether NRG1 associations with EDS1 and SAG101 are active or passive requires follow-up investigation. Potential upstream activation signals will be discussed in further detail in section 6.3.

Slower migrating forms of NRG1 are present in BN-PAGE upon Pf0-1 delivery of empty vector (PTI activation). Yet, EDS1 and SAG101 do not associate with NRG1 until Pf0-1 delivery of AvrRps4 (PTI+ETI activation). While accumulation of these higher-order states increases between PTI and PTI+ETI activation, no band shifts are observed that would indicate formation of NRG1-EDS1-SAG101 associations upon PTI+ETI activation. These data may indicate that PTI activation primes NRG1 for associations with EDS1 and SAG101, or that formation of higher-order NRG1 states is not due to self-associations. It could be that EDS1-SAG101 do not promote oligomerization of NRG1 but are only able to associate once NRG1 oligomers have formed (Figure 6.1C & D). If so, the stoichiometric ratio of NRG1 protomers to EDS1-SAG101 heterodimers may not be linear. Taken together, these lines of evidence are not enough to fully explain the mode of interaction between NRG1 and the EDS1-SAG101 heterodimer, yet the requirement of ETI+PTI for full activation of NRG1 is clear.

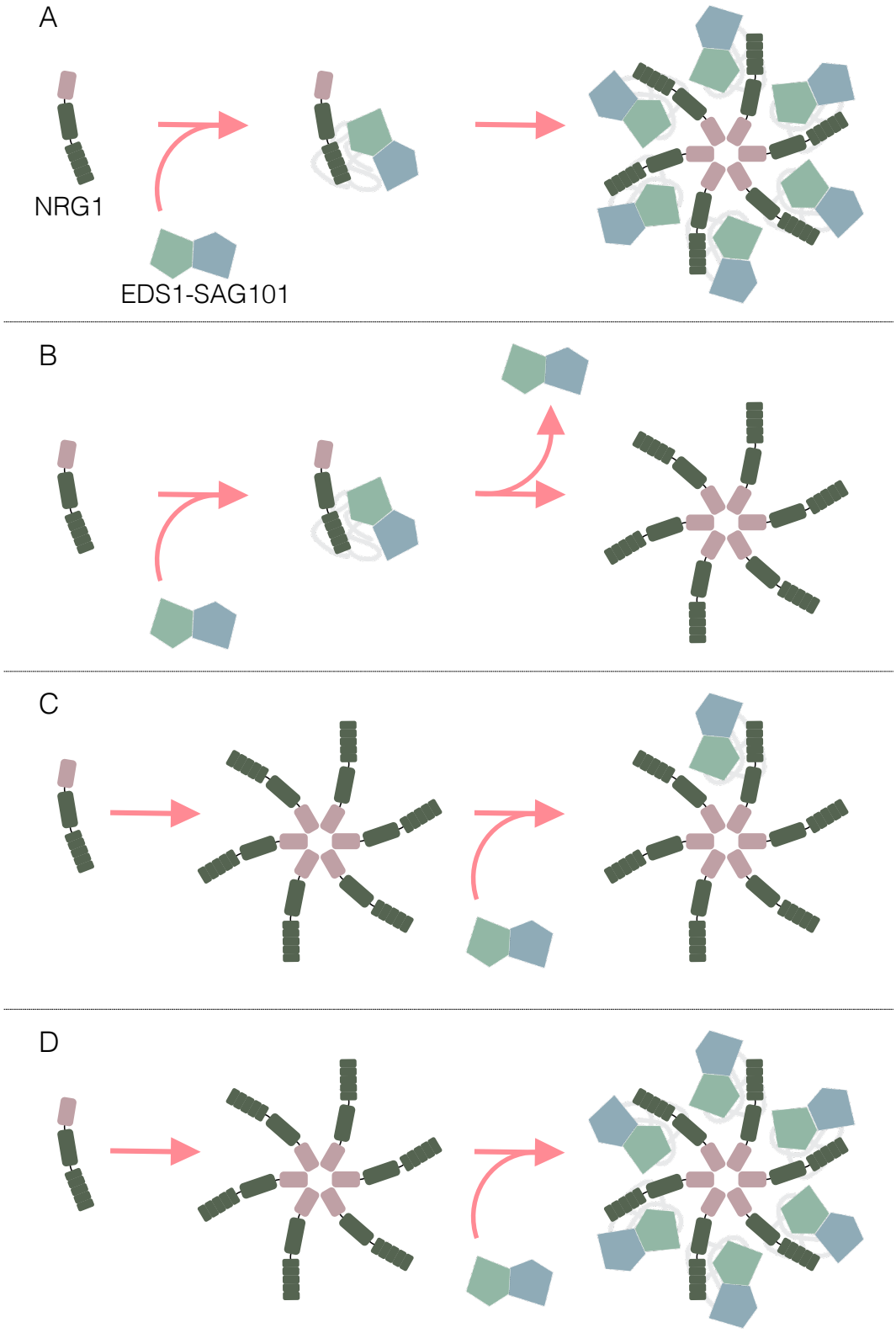

Figure 6.1 Potential NRG1 activation models. (A) EDS1 and SAG101 association with NRG1 may be required to facilitate NRG1 oligomerization. (B) EDS1 and SAG101 may transiently associate with NRG1 before dissociation to facilitate NRG1 oligomerization. (C & D) EDS1 and SAG101 heterodimers may association with oligomerized NRG1 at unknown stoichiometries.

6.2.2 SAG101 may contribute to cell death via undetermined lipase activity

The N-terminal RPW8 domain of NRG1 shares homology to the HeLo domain of the fungal HET-S protein (Daskalov et al., 2016). In heterokaryon incompatibility, incompatible interactions induce aggregation of HET-S via prion-forming domains which leads to partial unfolding of the HeLo domain. This unfolding exposes a previously buried N-terminal transmembrane segment which targets HET-S to membranes for further oligomerizations (Seuring et al., 2012). HET-S transmembrane homooligomerizations have been shown to be "toxic", leading to loss of membrane integrity and cell death. The HeLo-like domain-containing mammalian MLKL also requires homotrimer formation at plasma membranes for inducing death (Cai et al., 2014, Chen et al., 2014). Formation of transmembrane homooligomers has also been proposed for the ZAR1 resistosome, although it does not contain a HeLo-like N-terminal domain (Wang et al., 2019a). As NRG1 contains a HeLo-like domain homologous to HET-S, it is conceivable that NRG1 mediates cell death via formation of toxic N-terminal transmembrane homooligomers.

However, if toxicity via transmembrane associations is sufficient for cell death, why does NRG1 require EDS1 and SAG101 to mediate cell death (Qi et al., 2018, Lapin et al., 2019)? The data presented in this thesis indicate that either EDS1 and SAG101 facilitate progression of NRG1 to higher-order states, or EDS1 and SAG101 bind after formation of NRG1 oligomers (Figure 6.1). If EDS1 and SAG101 bind prior to NRG1 oligomerization, then likely cell death is mediated via NRG1 transmembrane homooligomers; however, if EDS1 and SAG101 bind after oligomerization, a more direct role in cell-death mechanisms is implied. Notably, EDS1 carries a lipase-like domain, and lipase activity could contribute to alteration of membrane integrity. Although EDS1 shows conservation of a functional lipase catalytic triad, mutation of these residues has unambiguously shown that they are dispensable for EDS1-mediated immune responses (Wagner et al., 2013, Voss et al., 2019). Instead, it appears that the lipase-like domain of EDS1 is required to facilitate heterodimer formation with PAD4 or SAG101 (Wagner et al., 2013).

However, the lipase-like domain of SAG101 was not found to retain key features of a functional catalytic site (Wagner et al., 2013). As a consequence, lipase mutants have not been evaluated for immune function. Yet, when SAG101 was first characterized, it was shown to have in vitro acyl hydrolase activity after purification from *E. coli* expression systems (He and Gan, 2002). This presents a paradox as SAG101 is missing a key GxSxG lipase motif; however, a similar GxSxA motif located

slightly downstream could be mediating activity (He and Gan, 2002). Indeed, examples exist wherein either a pathogen-secreted esterase (Raymer et al., 1990) or a host-encoding patatin-like phospholipase (Li et al., 2011) show acyl hydrolase activity in plants without the canonical GxSxG motif. Therefore, while lipase activity for EDS1 and PAD4 has been shown to be dispensable, whether SAG101 does indeed function as a lipase, and whether that activity would have a role in cell death, remains unknown. It is tempting to postulate that EDS1 recruits SAG101 to oligomerized NRG1 at membranes to carry out some membrane-disrupting lipase activity to induce cell death. However, this remains highly speculative.

6.2.3 EDS1-SAG101 may target NRG1 to membranes to activate cell death

By whatever means EDS1 and SAG101 contribute to NRG1-mediated cell death, the differences in their localizations presents another paradox. NRG1 seems primarily localized to endomembrane networks (Wu et al., 2019) while SAG101-EDS1 heterodimers seem primarily nuclear-localized (Feys et al., 2005, Zhu et al., 2011). The association observed between EDS1 and SAG101 with NRG1 suggests that upon effector recognition they are in close proximity. These data would indicate that either NRG1 localizes to nuclei or EDS1-SAG101 heterodimers re-localize to extranuclear spaces. As evidence exists for EDS1 trafficking between cytoplasm and nuclei (García et al., 2010), it is most likely that EDS1-SAG101 are re-localized to extranuclear spaces to associate with NRG1 (Figure 6.2A). However, potential mechanisms that would mediate localization-changes are obscure.

Yet, it is plausible that EDS1-SAG101 heterodimers are present in extranuclear spaces at low abundance to mediate cell death responses. Indeed, extra-nuclear SAG101 may be required to mediate cell death. The non-functional *Solanum lycopersicum* SAG101a isoform is exclusively nuclear localized when transiently expressed in *N. benthamiana* while the functional *Sl*SAG101b is nucleo-cytosolic (Gantner et al., 2019). Importantly, *Sl*SAG101b can signal with *N. benthamiana* alleles of EDS1 and NRG1. Notably, reports for Arabidopsis SAG101 localizations to nuclei have been in the absence of PAD4 (Feys et al., 2005). When PAD4 was co-expressed with SAG101, a more evenly distributed signal is observed (Zhu et al., 2011). Indeed, my own evaluation of SAG101-mCherry shows some signal is present in cytoplasmic spaces (Appendix XXI). These data would indicate that SAG101 may not be exclusively nuclear-localized, as previous reports suggest.

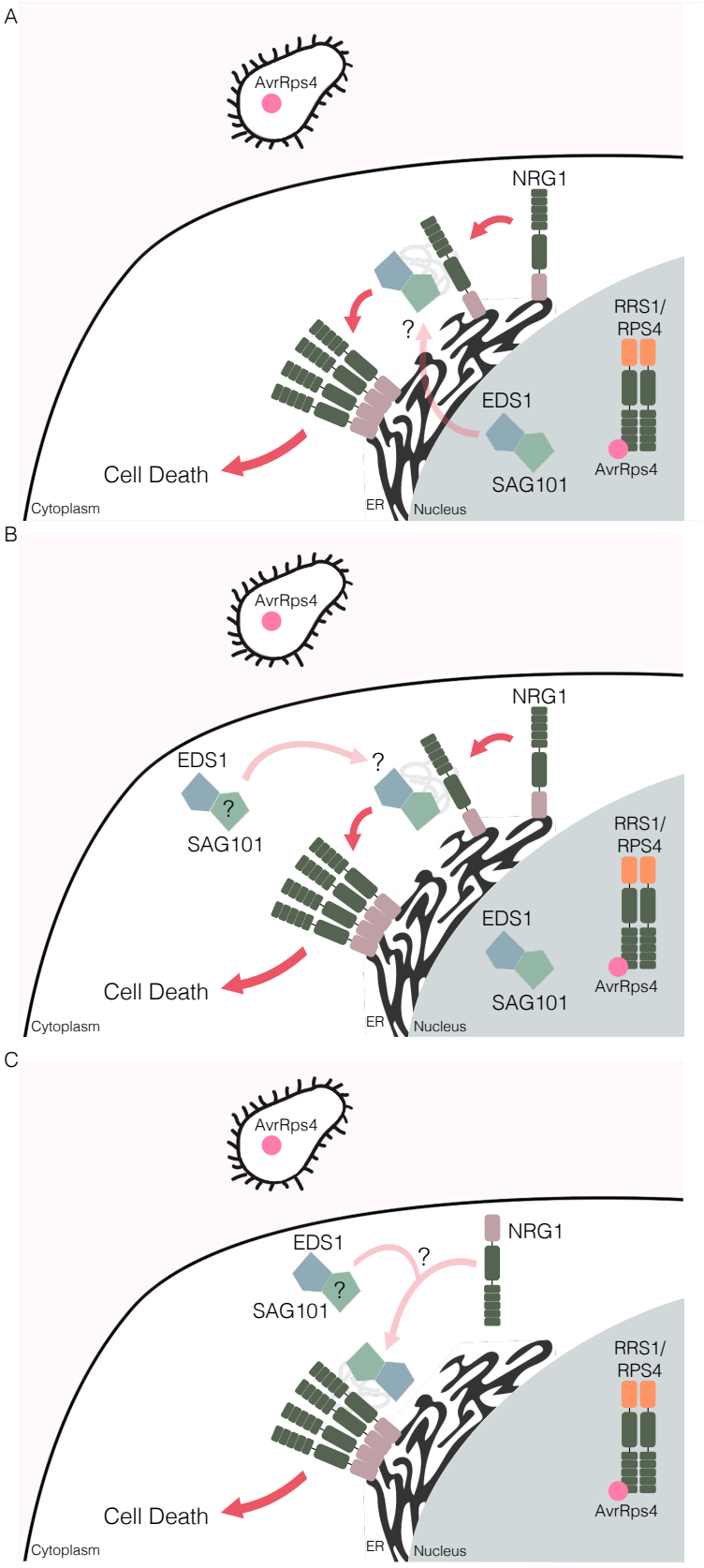

Figure 6.2 Potential models for EDS1-SAG101 localization changes upon immune activation required for associations with NRG1. (A) EDS1-SAG101 may need to re-localize from nuclei to extranuclear spaces to associate with NRG1 upon activation by unknown mechanisms. (B) EDS1-SAG101 may already be present in extracellular spaces prior to associations with NRG1 upon activation by unknown mechanisms. (C) EDS1-SAG101 associations in the cytosol with NRG1 may target NRG1 to membranes

It could be that upon immune activation, extra-nuclear EDS1-SAG101 re-localize from cytosol to endomembranes to form associations with NRG1 (Figure 6.2B). Alternatively, perhaps associations with EDS1-SAG101 are required to target NRG1 to endomembranes (Figure 6.2C). This would mimic the fungal HET-S and mammalian MLKL systems wherein formation of aggregates is required to unfold the N-terminal domain which is subsequently targeted to membranes for insertion (Seuring et al., 2012, Wang et al., 2014, Chen et al., 2014, Cai et al., 2014). Therefore, the observed compartmental restrictions may act to prevent passive associations that might provoke auto-active immune responses.

Resolving localizations pre- and post-immune activation may help elucidate the contribution NRG1 and EDS1-SAG101 make to TNL-mediated cell death. I have tried to investigate these states using transient expression in *N. benthamiana*, but the system potentially used variants of NRG1 and SAG101 that were rendered non-functional by fusion-tags. Yet, as some signal was present for EDS1-SAG101 outside nuclei, the qualitative approach I took to investigate co-localization may not facilitate definitive conclusions on EDS1-SAG101 associations with NRG1. Therefore, future assays, utilizing functionally-confirmed components, could employ quantitative methodologies such as FRET-FLIM (Forster resonance electron transfer and fluorescence lifetime imaging microscopy) to investigate NRG1 associations with EDS1-SAG101 pre- and post-immune activation. Furthermore, biochemical assays to investigate localizations of NRG1, EDS1, and SAG101 in nuclear, cytosolic, and microsomal compartments pre- and post-immune activation may help resolve the space(s) in which associations occur. A clearer understanding of where these components are localized may guide investigations of how they mediate cell death together.

6.2.4 PTI and ETI activation both seem to be required for NRG1-EDS1-SAG101 associations that lead to cell death

As Ngou et al. (2020) have found that PTI- and ETI-activation are both required for cell death, this begs the question: what role does PTI play in NRG1-mediated cell death? Hallmarks of PTI activation such as MAPK phosphorylation and ROS production are maintained in *nrg1a/b* mutants treated with flg22 (Bruno Ngou, personal communication with permission). Additionally, neither NRG1 nor ADR1 contribute to bacterial growth restriction upon PTI activation only (Saile et al., 2020). These data indicate that NRG1 does not function in PTI. However, as previously mentioned, higher-order NRG1 species are formed upon PTI activation alone. It could

be that PTI primes NRG1 for ETI activation—possibly by inducing self-associations. Conceivably, ETI activation acts to specifically induce EDS1-SAG101 associations with self-associated NRG1 (Figure 6.3); thus, PTI and ETI may both contribute to the stepwise activation of NRG1 to carry out cell death with EDS1 and SAG101.

To test these hypotheses, two Arabidopsis complementation lines with with inducible effectors could be generated: one with two differently-tagged NRG1 variants for PTI-induced self-associations, the other with fusion-tagged copies of NRG1, SAG101, EDS1 for ETI-induced heteromeric associations. Each would be tested for associations upon PTI-, PTI+ETI-, and ETI-activation, mediated by flg22 treatment, Pf0-1 delivery of AvrRps4, and β-estradiol-induction of AvrRps4, respectively. As mentioned previously, it may be that NRG1 self-associations are required for EDS1-SAG101 associations, or that EDS1-SAG101 facilitate NRG1 oligomerization.

If PTI activation induces NRG1 self-associations, the mechanism by which this is accomplished is obscure. While cross-talk between PTI and ETI has conclusively been shown (Ngou et al., 2020a, Yuan et al., 2020), this is primarily through restoration of PTI components. Future investigations could be performed in mutant backgrounds for conserved PTI-signalling components. These data could genetically link NRG1 self-associations with PTI activation. Potentially, formation of higher-order NRG1 states upon PTI activation is mediated by phosphorylation imposed by PTI signalling components. A role for PTI activation in promotion of NRG1 self-associations would represent a highly novel discovery in plant immunity.

Conceivably, some ETI signal specifically induces EDS1-SAG101 associations with NRG1. It's unlikely that PTI-mediated self-association of NRG1 is sufficient—heterologous expression in *N. benthamiana* would be under PTI as it includes *Agro*-infiltration, and convincing association between NRG1 with EDS1 or SAG101 is not observed in these conditions. Furthermore, over-expression of Arabidopsis alleles in *N. benthamiana* requires co-delivery of a recognized effector to recapitulate cell death. Therefore, it appears that PTI and ETI both contribute to the cell death mechanism of NRG1. Future investigations to dissect these distinct contributions may reveal key immune mechanisms mediated by NRG1 with EDS1 and SAG101.

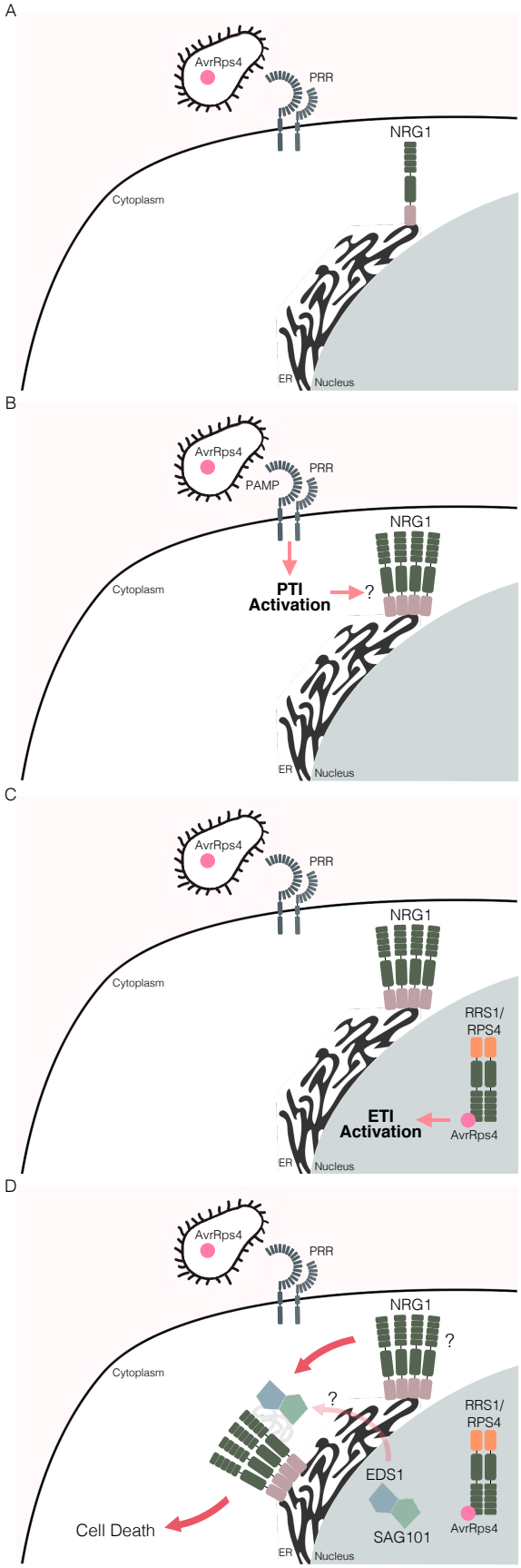

Figure 6.3 PTI and ETI activation may each be required for NRG1-EDS1-SAG101 associations that lead to cell death. Potential activation model for NRG1. (A) NRG1 is localized to endomembrane networks in monomeric states. (B) PTI activation induces NRG1 self-associations. (C and D) ETI activation induces EDS1-SAG101 associations with oligomerized NRG1.

6.3 The NRG1 pre-activation state is poorly understood

Although the data presented in this thesis has facilitated insight into activated forms of NRG1, the pre-activation state remains somewhat ambiguous. Negative stain EM indicates that NRG1B-HF is purified as a monomer (~ 99 kDa) after heterologous expression in *N. benthamiana*. However, SEC and BN-PAGE of those samples indicate that NRG1B-HF exists as ~ 200, ~ 400, and ~ 600 kDa species, which could correlate to dimers, tetramers, and hexamers. These data roughly correlate with BN-PAGE of Arabidopsis lysates: ~ 200 kDa species are observed prior to immune activation, but upon PTI or PTI+ETI activation, NRG1B-HF also forms ~ 400 and ~ 800 kDa species (and possibly a ~ 600 kDa species). As mentioned, *Agro*-infiltration in *N. benthamiana* likely triggers PTI activation. As such, it is expected to purify the PTI-activated states of NRG1B-HF with this methodology. However, it is not expected to purify ~ 99 kDa monomers of NRG1B-HF. Therefore, follow-up investigations are required to resolve the pre-activation state of NRG1, and whether we are falsely assigning negative stain EM noise as NRG1B-HF monomer particles.

The ~ 200 kDa pre-activation state for NRG1B-HF may represent dimers, associations with detergent, or associations with co-purifying components. Co-IP assays utilizing Arabidopsis complementation lines carrying differently-tagged NRG1 copies (mentioned in section 6.2.4) would reveal whether the pre-activation state of NRG1 is a dimer. Additionally, composition of the pre-activation state could be determined by excising the ~ 200 kDa band from BN-PAGE gels for LC-MS analysis. As we hope to solve structures of pre- and post-activated forms of NRG1, it will be important to definitively resolve the pre-activation state of NRG1.

Notably, a slight difference in higher-order species is observed between Arabidopsis and transient *N. benthamiana* lysates upon PTI activation. This may indicate that additional components—which cannot be EDS1 or SAG101 as they do not associate before effector delivery—are being assembled in Arabidopsis to form the ~ 800 kDa state. However, follow-up work is required to resolve more clearly the molecular weights of these higher-order species. These slower-migrating bands on BN-PAGE could also be subjected to LC-MS to determine composition. Nevertheless, although there are slight differences observed between Arabidopsis and *N. benthamiana* lysates, these data point to the formation of higher-order states that are relatively consistent between transient expression in *N. benthamiana* and stable expression in Arabidopsis.

6.4 How NRG1, EDS1-SAG101 perceive TNL activation is not known

Although NRG1, EDS1, and SAG101 are each genetically required in TNL immune-signalling pathways, the mechanism for downstream signalling has not been revealed. Yet, data indicates some direct or indirect perception of their TIR domains. This domain contains a conserved glutamic acid residue that is shared in the TIR proteins of prokaryotes and the mammalian SARM1 (STERILE ALPHA AND TIR MOTIF CONTAINING 1). It appears that these TIR proteins have intrinsic enzymatic activity, capable of degrading nicotinamide adenine dinucleotide in its oxidized form (NAD+) (Essuman et al., 2017, Essuman et al., 2018). Recently, the TIR domain of plant TNLs, and truncated variants, have been shown to exhibit NADase activity (Wan et al., 2019, Horsefield et al., 2019). Indeed, this NADase activity of plant TIRs is necessary to induce plant defence (Duxbury et al., 2020).

Notably, the NADase activity of SARM1 or a bacterial TIR is not sufficient for defence activation when heterologously expressed in plants (Duxbury et al., 2020). A subset of prokaryote TIRs are capable of producing a variant-cyclic-ADP-ribose (vcADPR) product (Essuman et al., 2018). Unlike SARM1, plant TIRs have recently been shown to produce a seemingly identical product (Wan et al., 2019). These data indicate that although a similar product is produced between plant and bacterial TIRs, it is not sufficient to elicit defence responses. Indeed, NADase activity of plant TIRs requires EDS1 to trigger cell death, while SARM1 does not (Wan et al., 2019, Horsefield et al., 2019). These data indicate some specialization between plant TIR NADase activity and EDS1.

Therefore, it is possible that EDS1 indirectly mediates signalling between TNL sensors and RNL helpers via perception of vcADPR produced by TNL NADase activity (Figure 6.4). Notably, the EDS1-SAG101 structure shows the presence of a highly conserved cavity between the EP domains (Wagner et al., 2013). As previously mentioned, mutating residues in this cavity do not interfere with heterodimer associations but does lead to disruption of TNL immune signalling pathways (Bhandari et al., 2019). Interactions between EDS1-SAG101 heterodimers and vcADPR have not yet been investigated; however, it is tempting to speculate that vcADPR may bind in the EDS1-SAG101 cavity, inducing conformation changes that facilitate association with NRG1 to carry out cell-death mechanisms (Figure 6.4). Future experiments could investigate EDS1-SAG101 associations with NRG1 in the presence of loss-of-function TNL RPS4^{E88A} mutant which substitutes the catalytic glutamic acid for an alanine (Duxbury et al., 2020). These assays would help reveal whether EDS1-SAG101

associations with NRG1 are dependent on the NADase activity of the RPS4 TIR domain.

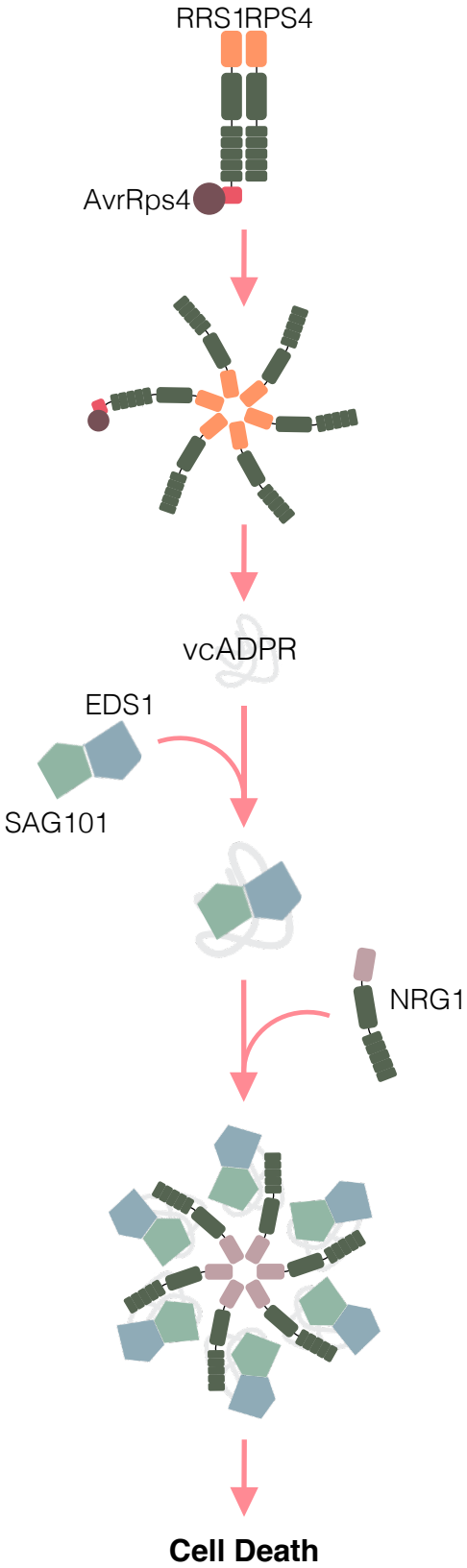

Figure 6.4 Potential signalling pathway from TNLs to RNLs. Upon effector recognition TNLs oligomerize and NADase activity is promoted producing vcADPR, which is perceived by EDS1-SAG101. This perception facilitates associations with NRG1 which activates cell death responses.

It's also possible that direct association of EDS1 with TNLs mediates signalling to downstream helper RNLs. Perhaps oligomerization of TNLs allows associations with EDS1 that lead to activation of RNLs. Indeed, EDS1 has been shown to associate with RPS4 in nuclei (Huh et al., 2017). It is notable that spectra for peptides derived from the TNL RRS1-R were observed in LC-MS data after IP of NRG1B-HF. These data could indicate the direct association of NRG1 with TNLs, mediated by EDS1. However, in this particular LC-MS dataset, EDS1 spectra were not also present alongside RRS1-R. Furthermore, RRS1-R spectra were present in the mock-, empty vector-, and AvrRps4-treated samples. As EDS1 and SAG101 were shown to associate with NRG1 only upon effector delivery, these data would indicate that RRS1-R associations with NRG1 are EDS1-independent. Thus, future investigations are required to more clearly elucidate the mechanism for perception of activated TNLs by NRG1 and EDS1-SAG101 components.

6.5 Cell death may mediate discrete defence against different pathogens

As mentioned, NRG1-EDS1-SAG101 are required for cell death in Arabidopsis while ADR1-EDS1-PAD4 are required for transcriptional activation of defence-related genes. One of the more interesting details to emerge from the literature is the observation that different pathogens are differentially inhibited by RNLs and EDS1-family proteins. NRG1 can suppress viral accumulation (Peart et al., 2005)—the RPW8 domain is alone sufficient (Collier et al., 2011)—but cannot restrict bacterial growth (Castel et al., 2019a, Saile et al., 2020). In contrast, ADR1 seems to have a role in bacterial growth restriction (Saile et al., 2020). While *nrg1* mutants are only partially compromised in resistance to the oomycete *H. arabidopsis* (Castel et al., 2019a, Saile et al., 2020), *adr1* mutants show a higher susceptibility (Saile et al., 2020). These observations are true as well for the respective SAG101 and PAD4 signalling partners: bacterial growth is the same on WT or *sag101* mutants while *pad4* mutants shows enhanced susceptibility (Feys et al., 2005). These data may reflect the distinct contribution of cell death in mediating immunity to different pathogen groups.

However, a paradox exists in that *sag101* mutants still show HR in response to the oomycete *H. arabidopsidis* while *pad4* mutants show a trailing necrosis phenotype (Feys et al., 2005). However, as ADR1-EDS1-PAD4 are able to compensate for NRG1-EDS1-SAG101, and vice versa (Lapin et al., 2019, Saile et al., 2020), perhaps transcriptional activation by ADR1-EDS1-PAD4 restricts growth from cell-to-cell, and

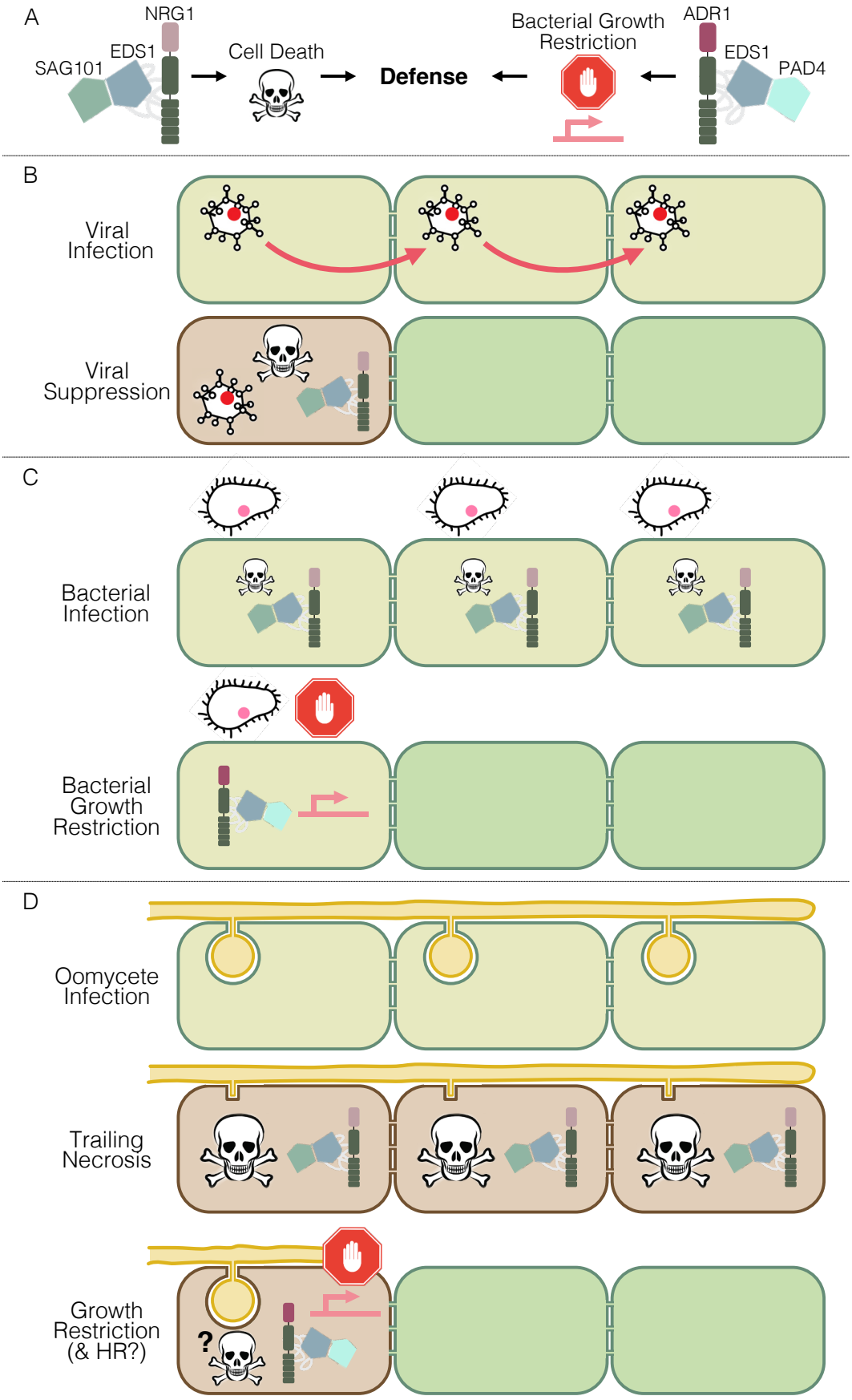

Figure 6.5 Cell death may mediate discrete defence against different pathogens. (A) In Arabidopsis, NRG1 signals with EDS1 and SAG101 to trigger cell death, while ADR1 signals with EDS1 and PAD4 to restrict bacterial growth. ADR1-EDS1-PAD4 induce transcriptional activation. (B)

NRG1-EDS1-SAG101 can restrict viral accumulation by triggering cell death of infected cells and restricting pathogen spread. (C) NRG1-EDS1-SAG101 cannot restrict bacterial growth by triggering cell death, but ADR1-EDS1-PAD4 restrict pathogen growth, possibly via transcriptional activation of defence genes. (D) NRG1-EDS1-SAG101 can induce cell death of oomycete-infected cells, but cannot restrict pathogen growth, which is observed as trailing necrosis. ADR1-EDS1-PAD4 can restrict oomycete growth and may be able to compensate for NRG1-EDS1-SAG101-mediated cell death for localized cell death.

is then able to carry out localized cell death. Likewise, perhaps NRG1-EDS1-SAG101 cannot restrict growth as well as ADR1-EDS1-PAD4, but produces a trailing necrosis phenotype by killing the cells as the hyphae migrate from cell-to-cell. Indeed, sporulation is restricted in a *sag101* mutant but not a *pad4* mutant (Feys et al., 2005), indicating that the pathogen can carry out its lifecycle in the presence of SAG101. These data support a model in which transcriptional activation generally restricts pathogen growth and spreading, and cell death terminates those cells which are already infected (Figure 6.5).

It could be that cell death is a more effective mechanism for managing pathogens that have colonized within cell-wall boundaries. As bacteria are localized in the apoplast, cell death would do little to negatively impact pathogenesis beyond generating danger-associated-molecular-patterns (DAMPs) to signal to neighbouring cells of pathogen presence. Since viral pathogens carry out their cycles from within the cell, terminating those cells inhabited by viruses prior to replication may be an effective way to contain the infection. Moreover, although fungi and oomycetes are technically in the apoplastic spaces, their hyphae invaginate plant cells and travel cell-to-cell. Preventing hyphal growth from cell-to-cell by killing those already colonized may be an effective way to limit further spread in host tissues. Therefore, a more thorough understanding of the contribution of cell death or transcriptional activation to pathogen-specific immunity may reveal knowledge central to understanding plant immunity, and potentially specializations between host and pathogens.

6.6 NRG1-EDS1-SAG101 may have sub-functionalized in Brassicaceae

RNLs and their respective EDS1-family proteins function differently given the genetic background. In Arabidopsis, NRG1-EDS1-SAG101 are required for cell death, while ADR1-EDS1-PAD4 mediate transcription and bacterial growth restriction; however, NRG1-EDS1-SAG101 seem to mediate both responses in *N. benthamiana*

(Lapin et al., 2019). Notably, the requirement for genetically compatible alleles of RNL or EDS1-family proteins may be exclusive to Arabidopsis. Cell death is recapitulated in *N. benthamiana* only when *At*NRG1, *At*EDS1, and *At*SAG101 are co-delivered with a recognized effector (Lapin et al., 2019). In contrast, heterologous expression in Arabidopsis does not seem to require genetically compatible alleles of RNL or EDS1-family signalling partners. It may be that the RNLs and EDS1-family proteins have sub-functionalized in Brassicaceae.

Delivery of *S. lycopersicum* SAG101b to *N. benthamiana* is sufficient to recapitulate HR alone (Gantner et al., 2019). This may be due to a closer relation in *N. benthamiana* to *S. lycopersicum* than to Arabidopsis. Yet, co-expression of *S. lycopersicum* alleles of PAD4 and EDS1 in Arabidopsis can restrict an oomycete pathogen (Gantner et al., 2019). Although it was not directly tested, these data indicate that *Sl*PAD4 and *Sl*EDS1 are able to signal with *At*ADR1 to mediate resistance phenotypes. Additionally, overexpression of *Nb*NRG1 in Arabidopsis restricts bacterial growth (Brendolise et al., 2018), and *Triticum aestivum* EDS1 can complement powdery mildew resistance in *eds1* mutant Arabidopsis (Chen et al., 2018). Lapin et al. (2020) have noted that PAD4 orthologues lack an extended α-helix that is present in EDS1 and non-Brassicaceae PAD4 alleles (Lapin et al., 2020). These data indicate that Brassicaceae alleles of RNL and EDS1-family proteins have sub-functionalized, while the Solanaceae alleles can function in broader contexts. Whether RNL and EDS1-family proteins from other genetic backgrounds will show broad or specialized functions has yet to be revealed.

6.7 ADR1 may have a helper NLR role beyond TNL immune signalling

While a role for NRG1 in mediating cell death upon TNL activation has been demonstrated, the function of ADR1 as a helper NLR is less well understood. ADR1 functions with EDS1-PAD4 downstream of TNLs to regulate transcriptional activation in Arabidopsis (Lapin et al., 2019, Saile et al., 2020), yet in *N. benthamiana*, ADR1 does not appear to contribute to TNL-mediated resistance (Lapin et al., 2019). ADR1 is required by the CNL RPS2 in Arabidopsis (Bonardi et al., 2011, Saile et al., 2020), but whether this requires EDS1 is not fully understood (Aarts et al., 1998, Venugopal et al., 2009, Bhandari et al., 2019). A potential role for ADR1 in those genetic backgrounds missing NRG1, SAG101, and TNLs also remains to be determined. Therefore, elucidation of ADR1 signalling mechanisms are of high interest for follow-up research, and may reveal core functions of RNL-mediated immunity.

As the N-terminal domains of RNLs share homology to the HeLo domain of the fungal HET-S proteins, it raises the question: if ADR1 does not contribute to cell death, what does it do? It is notable that an intact P-loop is not required for function of ADR1-L2 in ETI, basal immunity, or SA accumulation (Bonardi et al., 2011). However, a functional P-loop is required for ADR1-L2^{D484V} auto-activity and for propagation of unregulated cell death in *lsd1* mutant backgrounds (Roberts et al., 2013). As the P-loop motif is involved in coordinating nucleotide binding, the requirement for a functional P-loop in this variant of ADR1 may indicate the role for oligomerization in immune function. Perhaps, ADR1 can carry out functions that are independent of oligomerization, but can oligomerize to propagate runaway cell death in *lsd1* backgrounds, or to compensate for NRG1 in cell death mechanisms. Indeed, ADR1 and NRG1 are unequally redundant but still show the ability to compensate for each other (Saile et al., 2020).

In contrast, the P-loop is required by *Nb*NRG1 to mediate cell death (Peart et al., 2005). Conceivably, in Arabidopsis, NRG1 has specialized for cell death while ADR1 has specialized for transcriptional activation. This could explain why *At*EDS1 has been observed to negatively regulate *At*ADR1-L2^{D484V} auto-activity (Roberts et al., 2013), and why *At*ADR1-L2^{D484V} requires *At*PAD4 for function (Wu et al., 2019)—possibly, EDS1-PAD4 bind ADR1 and divert signalling towards transcriptional activation pathways (Figure 6.6). This would point to SAG101 and PAD4 mediating EDS1 associations with NRG1 or ADR1, respectively. As such, solving the structures of the anticipated NRG1-EDS1-SAG101 complexes and ADR1-EDS1-PAD4 complexes may shed light on the potential sub-functionalization of RNLs in Brassicaceae. Future investigations are also required to evaluate whether EDS1-PAD4 associate with ADR1 in an effector-dependent manner, analogous to NRG1-EDS1-SAG101 associations.

It remains to be determined whether ADR1 also functions in CNL sensor signalling pathways in an EDS1-dependent manner. As mentioned, ADR1 is required downstream of the CNL RPS2 (Bonardi et al., 2011, Saile et al., 2020), but conflicting data exist on whether EDS1 is also required (Aarts et al., 1998, Venugopal et al., 2009, Bhandari et al., 2019). Yet, many CNLs do not signal through EDS1. It may be that ADR1 and EDS1 connect to CNL pathways via their roles in SA signalling.

ZAR1 and RPM1 represent examples of CNLs that do not require RNLs to mediate immune responses (Saile et al., 2020). However, ZAR1 forms resistosomes that may be able to induce cell death via homooligomerization in membranes (Wang

et al., 2019a), thus negating the requirement for helper NLRs. Furthermore, Saile et al. (2020) have found that RNLs and CNLs induce the same suite of genes upon activation, indicating a redundant function in transcriptional activation for RNLs. Therefore, perhaps only those CNLs that are cell death-incompetent require RNLs to mediate both transcription and cell death immune responses. It will be interesting to further characterize which CNLs require RNLs, and which do not, and why.

It is notable that ADR1 seems to not contribute to TNL-mediated immunity in *N. benthamiana*. Yet, ADR1 and NRG1 are redundant downstream of the potato-derived CNL Rx2 (Collier et al., 2011). Conceivably, ADR1 has specialized to function downstream of CNLs in Solanaceae, and mediates both cell death and transcriptional activation. As NRG1, SAG101, and TNLs have been lost in monocots and *Aquilegia coerulea* (Baggs et al., 2020), perhaps it will be revealed that ADR1s are accomplishing both cell death and transcriptional activation for defence in those genomic backgrounds.

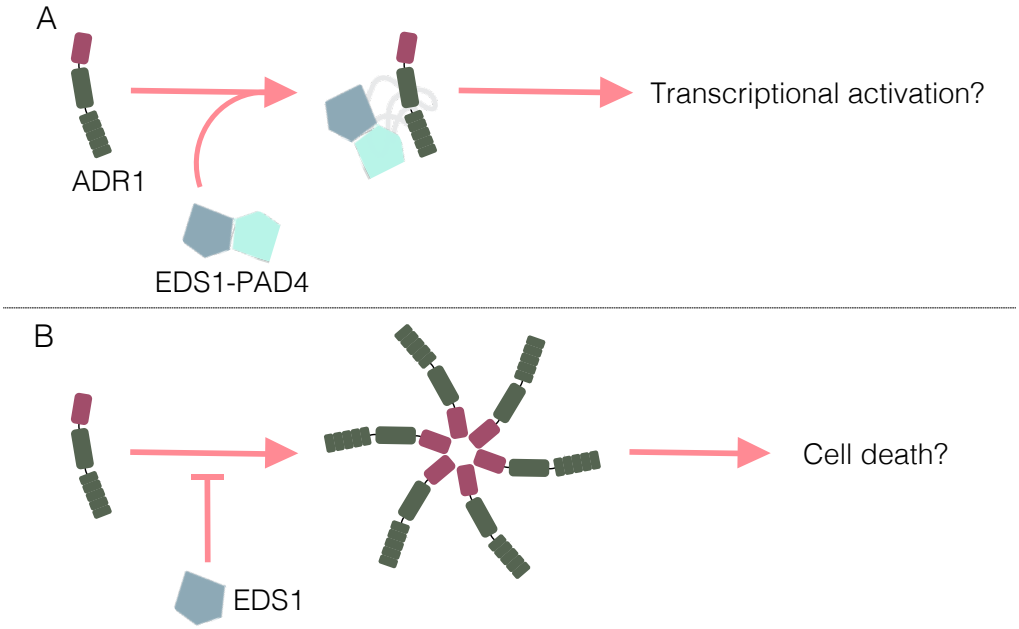

Figure 6.6 How does ADR1 mediate defence responses? (A) EDS1-PAD4 may direct ADR1 to induce transcription in the absence of ADR1 oligomerizations. (B) ADR1 can oligomerize to induce cell death, although EDS1 may inhibit formation of oligomers.

6.8 A loss-of-function NRG1 mutant may facilitate studies of activated forms

Future investigations should employ cell death-incompetent mutants of NRG1, as death of cells that contain activated species may be interfering with visualizing important intermediates. Daskalov et al. (2016) were able to generate loss-of-function

mutants of the fungal HELLP protein that, like NRG1, carries homology to the HeLo domain of HET-S. They discovered that HELLP carries a “glycine zipper” motif—a common sequence motif that facilitates transmembrane helix packing in channel proteins (Kim et al., 2005). Indeed, the N-terminus of NRG1 is also predicted to carry a glycine zipper (Daskalov et al., 2016). Mutation of residues in this motif may render NRG1 cell death-incompetent, while still capable of effector-dependent association with EDS1 and SAG101.

Data presented in this thesis indicate that EDS1 associates with NRG1 4-8 hpd by Pf0-1 infiltration, and that weak EDS1-NRG1 associations persist until 12 hpd. Either EDS1 dissociates from NRG1 over time, or those cells that produced NRG1-EDS1-SAG101 associations lost viability by 12 hpd. Utilizing NRG1 loss-of-function glycine zipper mutants in time-course assays would resolve the persistence of EDS1-SAG101 associations with NRG1 post-effector delivery. If EDS1-SAG101 are still associated with the glycine zipper NRG1 mutant 12 hpd, this would indicate the formation of stable NRG1-EDS1-SAG101 activated complexes. If EDS1-SAG101 are not associated 12 h post-effector delivery, this would indicate transient associations of EDS1-SAG101 with NRG1 during activation. Further understanding of the persistence of these associations would help delimit the contribution of EDS1-SAG101 to NRG1-mediated cell death.

Notably, glycine zipper motifs are found in membrane proteins that form ion channels (Kim et al., 2005, Kim et al., 2004). Therefore, it is possible the glycine zipper motif mediates the same channel formation in NRG1 upon activation and transmembrane self-associations. Influx of ions may lead to perception by immune signalling components to activate downstream signalling processes, or perhaps leakage induces toxicity to mediate cell death. Indeed, formation of MLKL homotrimers in mammalian cell membranes correlates with ion flux that disrupts membrane integrity (Chen et al., 2014, Cai et al., 2014). However, further investigation is required to determine whether NRG1 does form ion channels and the contribution of those channels to immunity.

However, as glycine zipper motifs may directly drive the formation of homooligomeric bundles (Kim et al., 2005), mutations in these residues could interfere with either oligomerization or membrane insertion, or both. Indeed, Daskalov et al. (2016) found that glycine zipper HELLP mutants formed aggregates via prion-forming domains in cytoplasm rather than at membranes (Daskalov et al., 2016). Therefore, it

should first be determined whether NRG1 does self-associate upon effector delivery, and whether glycine zipper mutants can also self-associate.

6.9 Future goals for structural investigations

The structural investigations I undertook in this project were able to produce a low-resolution NRG1 monomer structure through 2D reconstruction of particles imaged on negative stain EM grids. However, the reconstruction map was too low resolution to form any conclusions on biological mechanisms. Furthermore, obtaining both pre- and post-activation structures for NRG1 would better facilitate hypothesis formulation about cell death mechanisms. Structures of activated NRG1 may reveal whether associations with EDS1 and SAG101 are direct or indirect, stable or transient. Moreover, structures of PTI-activated and PTI+ETI-activated forms of NRG1 may reveal whether EDS1 and SAG101 are required to induce NRG1 oligomerizations, or whether they are associated with oligomerized NRG1. Therefore, the purification protocol described in this thesis serves primarily as a foundation for follow-up work to solve NRG1 structures

If the pre-activation state of NRG1 is a ~ 99 kDa monomer, solving structures by cryo-EM may be impossible. Currently, technical limitations exist for solving structures of < 200 kDa particles (Wu and Lander, 2020). As mentioned previously, X-ray crystallography of NRG1 monomers will not be possible with current purification methodologies as protein yields are limiting. However, if pre-activated NRG1 is a dimer at ~ 200 kDa, this is within range for structure determination by cryo-EM. Indeed, the data presented in this thesis are conflicting on whether NRG1 exists as a monomer or dimer in pre-activation states. If the pre-activation state for NRG1 could be determined through co-IP assays in Arabidopsis, these data would better guide downstream structure-determination methodology.

Importantly, if PTI does induce NRG1 self-associations, it may not be possible to solve pre-activation structures by *Agro*-mediated expression in *N. benthamiana*. The presence of *Agrobacterium* would likely trigger PTI activation. Indeed, purification of NRG1B-HF from *N. benthamiana* showed ~ 200, ~ 400, and ~ 600 kDa species like similar to those observed in PTI-activated Arabidopsis lysates. Therefore, perhaps ~ 200 kDa species should be resolved by SEC and isolated prior to negative stain EM. This may ensure that we are imaging pre-activation forms and not heterogenous mixtures of pre- and post-activation states.

Post-activation states for NRG1 may exist as PTI-primed homooligomers and PTI+ETI-induced EDS1-SAG101 associations with oligomerized NRG1. If biochemical assays in Arabidopsis show support for the existence of these individual species, solving the structures for each would greatly inform the activation mechanism for NRG1. However, it is equally possible that PTI-induced higher-order states for NRG1 are not self-associations but heteromers with chaperones or unknown components. Therefore, it is important that follow-up investigations first confirm that composition of higher-order PTI- and PTI+ETI-activated NRG1 states.

Notably, as we hope to solve structures for activated forms of NRG1, leveraging cell death-incompetent glycine zipper motif mutants would allow purification of activated forms from live tissues. Additionally, perhaps we could purify activated forms of NRG1 in the absence of effectors by also mutating the methionine-histidine-aspartate (MHD) motif in the NB-ARC domain, as MHD mutants may be prone to spontaneous formation of effector-independent homooligomers. While mutation of both the glycine zipper and MHD motif may simplify protein purifications, mutation of the glycine zipper motif may interfere with functional interpretations. If the glycine zipper motif is important for transmembrane homooligomerizations of NRG1, structure determination from mutants may interfere with our ability to deduce cell death mechanisms. Nevertheless, purification of activated forms of NRG1, even with distorted N-terminal organizations, promises to greatly inform our understanding of NRG1-mediated cell death mechanisms.

Solving structures for NRG1 and ADR1 proteins from *N. benthamiana* and Arabidopsis could reveal the distinct mechanisms for cell death and transcriptional activation accomplished by RNLs. If *At*NRG1 can only mediate cell death, but *Nb*NRG1 can do both, we may be able to deduce what is required for cell death by comparing these structures. Likewise, if *At*ADR1 can regulate transcription while *Nb*ADR1 has lost genetic redundancy, we may better understand what is required for transcriptional activation by comparing these structures. Perhaps, further comparisons to *Nb*NRG1 in this regard would also be informative. These lines of investigation likely represent at least several years of work. Yet, it is tempting to state that this may be the perfect system to better understand the discrete mechanisms by which RNLs mediate downstream immune responses.

6.10 Summary and outlook

This project aimed to further our understanding of NLR-mediated immunity by investigating the signalling mechanisms of NRG1. I discovered the effector-dependent association of NRG1 with EDS1 and SAG101. As NRG1 was previously shown to be genetically required with EDS1 and SAG101 downstream of TNL-mediated immune activation, the discovery of associations that may mediate function represents a significant advancement. I also optimized a protocol for purification of full-length NRG1 for structural investigations that resulted in a low-resolution map. These data provide a foundation for future investigations of NRG1-mediated cell death mechanisms in plant immunity.

Although data indicate several possibilities for the formation NRG1-EDS1-SAG101 associations, the most intriguing prospect is the requirement for PTI-primed NRG1 self-associations. Future investigations could utilise Arabidopsis lines carrying two variants of differently-tagged NRG1 to determine whether PAMP treatment alone induces self-associations. Likewise, Arabidopsis lines carrying inducible effectors and tagged copies of NRG1, EDS1, and SAG101 could investigate whether delivery of effectors in the absence of PTI still promotes EDS1-SAG101 associations with NRG1. These lines of investigation would not only shed light on the influence of activation state on NRG1-EDS1-SAG101 associations, but help reveal the minimal requirements for NRG1-mediated cell death. As mentioned, both PTI and ETI activation are required for cell death; therefore, if ETI induces EDS1-SAG101 associations with NRG1 in the absence of PTI, these associations are insufficient to mediate cell death. Likewise, if PTI does induce self-associations of NRG1, these would also be insufficient for cell-death. If these two “checkpoints” for activation of NRG1 are both required, this would represent a novel activation mechanism for NLRs.

Resolving the inconsistencies in localization differences for NRG1 and EDS1-SAG101 would greatly illuminate their function(s). I think it is most likely that NRG1 and EDS1-SAG101 exist separately in low abundance in the cytosol. It does not make sense for NRG1 to have a constitutive association with ER membranes, as it does not contain a constitutive transmembrane domain. It is most likely that only upon activation does unfolding of the N-terminal domain result in insertion into the membrane. Indeed, HeLo/HeLo-like domain-containing HET-S and MLKL are both targeted to membranes only after induced oligomerizations. Therefore, I would hypothesize that NRG1 oligomerizes in the cytosol and is targeted to membranes by EDS1 and SAG101 associations. Therefore, future investigations into the localization

changes of NRG1 and EDS1-SAG101 in pre- and post-immune activation states are of high interest.

Future structural investigations should come after biochemical determination of PTI and PTI+ETI activation states of NRG1. They should also employ the use of cell death incompetent mutants, possibly a glycine zipper mutant. The most interesting structures would be a pre-activated NRG1 monomer, a PTI-activated NRG1 homooligomer, and a PTI+ETI-activated NRG1-EDS1-SAG101 heteromer—if these are indeed the activation states for NRG1. Once biochemical assays more clearly define pre- and post-immune activation states for NRG1, the purification protocol presented in this thesis could be used to isolate those species for structural investigations, likely using cryo-EM. Solving the structures of pre- and post-immune activation states of NRG1 would allow the most direct interpretations of cell death mechanism.

Therefore, the insights gained from this thesis open several new avenues of investigation into NRG1 mechanisms, which may eventually guide structural studies. As NRG1 belongs to a core signalling hub of immune-signalling NLRs in plants, future studies of NRG1 can provide both a biological and structural framework for investigating other NLRs.

Bibliography

AARTS, N., METZ, M., HOLUB, E., STASKAWICZ, B. J., DANIELS, M. J. & PARKER, J. E. 1998. Different requirements for EDS1 and NDR1 by disease resistance genes define at least two R gene-mediated signaling pathways in Arabidopsis. *Proceedings of the National Academy of Sciences,* 95**,** 10306-10311.

ADACHI, H., CONTRERAS, M. P., HARANT, A., WU, C. H., DEREVNINA, L., SAKAI, T., DUGGAN, C., MORATTO, E., BOZKURT, T. O., MAQBOOL, A., WIN, J. & KAMOUN, S. 2019. An N-terminal motif in NLR immune receptors is functionally conserved across distantly related plant species. *Elife,* 8**,** e49956.

AXTELL, M. J. & STASKAWICZ, B. J. 2003. Initiation of RPS2-specified disease resistance in Arabidopsis is coupled to the AvrRpt2-directed elimination of RIN4. *Cell,* 112**,** 369-77.

AZEVEDO, C., BETSUYAKU, S., PEART, J., TAKAHASHI, A., NOËL, L., SADANANDOM, A., CASAIS, C., PARKER, J. & SHIRASU, K. 2006. Role of SGT1 in resistance protein accumulation in plant immunity. *Embo j,* 25**,** 2007-16.

AZEVEDO, C., SADANANDOM, A., KITAGAWA, K., FREIALDENHOVEN, A., SHIRASU, K. & SCHULZE-LEFERT, P. 2002. The RAR1 Interactor SGT1, an Essential Component of R Gene-Triggered Disease Resistance. *Science,* 295**,** 2073.

BAGGS, E. L., MONROE, J. G., THANKI, A. S., O'GRADY, R., SCHUDOMA, C., HAERTY, W. & KRASILEVA, K. V. 2020. Convergent Loss of an EDS1/PAD4 Signaling Pathway in Several Plant Lineages Reveals Coevolved Components of Plant Immunity and Drought Response. *The Plant Cell,* 32**,** 2158.

BARRAGAN, C. A., WU, R., KIM, S. T., XI, W., HABRING, A., HAGMANN, J., VAN DE WEYER, A. L., ZAIDEM, M., HO, W. W. H., WANG, G., BEZRUKOV, I., WEIGEL, D. & CHAE, E. 2019. RPW8/HR repeats control NLR activation in Arabidopsis thaliana. *PLoS Genet,* 15**,** e1008313.

BAUDIN, M., HASSAN, J. A., SCHREIBER, K. J. & LEWIS, J. D. 2017. Analysis of the ZAR1 Immune Complex Reveals Determinants for Immunity and Molecular Interactions. *Plant Physiol,* 174**,** 2038-2053.

BENDER, K. W., BLACKBURN, R. K., MONAGHAN, J., DERBYSHIRE, P., MENKE, F. L. H., ZIPFEL, C., GOSHE, M. B., ZIELINSKI, R. E. & HUBER, S. C. 2017. Autophosphorylation-based Calcium (Ca(2+)) Sensitivity Priming and Ca(2+)/Calmodulin Inhibition of Arabidopsis thaliana Ca(2+)-dependent Protein Kinase 28 (CPK28). *The Journal of biological chemistry,* 292**,** 3988-4002.

BENTHAM, A., BURDETT, H., ANDERSON, P. A., WILLIAMS, S. J. & KOBE, B. 2017. Animal NLRs provide structural insights into plant NLR function. *Ann Bot,* 119**,** 827-702.

BENTHAM, A. R., ZDRZALEK, R., DE LA CONCEPCION, J. C. & BANFIELD, M. J. 2018. Uncoiling CNLs: Structure/Function Approaches to Understanding CC Domain Function in Plant NLRs. *Plant Cell Physiol,* 59**,** 2398-2408.

BERKEY, R., ZHANG, Y., MA, X., KING, H., ZHANG, Q., WANG, W. & XIAO, S. 2017. Homologues of the RPW8 Resistance Protein Are Localized to the Extrahaustorial Membrane that Is Likely Synthesized De Novo. *Plant Physiol,* 173**,** 600-613.

BERNOUX, M., VE, T., WILLIAMS, S., WARREN, C., HATTERS, D., VALKOV, E., ZHANG, X., ELLIS, J. G., KOBE, B. & DODDS, P. N. 2011. Structural and functional analysis of a plant resistance protein TIR domain reveals interfaces for self-association, signaling, and autoregulation. *Cell Host Microbe,* 9**,** 200-211.

BHANDARI, D. D., LAPIN, D., KRACHER, B., VON BORN, P., BAUTOR, J., NIEFIND, K. & PARKER, J. E. 2019. An EDS1 heterodimer signalling surface enforces timely reprogramming of immunity genes in Arabidopsis. *Nature Communications,* 10**,** 772.

BIERI, S., MAUCH, S., SHEN, Q.-H., PEART, J., DEVOTO, A., CASAIS, C., CERON, F., SCHULZE, S., STEINBIS, H.-H., SHIRASU, K. & SCHULZE-LEFERT, P. 2004. RAR1 Positively Controls Steady State Levels of Barley MLA Resistance Proteins and Enables Sufficient MLA6 Accumulation for Effective Resistance. *The Plant Cell,* 16**,** 3480.

BIRKER, D., HEIDRICH, K., TAKAHARA, H., NARUSAKA, M., DESLANDES, L., NARUSAKA, Y., REYMOND, M., PARKER, J. E. & O'CONNELL, R. 2009. A locus conferring resistance to Colletotrichum higginsianum is shared by four geographically distinct Arabidopsis accessions. *The Plant Journal,* 60**,** 602-613.

BONARDI, V., TANG, S., STALLMANN, A., ROBERTS, M., CHERKIS, K. & DANGL, J. L. 2011. Expanded functions for a family of plant intracellular immune receptors beyond specific recognition of pathogen effectors. *Proc Natl Acad Sci U S A,* 108**,** 16463-8.

BOTËR, M., AMIGUES, B., PEART, J., BREUER, C., KADOTA, Y., CASAIS, C., MOORE, G., KLEANTHOUS, C., OCHSENBEIN, F., SHIRASU, K. & GUEROIS, R. 2007. Structural and Functional Analysis of SGT1 Reveals That Its Interaction with HSP90 Is Required for the Accumulation of Rx, an R Protein Involved in Plant Immunity. *The Plant Cell,* 19**,** 3791.

BRENDOLISE, C., MARTINEZ-SANCHEZ, M., MOREL, A., CHEN, R., DINIS, R., DEROLES, S., PEETERS, N., RIKKERINK, E. H. A. & MONTEFIORI, M. 2018. NRG1-mediated recognition of HopQ1 reveals a link between PAMP and Effector-triggered Immunity. *bioRxiv***,** 293050.

BURDETT, H., BENTHAM, A. R., WILLIAMS, S. J., DODDS, P. N., ANDERSON, P. A., BANFIELD, M. J. & KOBE, B. 2019. The Plant "Resistosome": Structural Insights into Immune Signaling. *Cell Host Microbe,* 26**,** 193-201.

CAI, Z., JITKAEW, S., ZHAO, J., CHIANG, H. C., CHOKSI, S., LIU, J., WARD, Y., WU, L. G. & LIU, Z. G. 2014. Plasma membrane translocation of trimerized MLKL protein is required for TNF-induced necroptosis. *Nat Cell Biol,* 16**,** 55-65.

CAO, H., BOWLING, S. A., GORDON, A. S. & DONG, X. 1994. Characterization of an Arabidopsis Mutant That Is Nonresponsive to Inducers of Systemic Acquired Resistance. *The Plant Cell,* 6**,** 1583.

CASEY, L. W., LAVRENCIC, P., BENTHAM, A. R., CESARI, S., ERICSSON, D. J., CROLL, T., TURK, D., ANDERSON, P. A., MARK, A. E., DODDS, P. N., MOBLI, M., KOBE, B. & WILLIAMS, S. J. 2016. The CC domain structure from the wheat stem rust resistance protein Sr33 challenges paradigms for dimerization in plant NLR proteins. *Proceedings of the National Academy of Sciences,* 113**,** 12856.

CASTEL, B., NGOU, P. M., CEVIK, V., REDKAR, A., KIM, D. S., YANG, Y., DING, P. & JONES, J. D. G. 2019a. Diverse NLR immune receptors activate defence via the RPW8-NLR NRG1. *New Phytol,* 222**,** 966-980.

CASTEL, B., WU, Y., XIAO, S. & JONES, J. D. G. 2019b. An rpw8 quadruple mutant of Arabidopsis Col-0 is partially compromised in bacterial and fungal resistance. *bioRxiv***,** 839308.

CESARI, S. 2018. Multiple strategies for pathogen perception by plant immune receptors. *New Phytologist,* 219**,** 17-24.

CESARI, S., BERNOUX, M., MONCUQUET, P., KROJ, T. & DODDS, P. N. 2014a. A novel conserved mechanism for plant NLR protein pairs: the "integrated decoy" hypothesis. *Front Plant Sci,* 5**,** 606.

CESARI, S., KANZAKI, H., FUJIWARA, T., BERNOUX, M., CHALVON, V., KAWANO, Y., SHIMAMOTO, K., DODDS, P., TERAUCHI, R. & KROJ, T. 2014b. The NB-LRR proteins RGA4 and RGA5 interact functionally and physically to confer disease resistance. *EMBO J,* 33**,** 1941-59.

CHAE, E., BOMBLIES, K., KIM, S.-T., KARELINA, D., ZAIDEM, M., OSSOWSKI, S., MARTÍN-PIZARRO, C., LAITINEN, ROOSA A. E., ROWAN, BETH A., TENENBOIM, H., LECHNER, S., DEMAR, M., HABRING-MÜLLER, A., LANZ, C., RÄTSCH, G. & WEIGEL, D. 2014. Species-wide Genetic Incompatibility Analysis Identifies Immune Genes as Hot Spots of Deleterious Epistasis. *Cell,* 159**,** 1341-1351.

CHEN, G., WEI, B., LI, G., GONG, C., FAN, R. & ZHANG, X. 2018. TaEDS1 genes positively regulate resistance to powdery mildew in wheat. *Plant Mol Biol,* 96**,** 607-625.

CHEN, H., LIU, F. & FU, Z. Q. 2019. Deceiving the chaperone. *Nature Plants,* 5**,** 1110-1111.

CHEN, L., HAMADA, S., FUJIWARA, M., ZHU, T., THAO, N. P., WONG, H. L., KRISHNA, P., UEDA, T., KAKU, H., SHIBUYA, N., KAWASAKI, T. & SHIMAMOTO, K. 2010. The Hop/Sti1-Hsp90 chaperone complex facilitates the maturation and transport of a PAMP receptor in rice innate immunity. *Cell Host Microbe,* 7**,** 185-96.

CHEN, Q. F., XU, L., TAN, W. J., CHEN, L., QI, H., XIE, L. J., CHEN, M. X., LIU, B. Y., YU, L. J., YAO, N., ZHANG, J. H., SHU, W. & XIAO, S. 2015. Disruption of the Arabidopsis Defense Regulator Genes SAG101, EDS1, and PAD4 Confers Enhanced Freezing Tolerance. *Mol Plant,* 8**,** 1536-49.

CHEN, X., LI, W., REN, J., HUANG, D., HE, W. T., SONG, Y., YANG, C., LI, W., ZHENG, X., CHEN, P. & HAN, J. 2014. Translocation of mixed lineage kinase domain-like protein to plasma membrane leads to necrotic cell death. *Cell Res,* 24**,** 105-21.

CHINI, A., GRANT, J. J., SEKI, M., SHINOZAKI, K. & LOAKE, G. J. 2004. Drought tolerance established by enhanced expression of the CC–NBS–LRR gene, ADR1, requires salicylic acid, EDS1 and ABI1. *The Plant Journal,* 38**,** 810-822.

COLLIER, S. M., HAMEL, L. P. & MOFFETT, P. 2011. Cell death mediated by the N-terminal domains of a unique and highly conserved class of NB-LRR protein. *Mol Plant Microbe Interact,* 24**,** 918-31.

CORMACK, B. P., VALDIVIA, R. H. & FALKOW, S. 1996. FACS-optimized mutants of the green fluorescent protein (GFP). *Gene,* 173**,** 33-8.

CUI, H., QIU, J., ZHOU, Y., BHANDARI, D. D., ZHAO, C., BAUTOR, J. & PARKER, J. E. 2018. Antagonism of Transcription Factor MYC2 by EDS1/PAD4 Complexes Bolsters Salicylic Acid Defense in Arabidopsis Effector-Triggered Immunity. *Mol Plant,* 11**,** 1053-1066.

DANOT, O., MARQUENET, E., VIDAL-INGIGLIARDI, D. & RICHET, E. 2009. Wheel of Life, Wheel of Death: A Mechanistic Insight into Signaling by STAND Proteins. *Structure,* 17**,** 172-82.

DASKALOV, A., HABENSTEIN, B., SABATE, R., BERBON, M., MARTINEZ, D., CHAIGNEPAIN, S., COULARY-SALIN, B., HOFMANN, K., LOQUET, A. & SAUPE, S. J. 2016. Identification of a novel cell death-inducing domain reveals that fungal amyloid-controlled programmed cell death is related to necroptosis. *Proc Natl Acad Sci U S A,* 113**,** 2720-5.

DI DONATO, M. & GEISLER, M. 2019. HSP90 and co-chaperones: a multitaskers' view on plant hormone biology. *FEBS Lett,* 593**,** 1415-1430.

DONG, O. X., AO, K., XU, F., JOHNSON, K. C. M., WU, Y., LI, L., XIA, S., LIU, Y., HUANG, Y., RODRIGUEZ, E., CHEN, X., CHEN, S., ZHANG, Y., PETERSEN, M. & LI, X. 2018. Individual components of paired typical NLR immune receptors are regulated by distinct E3 ligases. *Nat Plants,* 4**,** 699-710.

DONG, O. X., TONG, M., BONARDI, V., EL KASMI, F., WOLOSHEN, V., WÜNSCH, L. K., DANGL, J. L. & LI, X. 2016. TNL-mediated immunity in Arabidopsis requires complex regulation of the redundant ADR1 gene family. *New Phytologist,* 210**,** 960-973.

DONGUS, J. A., BHANDARI, D. D., PATEL, M., ARCHER, L., DIJKGRAAF, L., DESLANDES, L., SHAH, J. & PARKER, J. E. 2020. The Arabidopsis PAD4 Lipase-Like Domain Is Sufficient for Resistance to Green Peach Aphid. *Mol Plant Microbe Interact,* 33**,** 328-335.

DRULYTE, I., JOHNSON, R. M., HESKETH, E. L., HURDISS, D. L., SCARFF, C. A., PORAV, S. A., RANSON, N. A., MUENCH, S. P. & THOMPSON, R. F. 2018. Approaches to altering particle distributions in cryo-electron microscopy sample preparation. *Acta Crystallogr D Struct Biol,* 74**,** 560-571.

DUXBURY, Z., WANG, S., MACKENZIE, C. I., TENTHOREY, J. L., ZHANG, X., HUH, S. U., HU, L., HILL, L., NGOU, P. M., DING, P., CHEN, J., MA, Y., GUO, H., CASTEL, B., MOSCHOU, P. N., BERNOUX, M., DODDS, P. N., VANCE, R. E. & JONES, J. D. G. 2020. Induced proximity of a TIR signaling domain on a plant-mammalian NLR chimera activates defense in plants. *Proceedings of the National Academy of Sciences,* 117**,** 18832.

DYRKA, W., COUSTOU, V., DASKALOV, A., LENDS, A., BARDIN, T., BERBON, M., KAUFFMANN, B., BLANCARD, C., SALIN, B., LOQUET, A. & SAUPE, S. J. 2020. Identification of NLR-associated amyloid signaling motifs in filamentous bacteria. *bioRxiv***,** 2020.01.06.895854.

DYRKA, W., LAMACCHIA, M., DURRENS, P., KOBE, B., DASKALOV, A., PAOLETTI, M., SHERMAN, D. J. & SAUPE, S. J. 2014. Diversity and variability of NOD-like receptors in fungi. *Genome Biol Evol,* 6**,** 3137-58.

ENGLER, C., KANDZIA, R. & MARILLONNET, S. 2008. A one pot, one step, precision cloning method with high throughput capability. *PLoS One,* 3**,** e3647.

ENGLER, C., YOULES, M., GRUETZNER, R., EHNERT, T. M., WERNER, S., JONES, J. D., PATRON, N. J. & MARILLONNET, S. 2014. A golden gate modular cloning toolbox for plants. *ACS Synth Biol,* 3**,** 839-43.

ESSUMAN, K., SUMMERS, D. W., SASAKI, Y., MAO, X., DIANTONIO, A. & MILBRANDT, J. 2017. The SARM1 Toll/Interleukin-1 Receptor Domain Possesses Intrinsic NAD(+) Cleavage Activity that Promotes Pathological Axonal Degeneration. *Neuron,* 93**,** 1334-1343.e5.

ESSUMAN, K., SUMMERS, D. W., SASAKI, Y., MAO, X., YIM, A. K. Y., DIANTONIO, A. & MILBRANDT, J. 2018. TIR Domain Proteins Are an Ancient Family of NAD(+)-Consuming Enzymes. *Current biology : CB,* 28**,** 421-430.e4.

FALK, A., FEYS, B. J., FROST, L. N., JONATHAN, D. G. J., DANIELS, M. J. & PARKER, J. E. 1999. EDS1, an Essential Component of R Gene-Mediated Disease Resistance in Arabidopsis Has Homology to Eukaryotic Lipases. *Proceedings of the National Academy of Sciences of the United States of America,* 96**,** 3292-3297.

FAUSTIN, B., LARTIGUE, L., BRUEY, J. M., LUCIANO, F., SERGIENKO, E., BAILLY-MAITRE, B., VOLKMANN, N., HANEIN, D., ROUILLER, I. & REED, J. C. 2007. Reconstituted NALP1 inflammasome reveals two-step mechanism of caspase-1 activation. *Mol Cell,* 25**,** 713-24.

FEEHAN, J. M., CASTEL, B., BENTHAM, A. R. & JONES, J. D. 2020. Plant NLRs get by with a little help from their friends. *Curr Opin Plant Biol,* 56**,** 99-108.

FEYS, B. J., MOISAN, L. J., NEWMAN, M. A. & PARKER, J. E. 2001. Direct interaction between the Arabidopsis disease resistance signaling proteins, EDS1 and PAD4. *Embo j,* 20**,** 5400-11.

FEYS, B. J., WIERMER, M., BHAT, R. A., MOISAN, L. J., MEDINA-ESCOBAR, N., NEU, C., CABRAL, A. & PARKER, J. E. 2005. Arabidopsis SENESCENCE-ASSOCIATED GENE101 stabilizes and signals within an ENHANCED DISEASE SUSCEPTIBILITY1 complex in plant innate immunity. *Plant Cell,* 17**,** 2601–2613.

FLOR, H. H. 1971. Current Status of the Gene-For-Gene Concept. *Annual Review of Phytopathology,* 9**,** 275-296.

FRYE, C. A. & INNES, R. W. 1998. An Arabidopsis Mutant with Enhanced Resistance to Powdery Mildew. *The Plant Cell,* 10**,** 947.

GABRIELS, S. H., VOSSEN, J. H., EKENGREN, S. K., VAN OOIJEN, G., ABD-EL-HALIEM, A. M., VAN DEN BERG, G. C., RAINEY, D. Y., MARTIN, G. B., TAKKEN, F. L., DE WIT, P. J. & JOOSTEN, M. H. 2007. An NB-LRR protein required for HR signalling mediated by both extra- and intracellular resistance proteins. *Plant J,* 50**,** 14-28.

GABRIËLS, S. H., VOSSEN, J. H., EKENGREN, S. K., VAN OOIJEN, G., ABD-EL-HALIEM, A. M., VAN DEN BERG, G. C., RAINEY, D. Y., MARTIN, G. B., TAKKEN, F. L., DE WIT, P. J. & JOOSTEN, M. H. 2007. An NB-LRR protein required for HR signalling mediated by both extra- and intracellular resistance proteins. *Plant J,* 50**,** 14-28.

GANTNER, J., ORDON, J., KRETSCHMER, C., GUEROIS, R. & STUTTMANN, J. 2019. An EDS1-SAG101 Complex Is Essential for TNL-Mediated Immunity in Nicotiana benthamiana. *Plant Cell,* 31**,** 2456-2474.

GARCÍA, A. V., BLANVILLAIN-BAUFUMÉ, S., HUIBERS, R. P., WIERMER, M., LI, G., GOBBATO, E., RIETZ, S. & PARKER, J. E. 2010. Balanced Nuclear and Cytoplasmic Activities of EDS1 Are Required for a Complete Plant Innate Immune Response. *PLOS Pathogens,* 6**,** e1000970.

GIMPL, K., KLEMENT, J. & KELLER, S. 2016. Characterising protein/detergent complexes by triple-detection size-exclusion chromatography. *Biological procedures online,* 18**,** 4-4.

GLASS, N. L., JACOBSON, D. J. & SHIU, P. K. 2000. The genetics of hyphal fusion and vegetative incompatibility in filamentous ascomycete fungi. *Annu Rev Genet,* 34**,** 165-186.

GLAZEBROOK, J., ROGERS, E. E. & AUSUBEL, F. M. 1996. Isolation of Arabidopsis Mutants with Enhanced Disease Susceptibility by Direct Screening. *Genetics,* 143**,** 973-982.

GRANT, J. J., CHINI, A., BASU, D. & LOAKE, G. J. 2003. Targeted activation tagging of the Arabidopsis NBS-LRR gene, ADR1, conveys resistance to virulent pathogens. *Mol Plant Microbe Interact,* 16**,** 669-80.

GREENE, E. A., CODOMO, C. A., TAYLOR, N. E., HENIKOFF, J. G., TILL, B. J., REYNOLDS, S. H., ENNS, L. C., BURTNER, C., JOHNSON, J. E., ODDEN, A. R., COMAI, L. &

HENIKOFF, S. 2003. Spectrum of chemically induced mutations from a large-scale reverse-genetic screen in Arabidopsis. *Genetics,* 164**,** 731-40.

GREENWALD, J., BUHTZ, C., RITTER, C., KWIATKOWSKI, W., CHOE, S., MADDELEIN, M. L., NESS, F., CESCAU, S., SORAGNI, A., LEITZ, D., SAUPE, S. J. & RIEK, R. 2010. The mechanism of prion inhibition by HET-S. *Mol Cell,* 38**,** 889-99.

GUO, H., AHN, H. K., SKLENAR, J., HUANG, J., MA, Y., DING, P., MENKE, F. L. H. & JONES, J. D. G. 2020. Phosphorylation-Regulated Activation of the Arabidopsis RRS1-R/RPS4 Immune Receptor Complex Reveals Two Distinct Effector Recognition Mechanisms. *Cell Host Microbe,* 27**,** 1–13.

HAMMOND-KOSACK, K. E. & JONES, J. D. 1997. Plant disease resistance genes. *Annu Rev Plant Physiol Plant Mol Biol,* 48**,** 575-607.

HAO, W., COLLIER, S. M., MOFFETT, P. & CHAI, J. 2013. Structural basis for the interaction between the potato virus X resistance protein (Rx) and its cofactor Ran GTPase-activating protein 2 (RanGAP2). *J Biol Chem,* 288**,** 35868-76.

HE, Y. & GAN, S. 2002. A Gene Encoding an Acyl Hydrolase Is Involved in Leaf Senescence in Arabidopsis. *The Plant Cell,* 14**,** 805-815.

HEBERT, H. 2019. CryoEM: a crystals to single particles round-trip. *Curr Opin Struct Biol,* 58**,** 59-67.

HEIDRICH, K., WIRTHMUELLER, L., TASSET, C., POUZET, C., DESLANDES, L. & PARKER, J. E. 2011. Arabidopsis EDS1 Connects Pathogen Effector Recognition to Cell Compartment–Specific Immune Responses. *Science.*

HELLER, J., CLAVÉ, C., GLADIEUX, P., SAUPE, S. J. & GLASS, N. L. 2018. NLR surveillance of essential SEC-9 SNARE proteins induces programmed cell death upon allorecognition in filamentous fungi. *Proceedings of the National Academy of Sciences*.

HOFMANN, K. 2019. The Evolutionary Origins of Programmed Cell Death Signaling. *Cold Spring Harb Perspect Biol*.

HOLT, B. F., 3RD, BELKHADIR, Y. & DANGL, J. L. 2005. Antagonistic control of disease resistance protein stability in the plant immune system. *Science,* 309**,** 929-32.

HORSEFIELD, S., BURDETT, H., ZHANG, X., MANIK, M. K., SHI, Y., CHEN, J., QI, T., GILLEY, J., LAI, J. S., RANK, M. X., CASEY, L. W., GU, W., ERICSSON, D. J., FOLEY, G., HUGHES, R. O., BOSANAC, T., VON ITZSTEIN, M., RATHJEN, J. P., NANSON, J. D., BODEN, M., DRY, I. B., WILLIAMS, S. J., STASKAWICZ, B. J., COLEMAN, M. P., VE, T., DODDS, P. N. & KOBE, B. 2019. NAD(+) cleavage activity by animal and plant TIR domains in cell death pathways. *Science,* 365**,** 793-799.

HU, Z., YAN, C., LIU, P., HUANG, Z., MA, R., ZHANG, C., WANG, R., ZHANG, Y., MARTINON, F., MIAO, D., DENG, H., WANG, J., CHANG, J. & CHAI, J. 2013. Crystal Structure of NLRC4 Reveals Its Autoinhibition Mechanism. *Science,* 341**,** 172-175.

HU, Z., ZHOU, Q., ZHANG, C., FAN, S., CHENG, W., ZHAO, Y., SHAO, F., WANG, H. W., SUI, S. F. & CHAI, J. 2015. Structural and biochemical basis for induced self-propagation of NLRC4. *Science,* 350**,** 399-404.

HUANG, Y., CHEN, X., LIU, Y., ROTH, C., COPELAND, C., MCFARLANE, H. E., HUANG, S., LIPKA, V., WIERMER, M. & LI, X. 2013. Mitochondrial AtPAM16 is required for plant survival and the negative regulation of plant immunity. *Nature Communications,* 4**,** 2558.

HUH, S. U., CEVIK, V., DING, P., DUXBURY, Z., MA, Y., TOMLINSON, L., SARRIS, P. F. & JONES, J. D. G. 2017. Protein-protein interactions in the RPS4/RRS1 immune receptor complex. *PLOS Pathogens,* 13**,** e1006376.

JANDER, G., BAERSON, S. R., HUDAK, J. A., GONZALEZ, K. A., GRUYS, K. J. & LAST, R. L. 2003. Ethylmethanesulfonate saturation mutagenesis in Arabidopsis to determine frequency of herbicide resistance. *Plant physiology,* 131**,** 139-146.

JELENSKA, J., VAN HAL, J. A. & GREENBERG, J. T. 2010. Pseudomonas syringae hijacks plant stress chaperone machinery for virulence. *Proceedings of the National Academy of Sciences,* 107**,** 13177.

JIRAGE, D., TOOTLE, T. L., REUBER, T. L., FROST, L. N., FEYS, B. J., PARKER, J. E., AUSUBEL, F. M. & GLAZEBROOK, J. 1999. Arabidopsis thaliana PAD4 encodes a lipase-like gene that is important for salicylic acid signaling. *Proc Natl Acad Sci U S A,* 96**,** 13583-8.

JOHNSON, K. C., DONG, O. X., HUANG, Y. & LI, X. 2012. A rolling stone gathers no moss, but resistant plants must gather their moses. *Cold Spring Harb Symp Quant Biol,* 77**,** 259-68.

JONES, J. D. & DANGL, J. L. 2006. The plant immune system. *Nature,* 444**,** 323-9.

JONES, J. D. G., VANCE, R. E. & DANGL, J. L. 2016. Intracellular innate immune surveillance devices in plants and animals. *Science,* 354.

KADOTA, Y. & SHIRASU, K. 2012. The HSP90 complex of plants. *Biochimica et Biophysica Acta (BBA) - Molecular Cell Research,* 1823**,** 689-697.

KANYUKA, K. & RUDD, J. J. 2019. Cell surface immune receptors: the guardians of the plant's extracellular spaces. *Current Opinion in Plant Biology,* 50**,** 1-8.

KANZAKI, H., SAITOH, H., ITO, A., FUJISAWA, S., KAMOUN, S., KATOU, S., YOSHIOKA, H. & TERAUCHI, R. 2003. Cytosolic HSP90 and HSP70 are essential components of INF1-mediated hypersensitive response and non-host resistance to Pseudomonas cichorii in Nicotiana benthamiana. *Mol Plant Pathol,* 4**,** 383-91.

KIM, S., CHAMBERLAIN, A. K. & BOWIE, J. U. 2004. Membrane channel structure of Helicobacter pylori vacuolating toxin: role of multiple GXXXG motifs in cylindrical channels. *Proc Natl Acad Sci U S A,* 101**,** 5988-91.

KIM, S., JEON, T.-J., OBERAI, A., YANG, D., SCHMIDT, J. J. & BOWIE, J. U. 2005. Transmembrane glycine zippers: Physiological and pathological roles in membrane proteins. *Proceedings of the National Academy of Sciences of the United States of America,* 102**,** 14278.

KIM, Y., SCHUMAKER, K. S. & ZHU, J.-K. 2006. EMS Mutagenesis of Arabidopsis. *In:* SALINAS, J. & SANCHEZ-SERRANO, J. J. (eds.) *Arabidopsis Protocols.* Totowa, NJ: Humana Press.

KITAGAWA, K., SKOWYRA, D., ELLEDGE, S. J., HARPER, J. W. & HIETER, P. 1999. SGT1 encodes an essential component of the yeast kinetochore assembly pathway and a novel subunit of the SCF ubiquitin ligase complex. *Mol Cell,* 4**,** 21-33.

KONTRA, L., CSORBA, T., TAVAZZA, M., LUCIOLI, A., TAVAZZA, R., MOXON, S., TISZA, V., MEDZIHRADSZKY, A., TURINA, M. & BURGYÁN, J. 2016. Distinct Effects of p19 RNA Silencing Suppressor on Small RNA Mediated Pathways in Plants. *PLOS Pathogens,* 12**,** e1005935.

KOURELIS, J. & VAN DER HOORN, R. A. L. 2018. Defended to the Nines: 25 Years of Resistance Gene Cloning Identifies Nine Mechanisms for R Protein Function. *The Plant Cell,* 30**,** 285.

KRASILEVA, K. V., DAHLBECK, D. & STASKAWICZ, B. J. 2010. Activation of an Arabidopsis resistance protein is specified by the in planta association of its leucine-rich repeat domain with the cognate oomycete effector. *Plant Cell,* 22**,** 2444-58.

LAPIN, D., BHANDARI, D. D. & PARKER, J. E. 2020. Origins and Immunity Networking Functions of EDS1 Family Proteins. *Annu Rev Phytopathol*.

LAPIN, D., KOVACOVA, V., SUN, X., DONGUS, J. A., BHANDARI, D. D., VON BORN, P., BAUTOR, J., GUARNERI, N., RZEMIENIEWSKI, J., STUTTMANN, J., BEYER, A. & PARKER, J. E. 2019. A coevolved EDS1-SAG101-NRG1 module mediates cell death signaling by TIR-domain immune receptors. *Plant Cell,* 31**,** 2430–2455.

LE MAIRE, M., CHAMPEIL, P. & MOLLER, J. V. 2000. Interaction of membrane proteins and lipids with solubilizing detergents. *Biochim Biophys Acta,* 1508**,** 86-111.

LE ROUX, C., HUET, G., JAUNEAU, A., CAMBORDE, L., TREMOUSAYGUE, D., KRAUT, A., ZHOU, B., LEVAILLANT, M., ADACHI, H., YOSHIOKA, H., RAFFAELE, S., BERTHOME, R., COUTE, Y., PARKER, J. E. & DESLANDES, L. 2015. A receptor pair with an integrated decoy converts pathogen disabling of transcription factors to immunity. *Cell,* 161**,** 1074-88.

LI, L., HABRING, A., WANG, K. & WEIGEL, D. 2020a. Atypical Resistance Protein RPW8/HR Triggers Oligomerization of the NLR Immune Receptor RPP7 and Autoimmunity. *Cell Host Microbe,* 27**,** 405-417.e6.

LI, M., BAHN, S. C., GUO, L., MUSGRAVE, W., BERG, H., WELTI, R. & WANG, X. 2011. Patatin-Related Phospholipase pPLAIIIβ-Induced Changes in Lipid Metabolism Alter Cellulose Content and Cell Elongation in <em>Arabidopsis</em&gt. *The Plant Cell,* 23**,** 1107.

LI, Q., WANG, J., BAI, T., ZHANG, M., JIA, Y., SHEN, D., ZHANG, M. & DOU, D. 2020b. A Phytophthora capsici effector suppresses plant immunity via interaction with EDS1. *Mol Plant Pathol,* 21**,** 502-511.

LIU, S., LIU, H., JOHNSTON, A., HANNA-ADDAMS, S., REYNOSO, E., XIANG, Y. & WANG, Z. 2017. MLKL forms disulfide bond-dependent amyloid-like polymers to induce necroptosis. *Proc Natl Acad Sci U S A,* 114**,** E7450-e7459.

LIU, Y., SCHIFF, M., MARATHE, R. & DINESH-KUMAR, S. P. 2002. Tobacco Rar1, EDS1 and NPR1/NIM1 like genes are required for N-mediated resistance to tobacco mosaic virus. *Plant J,* 30**,** 415-29.

LOLLE, S., STEVENS, D. & COAKER, G. 2020. Plant NLR-triggered immunity: from receptor activation to downstream signaling. *Curr Opin Immunol,* 62**,** 99-105.

LOUIS, J., GOBBATO, E., MONDAL, H. A., FEYS, B. J., PARKER, J. E. & SHAH, J. 2012. Discrimination of Arabidopsis PAD4 Activities in Defense against Green Peach Aphid and Pathogens. *Plant Physiology,* 158**,** 1860.

LUKASIK, E. & TAKKEN, F. L. W. 2009. STANDing strong, resistance proteins instigators of plant defence. *Current Opinion in Plant Biology,* 12**,** 427-436.

MA, Y., GUO, H., HU, L., MARTINEZ, P. P., MOSCHOU, P. N., CEVIK, V., DING, P., DUXBURY, Z., SARRIS, P. F. & JONES, J. D. G. 2018. Distinct modes of derepression of an Arabidopsis immune receptor complex by two different bacterial effectors. *Proc Natl Acad Sci U S A,* 115**,** 10218-10227.

MAEKAWA, T., CHENG, W., SPIRIDON, L. N., TOLLER, A., LUKASIK, E., SAIJO, Y., LIU, P., SHEN, Q. H., MICLUTA, M. A., SOMSSICH, I. E., TAKKEN, F. L. W., PETRESCU, A. J., CHAI, J. & SCHULZE-LEFERT, P. 2011. Coiled-coil domain-dependent homodimerization of intracellular barley immune receptors defines a minimal functional module for triggering cell death. *Cell Host Microbe,* 9**,** 187-199.

MAHDI, L. K., HUANG, M., ZHANG, X., NAKANO, R. T., KOPP, L. B., SAUR, I. M. L., JACOB, F., KOVACOVA, V., LAPIN, D., PARKER, J. E., MURPHY, J. M., HOFMANN, K., SCHULZE-LEFERT, P., CHAI, J. & MAEKAWA, T. 2020. Discovery of a Family of Mixed Lineage Kinase Domain-like Proteins in Plants and Their Role in Innate Immune Signaling. *Cell Host & Microbe*.

MARTIN, R., QI, T., ZHANG, H., LIU, F., KING, M., TOTH, C., NOGALES, E. & STASKAWICZ, B. J. 2020. Structure of the activated Roq1 resistosome directly recognizing the pathogen effector XopQ. *bioRxiv***,** 2020.08.13.246413.

MAYOR, A., MARTINON, F., DE SMEDT, T., PÉTRILLI, V. & TSCHOPP, J. 2007. A crucial function of SGT1 and HSP90 in inflammasome activity links mammalian and plant innate immune responses. *Nature Immunology,* 8**,** 497-503.

MESTRE, P. & BAULCOMBE, D. C. 2006. Elicitor-mediated oligomerization of the tobacco N disease resistance protein. *Plant Cell,* 18**,** 491-501.

MEYER, P., LINN, F., HEIDMANN, I., MEYER, H., NIEDENHOF, I. & SAEDLER, H. 1992. Endogenous and environmental factors influence 35S promoter methylation of a maize A1 gene construct in transgenic petunia and its colour phenotype. *Molecular and General Genetics MGG,* 231**,** 345-352.

MUSKETT, P. R., KAHN, K., AUSTIN, M. J., MOISAN, L. J., SADANANDOM, A., SHIRASU, K., JONES, J. D. & PARKER, J. E. 2002. Arabidopsis RAR1 exerts rate-limiting control of R gene-mediated defenses against multiple pathogens. *Plant Cell,* 14**,** 979-92.

NANDETY, R. S., CAPLAN, J. L., CAVANAUGH, K., PERROUD, B., WROBLEWSKI, T., MICHELMORE, R. W. & MEYERS, B. C. 2013. The role of TIR-NBS and TIR-X proteins in plant basal defense responses. *Plant Physiol,* 162**,** 1459-72.

NARUSAKA, M., SHIRASU, K., NOUTOSHI, Y., KUBO, Y., SHIRAISHI, T., IWABUCHI, M. & NARUSAKA, Y. 2009. RRS1 and RPS4 provide a dual Resistance-gene system against fungal and bacterial pathogens. *Plant J,* 60**,** 218-26.

NEUBAUER, M., SERRANO, I., RODIBAUGH, N., BHANDARI, D. D., BAUTOR, J., PARKER, J. E. & INNES, R. W. 2020. Arabidopsis EDR1 Protein Kinase Regulates the Association of EDS1 and PAD4 to Inhibit Cell Death. *Mol Plant Microbe Interact,* 33**,** 693-703.

NGOU, B. P. M., AHN, H.-K., DING, P. & JONES, J. D. G. 2020a. Mutual Potentiation of Plant Immunity by Cell-surface and Intracellular Receptors. *bioRxiv***,** 2020.04.10.034173.

NGOU, B. P. M., AHN, H. K., DING, P., REDKAR, A., BROWN, H., MA, Y., YOULES, M., TOMLINSON, L. & JONES, J. D. G. 2020b. Estradiol-inducible AvrRps4 expression reveals distinct properties of TIR-NLR-mediated effector-triggered immunity. *J Exp Bot,* 71**,** 2186-2197.

NIELSEN, H. 2017. Predicting Secretory Proteins with SignalP. *In:* KIHARA, D. (ed.) *Protein Function Prediction: Methods and Protocols.* New York, NY: Springer New York.

NISHIMURA, M. T., ANDERSON, R. G., CHERKIS, K. A., LAW, T. F., LIU, Q. L., MACHIUS, M., NIMCHUK, Z. L., YANG, L., CHUNG, E.-H., EL KASMI, F., HYUNH, M., OSBORNE NISHIMURA, E., SONDEK, J. E. & DANGL, J. L. 2017. TIR-only protein RBA1 recognizes a pathogen effector to regulate cell death in Arabidopsis. *Proceedings of the National Academy of Sciences*.

NOËL, L. D., CAGNA, G., STUTTMANN, J., WIRTHMÜLLER, L., BETSUYAKU, S., WITTE, C.-P., BHAT, R., POCHON, N., COLBY, T. & PARKER, J. E. 2007. Interaction between SGT1 and cytosolic/nuclear HSC70 chaperones regulates Arabidopsis immune responses. *The Plant cell,* 19**,** 4061-4076.

NTOUKAKIS, V., SAUR, I. M. L., CONLAN, B. & RATHJEN, J. P. 2014. The changing of the guard: the Pto/Prf receptor complex of tomato and pathogen recognition. *Current Opinion in Plant Biology,* 20**,** 69-74.

PARK, C. J. & SEO, Y. S. 2015. Heat Shock Proteins: A Review of the Molecular Chaperones for Plant Immunity. *Plant Pathol J,* 31**,** 323-33.

PARKER, J. E., HOLUB, E. B., FROST, L. N., FALK, A., GUNN, N. D. & DANIELS, M. J. 1996. Characterization of eds1, a mutation in Arabidopsis suppressing resistance to Peronospora parasitica specified by several different RPP genes. *Plant Cell,* 8**,** 2033-46.

PEART, J. R., COOK, G., FEYS, B. J., PARKER, J. E. & BAULCOMBE, D. C. 2002. An EDS1 orthologue is required for N-mediated resistance against tobacco mosaic virus. *Plant J,* 29**,** 569-79.

PEART, J. R., MESTRE, P., LU, R., MALCUIT, I. & BAULCOMBE, D. C. 2005. NRG1, a CC-NB-LRR protein, together with N, a TIR-NB-LRR protein, mediates resistance against tobacco mosaic virus. *Curr Biol,* 15**,** 968-73.

PEGADARAJU, V., LOUIS, J., SINGH, V., REESE, J. C., BAUTOR, J., FEYS, B. J., COOK, G., PARKER, J. E. & SHAH, J. 2007. Phloem-based resistance to green peach aphid is controlled by Arabidopsis PHYTOALEXIN DEFICIENT4 without its signaling partner ENHANCED DISEASE SUSCEPTIBILITY1. *Plant J,* 52**,** 332-41.

PRASHER, D. C., ECKENRODE, V. K., WARD, W. W., PRENDERGAST, F. G. & CORMIER, M. J. 1992. Primary structure of the Aequorea victoria green-fluorescent protein. *Gene,* 111**,** 229-233.

PRIVÉ, G. G. 2009. Lipopeptide detergents for membrane protein studies. *Curr Opin Struct Biol,* 19**,** 379-85.

QI, D., DUBIELLA, U., KIM, S. H., SLOSS, D. I., DOWEN, R. H., DIXON, J. E. & INNES, R. W. 2014. Recognition of the protein kinase AVRPPHB SUSCEPTIBLE1 by the disease resistance protein RESISTANCE TO PSEUDOMONAS SYRINGAE5 is dependent on s-acylation and an exposed loop in AVRPPHB SUSCEPTIBLE1. *Plant Physiol,* 164**,** 340-51.

QI, T., SEONG, K., THOMAZELLA, D. P. T., KIM, J. R., PHAM, J., SEO, E., CHO, M. J., SCHULTINK, A. & STASKAWICZ, B. J. 2018. NRG1 functions downstream of EDS1 to regulate TIR-NLR-mediated plant immunity in Nicotiana benthamiana. *Proc Natl Acad Sci U S A,* 115**,** E10979-e10987.

RAJEEVKUMAR, S., ANUNANTHINI, P. & SATHISHKUMAR, R. 2015. Epigenetic silencing in transgenic plants. *Frontiers in plant science,* 6**,** 693-693.

RAVENSDALE, M., BERNOUX, M., VE, T., KOBE, B., THRALL, P. H., ELLIS, J. G. & DODDS, P. N. 2012. Intramolecular interaction influences binding of the Flax L5 and L6 resistance proteins to their AvrL567 ligands. *PLoS Pathog,* 8**,** e1003004.

RAYMER, G., WILLARD, J. M. & SCHOTTEL, J. L. 1990. Cloning, sequencing, and regulation of expression of an extracellular esterase gene from the plant pathogen Streptomyces scabies. *J Bacteriol,* 172**,** 7020-6.

ROBERTS, M., TANG, S., STALLMANN, A., DANGL, J. L. & BONARDI, V. 2013. Genetic requirements for signaling from an autoactive plant NB-LRR intracellular innate immune receptor. *PLoS Genet,* 9.

RUSTERUCCI, C., AVIV, D. H., HOLT, B. F., 3RD, DANGL, J. L. & PARKER, J. E. 2001. The disease resistance signaling components EDS1 and PAD4 are essential regulators of the cell death pathway controlled by LSD1 in Arabidopsis. *Plant Cell,* 13**,** 2211-24.

SAILE, S. C., JACOB, P., CASTEL, D., JUBIC, L. M., GONZALEZ, I. S., BÄCKER, M., JONES, J. D. G., DANGL, J. L. & EL KASMI, F. 2020. Two unequally redundant "helper" immune receptor families mediate Arabidopsis thaliana intracellular "sensor" immune receptor functions. *PLoS Biology*.

SANO, S., AOYAMA, M., NAKAI, K., SHIMOTANI, K., YAMASAKI, K., SATO, M. H., TOJO, D., SUWASTIKA, I. N., NOMURA, H. & SHIINA, T. 2014. Light-dependent expression of flg22-induced defense genes in Arabidopsis. *Frontiers in Plant Science,* 5**,** 531.

SARAVANAN, R. S., SLABAUGH, E., SINGH, V. R., LAPIDUS, L. J., HAAS, T. & BRANDIZZI, F. 2009. The targeting of the oxysterol-binding protein ORP3a to the endoplasmic reticulum relies on the plant VAP33 homolog PVA12. *Plant J,* 58**,** 817-30.

SARRIS, P. F., CEVIK, V., DAGDAS, G., JONES, J. D. G. & KRASILEVA, K. V. 2016. Comparative analysis of plant immune receptor architectures uncovers host proteins likely targeted by pathogens. *BMC Biology,* 14**,** 8.

SARRIS, P. F., DUXBURY, Z., HUH, S. U., MA, Y., SEGONZAC, C., SKLENAR, J., DERBYSHIRE, P., CEVIK, V., RALLAPALLI, G., SAUCET, S. B., WIRTHMUELLER, L., MENKE, F. L., SOHN, K. H. & JONES, J. D. 2015. A Plant Immune Receptor Detects Pathogen Effectors that Target WRKY Transcription Factors. *Cell,* 161**,** 1089-100.

SAUCET, S. B., MA, Y., SARRIS, P. F., FURZER, O. J., SOHN, K. H. & JONES, J. D. 2015. Two linked pairs of Arabidopsis TNL resistance genes independently confer recognition of bacterial effector AvrRps4. *Nat Commun,* 6**,** 6338.

SCHUBERT, D., LECHTENBERG, B., FORSBACH, A., GILS, M., BAHADUR, S. & SCHMIDT, R. 2004. Silencing in Arabidopsis T-DNA Transformants: The Predominant Role of a Gene-Specific RNA Sensing Mechanism versus Position Effects. *The Plant Cell,* 16**,** 2561.

SCHULTINK, A., QI, T., LEE, A., STEINBRENNER, A. D. & STASKAWICZ, B. 2017. Roq1 mediates recognition of the Xanthomonas and Pseudomonas effector proteins XopQ and HopQ1. *Plant J,* 92**,** 787-795.

SERRANO, M., HUBERT, D. A., DANGL, J. L., SCHULZE-LEFERT, P. & KOMBRINK, E. 2010. A chemical screen for suppressors of the avrRpm1-RPM1-dependent hypersensitive cell death response in Arabidopsis thaliana. *Planta,* 231**,** 1013-1023.

SEURING, C., GREENWALD, J., WASMER, C., WEPF, R., SAUPE, S. J., MEIER, B. H. & RIEK, R. 2012. The Mechanism of Toxicity in HET-S/HET-s Prion Incompatibility. *PLOS Biology,* 10**,** e1001451.

SHANER, N. C., CAMPBELL, R. E., STEINBACH, P. A., GIEPMANS, B. N., PALMER, A. E. & TSIEN, R. Y. 2004. Improved monomeric red, orange and yellow fluorescent proteins derived from Discosoma sp. red fluorescent protein. *Nat Biotechnol,* 22**,** 1567-72.

SHANER, N. C., LAMBERT, G. G., CHAMMAS, A., NI, Y., CRANFILL, P. J., BAIRD, M. A., SELL, B. R., ALLEN, J. R., DAY, R. N., ISRAELSSON, M., DAVIDSON, M. W. & WANG, J. 2013. A bright monomeric green fluorescent protein derived from Branchiostoma lanceolatum. *Nature methods,* 10**,** 407-409.

SHAO, Z.-Q., XUE, J.-Y., WU, P., ZHANG, Y.-M., WU, Y., HANG, Y.-Y., WANG, B. & CHEN, J.-Q. 2016. Large-Scale Analyses of Angiosperm Nucleotide-Binding Site-Leucine-Rich Repeat Genes Reveal Three Anciently Diverged Classes with Distinct Evolutionary Patterns. *Plant Physiology,* 170**,** 2095-2109.

SHAO, Z. Q., ZHANG, Y. M., HANG, Y. Y., XUE, J. Y., ZHOU, G. C., WU, P., WU, X. Y., WU, X. Z., WANG, Q., WANG, B. & CHEN, J. Q. 2014. Long-term evolution of nucleotide-binding site-leucine-rich repeat genes: understanding gained from and beyond the legume family. *Plant Physiol,* 166**,** 217-34.

SHIMADA, T. L., SHIMADA, T. & HARA-NISHIMURA, I. 2010. A rapid and non-destructive screenable marker, FAST, for identifying transformed seeds of Arabidopsis thaliana. *Plant J,* 61**,** 519-28.

SHIRASU, K. 2009. The HSP90-SGT1 Chaperone Complex for NLR Immune Sensors. *Annual Review of Plant Biology,* 60**,** 139-164.

SHIRASU, K., LAHAYE, T., TAN, M.-W., ZHOU, F., AZEVEDO, C. & SCHULZE-LEFERT, P. 1999. A Novel Class of Eukaryotic Zinc-Binding Proteins Is Required for Disease Resistance Signaling in Barley and Development in C. elegans. *Cell,* 99**,** 355-366.

SHOEMAKER, S. C. & ANDO, N. 2018. X-rays in the Cryo-Electron Microscopy Era: Structural Biology's Dynamic Future. *Biochemistry,* 57**,** 277-285.

SILIGARDI, G., ZHANG, M. & PRODROMOU, C. 2018. The Stoichiometric Interaction of the Hsp90-Sgt1-Rar1 Complex by CD and SRCD Spectroscopy. *Front Mol Biosci,* 4**,** 95.

SILIGATO, R., WANG, X., YADAV, S. R., LEHESRANTA, S., MA, G., URSACHE, R., SEVILEM, I., ZHANG, J., GORTE, M., PRASAD, K., WRZACZEK, M., HEIDSTRA, R., MURPHY, A., SCHERES, B. & MÄHÖNEN, A. P. 2016. MultiSite Gateway-Compatible Cell Type-Specific Gene-Inducible System for Plants. *Plant physiology,* 170**,** 627-641.

SINAPIDOU, E., WILLIAMS, K., NOTT, L., BAHKT, S., TOR, M., CRUTE, I., BITTNER-EDDY, P. & BEYNON, J. 2004. Two TIR:NB:LRR genes are required to specify resistance to Peronospora parasitica isolate Cala2 in Arabidopsis. *Plant J,* 38**,** 898-909.

SOHN, K. H., HUGHES, R. K., PIQUEREZ, S. J., JONES, J. D. & BANFIELD, M. J. 2012. Distinct regions of the Pseudomonas syringae coiled-coil effector AvrRps4 are required for activation of immunity. *Proc Natl Acad Sci U S A,* 109**,** 16371-6.

SOHN, K. H., SEGONZAC, C., RALLAPALLI, G., SARRIS, P. F., WOO, J. Y., WILLIAMS, S. J., NEWMAN, T. E., PAEK, K. H., KOBE, B. & JONES, J. D. G. 2014. The Nuclear Immune Receptor RPS4 Is Required for RRS1SLH1-Dependent Constitutive Defense Activation in Arabidopsis thaliana. *PLOS Genetics,* 10**,** e1004655.

STEELE, J. F. C., HUGHES, R. K. & BANFIELD, M. J. 2019. Structural and biochemical studies of an NB-ARC domain from a plant NLR immune receptor. *bioRxiv***,** 557280.

STUTTMANN, J., PEINE, N., GARCIA, A. V., WAGNER, C., CHOUDHURY, S. R., WANG, Y., JAMES, G. V., GRIEBEL, T., ALCÁZAR, R., TSUDA, K., SCHNEEBERGER, K. & PARKER, J. E. 2016. Arabidopsis thaliana DM2h (R8) within the Landsberg RPP1-like Resistance Locus Underlies Three Different Cases of EDS1-Conditioned Autoimmunity. *PLOS Genetics,* 12**,** e1005990.

SU, L., QUADE, B., WANG, H., SUN, L., WANG, X. & RIZO, J. 2014. A plug release mechanism for membrane permeation by MLKL. *Structure,* 22**,** 1489-500.

SUNG, D. Y., VIERLING, E. & GUY, C. L. 2001. Comprehensive expression profile analysis of the Arabidopsis Hsp70 gene family. *Plant physiology,* 126**,** 789-800.

SWIDERSKI, M. R., BIRKER, D. & JONES, J. D. G. 2009. The TIR Domain of TIR-NB-LRR Resistance Proteins Is a Signaling Domain Involved in Cell Death Induction. *Molecular Plant-Microbe Interactions®,* 22**,** 157-165.

SZECHYNSKA-HEBDA, M., CZARNOCKA, W., HEBDA, M., BERNACKI, M. J. & KARPINSKI, S. 2016. PAD4, LSD1 and EDS1 regulate drought tolerance, plant biomass production, and cell wall properties. *Plant Cell Rep,* 35**,** 527-39.

TAKAHASHI, A., CASAIS, C., ICHIMURA, K. & SHIRASU, K. 2003. HSP90 interacts with RAR1 and SGT1 and is essential for RPS2-mediated disease resistance in Arabidopsis. *Proc Natl Acad Sci U S A,* 100**,** 11777-82.

TAKKEN, F. L. W. & TAMELING, W. I. L. 2009. To Nibble at Plant Resistance Proteins. *Science,* 324**,** 744.

TAMBORSKI, J. & KRASILEVA, K. V. 2020. Evolution of Plant NLRs: From Natural History to Precise Modifications. *Annual Review of Plant Biology,* 71**,** 355-378.

TAMELING, W. I. L., VOSSEN, J. H., ALBRECHT, M., LENGAUER, T., BERDEN, J. A., HARING, M. A., CORNELISSEN, B. J. C. & TAKKEN, F. L. W. 2006. Mutations in the NB-ARC domain of I-2 that impair ATP hydrolysis cause autoactivation. *Plant Physiol,* 140.

TANG, D., WANG, G. & ZHOU, J.-M. 2017. Receptor Kinases in Plant-Pathogen Interactions: More Than Pattern Recognition. *The Plant Cell,* 29**,** 618.

TENTHOREY, J. L., HALOUPEK, N., LÓPEZ-BLANCO, J. R., GROB, P., ADAMSON, E., HARTENIAN, E., LIND, N. A., BOURGEOIS, N. M., CHACÓN, P., NOGALES, E. & VANCE, R. E. 2017. The structural basis of flagellin detection by NAIP5: A strategy to limit pathogen immune evasion. *Science,* 358**,** 888.

THOMAS, W. J., THIREAULT, C. A., KIMBREL, J. A. & CHANG, J. H. 2009. Recombineering and stable integration of the Pseudomonas syringae pv. syringae 61 hrp/hrc cluster into the genome of the soil bacterium Pseudomonas fluorescens Pf0-1. *Plant J,* 60**,** 919-28.

TORNERO, P., CHAO, R. A., LUTHIN, W. N., GOFF, S. A. & DANGL, J. L. 2002. Large-Scale Structure –Function Analysis of the Arabidopsis RPM1 Disease Resistance Protein. *The Plant Cell,* 14**,** 435-450.

TRAN, D. T. N., CHUNG, E. H., HABRING-MULLER, A., DEMAR, M., SCHWAB, R., DANGL, J. L., WEIGEL, D. & CHAE, E. 2017. Activation of a Plant NLR Complex through Heteromeric Association with an Autoimmune Risk Variant of Another NLR. *Curr Biol,* 27**,** 1148-1160.

UEHLING, J., DEVEAU, A. & PAOLETTI, M. 2017. Do fungi have an innate immune response? An NLR-based comparison to plant and animal immune systems. *PLOS Pathogens,* 13**,** e1006578.

URBACH, J. M. & AUSUBEL, F. M. 2017. The NBS-LRR architectures of plant R-proteins and metazoan NLRs evolved in independent events. *Proceedings of the National Academy of Sciences of the United States of America,* 114**,** 1063-1068.

VAN DE WEYER, A. L., MONTEIRO, F., FURZER, O. J., NISHIMURA, M. T., CEVIK, V., WITEK, K., JONES, J. D. G., DANGL, J. L., WEIGEL, D. & BEMM, F. 2019. A Species-Wide Inventory of NLR Genes and Alleles in Arabidopsis thaliana. *Cell,* 178**,** 1260-1272.e14.

VAN DER BIEZEN, E. A. & JONES, J. D. 1998. The NB-ARC domain: a novel signalling motif shared by plant resistance gene products and regulators of cell death in animals. *Current Biology: CB,* 8**,** R226-R227.

VAN DER BURGH, A. M. & JOOSTEN, M. H. A. J. 2019. Plant Immunity: Thinking Outside and Inside the Box. *Trends in Plant Science,* 24**,** 587-601.

VAN DER HOORN, R. A. & KAMOUN, S. 2008. From Guard to Decoy: a new model for perception of plant pathogen effectors. *Plant Cell,* 20**,** 2009-17.

VENUGOPAL, S. C., JEONG, R. D., MANDAL, M. K., ZHU, S., CHANDRA-SHEKARA, A. C., XIA, Y., HERSH, M., STROMBERG, A. J., NAVARRE, D., KACHROO, A. & KACHROO, P. 2009. Enhanced disease susceptibility 1 and salicylic acid act redundantly to regulate resistance gene-mediated signaling. *PLoS Genet,* 5**,** e1000545.

VOSS, M., TOELZER, C., BHANDARI, D. D., PARKER, J. E. & NIEFIND, K. 2019. Arabidopsis immunity regulator EDS1 in a PAD4/SAG101-unbound form is a monomer with an inherently inactive conformation. *J Struct Biol,* 208**,** 107390.

WAGNER, S., STUTTMANN, J., RIETZ, S., GUEROIS, R., BRUNSTEIN, E., BAUTOR, J., NIEFIND, K. & PARKER, J. E. 2013. Structural basis for signaling by exclusive EDS1 heteromeric complexes with SAG101 or PAD4 in plant innate immunity. *Cell Host Microbe,* 14**,** 619-30.

WAN, L., ESSUMAN, K., ANDERSON, R. G., SASAKI, Y., MONTEIRO, F., CHUNG, E. H., OSBORNE NISHIMURA, E., DIANTONIO, A., MILBRANDT, J., DANGL, J. L. & NISHIMURA, M. T. 2019. TIR domains of plant immune receptors are NAD(+)-cleaving enzymes that promote cell death. *Science,* 365**,** 799-803.

WANG, D., ZHANG, L., HU, J., GAO, D., LIU, X. & SHA, Y. 2018. Comparative genomic analysis of the Lipase3 gene family in five plant species reveals distinct evolutionary origins. *Genetica,* 146**,** 179-185.

WANG, H., SUN, L., SU, L., RIZO, J., LIU, L., WANG, L. F., WANG, F. S. & WANG, X. 2014. Mixed lineage kinase domain-like protein MLKL causes necrotic membrane disruption upon phosphorylation by RIP3. *Mol Cell,* 54**,** 133-146.

WANG, J., HU, M., WANG, J., QI, J., HAN, Z., WANG, G., QI, Y., WANG, H. W., ZHOU, J. M. & CHAI, J. 2019a. Reconstitution and structure of a plant NLR resistosome conferring immunity. *Science,* 364**,** eaav5870.

WANG, J., WANG, J., HU, M., WU, S., QI, J., WANG, G., HAN, Z., QI, Y., GAO, N., WANG, H. W., ZHOU, J. M. & CHAI, J. 2019b. Ligand-triggered allosteric ADP release primes a plant NLR complex. *Science,* 364**,** eaav5868.

WANG, W., WEN, Y., BERKEY, R. & XIAO, S. 2009. Specific targeting of the Arabidopsis resistance protein RPW8.2 to the interfacial membrane encasing the fungal Haustorium renders broad-spectrum resistance to powdery mildew. *Plant Cell,* 21**,** 2898-913.

WHITHAM, S., DINESH-KUMAR, S. P., CHOI, D., HEHL, R., CORR, C. & BAKER, B. 1994. The product of the tobacco mosaic virus resistance gene N: similarity to toll and the interleukin-1 receptor. *Cell,* 78**,** 1101-15.

WIERMER, M., FEYS, B. J. & PARKER, J. E. 2005. Plant immunity: the EDS1 regulatory node. *Curr Opin Plant Biol,* 8**,** 383-9.

WILLIAMS, S. J., SOHN, K. H., WAN, L., BERNOUX, M., SARRIS, P. F., SEGONZAC, C., VE, T., MA, Y., SAUCET, S. B., ERICSSON, D. J., CASEY, L. W., LONHIENNE, T., WINZOR, D. J., ZHANG, X., COERDT, A., PARKER, J. E., DODDS, P. N., KOBE, B. &

JONES, J. D. 2014. Structural basis for assembly and function of a heterodimeric plant immune receptor. *Science,* 344**,** 299-303.

WILLIAMS, S. J., SORNARAJ, P., DECOURCY-IRELAND, E., MENZ, R. I., KOBE, B., ELLIS, J. G., DODDS, P. N. & ANDERSON, P. A. 2011. An autoactive mutant of the M flax rust resistance protein has a preference for binding ATP, whereas wild-type M protein binds ADP. *Mol Plant Microbe Interact,* 24**,** 897-906.

WRÓBLEWSKI, T., SPIRIDON, L., MARTIN, E. C., PETRESCU, A.-J., CAVANAUGH, K., TRUCO, M. J., XU, H., GOZDOWSKI, D., PAWŁOWSKI, K., MICHELMORE, R. W. & TAKKEN, F. L. W. 2018. Genome-wide functional analyses of plant coiled–coil NLR-type pathogen receptors reveal essential roles of their N-terminal domain in oligomerization, networking, and immunity. *PLOS Biology,* 16**,** e2005821.

WU, C.-H., ABD-EL-HALIEM, A., BOZKURT, T. O., BELHAJ, K., TERAUCHI, R., VOSSEN, J. H. & KAMOUN, S. 2017. NLR network mediates immunity to diverse plant pathogens. *Proceedings of the National Academy of Sciences,* 114**,** 8113-8118.

WU, C.-H., BELHAJ, K., BOZKURT, T. O., BIRK, M. S. & KAMOUN, S. 2016. Helper NLR proteins NRC2a/b and NRC3 but not NRC1 are required for Pto-mediated cell death and resistance in Nicotiana benthamiana. *New Phytologist,* 209**,** 1344-1352.

WU, M. & LANDER, G. C. 2020. How low can we go? Structure determination of small biological complexes using single-particle cryo-EM. *Curr Opin Struct Biol,* 64**,** 9-16.

WU, Z., LI, M., DONG, O. X., XIA, S., LIANG, W., BAO, Y., WASTENEYS, G. & LI, X. 2019. Differential regulation of TNL-mediated immune signaling by redundant helper CNLs. *New Phytol,* 222**,** 938-953.

XIAO, S., CALIS, O., PATRICK, E., ZHANG, G., CHAROENWATTANA, P., MUSKETT, P., PARKER, J. E. & TURNER, J. G. 2005. The atypical resistance gene, RPW8, recruits components of basal defence for powdery mildew resistance in Arabidopsis. *Plant J,* 42**,** 95-110.

XIAO, S., ELLWOOD, S., CALIS, O., PATRICK, E., LI, T., COLEMAN, M. & TURNER, J. G. 2001. Broad-spectrum mildew resistance in Arabidopsis thaliana mediated by RPW8. *Science,* 291**,** 118-20.

XIAO, S., EMERSON, B., RATANASUT, K., PATRICK, E., O'NEILL, C., BANCROFT, I. & TURNER, J. G. 2004. Origin and Maintenance of a Broad-Spectrum Disease Resistance Locus in Arabidopsis. *Molecular Biology and Evolution,* 21**,** 1661-1672.

XU, F., ZHU, C., CEVIK, V., JOHNSON, K., LIU, Y., SOHN, K., JONES, J. D., HOLUB, E. B. & LI, X. 2015. Autoimmunity conferred by chs3-2D relies on CSA1, its adjacent TNL-encoding neighbour. *Sci Rep,* 5**,** 8792.

YANG, Z., WANG, C., ZHOU, Q., AN, J., HILDEBRANDT, E., ALEKSANDROV, L. A., KAPPES, J. C., DELUCAS, L. J., RIORDAN, J. R., URBATSCH, I. L., HUNT, J. F. & BROUILLETTE, C. G. 2014. Membrane protein stability can be compromised by detergent interactions with the extramembranous soluble domains. *Protein Sci,* 23**,** 769-89.

YUAN, M., JIANG, Z., BI, G., NOMURA, K., LIU, M., HE, S. Y., ZHOU, J.-M. & XIN, X.-F. 2020. Pattern-recognition receptors are required for NLR-mediated plant immunity. *bioRxiv***,** 2020.04.10.031294.

YUAN, S. & AKEY, C. W. 2013. Apoptosome structure, assembly, and procaspase activation. *Structure,* 21**,** 501-15.

ZACHARIAS, D. A., VIOLIN, J. D., NEWTON, A. C. & TSIEN, R. Y. 2002. Partitioning of lipid-modified monomeric GFPs into membrane microdomains of live cells. *Science,* 296**,** 913-6.

ZHANG, L., CHEN, S., RUAN, J., WU, J., TONG, A. B., YIN, Q., LI, Y., DAVID, L., LU, A., WANG, W. L., MARKS, C., OUYANG, Q., ZHANG, X., MAO, Y. & WU, H. 2015a. Cryo-EM structure of the activated NAIP2-NLRC4 inflammasome reveals nucleated polymerization. *Science,* 350**,** 404-9.

ZHANG, M., KADOTA, Y., PRODROMOU, C., SHIRASU, K. & PEARL, L. H. 2010. Structural Basis for Assembly of Hsp90-Sgt1-CHORD Protein Complexes: Implications for Chaperoning of NLR Innate Immunity Receptors. *Molecular Cell,* 39**,** 269-281.

ZHANG, Q., BERKEY, R., PAN, Z., WANG, W., ZHANG, Y., MA, X., KING, H. & XIAO, S. 2015b. Dominant negative RPW8.2 fusion proteins reveal the importance of haustorium-oriented protein trafficking for resistance against powdery mildew in Arabidopsis. *Plant Signal Behav,* 10**,** e989766.

ZHANG, X., BERNOUX, M., BENTHAM, A. R., NEWMAN, T. E., VE, T., CASEY, L. W., RAAYMAKERS, T. M., HU, J., CROLL, T. I., SCHREIBER, K. J., STASKAWICZ, B. J., ANDERSON, P. A., SOHN, K. H., WILLIAMS, S. J., DODDS, P. N. & KOBE, B. 2017. Multiple functional self-association interfaces in plant TIR domains. *Proceedings of the National Academy of Sciences*.

ZHANG, Y., DOREY, S., SWIDERSKI, M. & JONES, J. D. 2004. Expression of RPS4 in tobacco induces an AvrRps4-independent HR that requires EDS1, SGT1 and HSP90. *Plant J,* 40**,** 213-24.

ZHOU, J. M. & ZHANG, Y. 2020. Plant Immunity: Danger Perception and Signaling. *Cell,* 181**,** 978-989.

ZHOU, N., TOOTLE, T. L., TSUI, F., KLESSIG, D. F. & GLAZEBROOK, J. 1998. PAD4 functions upstream from salicylic acid to control defense responses in Arabidopsis. *Plant Cell,* 10**,** 1021-30.

ZHU, S., JEONG, R.-D., VENUGOPAL, S. C., LAPCHYK, L., NAVARRE, D., KACHROO, A. & KACHROO, P. 2011. SAG101 Forms a Ternary Complex with EDS1 and PAD4 and Is Required for Resistance Signaling against Turnip Crinkle Virus. *PLOS Pathogens,* 7**,** e1002318.

ZUO, J., NIU, Q. & CHUA, N. 2000. An estrogen receptor -based transactivator XVE mediates highly inducible gene expression in transgenic plants. *Plant J,* 24.

Appendices

Appendix I Sequences for synthetic EDS1 promoter and terminators

pEDS1-domestication-synthetic

BbsI
Overhangs
terminator
Mutations (all C>T)

ggGAAGACttGGAG**ATTTTAAGCGTTGGTTGGAACACTTTACATGGCTTTTCGTAGAAATTTCCCCAA**
GTTGGGTTTTATTAAGACCAAGAAAATTCTAGTCTCCTAGACTTTTTTTTGTTTCTTTTGTTAATTTA
GTCTCCTAGGCTTTTTCATTCTATCTGAAAGCAAAATATGGTTATGCAATTTGGTTTAGCCAAAAAAA
CAAACTAAATTTTTCTAGTCCGGTTCATGTAACTTCATAATCAAACAAGTAAAAGTCGAATGTGACGC
GTCTTGCCGAACGCAAAAACGGACCAGGCAAGAAGGTGTAGTTAGTTAATTCGGTTAATATTCAGCTG
AGAGAAATCGAACCGGTTCCATATCTTGTAGATTATCCGGTTTACTTTCCGGATAAGATTTATAAGCA
AAACAGAGTTAAAGTAGTAGATTTCTTCTATACGAGACT**AAATCTGAAAACCCAAGTCAAGCTACAA**A
AACTTAACTCCAAGCGAACAAATCTCCTCATTCATTAAACAACAAAATTGTTTTCCGACAAAAAAGTG
AATATCATTGAGTTACTGCGAAATCCCAACCGAGAGTGACATCTCAAACCAAAAGATGGAGTCTATAT
TAAAGAGACGAAGATTCCAAAGTCAAGCTACAAAATTTCCAAGCAAAGATTACACAGAGAAAACTTTC
CGACCAAATGTGAATGTTTATGAAAGTTTCTGCGAAACTCCAGTCATGTCGGATGTACAAAGCCATAC
ACCAATGTAAAACCGACACGTGGAAAGCTAAGATTCCTAGCTTTTCTTTCTTCATGAGTCTCCAATAG
CCAAAGAGTCAACTCCAAAAAAAAACCCATTTTTGCATTGAAATAGTCTCATGATGGGGTATTTTGGG
TAACTAATTAGTCCTGTCTACATCTTCCCATAAATTAACAGAGTAGGAGCGGATTAAAGAAGCAAGAC
GATTCAAAAGAAAAAAGAGAGAAGAAAGTCCACTAAAGAAAAGAGAATAGATATAGATCAAATGaaGT
CTTCCcc

EDS1ter-domestication-synthetic

BbsI
Overhangs
BsaI
mutation
terminator

ggGAAGACttGCTTACCTTAGGTGGTGGAGTATTTAAGCTATTAGAACACTTGCTTCTCTTAATTTGT
GCAATAAGAAATGTTTATCAATCTGGTTTCCACTTCATGATGATCTTAGAATAAGAAACATGTTGTAT
GATCATTGTGAAGTAATGTAATAGCTCTCTATTCTAATGTCAAATTTGGTTTCCACTTTACAGTGATC
TTAGAATATATACGTTACTCTACTAAAGCCTAAAGCCATCTCAAATAGCATGAACCAGTAACAAACAA
CCTTCCTTAGATTGAAATGGTCTTATGATGGGGTATTTTGGGTAATTACTCCTGTCTACATCTTCCTA
CTATATTAACAGAGTAGGAGGACTAACGCTaaGTCTTCcc

Appendix II Design details for JFJJ constructs

ID	BB	P1	P2	P3	P4	P5	P6	P7
JFJJ14	pICH47732	pICH51266	pICSL80016	pICSL50010	pICH41432			
JFJJ19	pICH47732	pICH51277	BCJJ292A	pICSL50010	pICH41414			
JFJJ25	L1 01005	frag 1	frag 2	frag 3	frag 4			
JFJJ26	pICSL01005	pJFJJ25A						
JFJJ27	pICH47751	JFJJ34	pICSL80080	pICSL50004	pICSL60008			
JFJJ29	pICH47751	JFJJ34	pICSL80080	pICSL50044	pICSL60008			
JFJJ34	pICH41295	JFJJ33_pSAG101-L1_inv						
JFJJ36	pICH41295	pEDS1_GGAG-AATG						
JFJJ37	pICH41276	EDS1ter_GCTT-CGCT						
JFJJ38	pICH47751	JFJJ34	pICSL80080	pICSL50009	pICSL60008			
JFJJ42	pICSL01005	HopQ1 BpiI pcr prod						
JFJJ43	pICSL12005	JFJJ42	pICSL50010	pICH41432	pICH47772			
JFJJ45	pICSL4723	pICH54011	pICH54022	JFJJ70	JFJJ38	JFJJ43	pICSL11153	pICH41822
JFJJ55	pICSL86977OD	BCJJ292	pICSL50012					
JFJJ70	pICH47751	LBJJ5	pICSL50009	pICSL60008				
JFJJ72	pICH41295	JFJJ32_pNRG1B-L1_inv						
JFJJ79	pICH41276	NRG1Bter pcr product						
JFJJ125	pICSL4723	pICH54011	JFJJ64	JFJJ27	pICH41766			

Appendix III Optimized large-scale purification protocol

Purification of NLR-FLAG from *Nicotiana benthamiana* leaves by anti-FLAG IP

Buffers required

All buffers should be made fresh before use (maximum 2 days beforehand). Buffers must also be filtered and degassed.

GHMN buffer (500 mL):
10 % Glycerol (50 mL)
100 mM HEPES (pH 7.5) (50mL of 1M)
300 mM NaCl (30 mL of 5M)
5 mM $MgCl_2$ (2.5 mL of 1M)
0.5 % Nonidet-P40 (2.5 mL)

Extraction buffer (100 mL):
GHMN buffer (100 mL)
2 % Polyvinylpolypyrrolidone (PVPP) (2g)
cOmplete™, EDTA-free Protease Inhibitor Cocktail (2 tablets)
10mM DTT (added fresh) (1 mL 1M)

IP buffer:
GHMN buffer

Elution buffer: (80 uL aliquots of 5 mg/mL 3XFLAG peptide)
GHMN buffer
30 uL in 1 mL = 150 ng/µl peptide for 30min
50 uL in 1 mL = 250 ng/µl peptide overnight

Gel Filtration buffer (1 L):
10 mM HEPES pH 7.5 (2.38 g)
150 mM NaCl (8.77 g)
5 mM $MgCl_2$ (1.02 g)
5 % Glycerol (50 mL)
1 mM DTT (1 mL 1M)

PROTEIN ISOLATION

1. Grind tissue in LN_2; separate into ~22.5 mL aliquots in 50 mL falcon etubes; add 24 mL extraction buffer.

2. Incubate 15 min rolling in cold room

3. Spin 4000 RPM for 35min at 4°C

4. Filter supernatant through Miracloth and collect into a cold beaker. Sample 60 µL (Total Protein sample [TP]).

5. Split protein solution into 40-mL ultra-centrifuge tubes (compatible ones with A27-8x50 rotor). Centrifuge at 50,000 x g at 4°C for 90 min (LYNX ultracentrifuge, A27-8x50 rotor).

6. Collect supernatant into a cold beaker. Sample 60 µl (Clarified Lysate sampe [L]).

ANTI-FLAG IMMUNOPRECIPITATION

Equilibrating the resin

1. Pipette anti-FLAG resin with a 1 mL cut tip into 50 mL falcon tube for equilibration with IP buffer. After pipetting the required amount of beads, add 45 mL of IP buffer and incubate at 4°C with gentle inversion for ~60 minutes (start during lysate centrifugation steps).

(Use 1 mL bead resin total for each planned binding step.)

2. Centrifuge the falcon tube with resin at 800 x g for 5 minutes at 4°C to pellet beads, and remove the supernatant. Resuspend the beads in IP buffer with the original volume of resin (ie 1 mL resin = 1 mL IP buffer) to produced a 50 % buffer:resin slurry.

Binding of protein to the resin and washing

3. Add 500 µl of the equilibrated resin to each 50 mL tube; add 45 mL of protein solution to resin. Incubate at 4 °C for 30 min - 1 h with gentle inversion or rotation.

First binding step 30 minutes, following steps can be 1 h.

4. Centrifuge at 800 x g for 5 minutes at 4°C. Collect the supernatant of all tubes in a beaker without disturbing the pellet. Sample 60 µl (Supernatant samples [S1], [S2]…).

5. Gently resuspend each of the pellets in 1 mL of IP Buffer and combine the resin from all of the falcon tubes into one.

6. Top-up the falcon tube to 45 mL with IP buffer and mix by gentle inversion for 5 minutes at 4°C to wash the beads. Centrifuge at 800 x g for 5 minutes at 4°C. Sample 60 µL (Wash sample [W]). Discard wash supernatant without disturbing the pellet, resuspend in 45 mL of IP. Repeat the wash step a further 2 times for a total of 3 washes.

Binding 1	*Binding 2*
Wash 1	*Wash 1*
Wash 2	*Wash 2*
Wash 3	*Wash 3*

7. Add fresh 500 µL FLAG resin to the supernatant. Repeat steps 3-6. Repeat again for 2 total binding incubations. (S*tart during the previous washing steps)*

Elution of protein from the resin

8. Centrifuge falcon tubes containing resin with bound & washed protein at 800 x g for 5 minutes at 4°C. Discard supernatant without disturbing the pellet. Gently resuspend the pellet

in 1 mL of IP buffer and transfer to a 1.5 mL eppendorf. (*you can spin again and remove extra supernatant, and top-up to 1 mL mark)*

9. Add 30 µL of 5 mg/mL 3XFLAG peptide per mL of resin/IP buffer slurry (final concentration of 150 ng/µL 3XFLAG peptide). Incubate at 4°C 30 min under gentle inversion.

9a. centrifuge at 800 x g at 4°C for 1 min

9b. transfer supernatant (~ 500 uL) to lobind 1.5 mL eppendorf, through chilled spin column; do not remove beads as another elution step required

9c. Sample 20 µl (Elution sample [Ex]).

9d. add fresh IP buffer to 1mL line

10. Add 50 µL of 5 mg/mL 3XFLAG peptide per mL of resin/IP buffer slurry (final concentration of 250 ng/µL 3XFLAG peptide). Incubate at 4°C overnight under gentle inversion.

- NEXT DAY -

12. Transfer overnight eluate to chilled spin column (sigmaprep spin column SC1000-1KT) and centrifuge at 800 x g at 4°C for 30 seconds. Sample 20 µl (Elution sample [Ex]).

12b. Combine eluates into a new 15 mL faclon tube. Sample 20 µl (Elution Combined sample [EC]).

12c. immediately proceed with bead regeneration (next page)

CONCENTRATION AND ULTRAFILTRATION OF PROTEIN (50 kDa MWCO)

(Prepared first day)

1. Prepare 4 mL Merck and 0.5 mL Sartorious concentrators membranes for overnight incubation at room temperature

11a. Wash the concentrators once with dH_2O, spin the liquid through according to the respective protocol.

11b. Remove residual dH_2O thoroughly by pipetting. (Take care not to damage the membrane with the pipette tip.)

11c. Fill concentrators with dH_2O

11d. Incubate the filled concentrators at room temperature overnight (or for at least 2 hours)

11e. Pour out dH_2O

11f. Rinse the device with dH_2O and finally spin through

- NEXT DAY -

2. Dilute protein solution up to 10 mL* with GF buffer. Transfer 4 mL to water-equilibrated 4 mL Merck concentrator. Centrifuge 4000 x g (swing bucket) in 4-12 minute sessions at 4°C, mixing via pipetting between spins. Sample 20 µl when all the protein has been concentrated down to a volume of ~500 µL (Ultrafiltration sample [UF1]).

1b. Transfer to 0.5 mL concentrator to concentrate down from ~500 uL to ~200 uL.

1c. Sample 20 µl when ~200 uL (Ultrafiltration sample [UF2]).

10 mL is important because this dilutes ~ 2 mL of eluates at 0.5% NIDP40 to10 mL at 0.1% NIDP40 which helps maintain protein stability throughout ultracentrifugation

2. Transfer protein to a low-bind 1.5 mL eppendorf with gel loading pipette tip.
For subsequent use, store the concentrator at 4°C in enough dH_2O to cover membrane.

3. Centrifuge protein at 15,000 x g for 5 minutes at 4°C to pellet protein aggregates. Load 200 µl supernatant in Hamilton syringe for Gel Filtration injection. Save ~5 µL for Loading Control sample (LC).

Proceed with Gel Filtration.

After gel filtration, concentrate with 0.5 mL Sartorious concentrator pre-equilibrated with water as described above. ***May need to add detergent to 0.1 - 0.5% to avoid protein losses***

FLAG BEAD/RESIN REGENERATION

1. Resuspend the beads remaining the spin column in ~500 µL of 0.2 M Tris-Glycine pH 3.5 (10X TG lab stock) and transfer to 50 mL falcon tube. Continue to flush spin column with Tris-Glycine until all the beads have been recovered. Do this for all spin columns used, transferring the beads all to the same falcon tube.

2. After transferring all the beads to the faclon tube, fill the falcon tube with Tris-Glycine to the 45 mL mark and incubate at 4°C with rotations for 20 mins.

3. Pellet the beads by centrifuging at 800 x g for 5 min at 4°C. Carefully remove the supernatant, and resuspend the beads in 45 mL of TBS to wash out Tris-Glycine. Incubate rotating for 5 min at 4°C, and pellet beads by centrifuging at 800 x g for 5 min at 4°C. Repeat 3 times, or until confident the Tris-Glycine has been removed.

4. Resuspend the beads in equal w/v of TBS + 50% glycerol. These beads can now be stored at -20°C to be used again.

Appendix IV Expanded pool count summary

Count	Pool	Number of seedlings insensitive to β-estradiol	Number of seedlings positive for mNeon in roots	Number of seedlings negative for mNeon in roots
1	369	4	3	1
2	366	15	1	14
3	365	5	3	2
4	364	2	2	0
5	363	-	-	-
6	362	10	2	8
7	361	8	1	7
8	360	8	4	4
9	358	17	3	14
10	357	9	3	6
11	356	10	6	4
12	355	4	1	3
13	354	8	1	7
14	353	4	0	4
15	352	1	0	1
16	351	0	0	0
17	350	3	0	3
18	348	0	0	0
19	347	4	2	2
20	346	1	0	1
21	345	1	1	0
22	344			
23	342	4	0	4
24	341	9	1	8
25	340	10	0	10
26	339	3	3	0
27	338	26	3	23
28	337	6	1	5
29	335	13	5	8
30	334	9	0	9
31	332	30	1	29
32	331	21	4	17
33	329	29	0	29
34	328	5	3	2
35	327	30	3	27
36	326	26	0	26
37	325	6	4	2
38	324	38	5	33
39	322	22	2	20
40	320	7	5	2
41	319	5	0	5
42	318	0	0	0
43	317	1	0	1
44	314	2	0	2
45	313	3	0	3
46	312	2	0	2
47	308	19	1	18
48	306	0	0	0
49	303	8	1	7
50	302	12	0	12
51	301	0	0	0
52	300	26	0	26
53	298	11	0	11
54	398	6	0	6
55	297	7	1	6
56	296	9	3	6
57	295	12	2	10
58	294	1	0	1
59	**1**	0	0	-
60	**2**	4	4	-
61	**3**	3	3	-
62	**4**	1	1	-
63	**6**	1	1	-
64	**9**	1	1	-
65	**11**	2	2	-
66	**12**	0	0	-
67	**13**	0	0	-
68	**14**	0	0	-
69	**15**	0	0	-
70	**17**	0	0	-
71	**18**	0	0	-
72	**19**	0	0	-
73	**20**	0	0	-
74	**21**	0	0	-
75	**22**	0	0	-
76	**23**	1	1	-
77	**24**	0	0	-
78	**25**	0	0	-
79	**27**	0	0	-
80	**28**	0	0	-
81	**30**	0	0	-
82	**31**	0	0	-
83	**32**	2	2	-
84	**33**	0	0	-
85	**34**	1	1	-
86	**37**	0	0	-
87	**39**	1	1	-
88	**45**	1	1	-
89	**47**	0	0	-
90	**49**	1	1	-
91	**50**	1	1	-
92	**52**	1	1	-
93	**53**	1	1	-
94	**54**	2	2	-
95	**55**	2	2	-
96	**56**	0	0	-
97	**57**	0	0	-
98	**60**	0	0	-
99	**61**	0	0	-
100	**65**	0	0	-

101	**67**	2	2	-
102	**69**	1	1	-
103	**71**	0	0	-
104	**72**	0	0	-
105	**73**	0	0	-
106	**75**	1	1	-
107	**76**	0	0	-
108	**77**	0	0	-
109	**79**	0	0	-
110	**80**	0	0	-
111	**81**	0	0	-
112	**82**	0	0	-
113	**84**	0	0	-
114	**85**	1	1	-
115	**90**	1	1	-
116	**91**	0	0	-
117	**92**	0	0	-
118	**97**	0	0	-
119	**100**	0	0	-
120	**101**	0	0	-
121	**104**	0	0	-
122	**108**	0	0	-
123	**109**	1	1	-
124	**113**	1	1	-
125	**116**	0	0	-
126	**118**	0	0	-
127	**119**	0	0	-
128	**120**	0	0	-
129	**121**	0	0	-
130	**122**	1	1	-
131	**123**	2	2	-
132	**124**	0	0	-
133	**125**	1	1	-
134	**126**	2	2	-
135	**127**	0	0	-
136	**130**	0	0	-
137	**133**	0	0	-
138	**136**	0	0	-
139	**137**	1	1	-
140	**140**	0	0	-
141	**142**	0	0	-
142	**143**	1	1	-
143	**144**	1	1	-
144	**146**	0	0	-
145	**148**	0	0	-
146	**149**	1	1	-
147	**150**	3	3	-
148	**151**	0	0	-
149	**152**	0	0	-
150	**153**	0	0	-
151	**154**	0	0	-
152	**155**	0	0	-
153	**156**	2	2	-
154	**159**	0	0	-
155	**160**	1	1	-
156	**161**	1	1	-
157	**162**	0	0	-
158	**163**	0	0	-
159	**164**	0	0	-
160	**165**	0	0	-
161	**171**	0	0	-
162	**172**	0	0	-
163	**173**	1	1	-
164	**174**	0	0	-
165	**175**	1	1	-
166	**176**	0	0	-
167	**177**	2	2	-
168	**178**	0	0	-
169	**179**	0	0	-
170	292	18	3	15
171	290	25	1	24
172	289	34	0	34
173	288	13	0	13
174	286	23	4	19
175	283	9	2	7
176	281	5	2	3
177	280	5	0	5
178	279	14	3	11
179	277	3	1	2
180	276	1	0	1
181	275	7	2	5
182	274	9	3	6
183	272	28	1	27
184	270	32	3	29
185	269	7	3	4
186	58	10	1	9
187	282	18	0	18
188	102	8	0	8
189	211	18	2	16
190	5	10	0	10
191	43	47	2	45
192	62	18	1	17
193	99	18	4	14
194	36	18	3	15
195	169	20	1	19
196	147	31	0	31
197	63	19	2	17
198	64	15	1	14
199	70	5	2	3
200	196	8	1	7
201	198	9	2	7
202	231	1	0	1
203	238	8	2	6
204	250	11	0	11
205	370	15	0	15
206	382	26	1	25
207	383	22	0	22
208	384	19	8	11
209	399	11	3	8
210	381	11	0	11

211	379	40	0	40
212	377	17	4	13
213	309	7	3	4
214	78	8	2	6
215	46	16	2	14
216	41	12	0	12
217	284	14	0	14
218	38	19	4	15
219	103	22	5	17
220	359	19	2	17
221	343	13	1	12
222	310			
223	16	25	2	23
224	51	9	2	7
225	191	29	3	26
226	220			
227	233	6	3	3
228	263	3	0	3
229	271	4	0	4
230	316	2	0	2
231	321	5	1	4
232	336	5	1	4
233	374	4	0	4
234	380	4	0	4
235	392	2	0	2
236	311	9	0	9
237	106	5	2	3
238	170	19	2	17
239	35	5	0	5
240	44	10	0	10
241	157	4	0	4
242	393	9	2	7
243	115	3	0	3
244	389	9	4	5
245	299	8	5	3
246	267	4	3	1
247	395	6	0	6
248	397	4	1	3
249	10	14	1	13
250	29	11	1	10
251	74	4	1	3
252	83	5	2	3
253	93	15	3	12
254	107	5	0	5
255	110	3	2	1
256	129	7	4	3
257	158	17	1	16
258	291	21	0	21
259	307	11	3	8
260	378	0	0	0
261	390	6	2	4
262	385	1	1	0
263	7	0	0	0
264	376	16	0	16
265	375	8	0	8
266	373	13	0	13
267	372	7	2	5
268	371	1	0	1
269	234	0	0	0
270	323	11	2	9
271	68	1	0	1
272	349	4	1	3
273	333	0	0	0
274	66	2	1	1
275	59	3	0	3
276	117	5	0	5
277	387	0	0	0
278	400	0	0	0
279	134	0	0	0
280	367	4	0	4
281	89	1	0	1
282	94	0	0	0
283	285	0	0	0
284	139	4	0	4
285	105	0	0	0
286	128	6	0	6
287	114	0	0	0
288	42	0	0	0
289	111	2	2	0
290	8	2	1	1
291	112	3	1	2
292	138	2	0	2
293	131	3	1	2
294	98			
295	388	5	1	4
296	141	0	0	0
297	88	8	1	7
298	132	4	1	3
299	230	7	1	6
300	40	13	3	10
301	215	2	0	2
302	330	5	2	3
303	391	8	1	7
304	96	12	1	11
305	368	5	1	4
306	396	15	3	12
307	394	4	0	4
308	135	3	1	2
309	287	3	1	2
310	48 (or 13)	11	1	10
311	95	11	4	7
312	386	8	0	8
313	344	22	0	22
314	180	25	1	24
315	182	21	3	18
316	183	7	1	6
317	197	8	0	8
318	199			
319	200			
320	201			

321	202	17	1	16
322	203			
323	204			
324	205			
325	206	13	2	11
326	207	1	0	1
327	208			
328	209			
329	210	2	1	1
330	212	3	1	2
331	213	9	0	9
332	214	15	2	13
333	216	6	2	4
334	217	6	0	6
335	218	8	0	8
336	219	4	0	4

Cells highlighted in dark grey were contaminated and not counted; cells highlighted in dark purple were not counted due to poor seed quality

Pool IDs corresponding to images below for M2 seedling phenotypes

	A	B	C	D	E	F	G	H	I	J	K	L
1	131	8	132	138	281	289	376	349	333	234	299	267
2	111	112	141	230	99	380	372	385	373	7	395	157
3	42	88	36	282	115	35	374	316	220	16	211	270
4	98	40	5	62	397	170	271	233	263	51	269	102
5	388		58	43	106	44	336	321	191	392	169	147
6	276	275	272	283	323	371	41	46	393		381	284
7	277	274	290	292	68	375	78		389	311	377	343
8	279	286	288	280	66		359	310	309	379	103	38

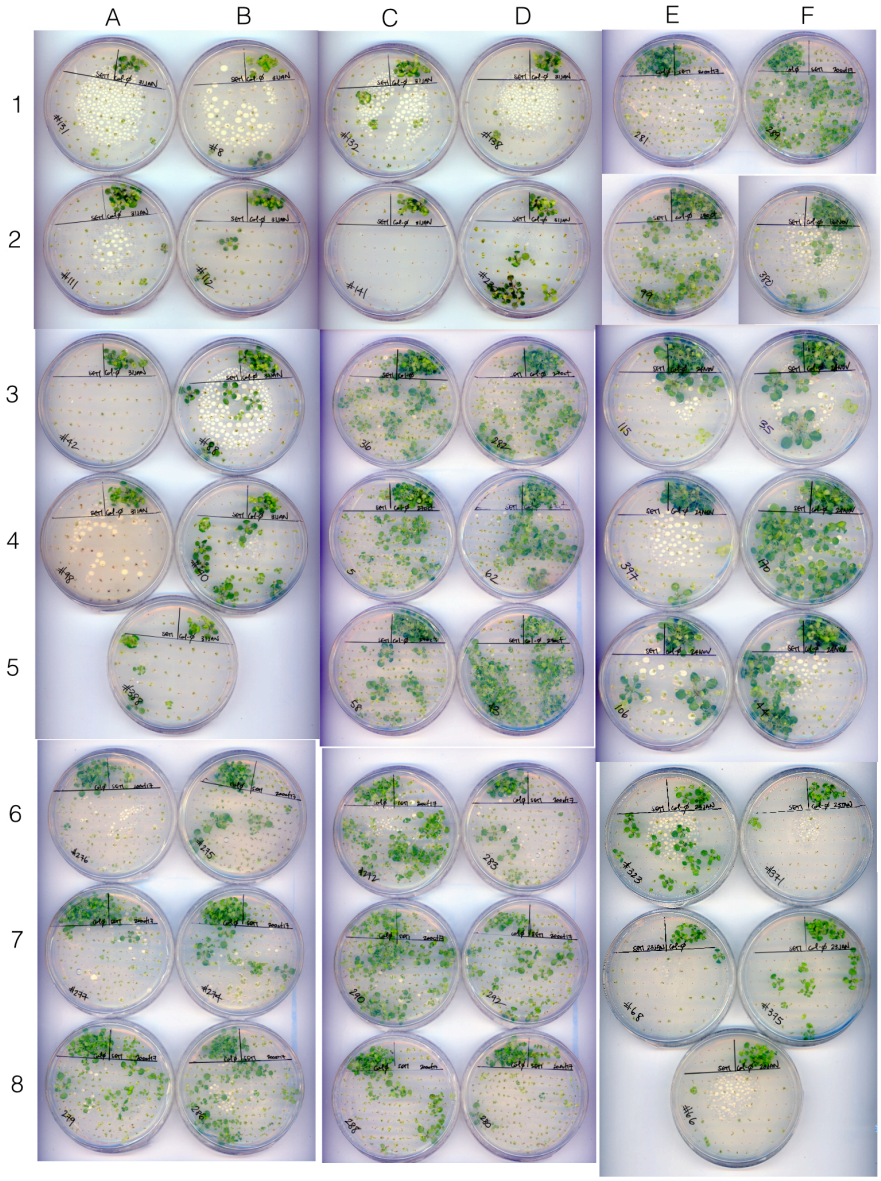

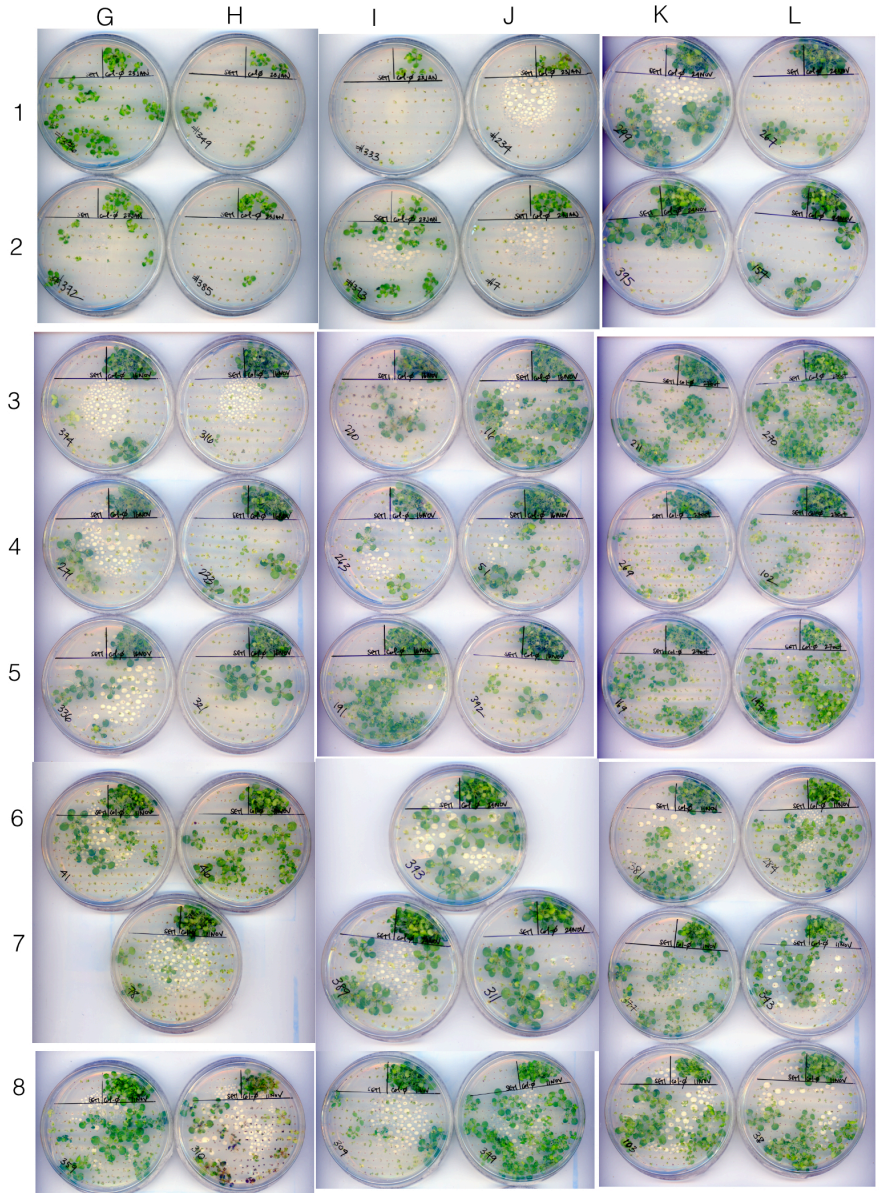
G
H
I
J
K
L
1
2
3
4
5
6
7
8

Appendix V Retention of β-estradiol insensitivity in putants

Putant IDs corresponding to images below for M3 seedling phenotypes

plate/ position	A	B	C	D	E	F	G	H	I	J	K	L
1	SETI	Col-0	325-1	327-1	328-1	331-1	332-1	335-1	337-1	338-1	339-1	345-1
2	SETI	Col-0	354-1	347-1	365-1	366-1	369-1	-	-	-	-	-
3	SETI	Col-0	11-1	34-1	90-1	109-1	113-1	149-1	150-1	156-1	160-1	161-1
4	SETI	Col-0	175-1	177-1	295-1	296-1	297-1	303-1	308-1	320-1	322-1	324-2
5	SETI	Col-0	45-1	46-1	49-1	50-1	51-1	52-1	53-1	54-1	55-1	58-1
6	SETI	Col-0	4-1	10-1	16-1	23-1	29-1	32-1	36-1	38-1	39-1	43-1
7	SETI	Col-0	93-1	99-1	102-1	103-1	106-1	122-1	123-1	125-1	126-1	129-1
8	SETI	Col-0	62-1	63-1	64-1	67-1	69-1	70-1	74-1	75-1	78-1	85-1
9	SETI	Col-0	233-2	238-1	267-1	269-1	270-1	272-1	274-1	275-1	277-1	279-1
10	SETI	Col-0	137-1	143-1	144-1	169-1	170-1	173-1	191-1	196-1	198-1	211-1
11	SETI	Col-0	335-1	336-1	343-1	355-1	356-1	357-1	359-1	364-1	372-1	377-1
12	SETI	Col-0	281-1	283-1	286-1	290-1	292-1	299-1	307-1	309-1	321-1	323-2
13	SETI	Col-0	385-1	382-1	384-1	389-1	390-1	393-1	397-1	399-1	-	-

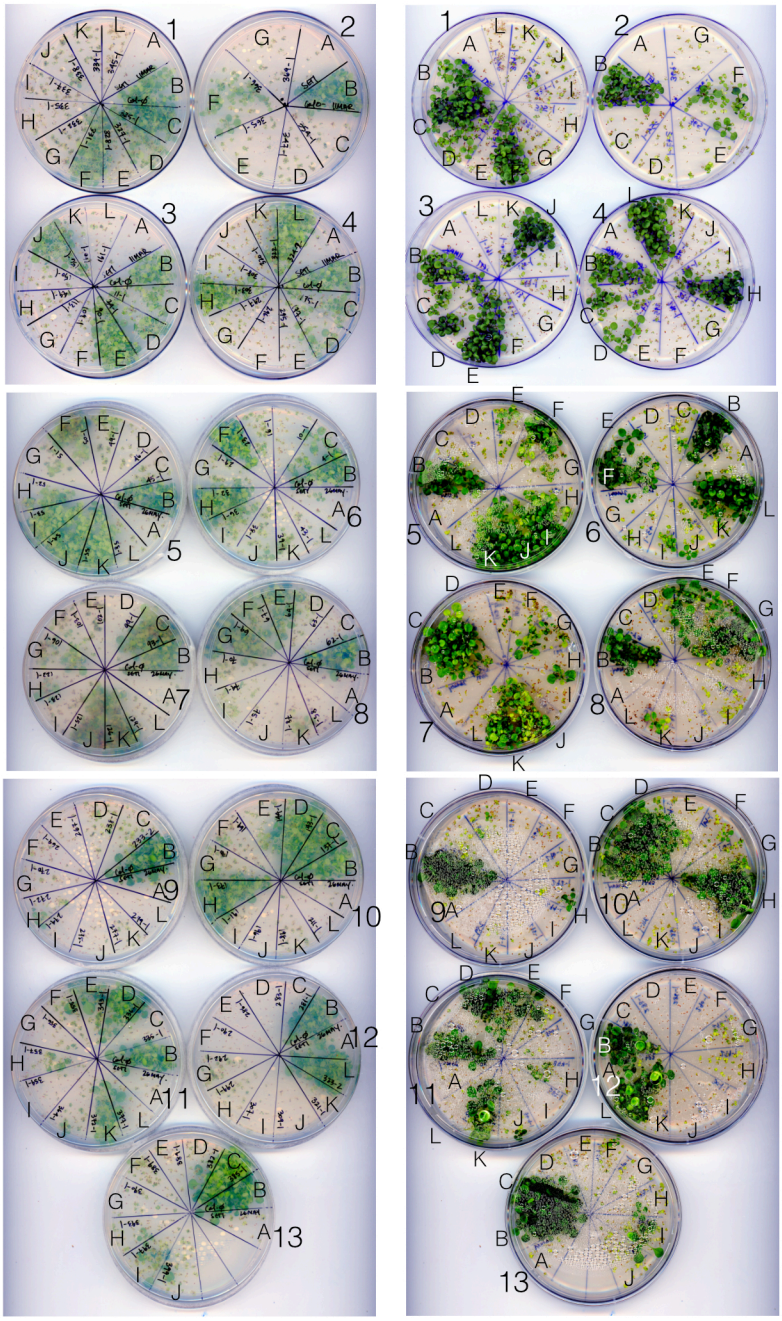

Appendix VI Full putant HR phenotypes

HR assays in M3 generation of putants. Pf0-1 (at OD_{600} = 0.3) delivery in rosette leave of 5-6-week-old plants shows maintenance of AvrRps4 recognition, and partial loss of PopP2 recognition 24 hours-post infiltration (hpi).

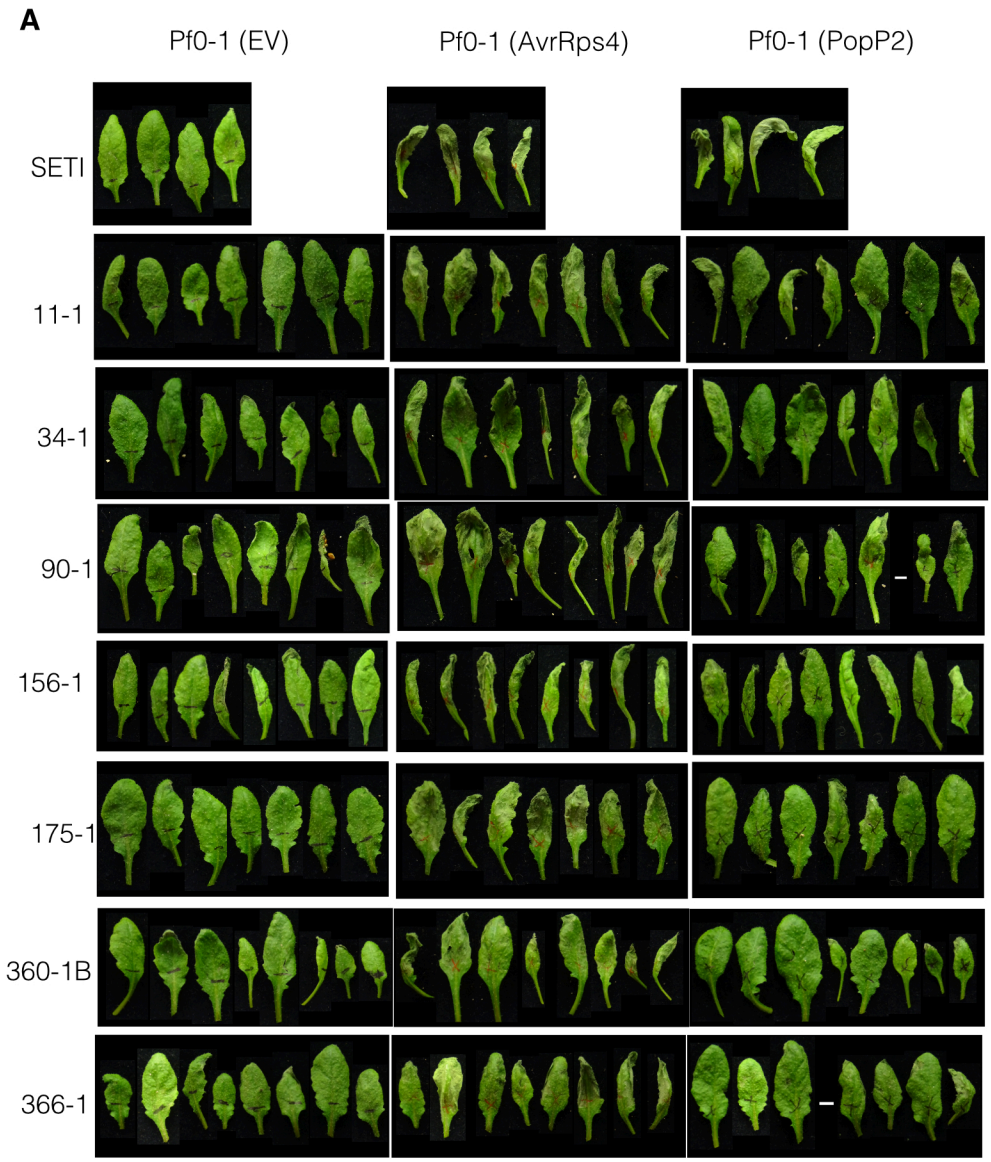

Appendix VII mNeon signal in roots of M2 seedlings from “uniform” M1 seed

The dsRed channel shows FAST-R signal in putant M2 seed while the mNeon channel shows AvrRps4-mNeon localized to root cell nuclei in M2 seedlings during screening

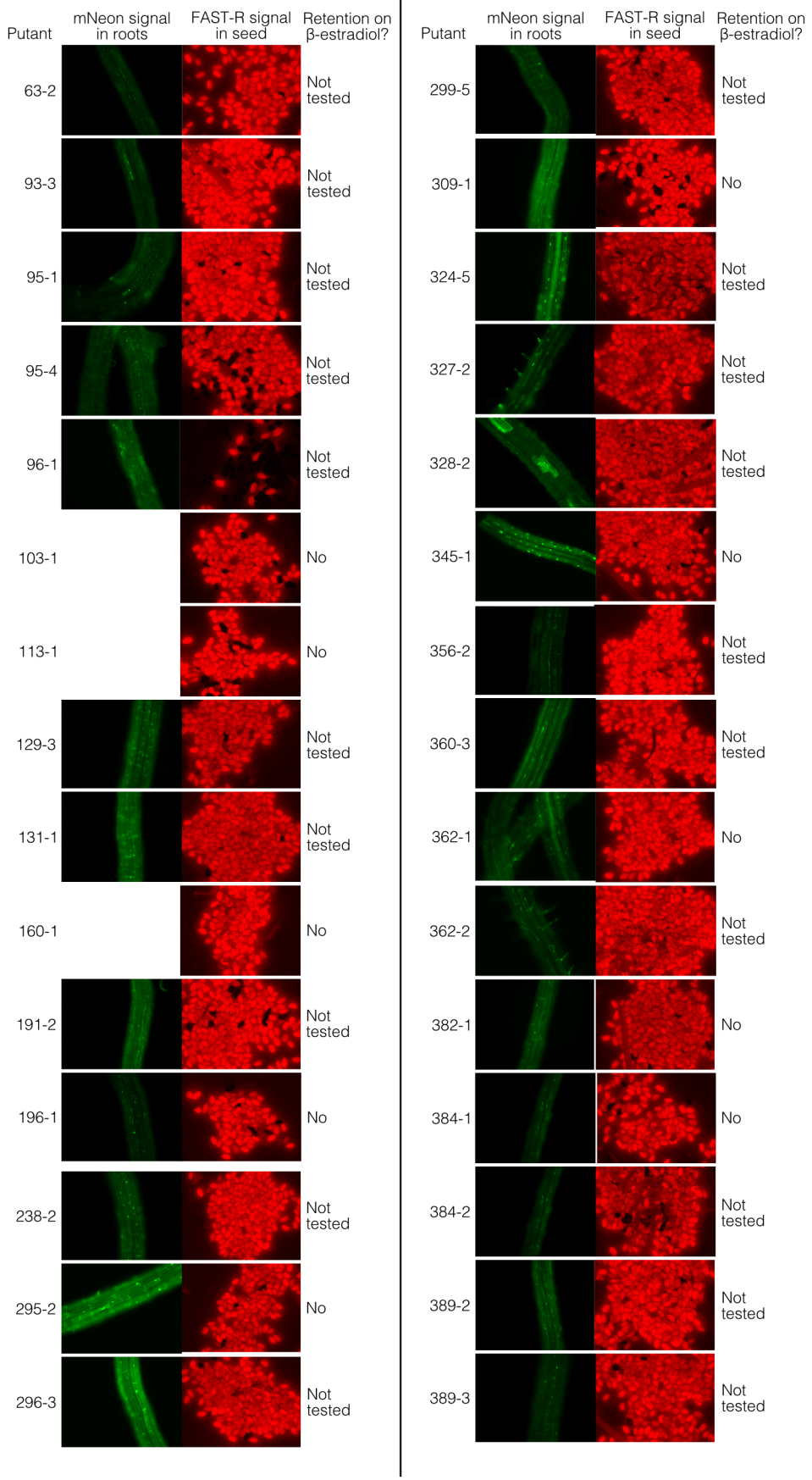

Appendix VIII HR assays with most promising putants

HR assays in M3 (M4 for 67-1) generation of putants. Pf0-1 (at OD_{600} = 0.3) delivery in rosette leave of 5-6-week-old plants shows maintenance of AvrRps4 recognition no cell death with empty vector negative control. HR was evaluated 24 hours post-infiltration (hpi).

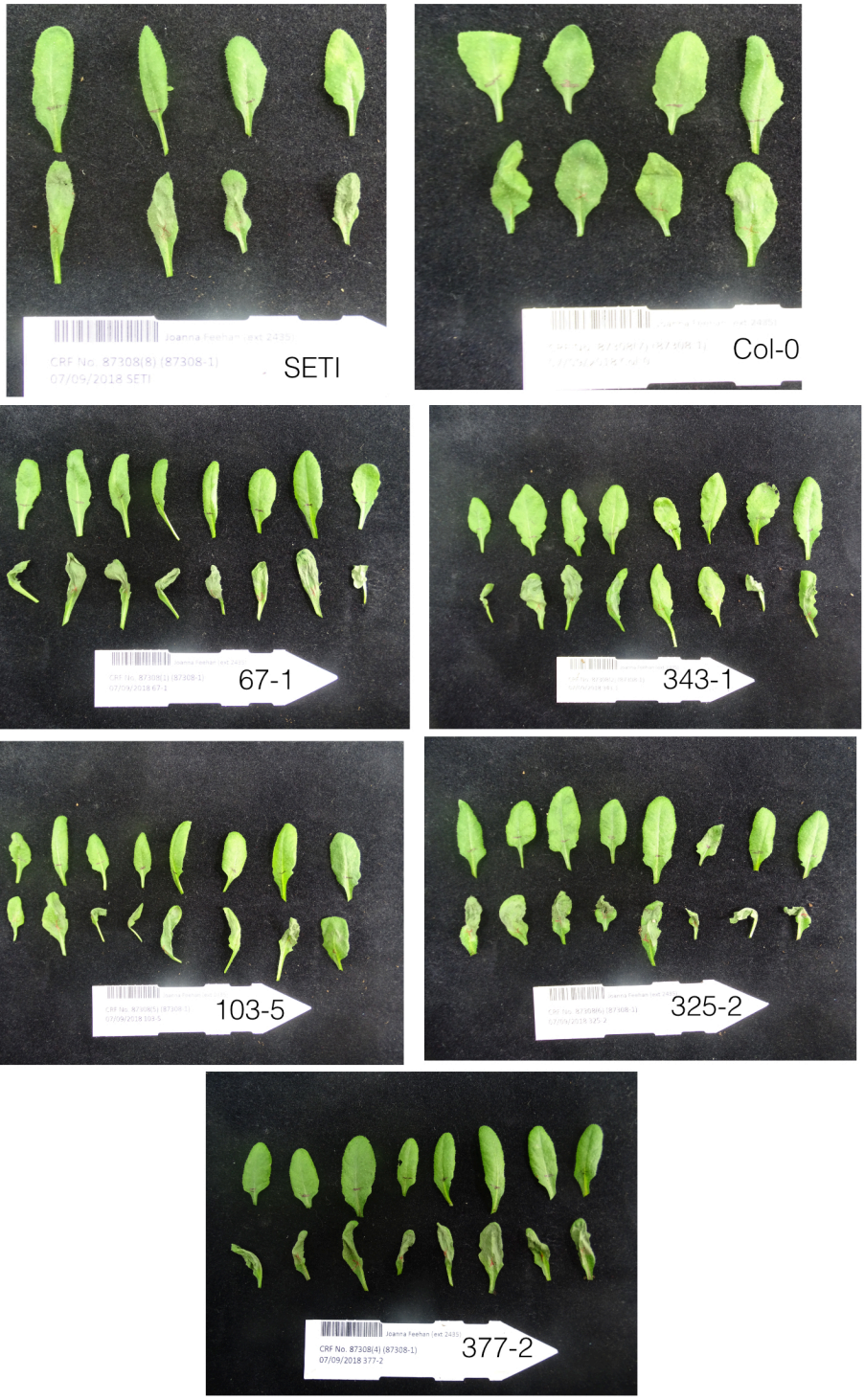

Appendix IX Full summary of putant phenotypes

Count	Putant	Retains insensitivity to β-estradiol?	mNeon signal in sister roots	HR on soil? Pf0-1 (AvrRps4)	HR on soil? Pf0-1 (PopP2)	Description of FAST-R signal of seed
1	4-1	Yes	-	-	-	None
2	8-1	-	-	-	-	Variable
3	10-1	No	-	-	-	Even (Slightly Variable)
4	11-1	Yes	0 of 8	Full	Partial	Variable
5	11-2	-	-	-	-	Variable
6	16-1 (M2)	-	-	-	-	Variable
7	16-2 (M3)	Yes	-	-	-	Variable
8	23-1 (M2)	-	-	-	-	None
9	23-1 (M3)	Yes	-	-	-	None
10	29-1	No	-	-	-	Variable
11	32-1	Yes	-	-	-	None
12	32-1	-	-	-	-	None
13	32-2 (M2)	-	-	-	-	Variable
14	32-2 (M3)	-	-	-	-	Variable
15	34-1	Yes	0 of 8	Partial	Partial	Variable
16	36-1	Yes	-	-	-	Variable
17	36-2	-	-	-	-	Variable
18	36-3	-	-	-	-	Variable
19	38-1	Yes	-	-	-	Variable
20	38-2	-	-	-	-	Variable
21	38-3	-	-	-	-	None
22	38-4	-	-	-	-	Variable
23	39-1 (M2)	-	-	-	-	Variable
24	39-1 (M3)	Yes	-	-	-	Variable
25	40-1	-	-	-	-	None
26	40-2	-	-	-	-	Variable
27	40-3	-	-	-	-	Variable
28	43-1	No	-	-	-	Variable
29	43-2	-	-	-	-	Variable
30	45-1 (M2)	-	-	-	-	Variable
31	45-1 (M3)	No	-	-	-	Variable
32	46-1	No	-	-	-	Even
33	46-2	-	-	-	-	Variable
34	48-1	-	-	-	-	Variable
35	49-1 (M2)	-	-	-	-	Even
36	49-1 (M3)	Yes	-	-	-	Variable
37	50-1 (M2)	-	-	-	-	None
38	50-1 (M3)	Yes	-	-	-	None
39	51-1	Yes	-	-	-	Variable
40	52-1 (M2)	-	-	-	-	Variable
41	52-1 (M3)	Yes	-	-	-	Variable
42	53-1 (M2)	-	-	-	-	Variable
43	53-1 (M3)	Yes	-	-	-	Variable
44	54-1 (M2)	-	-	-	-	Variable
45	54-1 (M3)	Yes	-	-	-	None
46	55-1 (M2)	-	-	-	-	None
47	55-1 (M3)	Yes	-	-	-	None
48	58-1	No	-	-	-	Variable
49	62-1	No	-	-	-	Variable
50	63-1	Yes	-	-	-	Even
51	63-2	-	-	-	-	Even
52	64-1	Yes	-	-	-	Variable
53	66-1	-	-	-	-	Variable
54	67-1 (M2)	-	-	-	-	Even
55	67-1 (M3)	Yes	-	Full	-	Even
56	67-2 (M2)	-	-	-	-	Variable
57	67-2 (M3)	-	-	-	-	Variable
58	69-1 (M2)	-	-	-	-	None
59	69-1 (M3)	Yes	-	-	-	None
60	70-1	Yes	-	-	-	Weak & Variable

61	70-2	-	-	-	-	Even
62	74-1	No	-	-	-	None
63	75-1 (M2)	-	-	-	-	Even
64	75-1 (M3)	No	-	-	-	Even
65	78-1	Yes	-	-	-	Variable
66	78-2	-	-	-	-	Variable
67	85-1 (M2)	-	-	-	-	Even? Variable?
68	85-1 (M3)	No	-	-	-	Variable
69	88-1	-	-	-	-	Variable
70	90-1	Yes	0 of 8	Full	Partial	None
71	93-1	Yes	-	-	-	Variable
72	93-2	-	-	-	-	Weak & Variable
73	93-3	-	-	-	-	Even
74	95-1	-	-	-	-	Even
75	95-2	-	-	-	-	Weak & Variable
76	95-4	-	-	-	-	Even
77	96-1	-	-	-	-	Even
78	99-1	No	-	-	-	Even? Variable?
79	99-2	-	-	-	-	Variable
80	99-3	-	-	-	-	Very weak & Variable
81	99-4	-	-	-	-	Even? Variable?
82	102-1	No	-	-	-	Even? Variable?
83	103-1	No	-	-	-	Even
84	103-2	-	-	-	-	Variable
85	103-3	-	-	-	-	Even
86	103-4	-	-	-	-	Variable
87	103-5	-	-	Partial	-	Variable
88	106-1	No	-	-	-	Variable
89	106-2	-	-	-	-	Even
90	109-1	No	-	-	-	Variable
91	111-1	-	-	-	-	Variable
92	111-2	-	-	-	-	None
93	113-1	No	-	-	-	Even
94	122-1 (M2)	-	-	-	-	Variable
95	122-1 (M3)	No	-	-	-	Variable
96	123-1 (M2)	-	-	-	-	Variable
97	123-1 (M3)	Yes	-	-	-	Variable
98	123-2 (M2)	-	-	-	-	Variable
99	123-2 (M3)	-	-	-	-	Variable
100	125-1 (M2)	-	-	-	-	Variable
101	125-1 (M3)	Yes	-	-	-	None
102	126-1 (M2)	-	-	-	-	Variable
103	126-1 (M3)	Yes	-	-	-	Variable
104	126-2 (M2)	-	-	-	-	Variable
105	126-2 (M3)	-	-	-	-	Variable
106	129-1	No	-	-	-	Variable
107	129-2	-	-	-	-	Variable
108	129-3	-	-	-	-	Even
109	129-4	-	-	-	-	Variable
110	131-1	-	-	-	-	Even
111	137-1 (M2)	-	-	-	-	Variable
112	137-1 (M3)	Yes	-	-	-	Variable
113	143-1 (M2)	-	-	-	-	Variable
114	143-1 (M3)	Yes	-	-	-	Variable
115	144-1 (M2)	-	-	-	-	None
116	144-1 (M3)	No	-	-	-	None
117	149-1	No	-	-	-	Variable
118	150-1	No	-	-	-	None
119	150-2	-	-	-	-	Variable
120	150-3	-	-	-	-	Variable
121	156-1	Yes	2 of 8	Full	Partial	Variable
122	156-2	-	-	-	-	Variable
123	160-1	No	-	-	-	Even
124	161-1	No	-	-	-	Variable
125	169-1	No	-	-	-	Variable
126	170-1	No	-	-	-	Variable
127	170-2	-	-	-	-	Variable
128	173-1	Yes	-	-	-	Variable
129	173-1	-	-	-	-	Variable
130	175-1	Yes	0 of 8	Partial	Partial	Variable

131	177-1	Yes	0 of 8	-	-	Variable
132	177-2	-	-	-	-	Variable
133	180-1	-	-	-	-	Variable
134	182-1	-	-	-	-	None
135	182-2	-	-	-	-	Variable
136	191-1	No	-	-	-	Variable
137	191-2	-	-	-	-	Even
138	191-3	-	-	-	-	Variable
139	196-1	No	-	-	-	Even? Variable?
140	198-1	No	-	-	-	None
141	198-2	-	-	-	-	Variable
142	202-1	-	-	-	-	Variable
143	210-1	-	-	-	-	Variable
144	211-1	No	-	-	-	Variable
145	211-2	-	-	-	-	Even? Variable?
146	212-1	-	-	-	-	None
147	214-1	-	-	-	-	None
148	214-2	-	-	-	-	None
149	216-1	-	-	-	-	None
150	216-2	-	-	-	-	None
151	230-1	-	-	-	-	Variable
152	233-2	No	-	-	-	Variable
153	233-3	-	-	-	-	Variable
154	238-1	Yes	-	-	-	Even
155	238-2	-	-	-	-	Even
156	267-1	No	-	-	-	Variable
157	267-2	-	-	-	-	Even?
158	267-3	-	-	-	-	Variable
159	269-1	No	-	-	-	Variable
160	269-2	-	-	-	-	None
161	269-3	-	-	-	-	None
162	270-1	No	-	-	-	Variable
163	270-2	-	-	-	-	Variable
164	270-3	-	-	-	-	None
165	272-1	Yes	-	-	-	Variable
166	274-1	No	-	-	-	Variable
167	274-2	-	-	-	-	Variable
168	274-3	-	-	-	-	Variable
169	275-1	No	-	-	-	Variable
170	275-2	-	-	-	-	Variable
171	277-1	No	-	-	-	Variable
172	279-1	No	-	-	-	Variable
173	279-2	-	-	-	-	Variable
174	279-3	-	-	-	-	Variable
175	281-1	No	-	-	-	Variable
176	281-2	-	-	-	-	Variable
177	283-1	No	-	-	-	Variable
178	283-2	-	-	-	-	Variable
179	286-1	No	-	-	-	Variable
180	286-2	-	-	-	-	Variable
181	286-3	-	-	-	-	Variable
182	286-4	-	-	-	-	Variable
183	290-1	No	-	-	-	Variable
184	292-1	Yes	-	-	-	Variable
185	292-2	-	-	-	-	Variable
186	292-3	-	-	-	-	Variable
187	295-2	No	-	-	-	Even?
188	296-1	No	-	-	-	Variable
189	296-2	-	-	-	-	Variable
190	296-3	-	-	-	-	Even?
191	297-1	No	-	-	-	Variable
192	299-1	Yes	-	-	-	Variable
193	299-2	-	-	-	-	Variable
194	299-3	-	-	-	-	Variable
195	299-4	-	-	-	-	Variable
196	299-5	-	-	-	-	Even?
197	303-1	Yes	0 of 8	-	-	Variable
198	307-1	No	-	-	-	None
199	308-1	No	-	-	-	Variable
200	309-1	No	-	-	-	Even

201	309-2	-	-	-	-	Variable
202	309-3	-	-	-	-	Variable
203	320-1	No	-	-	-	Variable
204	320-2	-	-	-	-	Variable
205	320-3	-	-	-	-	None
206	320-4	-	-	-	-	None
207	320-5	-	-	-	-	Variable
208	321-1	No	-	-	-	Variable
209	322-1	No	-	-	-	Variable
210	322-2	-	-	-	-	None
211	323-1	-	-	-	-	None
212	323-2	Yes	-	-	-	None
213	324-2	Yes	0 of 8	-	-	Variable
214	324-3	-	-	-	-	None
215	324-4	-	-	-	-	Variable
216	324-5	-	-	-	-	Even?
217	325-1	Yes	0 of 8	-	-	None
218	325-2	-	-	Full	-	Variable
219	325-3	-	-	-	-	Variable
220	325-4	-	-	-	-	Variable
221	327-1	Yes	2 of 8	-	-	Variable
222	327-2	-	-	-	-	Even?
223	328-1	No	-	-	-	Variable
224	328-2	-	-	-	-	Even?
225	328-3	-	-	-	-	Variable
226	330-1	-	-	-	-	Variable
227	330-2	-	-	-	-	Variable
228	331-1	Yes	0 of 8	Full	Partial	Variable
229	331-2	-	-	-	-	None
230	331-3	-	-	-	-	Variable
231	331-4	-	-	-	-	Variable
232	332-1	No	-	-	-	Variable
233	335-1	No	-	-	-	Variable
234	335-2	-	-	-	-	Variable
235	335-3	-	-	-	-	Variable
236	335-4	-	-	-	-	Variable
237	336-1	Yes	-	-	-	Variable
238	337-1	No	-	-	-	Variable
239	338-1	No	-	-	-	Variable
240	338-2	-	-	-	-	Variable
241	338-3	-	-	-	-	Variable
242	339-1	No	-	-	-	Variable
243	339-2	-	-	-	-	Weak & Variable
244	339-3	-	-	-	-	Variable
245	343-1	Yes	-	Partial	-	Even?
246	345-1	No	-	-	-	Even? Variable?
247	347-1	No	-	-	-	Even? Variable?
248	349-1	-	-	-	-	None
249	354-1	No	-	-	-	Variable
250	355-1	Yes	-	-	-	Variable
251	356-1	Yes	-	-	-	Even? Variable?
252	356-2	-	-	-	-	Even? Variable?
253	356-3	-	-	-	-	Variable
254	356-4	-	-	-	-	Even? Variable?
255	356-5	-	-	-	-	Variable
256	356-6	-	-	-	-	Variable
257	357-1	Yes	-	-	-	None
258	357-2	-	-	-	-	Weak & Variable
259	357-3	-	-	-	-	Even? Variable?
260	358-1	-	-	-	-	Variable
261	358-2	-	-	-	-	Variable
262	358-3	-	-	-	-	Variable
263	359-1	No	-	-	-	Variable
264	359-2	-	-	-	-	None
265	360-1A	-	-	-	-	Variable
266	360-1B	Yes	0 of 8	Partial	No	None
267	360-2	-	-	-	-	Weak & Variable
268	360-3	-	-	-	-	Even? Variable?
269	360-4	-	-	-	-	Even
270	362-1	No	-	-	-	Even? Variable?

271	362-2	-	-	-	-	Even? Variable?
272	364-1	Yes	-	-	-	Variable
273	364-2	-	-	-	-	Even
274	365-1	No	-	-	-	Weak & Variable
275	365-2	-	-	-	-	Variable
276	366-1	Yes	4 of 8	Partial	Partial	Variable
277	369-1	No	-	-	-	Even? Variable?
278	369-2	-	-	-	-	Variable
279	369-3	-	-	-	-	Variable
280	372-1	Yes	-	-	-	None
281	372-2	-	-	-	-	Variable
282	377-1	No	-	-	-	Variable
283	377-2	-	-	Full	-	None
284	377-3	-	-	-	-	Variable
285	377-4	-	-	-	-	Variable
286	382-1	No	-	-	-	Even?
287	384-1	No	-	-	-	Even?
288	384-2	-	-	-	-	Even? Variable?
289	384-3	-	-	-	-	Variable
290	384-4	-	-	-	-	Weak & Variable
291	384-6	-	-	-	-	Weak & Variable
292	384-7	-	-	-	-	Variable
293	384-8	-	-	-	-	Variable
294	385-1	Yes	-	-	-	None
295	389-1	Yes	-	-	-	Variable
296	389-2	-	-	-	-	Even? Variable?
297	389-3	-	-	-	-	Even? Variable?
298	389-4	-	-	-	-	Variable
299	390-1	No	-	-	-	Even? Variable?
300	390-2	-	-	-	-	Variable
301	391-1	-	-	-	-	Variable
302	393-1	Yes	-	-	-	Variable
303	393-2	-	-	-	-	Variable
304	396-1	-	-	-	-	None
305	396-2	-	-	-	-	None
306	396-3	-	-	-	-	Variable
307	397-1	Yes	-	-	-	Variable
308	399-1	Yes	-	-	-	Variable
309	399-2	-	-	-	-	Variable
310	399-3	-	-	-	-	Weak & Variable

Appendix X SETI β-estradiol dosage response assays

Dosage response assay to β-estradiol in Col-0 and SETI seedlings plated on GM + 50 μM β-estradiol and evaluated 14 days post-germination (DPG). We observe escapes of SETI seedlings up to 20 μM β-estradiol, with 35 μM β-estradiol inhibiting SETI growth. We observe some toxicity to 50 μM β-estradiol in Col-0 plants. 35 μM β-estradiol is the most appropriate dosage for SETI assays.

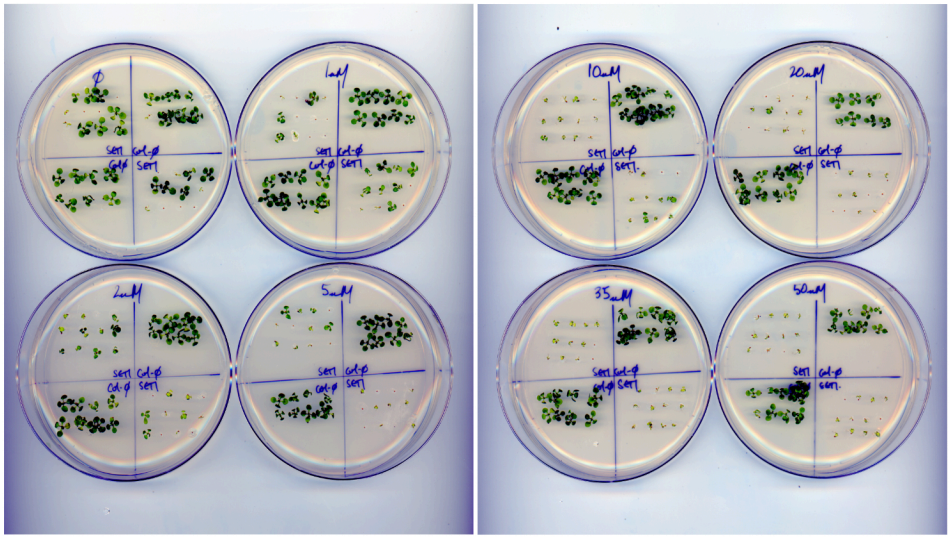

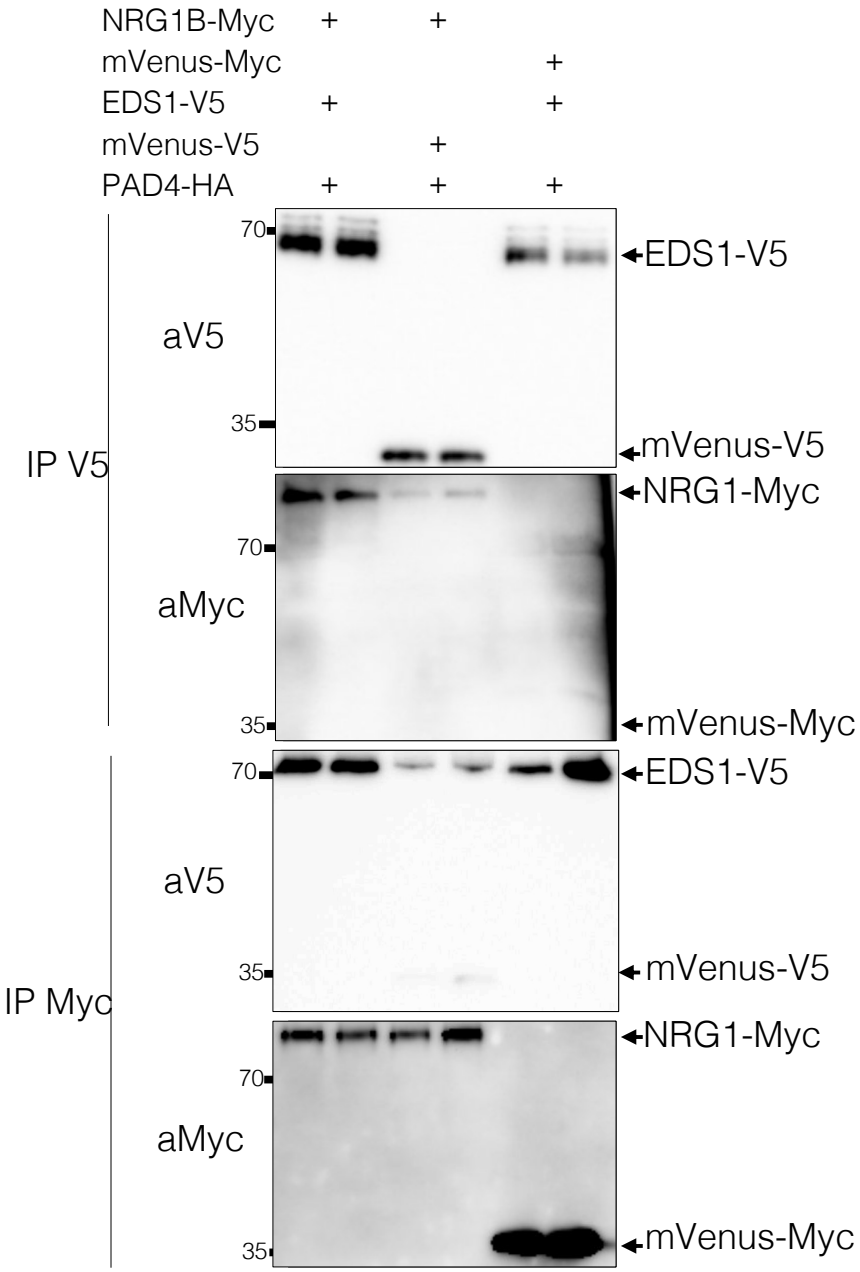
NRG1B-Myc + +
mVenus-Myc +
EDS1-V5 + +
mVenus-V5 +
PAD4-HA + + +
IP V5
aV5
70
35
EDS1-V5
mVenus-V5
aMyc
70
35
NRG1-Myc
mVenus-Myc
IP Myc
aV5
70
35
EDS1-V5
mVenus-V5
aMyc
70
35
NRG1-Myc
mVenus-Myc

Appendix XII Top 50 hits mass spectrometry jfe190130

jfe190130_CmOxP			NRG1B-HF		GUS-HF	
Identified Proteins (50/185)	Accession Number	MW	Band ID	co-IP	Band ID	co-IP
190130|NRG1B-HF|added_for_JoannaFeehan	190130|NRG1B-HF	99 kDa	69	55	0	2
RCA | rubisco activase | chr2:16570951-16573345 REVERSE LENGTH=474	AT2G39730.1	52 kDa	0	14	0	3
HSC70-1, HSP70-1, AT-HSC70-1, HSC70 | heat shock cognate protein 70-1 | chr5:554055-556334 REVERSE LENGTH=651	AT5G02500.1	71 kDa	0	11	7	0
HTB1 | Histone superfamily protein | chr1:2413049-2413495 FORWARD LENGTH=148	AT1G07790.1 (+5)	16 kDa	1	8	0	0
RBCL | ribulose-bisphosphate carboxylases | chrC:54958-56397 FORWARD LENGTH=479	ATCG00490.1	53 kDa	0	6	0	3
CAB1, AB140, CAB140, LHCB1.3 | chlorophyll A/B binding protein 1 | chr1:10478071-10478874 FORWARD LENGTH=267	AT1G29930.1	28 kDa	0	4	0	2
PVA12 | plant VAP homolog 12 | chr2:18611029-18612971 FORWARD LENGTH=239	AT2G45140.1	26 kDa	0	4	0	0
C2 calcium/lipid-binding plant phosphoribosyltransferase family protein | chr5:2127200-2129584 REVERSE LENGTH=794	AT5G06850.1	91 kDa	1	3	0	0
Ribosomal protein L11 family protein | chr2:15619559-15620059 REVERSE LENGTH=166	AT2G37190.1 (+1)	18 kDa	0	3	0	0
ATPA | ATP synthase subunit alpha | chrC:9938-11461 REVERSE LENGTH=507	ATCG00120.1	55 kDa	0	2	0	0
190130|GUS-HF|added_for_JoannaFeehan	190130|GUS-HF	75 kDa	0	0	575	144
CPHSC70-2EAT SHOCK PROTEIN 70-2, HSC70-7, cpHsc70-2 | chloroplast heat shock protein 70-2 | chr5:20303470-20306295 FORWARD LENGTH=718	AT5G49910.1	77 kDa	1	0	8	0
ACT7 | actin 7 | chr5:3052809-3054220 FORWARD LENGTH=377	AT5G09810.1	42 kDa	3	0	2	2
ATPANK2, PANK2 | pantothenate kinase 2 | chr4:15537724-15543715 REVERSE LENGTH=901	AT4G32180.1 (+2)	100 kDa	2	0	0	1
QWRF8 | Family of unknown function (DUF566) | chr4:14965538-14967881 REVERSE LENGTH=644	AT4G30710.1 (+1)	70 kDa	1	0	0	2
ATNOS1, NOS1, ATNOA1, NOA1, RIF1 | P-loop containing nucleoside triphosphate hydrolases superfamily protein | chr3:17483195-17486249 REVERSE LENGTH=561	AT3G47450.1 (+1)	62 kDa	1	0	0	2
Serine protease inhibitor (SERPIN) family protein | chr1:22973876-22975463 FORWARD LENGTH=433	AT1G62170.1 (+1)	48 kDa	2	0	0	1
O-Glycosyl hydrolases family 17 protein | chr2:7035463-7038326 REVERSE LENGTH=503	AT2G16230.1	54 kDa	2	0	0	1
Protein of unknown function (DUF1216) | chr3:10831233-10833020 FORWARD LENGTH=539	AT3G28830.1	56 kDa	2	0	0	1
LRR and NB-ARC domains-containing disease resistance protein | chr4:6634779-6637457 REVERSE LENGTH=892	AT4G10780.1	102 kDa	2	0	0	1
ATY1, TRX-Y1, TY1 | thioredoxin Y1 | chr1:28811873-28812948 REVERSE LENGTH=172	AT1G76760.1	19 kDa	0	0	0	2
Trypsin family protein | chr5:22240256-22241233 REVERSE LENGTH=198	AT5G54745.1	22 kDa	0	0	0	2
myosin heavy chain-related | chr3:11879235-11881788 REVERSE LENGTH=527	AT3G30230.1	59 kDa	0	0	0	3
AT59 | Pectate lyase family protein | chr1:4931844-4933405 REVERSE LENGTH=459	AT1G14420.1	51 kDa	0	0	0	2
RAP2.6 | related to AP2 6 | chr1:16263989-16264663 FORWARD LENGTH=192	AT1G43160.1	22 kDa	0	0	0	2
Disease resistance protein (TIR-NBS class) | chr1:27421086-27422999 FORWARD LENGTH=512	AT1G72870.1	59 kDa	0	0	0	2
HOS1 | ubiquitin-protein ligases | chr2:16612941-16617802 FORWARD LENGTH=927	AT2G39810.1	105 kDa	0	0	0	2
LOX5 | PLAT/LH2 domain-containing lipoxygenase family protein | chr3:7927011-7931167 FORWARD LENGTH=886	AT3G22400.1	101 kDa	0	0	0	2
			Total Spectrum Counts			

Protein threshold = 99%; minimum # peptides = 2; peptide threshold = 95%

Appendix XIII top 55 hits mass spectrometry jfe190320

jfe190320_CmOx			NRG1B-HF		GUS-HF	
Identified Proteins (55/218)	Accession Number	MW	EV	A4	EV	A4
| Disease resistance protein (CC-NBS-LRR class) family | Chr5:26718338-26721133 REVERSE LENGTH=815 | 201606	AT5G66910.1	93 kDa	170	144	0	0
| ribulose-bisphosphate carboxylase | ChrC:54958-56397 FORWARD LENGTH=479 | 201606	ATCG00490.1	53 kDa	51	95	19	17
| ATP synthase subunit beta | ChrC:52660-54156 REVERSE LENGTH=498 | 201606	ATCG00480.1	54 kDa	34	87	7	10
| rubisco activase | Chr2:16570951-16573345 REVERSE LENGTH=474 | 201606	AT2G39730.1	52 kDa	41	51	20	15
| heat shock cognate protein 70-1 | Chr5:554055-556334 REVERSE LENGTH=651 | 201606	AT5G02500.1	71 kDa	63	46	7	5
| ATP synthase subunit alpha | ChrC:9938-11461 REVERSE LENGTH=507 | 201606	ATCG00120.1	55 kDa	30	45	12	8
| Heat shock protein 70 (Hsp 70) family protein | Chr3:2903434-2905632 REVERSE LENGTH=649 | 201606	AT3G09440.1 (+3)	71 kDa	44	37	0	0
| Heat shock protein 70 (Hsp 70) family protein | Chr5:550296-552565 REVERSE LENGTH=653 | 201606	AT5G02490.1	71 kDa	45	36	0	0
| glyceraldehyde-3-phosphate dehydrogenase B subunit | Chr1:16127552-16129584 FORWARD LENGTH=447 | 201606	AT1G42970.1	48 kDa	17	31	6	3
| Transketolase | Chr3:22454004-22456824 FORWARD LENGTH=741 | 201606	AT3G60750.1 (+1)	80 kDa	10	29	0	0
| glutamate synthase 1 | Chr5:1130031-1138186 FORWARD LENGTH=1622 | 201606	AT5G04140.1 (+1)	177 kDa	5	27	0	0
| glyceraldehyde 3-phosphate dehydrogenase A subunit | Chr3:9795226-9796848 FORWARD LENGTH=396 | 201606	AT3G26650.1	42 kDa	14	26	0	0
| phosphoglycerate kinase 1 | Chr3:4061127-4063140 REVERSE LENGTH=481 | 201606	AT3G12780.1	50 kDa	11	26	0	0
| glyceraldehyde 3-phosphate dehydrogenase A subunit 2 | Chr1:4392634-4394283 REVERSE LENGTH=399 | 201606	AT1G12900.1 (+1)	43 kDa	15	25	0	0
| Cobalamin-independent synthase family protein | Chr5:5935771-5939195 FORWARD LENGTH=765 | 201606	AT5G17920.1 (+1)	84 kDa	11	25	2	0
| fructose-bisphosphate aldolase 2 | Chr4:18163714-18165659 REVERSE LENGTH=398 | 201606	AT4G38970.1	43 kDa	10	24	0	0
| C2 calcium/lipid-binding plant phosphoribosyltransferase family protein | Chr5:2127200-2129584 REVERSE LENGTH=794 | 201606	AT5G06850.1	91 kDa	30	23	0	0
| ENTH/ANTH/VHS superfamily protein | Chr5:13462463-13465581 REVERSE LENGTH=544 | 201606	AT5G35200.1 (+1)	61 kDa	17	22	0	0
| chaperonin 60 beta | Chr1:20715717-20718673 REVERSE LENGTH=600 | 201606	AT1G55490.1 (+4)	64 kDa	10	20	0	0
| CLPC homologue 1 | Chr5:20715710-20719800 REVERSE LENGTH=929 | 201606	AT5G50920.1	103 kDa	4	20	0	0
| chaperonin-60alpha | Chr2:11926603-11929184 FORWARD LENGTH=586 | 201606	AT2G28000.1	62 kDa	8	19	0	0
| serine transhydroxymethyltransferase 1 | Chr4:17831891-17834742 REVERSE LENGTH=517 | 201606	AT4G37930.1	57 kDa	7	19	0	0
| fructose-bisphosphate aldolase 1 | Chr2:9128416-9130152 REVERSE LENGTH=389 | 201606	AT2G21330.3	42 kDa	10	18	0	0
| RAB GTPase homolog E1B | Chr4:10990036-10991466 FORWARD LENGTH=476 | 201606	AT4G20360.1 (+1)	52 kDa	10	17	0	0
| epithiospecifier protein | Chr1:20170995-20173885 REVERSE LENGTH=341 | 201606	AT1G54040.2	37 kDa	5	17	5	0
| glycine decarboxylase P-protein 1 | Chr4:15926852-15931150 REVERSE LENGTH=1037 | 201606	AT4G33010.1	113 kDa	2	17	0	0
| carbonic anhydrase 2 | Chr5:4760536-4762382 FORWARD LENGTH=259 | 201606	AT5G14740.2 (+4)	28 kDa	6	16	0	0
| Aldolase-type TIM barrel family protein | Chr3:4818667-4820748 FORWARD LENGTH=367 | 201606	AT3G14415.1 (+1)	40 kDa	0	16	0	0
| Phosphoglycerate kinase family protein | Chr1:21028403-21030454 FORWARD LENGTH=478 | 201606	AT1G56190.1 (+1)	50 kDa	0	16	0	0
| photosystem II reaction center protein C | ChrC:33720-35141 FORWARD LENGTH=473 | 201606	ATCG00280.1	52 kDa	9	15	5	4
| Phosphoglycerate mutase%2C 2%2C3-bisphosphoglycerate-independent | Chr3:2608683-2611237 REVERSE LENGTH=560 | 201606	AT3G08590.1 (+1)	61 kDa	11	14	0	0
| Aldolase-type TIM barrel family protein | Chr3:4821804-4823899 FORWARD LENGTH=367 | 201606	AT3G14420.1 (+1)	40 kDa	9	14	0	0
| vacuolar ATP synthase subunit A | Chr1:29660463-29664575 FORWARD LENGTH=623 | 201606	AT1G78900.1 (+1)	69 kDa	6	14	0	0
| sedoheptulose-bisphosphatase | Chr3:20709640-20711421 FORWARD LENGTH=393 | 201606	AT3G55800.1	42 kDa	4	14	0	0
| lipoxygenase 2 | Chr3:16525437-16529233 FORWARD LENGTH=896 | 201606	AT3G45140.1	102 kDa	2	14	0	0
| ATP synthase alpha/beta family protein | Chr5:2821992-2824683 FORWARD LENGTH=559 | 201606	AT5G08680.1	60 kDa	0	14	0	0
| S-adenosyl-L-homocysteine hydrolase | Chr4:8054931-8056676 FORWARD LENGTH=485 | 201606	AT4G13940.1 (+1)	53 kDa	5	13	0	0
| high cyclic electron flow 1 | Chr3:20016951-20018527 FORWARD LENGTH=417 | 201606	AT3G54050.1 (+1)	45 kDa	0	13	0	0

| heat shock protein 70 (Hsp 70) family protein | Chr5:10540665-10543274 REVERSE LENGTH=669 | 201606	AT5G28540.1 (+2)	74 kDa	10	12	0	0
| carbonic anhydrase 1 | Chr3:194853-196716 REVERSE LENGTH=270 | 201606	AT3G01500.1 (+3)	30 kDa	4	12	0	2
| ATPase%2C F1 complex%2C gamma subunit protein | Chr4:2350761-2351882 REVERSE LENGTH=373 | 201606	AT4G04640.1	41 kDa	10	11	0	0
| DNA glycosylase superfamily protein | Chr1:6744520-6746144 FORWARD LENGTH=382 | 201606	AT1G19480.1 (+1)	42 kDa	10	11	0	0
| tubulin beta chain 2 | Chr5:25181560-25183501 FORWARD LENGTH=450 | 201606	AT5G62690.1 (+1)	51 kDa	9	11	0	0
| ATPase%2C F1 complex%2C alpha subunit protein | Chr2:3361474-3364028 FORWARD LENGTH=777 | 201606	AT2G07698.1	86 kDa	6	11	0	0
| ribosomal protein 1 | Chr1:16266992-16268631 FORWARD LENGTH=389 | 201606	AT1G43170.1 (+7)	45 kDa	4	11	0	0
| tubulin beta-5 chain | Chr1:6938033-6940481 REVERSE LENGTH=449 | 201606	AT1G20010.1	50 kDa	11	10	0	0
| ADP/ATP carrier 1 | Chr3:2605706-2607030 REVERSE LENGTH=381 | 201606	AT3G08580.1 (+1)	41 kDa	8	10	2	0
| chloroplast heat shock protein 70-2 | Chr5:20303470-20306295 FORWARD LENGTH=718 | 201606	AT5G49910.1	77 kDa	7	10	0	0
| chloroplast heat shock protein 70-1 | Chr4:12590094-12593437 FORWARD LENGTH=718 | 201606	AT4G24280.1	77 kDa	6	10	0	0
| Chlorophyll A-B binding family protein | Chr1:16871768-16873194 FORWARD LENGTH=265 | 201606	AT1G44575.1 (+1)	28 kDa	2	10	0	0
| photosystem I subunit D-1 | Chr4:1229247-1229873 REVERSE LENGTH=208 | 201606	AT4G02770.1	23 kDa	0	10	0	0
| plastid transcriptionally active 16 | Chr3:17228766-17231021 FORWARD LENGTH=510 | 201606	AT3G46780.1	54 kDa	0	10	0	0
| hydroxypyruvate reductase | Chr1:25493418-25495720 FORWARD LENGTH=386 | 201606	AT1G68010.1 (+1)	42 kDa	0	10	0	0
| plant VAP homolog 12 | Chr2:18611029-18612971 FORWARD LENGTH=239 | 201606	AT2G45140.1	26 kDa	12	9	0	0
| phosphoserine aminotransferase | Chr4:16904205-16905497 FORWARD LENGTH=430 | 201606	AT4G35630.1	47 kDa	8	9	0	0
				Total Spectrum Count		

Protein threshold = 99%; minimum # peptides = 2; peptide threshold = 95%

Appendix XIV Top 50 hits for mass spectrometry jfe190528

jfe190528_CmOx			NRG1B-HF		
Identified Proteins (50/150)	Accession Number	MW	mock	EV	A4
190130|NRG1B-HF|added_for_JoannaFeehan		99 kDa	196	185	134
HSC70-1, HSP70-1, AT-HSC70-1, HSC70 | heat shock cognate protein 70-1 | chr5:554055-556334 REVERSE LENGTH=651	AT5G02500.1	71 kDa	60	63	54
| Heat shock protein 70 (Hsp 70) family protein | chr3:2903434-2905632 REVERSE LENGTH=649	AT3G09440.1 (+1)	71 kDa	35	41	38
RCA | rubisco activase | chr2:16570951-16573345 REVERSE LENGTH=474	AT2G39730.1	52 kDa	51	37	27
GAPB | glyceraldehyde-3-phosphate dehydrogenase B subunit | chr1:16127552-16129584 FORWARD LENGTH=447	AT1G42970.1	48 kDa	27	23	22
RBCL | ribulose-bisphosphate carboxylases | chrC:54958-56397 FORWARD LENGTH=479	ATCG00490.1	53 kDa	42	41	16
ATPA | ATP synthase subunit alpha | chrC:9938-11461 REVERSE LENGTH=507	ATCG00120.1	55 kDa	25	23	14
GAPA, GAPA-1 | glyceraldehyde 3-phosphate dehydrogenase A subunit | chr3:9795226-9796848 FORWARD LENGTH=396	AT3G26650.1	42 kDa	18	22	13
GAPA-2 | glyceraldehyde 3-phosphate dehydrogenase A subunit 2 | chr1:4392634-4394283 REVERSE LENGTH=399	AT1G12900.1 (+2)	43 kDa	18	21	13
| DNA glycosylase superfamily protein | chr1:6744520-6746144 FORWARD LENGTH=382	AT1G19480.1 (+1)	42 kDa	19	17	10
ATPB, PB | ATP synthase subunit beta | chrC:52660-54156 REVERSE LENGTH=498	ATCG00480.1	54 kDa	21	18	9
CAB3, AB180, LHCB1.2 | chlorophyll A/B binding protein 3 | chr1:10472443-10473246 REVERSE LENGTH=267	AT1G29910.1 (+2)	28 kDa	20	15	9
| C2 calcium/lipid-binding plant phosphoribosyltransferase family protein | chr5:2127200-2129584 REVERSE LENGTH=794	AT5G06850.1	91 kDa	17	14	9
CA2, CA18, BETA CA2 | carbonic anhydrase 2 | chr5:4760536-4762382 FORWARD LENGTH=259	AT5G14740.2	28 kDa	13	13	9
AGD2 | Pyridoxal phosphate (PLP)-dependent transferases superfamily protein | chr4:16171847-16174630 REVERSE LENGTH=461	AT4G33680.1	50 kDa	13	8	9
| ENTH/ANTH/VHS superfamily protein | chr5:13462463-13465581 REVERSE LENGTH=544	AT5G35200.1	61 kDa	8	7	8
PVA12 | plant VAP homolog 12 | chr2:18611029-18612971 FORWARD LENGTH=239	AT2G45140.1	26 kDa	15	15	7
BIP1 | heat shock protein 70 (Hsp 70) family protein | chr5:10540665-10543274 REVERSE LENGTH=669	AT5G28540.1 (+1)	74 kDa	9	7	7
ESP, TASTY | epithiospecifier protein | chr1:20170995-20173885 REVERSE LENGTH=341	AT1G54040.2	37 kDa	15	14	6
LHCB2.1, LHCB2 | photosystem II light harvesting complex gene 2.1 | chr2:1823449-1824331 REVERSE LENGTH=265	AT2G05100.1	29 kDa	14	11	6
| Phosphoglycerate mutase, 2,3-bisphosphoglycerate-independent | chr3:2608683-2611237 REVERSE LENGTH=560	AT3G08590.1 (+1)	61 kDa	16	10	6
CPN60B, LEN1 | chaperonin 60 beta | chr1:20715717-20718673 REVERSE LENGTH=600	AT1G55490.1 (+1)	64 kDa	14	8	6
PMSR4 | peptide met sulfoxide reductase 4 | chr4:12898802-12899998 REVERSE LENGTH=258	AT4G25130.1	29 kDa	8	7	6
| Ribosomal protein L11 family protein | chr3:19809895-19810395 REVERSE LENGTH=166	AT3G53430.1	18 kDa	5	6	6
ESM1 | epithiospecifier modifier 1 | chr3:4729886-4731562 FORWARD LENGTH=392	AT3G14210.1	44 kDa	6	3	6
ATRAB8D, ATRABE1B, RABE1b | RAB GTPase homolog E1B | chr4:10990036-10991466 FORWARD LENGTH=476	AT4G20360.1	52 kDa	10	10	5
CA1, ATBCA1, SABP3, ATSABP3 | carbonic anhydrase 1 | chr3:194853-196716 REVERSE LENGTH=270	AT3G01500.1 (+2)	30 kDa	9	9	5
LHCA3 | photosystem I light harvesting complex gene 3 | chr1:22700152-22701149 FORWARD LENGTH=273	AT1G61520.1 (+1)	29 kDa	7	8	5
PSAF | photosystem I subunit F | chr1:11215011-11215939 REVERSE LENGTH=221	AT1G31330.1	24 kDa	7	8	5
PSBC | photosystem II reaction center protein C | chrC:33720-35141 FORWARD LENGTH=473	ATCG00280.1	52 kDa	6	8	5
PTAC5 | plastid transcriptionally active 5 | chr4:7948644-7950779 FORWARD LENGTH=387	AT4G13670.1	44 kDa	11	5	5
| Ribosomal protein S5 family protein | chr2:17460016-17461398 REVERSE LENGTH=285	AT2G41840.1	31 kDa	9	4	5
LHCB5 | light harvesting complex of photosystem II 5 | chr4:6408200-6409496 FORWARD LENGTH=280	AT4G10340.1	30 kDa	13	12	4
160201|RRS1-R-HF|for_Zane		162 kDa	11	11	4
LHB1B1, LHCB1.4 | light-harvesting chlorophyll-protein complex II subunit B1 | chr2:14524818-14525618 FORWARD LENGTH=266	AT2G34430.1	28 kDa	21	9	4
| GTP binding Elongation factor Tu family protein | chr4:1295751-1298354 REVERSE LENGTH=454	AT4G02930.1	49 kDa	5	9	4
PSAT | phosphoserine aminotransferase | chr4:16904205-16905497 FORWARD LENGTH=430	AT4G35630.1	47 kDa	12	7	4
| Histone superfamily protein | chr1:2369212-2369523 FORWARD LENGTH=103	AT1G07660.1 (+8)	11 kDa	6	7	4

| GTP binding Elongation factor Tu family protein | chr1:2455559-2457001 FORWARD LENGTH=449	AT1G07920.1 (+5)	50 kDa	9	6	4
ATPC1 | ATPase, F1 complex, gamma subunit protein | chr4:2350761-2351882 REVERSE LENGTH=373	AT4G04640.1	41 kDa	6	6	4
| Ribosomal protein S8e family protein | chr5:6851695-6853012 REVERSE LENGTH=222	AT5G20290.1	25 kDa	10	5	4
BGL1, BGLU18, ATBG1 | beta glucosidase 18 | chr1:19515250-19517930 FORWARD LENGTH=528	AT1G52400.1 (+1)	60 kDa	0	5	4
AAC1 | ADP/ATP carrier 1 | chr3:2605706-2607030 REVERSE LENGTH=381	AT3G08580.1 (+1)	41 kDa	9	10	3
VAP27-1, VAP, (AT)VAP, VAP27 | vesicle associated protein | chr3:22400537-22402408 FORWARD LENGTH=256	AT3G60600.1	28 kDa	8	7	3
ACT12 | actin-12 | chr3:17128567-17129981 FORWARD LENGTH=377	AT3G46520.1 (+2)	42 kDa	7	6	3
TUA6 | Tubulin/FtsZ family protein | chr4:8548753-8550319 REVERSE LENGTH=427	AT4G14960.1	47 kDa	4	5	3
| Ubiquitin supergroup;Ribosomal protein L40e | chr2:15172153-15173046 FORWARD LENGTH=128	AT2G36170.1 (+1)	15 kDa	4	5	3
| RNA polymerase II transcription elongation factor | chr1:26809987-26811645 REVERSE LENGTH=326	AT1G71080.1	35 kDa	6	4	3
| NAD(P)-binding Rossmann-fold superfamily protein | chr2:15795481-15796977 REVERSE LENGTH=325	AT2G37660.1	35 kDa	5	4	3
RPS6, RPS6A | ribosomal protein S6 | chr4:15346306-15347714 REVERSE LENGTH=250	AT4G31700.1	28 kDa	4	4	3
				Total Spectrum Counts	

Protein threshold = 99%; minimum # peptides = 2; peptide threshold = 95%

Appendix XV Replicates for PopP2 HR assays in Ws-2_*nrg1a/b*:NRG1B-HF

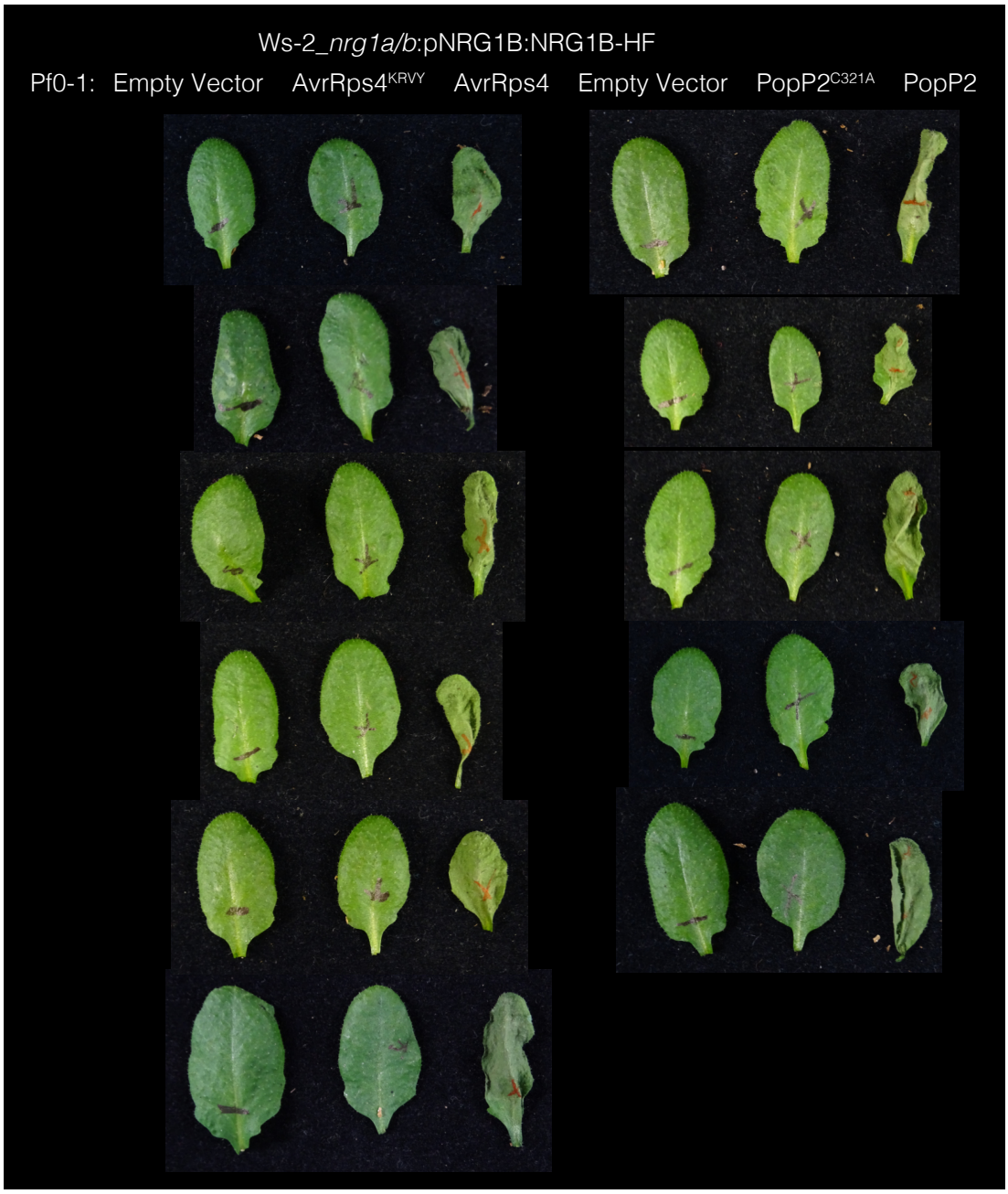

Appendix XVI Top 50 hits for mass spectrometry jfe190905

jfe190905_CmOx			NRG1B-HF				
Identified Proteins (50/477)	Accession Number	MW	EV	A4	KRVY	PopP2	C321A
| Disease resistance protein (CC-NBS-LRR class) family | Chr5:26718338-26721133 REVERSE LENGTH=815 | 201606	AT5G66910.1	93 kDa	237	228	277	247	248
| ribulose-bisphosphate carboxylase | ChrC:54958-56397 FORWARD LENGTH=479 | 201606	ATCG00490.1	53 kDa	104	118	125	143	124
| ATP synthase subunit beta | ChrC:52660-54156 REVERSE LENGTH=498 | 201606	ATCG00480.1	54 kDa	94	110	113	111	106
| rubisco activase | Chr2:16570951-16573345 REVERSE LENGTH=474 | 201606	AT2G39730.1	52 kDa	103	109	99	99	97
| heat shock cognate protein 70-1 | Chr5:554055-556334 REVERSE LENGTH=651 | 201606	AT5G02500.1	71 kDa	95	108	117	98	95
| Heat shock protein 70 (Hsp 70) family protein | Chr3:2903434-2905632 REVERSE LENGTH=649 | 201606	AT3G09440.1 (+3)	71 kDa	71	83	80	72	65
| Heat shock protein 70 (Hsp 70) family protein | Chr5:550296-552565 REVERSE LENGTH=653 | 201606	AT5G02490.1	71 kDa	56	71	64	58	57
| glyceraldehyde 3-phosphate dehydrogenase A subunit | Chr3:9795226-9796848 FORWARD LENGTH=396 | 201606	AT3G26650.1	42 kDa	64	59	59	75	58
| glyceraldehyde 3-phosphate dehydrogenase A subunit 2 | Chr1:4392634-4394283 REVERSE LENGTH=399 | 201606	AT1G12900.1	43 kDa	62	58	60	70	60
| ENTH/ANTH/VHS superfamily protein | Chr5:13462463-13465581 REVERSE LENGTH=544 | 201606	AT5G35200.1 (+1)	61 kDa	40	58	51	45	50
| heat shock protein 70 | Chr3:3991487-3993689 REVERSE LENGTH=650 | 201606	AT3G12580.1	71 kDa	42	55	0	0	49
| phosphoglycerate kinase 1 | Chr3:4061127-4063140 REVERSE LENGTH=481 | 201606	AT3G12780.1	50 kDa	43	54	51	48	46
| glyceraldehyde-3-phosphate dehydrogenase B subunit | Chr1:16127552-16129584 FORWARD LENGTH=447 | 201606	AT1G42970.1	48 kDa	69	53	58	69	58
| epithiospecifier protein | Chr1:20170995-20173885 REVERSE LENGTH=341 | 201606	AT1G54040.2	37 kDa	44	52	44	41	43
| Aldolase-type TIM barrel family protein | Chr3:4821804-4823899 FORWARD LENGTH=367 | 201606	AT3G14420.1 (+1)	40 kDa	29	51	52	51	43
| Aldolase-type TIM barrel family protein | Chr3:4818667-4820748 FORWARD LENGTH=367 | 201606	AT3G14415.1 (+1)	40 kDa	26	50	48	46	41
| ATP synthase subunit alpha | ChrC:9938-11461 REVERSE LENGTH=507 | 201606	ATCG00120.1	55 kDa	53	49	57	48	49
| Cobalamin-independent synthase family protein | Chr5:5935771-5939195 FORWARD LENGTH=765 | 201606	AT5G17920.1 (+1)	84 kDa	27	45	50	46	44
| fructose-bisphosphate aldolase 2 | Chr4:18163714-18165659 REVERSE LENGTH=398 | 201606	AT4G38970.1	43 kDa	39	44	47	46	46
| Transketolase | Chr3:22454004-22456824 FORWARD LENGTH=741 | 201606	AT3G60750.1 (+1)	80 kDa	34	42	43	45	42
| C2 calcium/lipid-binding plant phosphoribosyltransferase family protein | Chr5:2127200-2129584 REVERSE LENGTH=794 | 201606	AT5G06850.1	91 kDa	29	42	34	34	40
| lipoxygenase 2 | Chr3:16525437-16529233 FORWARD LENGTH=896 | 201606	AT3G45140.1	102 kDa	24	42	39	38	26
| photosystem II reaction center protein B | ChrC:72371-73897 FORWARD LENGTH=508 | 201606	ATCG00680.1	56 kDa	22	42	38	32	29
| carbonic anhydrase 1 | Chr3:194853-196716 REVERSE LENGTH=270 | 201606	AT3G01500.1 (+1)	30 kDa	37	40	40	37	38
| carbonic anhydrase 2 | Chr5:4760536-4762382 FORWARD LENGTH=259 | 201606	AT5G14740.2 (+4)	28 kDa	35	40	39	38	37
| serine transhydroxymethyltransferase 1 | Chr4:17831891-17834742 REVERSE LENGTH=517 | 201606	AT4G37930.1	57 kDa	29	40	34	34	36
| chaperonin-60alpha | Chr2:11926603-11929184 FORWARD LENGTH=586 | 201606	AT2G28000.1	62 kDa	25	37	36	36	33
| Phosphoglycerate mutase%2C 2%2C3-bisphosphoglycerate-independent | Chr3:2608683-2611237 REVERSE LENGTH=560 | 201606	AT3G08590.1 (+1)	61 kDa	25	36	24	19	18
| tubulin beta chain 2 | Chr5:25181560-25183501 FORWARD LENGTH=450 | 201606	AT5G62690.1 (+1)	51 kDa	17	36	25	25	28
| glyceraldehyde-3-phosphate dehydrogenase C2 | Chr1:4608465-4610494 REVERSE LENGTH=338 | 201606	AT1G13440.1	37 kDa	21	35	27	23	26
| fructose-bisphosphate aldolase 1 | Chr2:9128416-9130152 REVERSE LENGTH=399 | 201606	AT2G21330.1	43 kDa	29	34	37	38	35
| peroxisomal NAD-malate dehydrogenase 2 | Chr5:2993645-2995169 REVERSE LENGTH=333 | 201606	AT5G09660.2	35 kDa	22	34	27	34	30
| tubulin beta chain 4 | Chr5:17859442-17860994 REVERSE LENGTH=444 | 201606	AT5G44340.1	50 kDa	14	33	23	20	19
| RAB GTPase homolog E1B | Chr4:10990036-10991466 FORWARD LENGTH=476 | 201606	AT4G20360.1 (+1)	52 kDa	22	32	42	33	26
| photosystem II subunit QA | Chr4:11334446-11335587 FORWARD LENGTH=223 | 201606	AT4G21280.1	24 kDa	20	31	24	29	29
| glutamine synthetase 2 | Chr5:13831220-13833239 FORWARD LENGTH=430 | 201606	AT5G35630.1 (+2)	47 kDa	16	31	25	26	20
| tubulin beta-5 chain | Chr1:6938033-6940481 REVERSE LENGTH=449 | 201606	AT1G20010.1	50 kDa	15	31	24	23	22

| methionine synthase 2 | Chr3:957602-960740 FORWARD LENGTH=765 | 201606	AT3G03780.1 (+2)	85 kDa	14	31	31	30	27
| chloroplast heat shock protein 70-1 | Chr4:12590094-12593437 FORWARD LENGTH=718 | 201606	AT4G24280.1	77 kDa	28	30	36	42	36
| photosystem II subunit O-2 | Chr3:18891008-18892311 REVERSE LENGTH=331 | 201606	AT3G50820.1	35 kDa	27	30	32	28	26
| actin 8 | Chr1:18216539-18217947 FORWARD LENGTH=377 | 201606	AT1G49240.1 (+2)	42 kDa	31	29	31	32	27
| DNA glycosylase superfamily protein | Chr1:6744520-6746144 FORWARD LENGTH=382 | 201606	AT1G19480.1 (+1)	42 kDa	27	29	32	31	28
| GTP binding Elongation factor Tu family protein | Chr1:2455559-2457001 FORWARD LENGTH=449 | 201606	AT1G07920.1 (+8)	50 kDa	23	29	23	33	21
| CLPC homologue 1 | Chr5:20715710-20719800 REVERSE LENGTH=929 | 201606	AT5G50920.1	103 kDa	18	29	24	30	22
| ADP/ATP carrier 1 | Chr3:2605706-2607030 REVERSE LENGTH=381 | 201606	AT3G08580.1 (+1)	41 kDa	18	29	25	17	19
| light harvesting complex of photosystem II 5 | Chr4:6408200-6409496 FORWARD LENGTH=280 | 201606	AT4G10340.1	30 kDa	17	29	22	22	22
| chloroplast heat shock protein 70-2 | Chr5:20303470-20306295 FORWARD LENGTH=718 | 201606	AT5G49910.1	77 kDa	30	28	36	44	33
| actin 7 | Chr5:3052809-3054220 FORWARD LENGTH=377 | 201606	AT5G09810.1	42 kDa	26	28	24	28	25
| photosystem II reaction center protein C | ChrC:33720-35141 FORWARD LENGTH=473 | 201606	ATCG00280.1	52 kDa	24	28	26	25	20
| Pyridoxal phosphate (PLP)-dependent transferases superfamily protein | Chr4:16171847-16174630 REVERSE LENGTH=461 | 201606	AT4G33680.1	50 kDa	27	27	27	31	34
			Total Spectrum Count				

Protein threshold = 99%; minimum # peptides = 2; peptide threshold = 95%

Appendix XVII Top 50 hits for mass spectrometry jfe191114

jfe191114_CmOx			NRG1B-HF					
Identified Proteins (50/100)	Accession Number	MW	Un-infiltrated	KRVY	A4-3	A4-4	A4-6	A4-8
| Disease resistance protein (CC-NBS-LRR class) family | Chr5:26718338-26721133 REVERSE LENGTH=815 | 201606	AT5G66910.1	93 kDa	211	128	122	99	109	141
| ribulose-bisphosphate carboxylase | ChrC:54958-56397 FORWARD LENGTH=479 | 201606	ATCG00490.1	53 kDa	19	37	33	30	22	41
| rubisco activase | Chr2:16570951-16573345 REVERSE LENGTH=474 | 201606	AT2G39730.1	52 kDa	15	20	32	25	28	36
| ATP synthase subunit alpha | ChrC:9938-11461 REVERSE LENGTH=507 | 201606	ATCG00120.1	55 kDa	7	18	23	17	18	17
| glyceraldehyde 3-phosphate dehydrogenase A subunit 2 | Chr1:4392634-4394283 REVERSE LENGTH=399 | 201606	AT1G12900.1	43 kDa	6	18	0	17	14	25
| glyceraldehyde 3-phosphate dehydrogenase A subunit | Chr3:9795226-9796848 FORWARD LENGTH=396 | 201606	AT3G26650.1	42 kDa	6	18	20	17	18	24
| ATP synthase subunit beta | ChrC:52660-54156 REVERSE LENGTH=498 | 201606	ATCG00480.1	54 kDa	10	15	25	11	17	23
| glyceraldehyde-3-phosphate dehydrogenase B subunit | Chr1:16127552-16129584 FORWARD LENGTH=447 | 201606	AT1G42970.1	48 kDa	7	15	15	10	17	22
| heat shock cognate protein 70-1 | Chr5:554055-556334 REVERSE LENGTH=651 | 201606	AT5G02500.1	71 kDa	19	14	8	8	20	37
| epithiospecifier protein | Chr1:20170995-20173885 REVERSE LENGTH=341 | 201606	AT1G54040.2	37 kDa	5	3	8	8	7	7
| Heat shock protein 70 (Hsp 70) family protein | Chr3:2903434-2905632 REVERSE LENGTH=649 | 201606	AT3G09440.1 (+3)	71 kDa	13	9	6	7	16	24
| chlorophyll A/B binding protein 1 | Chr1:10478071-10478874 FORWARD LENGTH=267 | 201606	AT1G29930.1	28 kDa	8	11	11	7	9	13
| ADP/ATP carrier 1 | Chr3:2605706-2607030 REVERSE LENGTH=381 | 201606	AT3G08580.1 (+1)	41 kDa	3	1	4	7	5	7
| PSI type III chlorophyll a/b-binding protein | Chr1:22700152-22701149 FORWARD LENGTH=273 | 201606	AT1G61520.1 (+2)	29 kDa	4	4	6	6	2	5
| photosystem I subunit F | Chr1:11215011-11215939 REVERSE LENGTH=221 | 201606	AT1G31330.1	24 kDa	0	2	6	6	3	6
| photosystem II reaction center protein C | ChrC:33720-35141 FORWARD LENGTH=473 | 201606	ATCG00280.1	52 kDa	4	6	6	5	9	8
| photosystem II light harvesting complex protein 2.2 | Chr2:1799436-1800329 REVERSE LENGTH=265 | 201606	AT2G05070.1	29 kDa	8	0	0	4	6	9
| RAB GTPase homolog E1B | Chr4:10990036-10991466 FORWARD LENGTH=476 | 201606	AT4G20360.1 (+1)	52 kDa	4	9	5	4	6	10
| Transketolase | Chr3:22454004-22456824 FORWARD LENGTH=741 | 201606	AT3G60750.1 (+1)	80 kDa	4	4	5	4	6	8
| chaperonin-60alpha | Chr2:11926603-11929184 FORWARD LENGTH=586 | 201606	AT2G28000.1	62 kDa	4	2	2	4	2	5
| Phosphoglycerate mutase%2C 2%2C3-bisphosphoglycerate-independent | Chr3:2608683-2611237 REVERSE LENGTH=560 | 201606	AT3G08590.1 (+1)	61 kDa	4	2	5	4	5	3
| carbonic anhydrase 1 | Chr3:194853-196716 REVERSE LENGTH=270 | 201606	AT3G01500.1 (+1)	30 kDa	2	6	12	4	11	15
| light harvesting complex photosystem II subunit 6 | Chr1:5446685-5447676 REVERSE LENGTH=258 | 201606	AT1G15820.1	28 kDa	2	2	4	4	2	2
| Ribosomal protein L11 family protein | Chr2:15619559-15620059 REVERSE LENGTH=166 | 201606	AT2G37190.1 (+1)	18 kDa	1	2	2	4	2	4
| light harvesting complex of photosystem II 5 | Chr4:6408200-6409496 FORWARD LENGTH=280 | 201606	AT4G10340.1	30 kDa	0	7	9	4	6	4
| actin 8 | Chr1:18216539-18217947 FORWARD LENGTH=377 | 201606	AT1G49240.1	42 kDa	5	4	2	3	4	5
| fructose-bisphosphate aldolase 2 | Chr4:18163714-18165659 REVERSE LENGTH=398 | 201606	AT4G38970.1	43 kDa	4	9	10	3	2	8
| DNA glycosylase superfamily protein | Chr1:6744520-6746144 FORWARD LENGTH=382 | 201606	AT1G19480.1 (+1)	42 kDa	3	2	4	3	0	2

| GTP binding Elongation factor Tu family protein | Chr4:1295751-1298354 REVERSE LENGTH=454 | 201606	AT4G02930.1	49 kDa	3	1	2	3	0	0
| C2 calcium/lipid-binding plant phosphoribosyltransferase family protein | Chr5:2127200-2129584 REVERSE LENGTH=794 | 201606	AT5G06850.1	91 kDa	3	0	3	3	5	4
| carbonic anhydrase 2 | Chr5:4760536-4762382 FORWARD LENGTH=259 | 201606	AT5G14740.2 (+4)	28 kDa	1	4	10	3	8	17
| light harvesting complex photosystem II | Chr5:209084-210243 FORWARD LENGTH=290 | 201606	AT5G01530.1	31 kDa	0	1	2	3	4	2
| GTP binding Elongation factor Tu family protein | Chr1:2455559-2457001 FORWARD LENGTH=449 | 201606	AT1G07920.1 (+8)	50 kDa	5	2	2	2	2	7
| Cobalamin-independent synthase family protein | Chr5:5935771-5939195 FORWARD LENGTH=765 | 201606	AT5G17920.1 (+1)	84 kDa	3	3	3	2	4	4
| plant VAP homolog 12 | Chr2:18611029-18612971 FORWARD LENGTH=239 | 201606	AT2G45140.1	26 kDa	2	4	3	2	4	16
| catalase 2 | Chr4:16700937-16702955 REVERSE LENGTH=492 | 201606	AT4G35090.3	57 kDa	2	1	0	2	2	4
| chaperonin 60 beta | Chr1:20715717-20718673 REVERSE LENGTH=600 | 201606	AT1G55490.1 (+4)	64 kDa	2	1	4	2	2	0
| ENTH/ANTH/VHS superfamily protein | Chr5:13462463-13465581 REVERSE LENGTH=544 | 201606	AT5G35200.1 (+1)	61 kDa	0	4	4	2	0	4
| ATPase%2C F1 complex%2C gamma subunit protein | Chr4:2350761-2351882 REVERSE LENGTH=373 | 201606	AT4G04640.1	41 kDa	0	3	6	2	4	4
| DEA(D/H)-box RNA helicase family protein | Chr1:27378040-27379593 REVERSE LENGTH=414 | 201606	AT1G72730.1	47 kDa	0	3	2	2	2	0
| sedoheptulose-bisphosphatase | Chr3:20709640-20711421 FORWARD LENGTH=393 | 201606	AT3G55800.1	42 kDa	0	2	3	2	0	5
| Bifunctional inhibitor/lipid-transfer protein/seed storage 2S albumin superfamily protein | Chr2:4311160-4312035 REVERSE LENGTH=291 | 201606	AT2G10940.1 (+1)	30 kDa	0	2	2	2	0	3
| peroxisomal NAD-malate dehydrogenase 2 | Chr5:2993645-2995169 REVERSE LENGTH=333 | 201606	AT5G09660.2	35 kDa	0	1	3	2	1	5
| vesicle associated protein | Chr3:22400537-22402408 FORWARD LENGTH=256 | 201606	AT3G60600.1	28 kDa	0	0	1	2	1	10
| Ribosomal protein L3 family protein | Chr2:17894898-17895713 FORWARD LENGTH=271 | 201606	AT2G43030.1	29 kDa	0	0	2	2	0	3
| chloroplast heat shock protein 70-1 | Chr4:12590094-12593437 FORWARD LENGTH=718 | 201606	AT4G24280.1	77 kDa	4	2	2	1	1	4
| phosphoglycerate kinase 1 | Chr3:4061127-4063140 REVERSE LENGTH=481 | 201606	AT3G12780.1	50 kDa	2	1	8	1	5	3
| serine transhydroxymethyltransferase 1 | Chr4:17831891-17834742 REVERSE LENGTH=517 | 201606	AT4G37930.1	57 kDa	1	1	5	1	3	4
| tubulin beta chain 4 | Chr5:17859442-17860994 REVERSE LENGTH=444 | 201606	AT5G44340.1	50 kDa	1	0	3	1	2	1
| Ribulose bisphosphate carboxylase (small chain) family protein | Chr5:15381203-15381978 REVERSE LENGTH=181 | 201606	AT5G38420.1	20 kDa	0	3	3	1	5	5
			Total Spectrum Count					

Protein threshold = 99%; minimum # peptides = 2; peptide threshold = 95%

Appendix XVIII Optimizations for new lot of anti-EDS1 antibody

5% BSA TBS-T; Block overnight 4C ; Ladder, Ws-2, Ws-2_eds1
400 uL each pico, 100 uL each femto; high 14 x 45s increments

aEDS1:1° 1:3000 1 hr RT
aRb-HRP: 2° 1:10,000 1 hr RT

aEDS1:1° 1:3000 1 hr RT
aRb-HRP: 2° 1:25,000 1 hr RT

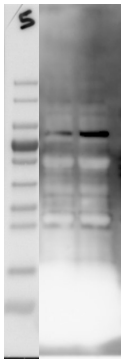

aEDS1:1° 1:5000 1 hr RT
aRb-HRP: 2° 1:10,000 1 hr RT

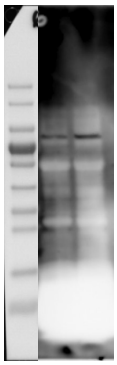

5% milk TBS-T; Block overnight 4C; Ladder, Ws-2, Ws-2_eds1
400 uL each pico, 100 uL each femto; high 23 x 60s increments

aEDS1: 1° 1:3000 1 hr RT
aRb-HRP: 2° 1:10,000 1 hr RT

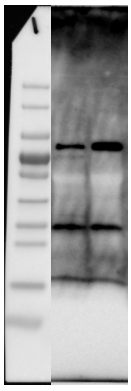

aEDS1: 1° 1:3000 1 hr RT
aRb-HRP: 2° 1:25,000 1 hr RT

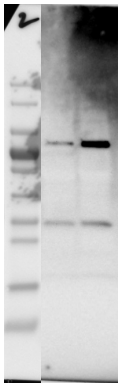

aEDS1: 1° 1:5000 1 hr RT
aRb-HRP: 2° 1:10,000 1 hr RT

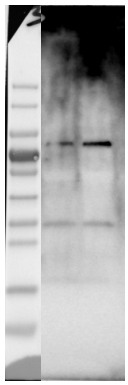

5% milk TBS-T; Block overnight 4C; Ladder, Ws-2, Ws-2_eds1
100 uL each femto; high 17 x 60s increments (plus adjustments)

aEDS1: 1O 1:1000 1 hr RT
aRb-HRP: 2O 1:25,000 1 hr RT

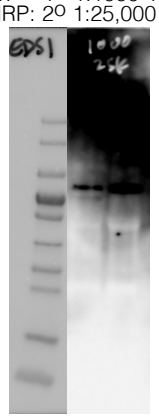

Lot 1908

aEDS1: 1O 1:1000 1 hr RT
aRb-HRP: 2O 1:50,000 1 hr RT

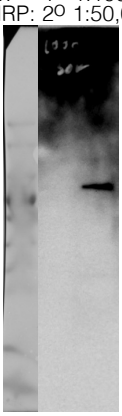

Lot 1908

aEDS1: 1O 1:2000 1 hr RT
aRb-HRP: 2O 1:25,000 1 hr RT

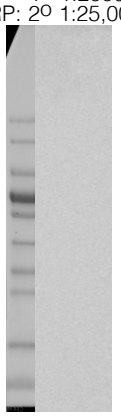

Lot 1809

Appendix XIX Leaky HopQ1-Myc expression induces HR

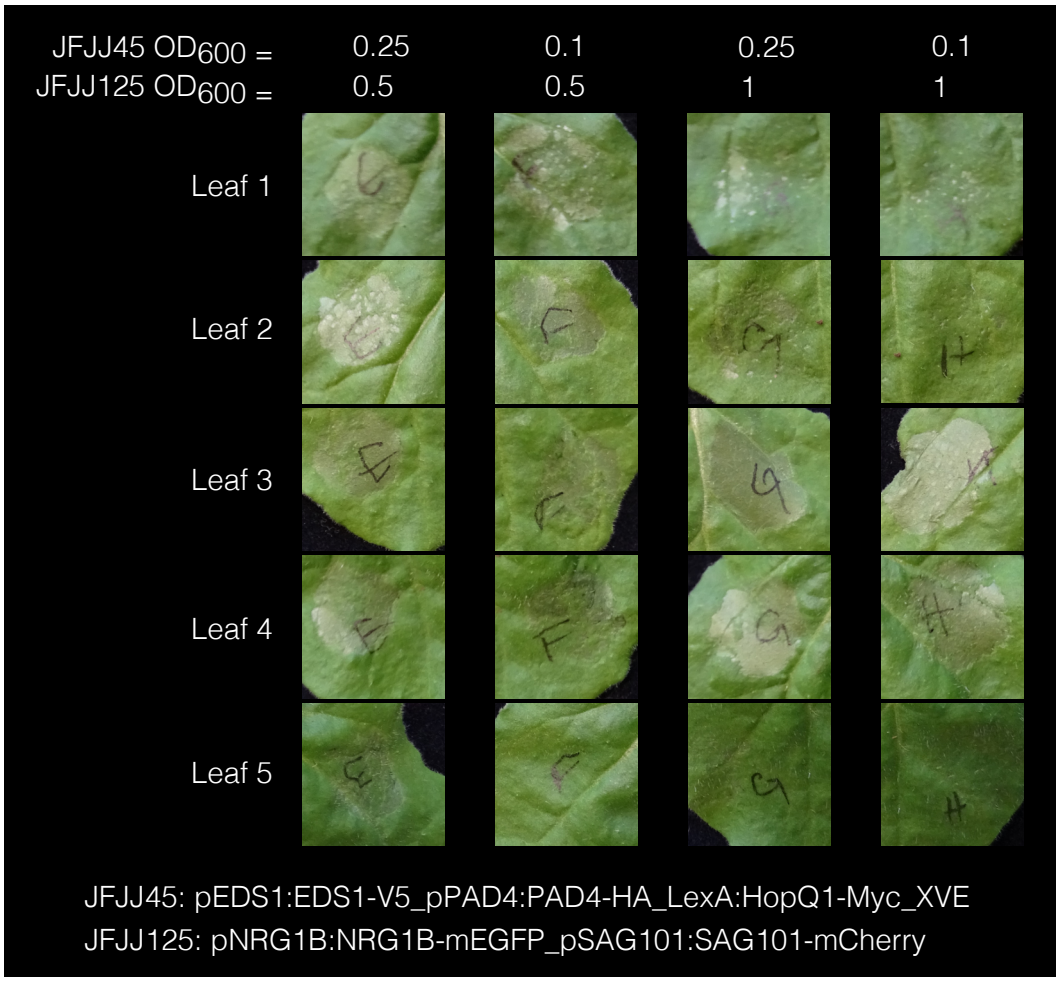

Appendix XX Replicates for localization change assays

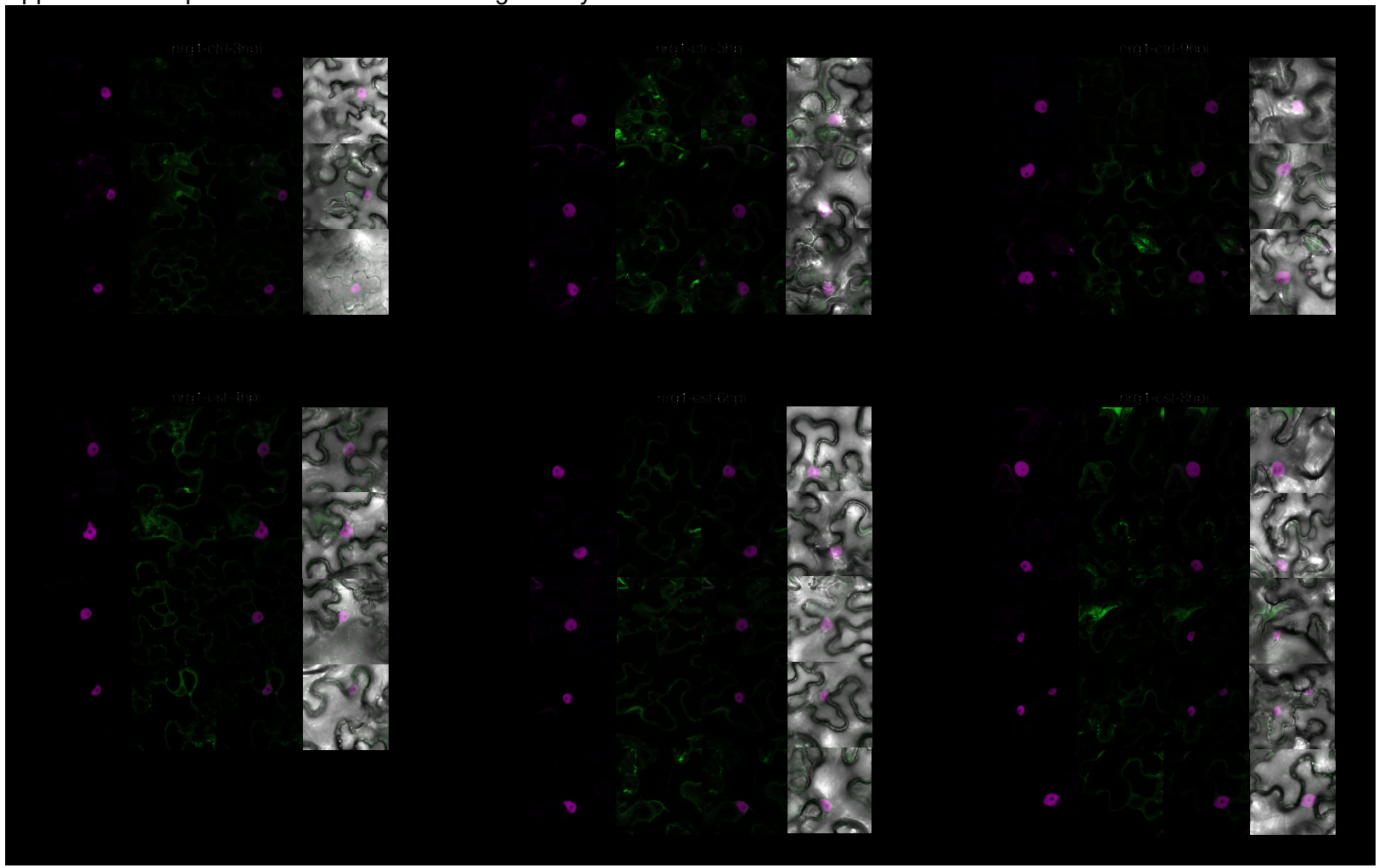

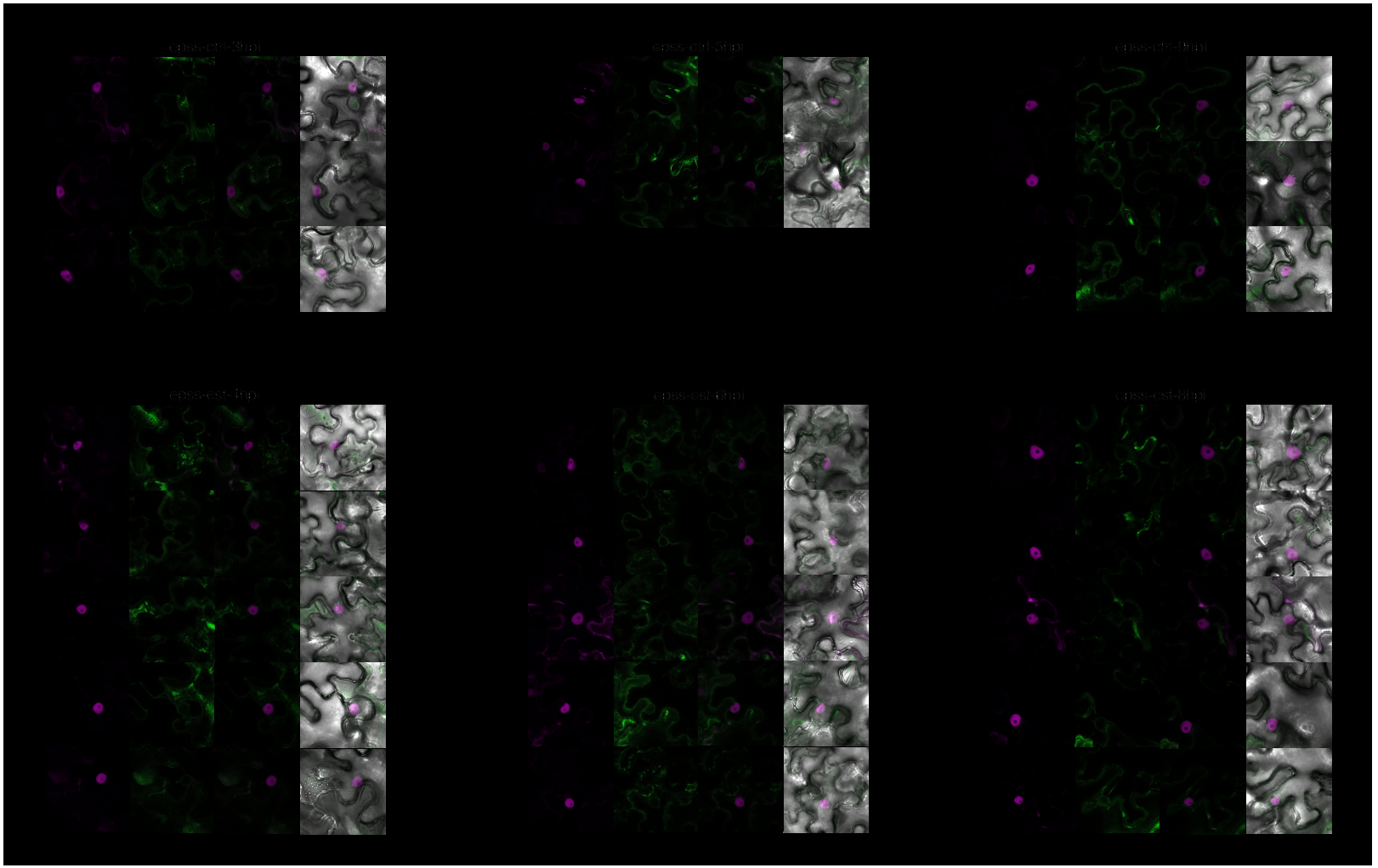

Appendix XXI Fluorescence signal with transient expression and stable lines